UNITED STATES PATENT AND TRADEMARK OFFICE

---

WESTERN DIGITAL TECHNOLOGIES, INC.,
Petitioner,

v.

GODO KAISHA IP BRIDGE 1,
Patent Owner.

---

Case No. IPR2024-01384
U.S. Patent No. 7,884,403

---

**DECLARATION OF JAMES L. MULLINS, Ph.D.**

I, James L. Mullins, declare as follows:

My name is James L. Mullins.

1. I have been retained by Godo Kaisha IP Bridge 1 ("Patent Owner") in the above-captioned *inter partes* review to provide opinions on various documents.

## I. INTRODUCTION

2. I am presently Dean Emeritus of Libraries and Esther Ellis Norton Professor Emeritus at Purdue University. My career as a professional and academic/research spanned more than 44 years including library positions at Indiana University, Villanova University, Massachusetts Institute of Technology, and Purdue University. Appendix A is a true and correct copy of my curriculum vitae describing my background and experience.

3. In January, 2018, I founded the firm Prior Art Documentation Librarian Services, LLC, located at 205 St. Cuthbert, Williamsburg, VA 23188 after purchasing the intellectual property of and successor to Prior Art Documentation, LLC located at 711 South Race Street, Urbana, IL 61801. Further information about my firm, Prior Art Documentation Librarian Services, LLC (PADLS), is available at https://www.priorartdoclib.com.

4. I have been retained by Patent Owner to offer my opinion on the authenticity and dates of public accessibility of various documents. For this service, I am being paid my usual hourly fee of $275.00/hour. I have no stake in the outcome

of this proceeding or any related litigation or administrative proceedings, and my compensation in no way depends on the substance of my testimony or the outcome of this proceeding.

## II. QUALIFICATIONS

5. I received a Bachelor of Arts degree in History, Religion and Political Science in 1972 as well as a Master of Arts degree in Library Science in 1973 from the University of Iowa. I received my Ph.D. in Academic Library Management in 1984 from Indiana University. Over the past fifty-years, I have held various positions in the field of library and information sciences.

6. I am presently Dean Emeritus of Libraries and Esther Ellis Norton Professor Emeritus at Purdue University, and have been since January 1, 2018. I have been previously employed as follows:

Dean of Libraries and Professor and Esther Ellis Norton Professor, Purdue University, West Lafayette, IN (2004-December 31, 2017)

Assistant/Associate Director for Administration, Massachusetts Institute of Technology (MIT) Libraries, Cambridge, MA (2000-2004)

University Librarian and Director, Falvey Memorial Library, Villanova University, Villanova, PA (1996-2000)

Director of Library Services, Indiana University South Bend, South Bend, IN (1978-1996)

Part-time Instructor, School of Library and Information Science, Indiana University, Bloomington, IN (1979-1996)

Associate Law Librarian, and associated titles, Indiana University School of Law, Bloomington, IN (1974-1978)

Catalog Librarian, Assistant Professor, Georgia Southern College (now University), Statesboro, GA (1973-1974)

7. I have been a member of the American Library Association ("ALA") since 1974. I served as the chair of the Research Committee of the Association of College and Research Libraries ("ACRL"). My service included the editorial board of the most prominent library journal, *College and Research Libraries*. I also served on the Standards Committee, College Section of the Association of College and Research Libraries, where I was instrumental in developing a re-issue of the *Standards for College Libraries* in 2000.

8. Over 20 years I was actively engaged in academic library professional associations on the international level including invited papers and lectures in Germany, Norway, Israel, Argentina, Australia, South Africa, New Zealand, Hong Kong, Israel, Turkey, Greece, Canada, France, Belgium, China, Japan, South Korea,

Finland, Sweden, Poland, Portugal, Spain, Switzerland, Singapore, and the United Kingdom.

9. I am an author of numerous publications in the field of library science, and have given presentations in library sciences at national and international conferences. During more than 44 years as an academic librarian and library science scholar, I have gained extensive experience with catalog records and online library management systems (LMS) built using Machine-Readable Cataloging ("MARC") standards. As a part-time instructor at the School of Library and Information Science, Indiana University, I taught, as well as other courses, the cataloging course, "Organization of Library Materials."

10. As an academic library administrator, I have had responsibility to ensure that students were educated to identify, locate, assess, and integrate information garnered from research library resources. I have also facilitated the research of faculty colleagues either directly or through the provision of and access to the requisite print and/or digital materials and services at the universities where I worked.

11. Based on my experience identified above and detailed in my curriculum vitae, which is attached hereto as Appendix A, I consider myself to be an expert in the field of library science and academic library administration. I have previously

offered my opinions on the public availability and authenticity of documents in over 147 cases. I have been deposed in three cases.

## III. BACKGROUND ON PUBLIC ACCESSIBILITY

### A. Scope of This Declaration

12. I am not a lawyer, and I am not rendering an opinion on the legal question of whether a particular document is, or is not, a "printed publication" under the law. I am, however, rendering my expert opinion on the authenticity of the document referenced herein and when and how this document was disseminated or otherwise made available to the extent that people interested and ordinarily skilled in the subject matter or art, exercising reasonable diligence, could have located the document.

13. I am informed by counsel that an item is considered authentic if there is sufficient evidence to support a finding that the item is what it is claimed to be. I am also informed that authenticity can be established based on the contents of the document itself, such as the appearance, content, substance, internal patterns, or other distinctive characteristics of the item.

14. I am informed by counsel that a given reference qualifies as "publicly accessible" if it were disseminated or otherwise made available such that a person interested in and ordinarily skilled in the relevant subject matter could locate it through the exercise of ordinary diligence.

15. While I understand that the determination of public accessibility under the foregoing standard rests on a case-by-case analysis of the facts particular to an individual publication, I also understand that a printed publication is rendered "publicly accessible" if it is cataloged and indexed by a library such that a person interested in the relevant subject matter could locate it (*i.e.*, I understand that cataloging and indexing by a library is sufficient, though there are other ways that a printed publication may qualify as "publicly accessible"). One manner of sufficient indexing is indexing according to subject matter. I understand that it is not necessary to prove someone actually looked at the printed publication in order to show it was publicly accessible by virtue of a library's cataloging and indexing thereof. I understand that cataloging and indexing by a single library of a single instance of a particular printed publication is sufficient. I understand that, even if access to a library is restricted, a printed publication that has been cataloged and indexed therein is publicly accessible so long as a presumption is raised that the portion of the public concerned with the relevant subject matter would know of the printed publication. I also understand that the cataloging and indexing of information that would guide a person interested in the relevant subject matter to the printed publication, such as the cataloging and indexing of an abstract for the printed publication, is sufficient to render the printed publication publicly accessible.

16. I understand that evidence showing the specific date when a printed publication became publicly accessible is not necessary. Rather, routine business practices, such as general library cataloging and indexing practices, can be used to establish an approximate date on which a printed publication became publicly accessible.

## B. Person of Ordinary Skill in the Art

17. In forming the opinions expressed in this declaration, I have reviewed the documents and appendices referenced herein. These materials are records created in the ordinary course of business by publishers, libraries, indexing services, and others. From my years of experience, I have been familiar with the process for creating many of these records, and I know that these records are created by people with knowledge of the information contained within the record. Further, these records are created with the expectation that researchers and other members of the public will use them. All materials cited in this declaration and its appendices are of a type that experts in my field would reasonably rely upon and refer to in forming their opinions.

18. Counsel has informed me that the subject matter of this proceeding relates to an advance to a special kind of solid-state electronics device known as a "magnetic tunnel junction" ("MTJ") device

19. I have been informed by counsel that a "person of ordinary skill in the art at the time of the inventions" (POSITA) is a hypothetical person who is presumed to be familiar with the relevant field and its literature at the time of the inventions. This hypothetical person is also a person of ordinary creativity, capable of understanding the scientific and/or engineering principles applicable to the pertinent field.

20. Counsel has informed me that for the purpose of the Preliminary Patent Owner Response, Patent Owner does not challenge Petitioner's person of ordinary skill in the art definition, and that Petitioner has asserted that people of ordinary skill in this subject matter or art would have included someone with:

- a Ph.D. in electrical engineering, physics, materials science, or a related field, and at least one year of experience in the research, design, and/or development of magnetic/spintronic devices, or the equivalent, or
- a Master's degree in electrical engineering, physics, materials science, or a related field, and four years of experience in the research, design, and/or development of magnetic/spintronic devices, or the equivalent.
- And that less work experience may be compensated by a higher level of relevant education, and vice versa.

21. It is my opinion that such a person would have been actively engaged in academic research and learning through study and practice in the field, and

possibly through formal instruction through the bibliographic resources relevant to his or her research. By the 2000s, such a person with the educational background and research expectation would have had access to a vast array of print resources, including at least the documents referenced below, as well as to a fast-changing set of online resources.

## C. Library Catalog Records and Other Resources

22. Some background on MARC (Machine-Readable Cataloging) formatted records, OCLC, and *WorldCat* is helpful to understand the library catalog records discussed in this declaration. I am fully familiar with the library cataloging standard known as the MARC standard, which is an industry-wide standard method of storing and organizing library catalog information.[1] MARC practices have been consistent since the MARC format was developed by the Library of Congress in the 1960s, and by the early 1970s became the U.S. national standard for disseminating bibliographic data. By the mid-1970s, MARC format became the international standard, and persists through the present. A MARC-compatible library is one that has a catalog consisting of individual MARC records for each of its items. The underlying MARC format (computer program) underpins the online public access catalog (OPAC) that is available to library users to locate a particular holding of a

[1] The full text of the standard is available from the Library of Congress at http://www.loc.gov/marc/bibliographic/.

library. Today, MARC is the primary communications protocol for the transfer and storage of bibliographic metadata in libraries.[2] The MARC practices discussed below were in place during the late 1990s time frame relevant to the documents referenced herein.

23. Online Computer Library Center (OCLC) is a not-for-profit worldwide consortium of libraries. Similar to MARC standards, OCLC's practices have been consistent since the 1970s through the present. Accordingly, the OCLC practices discussed below were in place during the time frame discussed in my opinions section. OCLC was created "to establish, maintain and operate a computerized library network and to promote the evolution of library use, of libraries themselves, and of librarianship, and to provide processes and products for the benefit of library users and libraries, including such objectives as increasing availability of library resources to individual library patrons and reducing the rate of rise of library per-unit costs, all for the fundamental public purpose of furthering ease of access to and use of the ever-expanding body of worldwide scientific, literary and educational knowledge and information."[3] Among other services, OCLC and its members are

[2] Almost every major library in the world uses a catalog that is MARC-compatible. *See, e.g.*, Library of Congress, *MARC Frequently Asked Questions (FAQ)*, https://www.loc.gov/marc/faq.html (last visited Jan. 24, 2018) ("MARC is the acronym for MAchine-Readable Cataloging. It defines a data format that emerged from a Library of Congress-led initiative that began nearly forty years ago. It provides the mechanism by which computers exchange, use, and interpret bibliographic information, and its data elements make up the foundation of most library catalogs used today."). MARC is the ANSI/NISO Z39.2-1994 (reaffirmed 2009) standard for Information Interchange Format.

[3] OCLC Online Computer Library Center, Inc., *Amended Articles of Incorporation of OCLC Online Computer Library Center, Inc.*, Third Article (OCLC, Dublin, Ohio) Revised November 30, 2016, https://www.oclc.org/content/dam/oclc/membership/articles-oA-incorporation.pdf.

responsible for maintaining the WorldCat database (http://www.worldcat.org/), used by libraries throughout the world.

24. Libraries worldwide use the machine-readable MARC format for catalog records. MARC-formatted records include a variety of subject access points based on the content of the document being cataloged. A MARC record for a particular work comprises several fields, each of which contains specific data about the work. Each field is identified by a standardized, unique, three-digit code corresponding to the type of data that follows. For example, a work's title is recorded in field 245, the primary author of the work is recorded in field 100, a work's International Standard Book Number ("ISBN") is recorded in field 020, and the work's Library of Congress call number (assigned by Library of Congress) is recorded in field 050. Some fields can contain subfields, which are indicated by letters. For example, a work's publication date is recorded in field 260 under the subfield "c."

25. The MARC Field 040, subfield "a," identifies the library or other entity that created the catalog record in the MARC format. MARC Field 008 identifies the date when this first MARC record was created.

26. MARC records also include several fields that include subject matter classification information. An overview of MARC record fields is available through the Library of Congress at http://www.loc.gov/marc/bibliographic/. For example,

6XX fields are termed "Subject Access Fields."[4] Among these, for example, is the 650 field; this is the "Subject Added Entry – Topical Term" field. *See* http://www.loc.gov/marc/bibliographic/bd650.html. The 650 field is a "[s]ubject added entry in which the entry element is a topical term." *Id.* The 650 field entries "are assigned to a bibliographic record to provide access according to generally accepted thesaurus-building rules (e.g., *Library of Congress Subject Headings* (LCSH), *Medical Subject Headings* (MeSH))." *Id.* Thus, a researcher can easily discover material relevant to a topic of interest with a search using the terms employed in MARC Fields 6XX.

27. *WorldCat* is the world's largest public online catalog, maintained by the OCLC, a not-for-profit international library consortium, built with the records created by the thousands of libraries that are members of OCLC. OCLC provides bibliographic and abstract information to the public based on MARC-compliant records through its OCLC *WorldCat* database. *WorldCat* requires no knowledge of MARC tags and code and does not require login or password. *WorldCat* is easily accessible through the World Wide Web to all who wish to search for it; there are no restrictions to being a member of a particular community, etc. The date a given catalog record was created (corresponding to the MARC Field 008) appears in some detailed *WorldCat* records as the Date of Entry but not necessarily all. WorldCat

[4] *See* http://www.loc.gov/marc/bibliographic/bd6xx.html.

does not provide a view of the underlying MARC format for a specific WorldCat record. In order to see the underlying MARC format the researcher must locate the book in a holding library listed among those shown in *WorldCat,* and search the online public catalog (OPAC) of a holding library. Whereas *WorldCat* records are widely available, the availability of library specific MARC formatted records varies from library to library. When a specific library wishes to make the underlying MARC format available there will be a link from the library's OPAC display, often identified as a MARC record or librarian/staff view.

28. When a MARC record is created by the Library of Congress or an OCLC member institution, the date of creation for that record is automatically populated in the fixed field (008), with characters 00 through 05 in year, month, day format (YYMMDD).[5] Therefore, the MARC record creation date reflects the date on which the publication associated with the record was first cataloged. Thereafter, the local library's computer system may automatically update the date in field 005 every time the library updates the MARC record (*e.g.*, to reflect that an item has been moved to a different shelving location within the library, or a reload of the bibliographic data with the introduction of a new library management system that creates and manages the OPAC.

### *D.* Monograph Publications

[5] Some of the newer library catalog systems also include hour, minute, second (HHMMSS).

29. Monograph publications are written on a single topic, presented at length, and distinguished from an article and include books, dissertations, and technical reports. A library typically creates a catalog record when the monograph is acquired by the library. First, it will search OCLC to determine if a record has already been created by the Library of Congress or a contributing member library. If the record is found in OCLC, the record is downloaded into the library's LMS (Library Management System) that includes typically the acquisitions, cataloging, and circulation integrated functions. Once the item is downloaded into the library's LMS, the library adds its identifier to the OCLC database so when a search is completed on WorldCat, the library will be indicated as an owner of the title. With the creation of the record in the LMS it is searchable and viewable through the library Online Public Access Catalog (OPAC), by author, title, and subject heading, at the library and from anywhere in the world through the internet. The OPAC also connects with the circulation function of the library which typically indicates whether the book, dissertation, tech report is available, in circulation, etc., with its call number and location in a specific departmental/disciplinary library. The OPAC not only provides immediate bibliographic access on site, it also facilitates interlibrary loan of items, that is, the loan of an item from one library to another to meet a research need.

## *E.* Dissertation/Thesis publications

30. Dissertation (doctoral level) and theses (masters and bachelors level) often exist in only one paper copy, held at the institution where it was written and cataloged, and shelved in the institution's archives or special collections. Often, there is only one library record and one holding library, the one in which the degree was granted. An additional copy may be added by another library when a copy is purchased and added to that library collection.

31. Dissertation/thesis in the past were made available in print and on microform, however, requested copies are now more often provided as a digital copy. During the past ten years many institutions no longer require the submission of a hard-copy of the dissertation/theses, and solely rely on the digital format. The originating cataloging would typically still be done by the degree granting institution's library.

## F. Database consulted

32. **ProQuest** - ProQuest's collections span six centuries, all disciplines and the diverse content types needed by researchers, providing the world's largest collection of dissertations and theses; three centuries of newspapers; more than 450,000 academic eBooks; collections of important scholarly journals and other content researchers need such as data; and unique digital vaults of primary source

materials ProQuest's renowned abstracting and indexing enables researchers to find sources in their area of study. https://about.proquest.com/libraries/academic/

33. ***HathiTrust Digital Library*** - Founded in 2008, HathiTrust is a not-for-profit collaborative of academic and research libraries preserving 18+ million digitized items. HathiTrust offers reading access to the fullest extent allowable by U.S. copyright law, computational access to the entire corpus for scholarly research, and other emerging services based on the combined collection. HathiTrust members steward the collection — the largest set of digitized books managed by academic and research libraries — under the aims of scholarly, not corporate, interests. https://www.hathitrust.org/

**OPINION REGARDING AUTHENTICITY AND PUBLIC ACCESSIBILITY:**

**Document A. EX2007 Rodney Joseph Soukup. *Hot Electron Transport in Vacuum Deposited Thin Film Emission Diodes*. A thesis submitted to the Graduate Faculty in Partial Fulfillment of the Requirements for the Degree of Doctor of Philosophy, June, 1969. University of Minnesota, 1969. ("Soukup")**

**A. Authentication**

34. I have been asked to opine on a thesis/dissertation authored by Rodney Joseph Soukup titled *Hot Electron Transport in Vacuum Deposited Thin Film Emission Diodes,* A Thesis submitted to the Graduate Faculty of the University of Minnesota in Partial Fulfillment of the Requirements for the Degree of Doctor of Philosophy, June, 1969, The University of Minnesota, 1969. ("Soukup")

35. EX2007 is an entire copy of Soukup provided to me by counsel. I will be comparing the results of my research to EX2007 to determine authenticity and public accessibility.

36. Attachment A-1 is the Purdue University Libraries OPAC record for Soukup providing access ("Online Access Available") to the digital version of Soukup through ProQuest.

37. Attachment A-2 is the Soukup dissertation accessible to, and downloaded by me, on November 10, 2024 through my emeritus faculty status at Purdue University from the *ProQuest* database URL: https://www.proquest.com/docview/302428580?accountid=13360&parentSessionId=SRFsb%2BfeCHVpkaFs8fMjx1GOKbYS2qj0lQFOXhgYz1E%3D&pq-origsite=primo&sourcetype=Dissertations%20&%20Theses

It is available for a fee at URL:

https://dissexpress.proquest.com/?author=Rodney%20joseph%20soukup

38. Attachment A-3 includes scans of the print copy of Soukup held by the University of Minnesota Libraries provided to me by the Purdue University Libraries Interlibrary Loan Department on November 13, 2024. Attachment A-3 includes transmittal page of PUL Libraries ILL, University of Minnesota Libraries MNU Lending, Soukup's title page, acknowledgements, Table of Contents, and List of Figures. Due to fair use restrictions it was not possible to request scans of the entire

print dissertation, however, included in the scans provided by the University of Minnesota from the print copy held by the library it is enough to ensure that the copy held in print is the same as held by ProQuest in digital format and transmitted to me as Attachment A-2.

39. After a careful review of EX2007 with Attachment A-2 and the comparable pages in Attachment A-3, it is my opinion, therefore, Soukup is an authentic document created as a dissertation and submitted for partial fulfillment for the degree of doctor of philosophy at the University of Minnesota in 1969.

40. This is documented by inclusion of Soukup in the *ProQuest* database, an authoritative digital repository for thesis/dissertations. In addition, the retrieval I made through the Purdue University Libraries, a major research university library, to access Soukup from *ProQuest* is further evidence that Soukup is authentic. Evidence that the University of Minnesota Libraries confirms its authenticity was my request through the Interlibrary Loan Department of Purdue University Libraries scans from the print copy held by the University of Minnesota Libraries. A scan of the entire print copy of Soukup held by the University of Minnesota Libraries was not possible due to limitations of 'fair use' under copyright law.

41. Therefore, I opine that Soukup is an authentic document. The authenticity of Soukup will be further examined in the Public Accessibility section below.

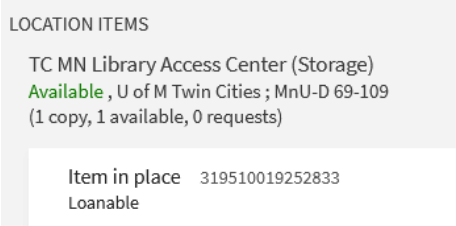
**Public Accessibility**

42. Attachment A-4 is the OCLC *WorldCat* entry for Soukup that I completed a search and created a screen capture on December 6, 2024 at URL: https://search.worldcat.org/title/763139404

43. The *WorldCat* holding record, Attachment A-4, shows Soukup is held by the University of Minnesota, as well as Hathi Trust Digital Library. Typically theses are only held by the degree granting institution. The HathiTrust Digital Library holding provides only access to the catalog record and not to the entire text due to copyright, a description of HathiTrust Digital Library is provided above.

44. Soukup could have been located in *WorldCat/FirstSearch* during the timeframe mid 1980s through 2005 by completing a search by author: Rodney Joseph Soukup; by title: *Hot Electron Transport in Vacuum Deposited Thin Film Emission Diodes* and/or by subject descriptors: *Electronic Emission* and/or *Metallic films*, among others.

45. Attachment A-5 is a download from the University of Minnesota Libraries OPAC that I completed on December 6, 2024. Upon review of the OPAC record it is possible to determine that Soukup is available in print as shown below in the OPAC record as shown below:




46. Attachment A-5 indicates that Soukup is available, in print, at "TC MN Library Access Center (Storage). Available, U of M Twin Cities ; MnU-D 69-109 (1 copy, 1 available, 0 requests). Item in Place 319510019252833 Loanable." Verification that this OPAC record reflects Soukup is indicated by author: Rodney Joseph Soukup; and by title: *Hot Electron Transport in Vacuum Deposited Thin Film Emission Diodes.*

47. Attachment A-6 is a download from the University of Minnesota Libraries OPAC that I completed on December 10, 2024. Upon review of the OPAC record it is possible to determine that Soukup is available digitally as shown below in the OPAC record as shown below:

48. The University of Minnesota Libraries OPAC record, as shown in Attachment A-5 and Attachment A-6, confirms that Soukup would have been publicly accessible through The University of Minnesota Libraries catalog by author: Rodney Joseph Soukup; by title: *Hot Electron Transport in Vacuum Deposited Thin Film Emission Diodes.*

and/or by Library of Congress subject descriptors: *Electrons – Emissions;* and/or *Metallic Films.*

49. Attachment A-7 is the MARC record for Soukup that I downloaded from the University of Minnesota Libraries OPAC on December 6, 2024. The MARC record provides information that populates the OPAC record and includes dates about the item that is not typically useful to a library researcher. Such is the case with 005 and 008 MARC Fields, a further description is above in the introductory paragraphs.

50. In most instances, the original cataloging (008 MARC field) of a published book is completed by the Library of Congress shortly after its publication and receipt by the Library of Congress, while the 005 MARC field indicates the date cataloged by the local library. The 005 and 008 MARC Fields for Soukup are shown below from Attachment A-7.

```
005     20240223061650.0
008     871109s1969    mnua     b    000 0 eng d
```

51. Original cataloging for a thesis/dissertation is completed by the library cataloging department of the university granting the degree. Therefore, the dates in the 008 MARC field is the date when Soukup was cataloged by the University of Minnesota Libraries, 871109s1969 (87=1987; 11=November; 09 = ninth day of November; s = single publication (not a serial); and 1969 = date of publication. Therefore, original cataloging by the University of Minnesota Libraries was completed on November 9, 1987.

52. The MARC 005 Field reads: 20240123061650.0, by this record appears that the record was "touched" by the University of Minnesota Libraries, that is, some additional information was added/changed in 2024, this could be a note about change in location or possibly the transfer of all catalog data from one library management system to another. However, ''touches' to the MARC record do not change access points as described above for author, title and subject headings.

53. Therefore, it is my opinion, that at least by November 9, 1987, Soukup, was searchable in the Library catalog of the University of Minnesota Library by author, title and the subject headings as delineated above.

54. Dissertations (doctoral level) and theses (masters and bachelors level) often exist in only one paper copy, held at the institution where it was written and cataloged, and shelved in the institution's archives or special collections. In addition, in order to document the research undertaken in the dissertation, in the past, at most universities, it was required that the dissertation be submitted to ProQuest so that it can be 'published' and made available to scholars and researchers.

55. Dissertation/theses in the past were made available for purchase in print and in microform by ProQuest (formerly known as University Microfilms). ProQuest is a database that can be searched online, both viewable and downloadable through a library or institution that has a subscription with ProQuest. If access is

not possible through a subscribing institution, it is possible to purchase a copy of a dissertation as shown above for Soukup.

56. In order to determine when and how public accessibility to Soukup was possible, I contacted customer service at ProQuest on November 25, 2024. Attachment A-8 is an email that is a follow-up to a chat that took place between Vicki Turner (ProQuest) and me on November 25, 2024 in which I described my need to document the deposit and accessibility of Soukup through ProQuest (in 1969 – University Microfilms). Ms. Turner informed me that it would be possible to obtain an affidavit from ProQuest detailing the questions I had about deposit and access of Soukup. This required payment which I made to cover this service.

57. On Tuesday, November 26, 2024, I received an affidavit, Attachment A-9, in which Heather Stewart, Manager, Content Curation, ProQuest, details the role of ProQuest/University Microfilms. In the affidavit Ms. Stewart describes the process of accepting and making dissertations available to the research community.

58. Paragraphs 1-2 of the affidavit describe her qualifications and experience at ProQuest as well as ProQuest's role within the research community by the acceptance and provision of access to dissertations and thesis

59. Paragraphs 3-7 describe the role of ProQuest (University Microfilms) from the 1980s through the 2010s, during which the transition took place from a print only publishing environment to a digital environment.

60. Paragraph 8, she states, “I have reviewed ProQuest’s records regarding the dissertation cited as:

| | |
|---|---|
| Dissertation No. | 7001819 |
| Title: | HOT ELECTRON TRANSPORT IN VACUUM DEPOSITED THIN FILM EMISSION DIODES |
| Author: | SOUKUP, RODNEY JOSEPH |
| Degree Date: | 1969 |
| University: | University of Minnesota |

| | |
|---|---|
| First Received by UMI/ProQuest: | n/a |
| First Made Available for Sale (print or electronic) | 01/1969 |
| DAI volume issue: | DAI-B 30/08, Dissertation Abstracts International |
| DAI publication month and year: | 01/1969 |
| Date full text is loaded into PQDT: | 01/1969 |
| Information available on restrictions: | no restrictions ever placed on document |

61. Paragraphs 9-10 read as follows:

9. At the time of the Dissertation’s publication, the Record of the Dissertation was made available directly from ProQuest in electronic format and online via third party vendors, including Dialog, as part of the Abstract Database which was made available via such vendors in the ordinary course of business.

10. The attached print copy of the Dissertation is a true and complete copy of the Record and the full Dissertation as originally published and kept by ProQuest in the ordinary course of its business.

62. Attachment A-10 is the copy referred to by Ms. Stewart in paragraph 10.

**Conclusion**

63. Based on the evidence presented here – thesis completed in 1969 at the University of Minnesota, and held in the University of Minnesota Libraries, it is my opinion EX2007, Soukup, is an authentic document that would have been available to the public, such that any person interested in Soukup could locate it through the University of Minnesota Libraries catalog by author, title and subject access at least by November 9, 1987. In addition, Soukup could be located and accessible through *ProQuest,* and its predecessor companies, from 1969 through 2005 by consulting Dissertation Abstracts International.

**RIGHT TO SUPPLEMENT**

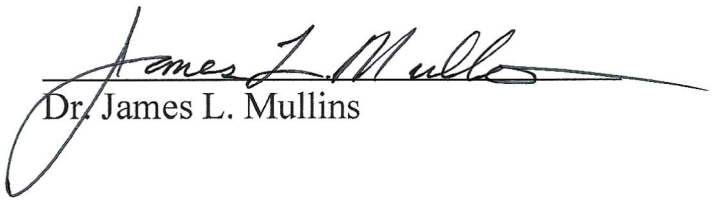
I reserve the right to supplement my opinions in the future to respond to any arguments that the Patent Owner raises and to take into account new information as it becomes available to me.

**JURAT**

I declare that all statements made herein of my own knowledge are true and that all statements made on information and belief are believed to be true; and further that these statements were made with the full knowledge that willful false statements

and the like so made are punishable by fine or imprisonment, or both, under Section 1001 of Title 18 of the U.S. Code.

Dated: December 11, 2024



Dr. James L. Mullins

# Attachment A-1

Screen capture created by J L Mullins from Purdue University Libraries OPAC on November 10, 2024 at URL:
https://purdue.primo.exlibrisgroup.com/discovery/fulldisplay?docid=cdi_proquest_journals_3024285 80&context=PC&vid=01PURDUE_PUWL:PURDUE&lang=en&search_scope=MyInst_and_CI&adaptor=Primo%20Central&tab=Everything&query=any,contains,Hot%20Electron%20Transport%20in%20Vacuum%20Deposited%20Thin%20Film%20Emission%20Diodes




DISSERTATION

**HOT ELECTRON TRANSPORT IN VACUUM DEPOSITED THIN FILM EMISSION DIODES**

SOUKUP, RODNEY JOSEPH

1969

*“ ...This dissertation has been microfilmed exactly as received 70-1819 SOUKUP, Rodney Joseph, 1939- HOT ELECTRON TRANSPORT IN VAC DEPOSITED THIN FILM EMISSION... ”*

Download PDF > Read Online >

TOP

Online access available >

## Details

| | |
|---|---|
| **Title** | HOT ELECTRON TRANSPORT IN VACUUM DEPOSITED THIN FILM EMISSION DIODES |
| **Author** | SOUKUP, RODNEY JOSEPH > |
| **Subjects** | Condensation > |
| **Publisher** | ProQuest Dissertations & Theses |
| **Creation Date** | 1969 |
| **Keywords** | Condensed matter physics |
| **Identifiers** | ISBN: 9798658445168 |
| **Citation Source** | ProQuest Dissertations & Theses Global |

# Attachment A-2

This dissertation has been
microfilmed exactly as received

70-1819

SOUKUP, Rodney Joseph, 1939-

HOT ELECTRON TRANSPORT IN VACUUM DEPOSITED THIN FILM EMISSION DIODES.

University of Minnesota, Ph.D., 1969
Physics, solid state

University Microfilms, Inc., Ann Arbor, Michigan

# HOT ELECTRON TRANSPORT IN VACUUM DEPOSITED THIN FILM EMISSION DIODES

A Thesis

Submitted to the Graduate Faculty

of the

University of Minnesota

by

Rodney Joseph Soukup

In Partial Fulfillment of the Requirements

for the

Degree of

Doctor of Philosophy

June, 1969

## ACKNOWLEDGMENTS

I wish to extend my sincere appreciation to Dr. D. E. Speliotis for his advice and helpful discussions.

I also wish to thank Dr. D. E. Anderson for suggesting the topic of study and for his interest and suggestions. To all associated with the Physical Electronics Laboratory, I extend thanks for the loan of equipment and for helpful suggestions.

I wish to acknowledge the support of this work by Aeronautical Systems Division, Air Force Systems Command, United States Air Force, under Contract Number AF 33(657)-10475 and Air Force Avionics Laboratory, Research and Technology Division, Air Force Systems Command, United States Air Force under Contract Number AF 33(615)-3434.

I thank my wife, Therese, for her constant encouragement and considerable help in preparing this manuscript.

TABLE OF CONTENTS


| | | Page |
|---|---|---|
| I. | Introduction | 1 |
| II. | Thin Film Sample Fabrication and Measurement Techniques | 9 |
| | A. General Considerations | 9 |
| | B. Preliminary Studies | 10 |
| | 1. Initial Vacuum System | 11 |
| | 2. Second Vacuum System | 14 |
| | 3. Six Port Vacuum System | 17 |
| | a. Metal Overlayer Tube | 19 |
| | b. Metal Underlayer Tube | 20 |
| | c. MgO Insulator Tube | 21 |
| | d. LEED Tube | 21 |
| | e. Measurements Tube | 22 |
| | f. Sputter Cleaning Tube | 23 |
| | g. Methods Used in the Fabrication of Sputtered Metal-MgO-Au Devices | 24 |
| | C. Experimental Vacuum System and Techniques Used in Final Approach | 29 |
| | 1. Description of Vacuum System | 29 |
| | 2. Description of Experimental Apparatus and Preliminary Results | 31 |

TABLE OF CONTENTS (continued)


| | | Page |
|---|---|---|
| 3. | Sample Preparation | 35 |
| | a. Glass Substrates | 35 |
| | b. MgO Substrates | 36 |
| | c. $CaF_2$ Substrates | 36 |
| 4. | Millisecond-Pulse Measurements of I-V Characteristics | 37 |
| 5. | Pulse Techniques Applied to Emission Measurements | 40 |
| 6. | DC Measurements of I-V Characteristics | 41 |
| III. | Results of Experimental Studies of Hot Electron Transport in Thin-Film Emission Diodes | 43 |
| A. | Introduction | 43 |
| B. | High Level I-V Characteristics of Thin Film Emission Diodes | 44 |
| C. | Temperature Measurements of the I-V Characteristics of Thin Film Emission Diodes | 56 |
| D. | Measurements Made on Devices Fabricated with Oxygen Gas Present During Deposition of the Oxide Film | 58 |

TABLE OF CONTENTS (continued)


| | | Page |
|---|---|---|
| | E. Low Level I-V Characteristics of Thin Film Emission Devices | 62 |
| | F. Measurements of Electron Emission into Vacuum from Thin Film Diodes | 63 |
| | G. Attempts to Fabricate a Device with a Single Crystal Oxide | 67 |
| IV. | Analysis of Hot Electron Transport Processes in Vacuum Deposited Thin-Film Emission Diodes | 71 |
| | A. Introduction | 71 |
| | B. Summary of Experimental Observations | 72 |
| | C. Discussion of a Model for Injection of Electrons into the Oxide Film | 74 |
| | D. Discussion of Emission into Vacuum | 93 |
| V. | Summary | 109 |
| APPENDICES | | |
| I. | Application of the Schottky Emission Problem to a Metal-Insulator-Metal Diode | 118 |
| II. | Barrier Height as a Function of Temperature and Excess Mg Concentration | 126 |

TABLE OF CONTENTS (continued)


| | Page |
|---|---|
| III. Calculation of the Fringing Field, F, at a Plane Electrode Beneath a Slot in an Opposing Plane Parallel Electrode | 132 |
| BIBLIOGRAPHY | 136 |
| FIGURES | |

## LIST OF FIGURES


| Figure Number | |
|---|---|
| 1 | Schematic Representation of Initial Vacuum System Used for Depositing Ordered Au-MgO-Au Emission Diodes. |
| 2a | Substrate Masks. |
| 2b | Substrate with Au-MgO-Au Thin Film Diode. |
| 3 | Schematic Representation of the Second Vacuum System Used for Depositing Ordered Au-MgO-Au Emission Diodes. |
| 4 | Six Port Vacuum System Top. |
| 5 | Schematic View of Six Port Vacuum System. |
| 6 | Detail of LEED Unit. |
| 7 | Schematic Representation of Bell Jar Section of Final Vacuum System. |
| 8a | Mask for Final Vacuum System. |
| 8b | Substrate with 3 Metal-Insulator-Metal Emission Diodes. |
| 9 | Circuit Used for Millisecond-Pulse Measurements of Thin-Film Hot Electron Emission Diodes. |
| 10 | Results of Millisecond-Pulse Measurement Technique, Showing I-V Characteristics and Expanded Traces. |

LIST OF FIGURES (continued)


| Figure Number | |
|---|---|
| 11 | Schematic of DC Measurement Technique for Au-MgO-Au Emission Diodes. |
| 12 | Tunnel I-V Characteristics of a Au-MgO-Au Device with an 89 Å Thick Oxide. |
| 13 | I-V Characteristics from Device PY-G-11, Overlayer 1. |
| 14 | Fowler-Nordheim Plot of the I-V Characteristics of Device PY-G-11, Overlayer 1. |
| 15 | Schottky Plot of the I-V Characteristics of Device PY-G-11, Overlayer 1. |
| 16 | Poole-Frenkel Plot of the I-V Characteristics of Device PY-G-11, Overlayer 1. |
| 17 | Comparison of Results of Devices with Thin (< 200 Å) Oxide Films. |
| 18 | Ln I vs. $V^{1/2}$ Plot for Two Devices with Thicker Oxide Films (680 Å). |
| 19 | Temperature Dependence of the I-V Characteristics of Device PY-G-11, Overlayer 1. |
| 20 | Ln I vs. $V^{1/2}$ as a Function of Temperature for Device PY-G-11, Overlayer 1. |
| 21 | $Ln(I_o/T^2)$ vs. 1/T for Device PY-G-11, Overlayer 1. |

LIST OF FIGURES (continued)

Figure Number

22 Comparison of Results with Different Pressures of Oxygen Present During Fabrication.

23 Arrhenius Plot of Devices Fabricated with Different Amounts of Oxygen Present During the MgO Deposition.

24 I-V Characteristics of Device PY-G-38(1).

25 Fowler-Nordheim Plot of I-V Characteristics of Device PY-G-38(1).

26 Comparison of Device Resistance as a Function of Temperature for Devices Fabricated with Different Amounts of Oxygen Present During Oxide Deposition.

27 Emission Transfer Ratio, $\alpha$, vs. Sample Voltage, $V_s$, for Device PY-G-11(1).

28 Comparison of Emission Transfer Ratio for Devices with Different Oxide Thicknesses.

29 Comparison of Emission Transfer Ratio for Devices with the MgO Film Deposited with Different Amounts of Oxygen Gas Admitted.

30 Potential Barrier Presented by a Dielectric Film Between Two Metals, Showing Electron Image Force Modification.

LIST OF FIGURES (continued)


| Figure Number | |
|---|---|
| 31 | Potential Energy Maximum of an Electron in a Dielectric with an Applied Field Present. |
| 32 | Ln I vs. $V^{.484}$ for Device PY-G-11(1). |
| 33 | $Ln(I_o/T^2)$ vs. $10^3/T$ for Device PY-G-11(1) where $I_o$ is Found from the Ln I vs. $V^{.484}$ Plots. |
| 34 | Comparison Between the Data for Device PY-G-21(3) and Equation (3). |
| 35 | Ln I vs. $V^{.484}$ for Devices Measured at High Fields Only. |
| 36 | Comparison of Results for Devices Fabricated with Different Amounts of $O_2$ Present During MgO Deposition. |
| 37 | Comparison Between Experimental Data and Equation (3) for Devices Fabricated with Oxygen Present During MgO Deposition. |
| 38 | Energy Bands as a Function of Interatomic Spacing for a Simple Linear Chain. |
| 39 | $Ln(I_o/T^2)$ vs. $10^3/T$ for Devices Fabricated with Different Amounts of Oxygen Present During MgO Deposition. |
| 40 | Barrier Heights as a Function of Temperature. |

LIST OF FIGURES (continued)


Figure Number

41 Results of Device PY-A-1 with Two Different Metal Electrodes.

42a Energy Band Picture for a Gold-Vacuum Interface.

42b Energy Band Picture for a Gold-MgO Interface if No Interface States Exist.

42c Energy Band Picture for a Gold-MgO Interface with a High Density of Donor Like Interface States.

43 Diagram Indicating Details of the Calculation of Electric Field Variation at a Plane Electrode Opposite a Slotted Electrode.

44a Energy Level Diagram for an Applied Sample Bias of 4 Volts Showing that No Electrons Should be Emitted through the Overlayer.

44b Energy Level Diagram Appropriate for Emission through Holes in the Gold Overlayer Film.

45 Field Strength at the Underlayer Beneath a Slot in the Overlayer.

46 $\alpha = \frac{I_e}{I_e+I_s}$ as a Function of Oxide Thickness Assuming No Energy Loss in the Oxide.

47 Evidence of Charging at an Emitting Slot, Device PY-G-17(1).

LIST OF FIGURES (continued)

Figure Number

48a Emission Transfer Ratio vs. Time Required to Reach $V_s$ = 2 Volts.

48b Emission Transfer Ratio vs. Total Charge Passed through the Device.

49 Time Constants for Charging of the Insulator Beneath a Slot.

## LIST OF TABLES


| | | Page |
|---|---|---|
| Table I | Barriers for different devices as obtained from the zero field intercept of the Schottky plot. | 53 |
| Table II | Barrier heights for different devices as obtained by the zero field intercept and the slope of the ln $(I_o/T^2)$ vs. 1/T plot. | 57 |
| Table III | Overlayer thicknesses for measured devices. | 64 |
| Table IV | Summary of device data. | 70 |
| Table V | Barrier heights for a number of devices with different parameters. | 81 |

# I. INTRODUCTION

Thin film metal-insulator-metal diode devices have been investigated quite extensively in recent years. The interest in these devices has arisen, in part, from the possible application of such devices as active circuit elements or electron sources, as suggested by Mead[1,2] and Geppert.[3] Additional motivation has been provided by interest in the transport of "hot electrons" in the insulator and in the metal overlayer with subsequent emission into vacuum. The term "hot electrons" is used to describe a nonequilibrium situation in solids where a group of electronic energy levels above the Fermi energy is characterized by a greater electron population than that which coincides with the lattice temperature. Well-known examples of this phenomenon include photoemission and secondary emission, in which the internal secondary electrons and photoexcited electrons can be characterized as hot electrons.

When an insulator and a metal are placed in contact the insulator presents a barrier to electron motion, which is part of its forbidden energy gap. However, when an electric field on the order of $10^6$ V/cm. is applied to a thin insulating film on the order of 100 Å thick, sandwiched between two metal films, a current is

observed. This current could be ionic current,[4] but, if the metal and insulator are stable during the application of this field, ionic current can be ignored. The current must then be an electron current. The electrons must either surmount the barrier, Richardson-Schottky current,[5,6] or penetrate through it. This penetration of electrons through a barrier is known as tunnelling and was first described by Fowler and Nordheim[7] in 1928. It has specifically been applied to thin film devices by other authors.[2,8-11] A combination of the two processes is also possible.[12,13] Another mechanism that has been proposed to explain the current observed is the Pool-Frenkel effect.[14] In this effect the current is limited by the field enhanced thermal emission of electrons from a discreet trap level into the conduction band of the oxide. Other possible processes for the conduction mechanism in thin oxide films have been summarized by Jonscher.[15] These processes could all be modified by space charge.[16-18] Thus, the electron process of importance in these devices is in some doubt. Under appropriate conditions a fraction of these electrons, accelerated by the electric field and injected into the overlayer metal film as hot electrons, can penetrate the overlayer film and arrive at the vacuum

interface with sufficient energy to escape, thus constituting an emission current.

Hot electron emission from such devices was first reported by Mead[2] in 1961 using Al-$Al_2O_3$-Al thin film devices. The fraction, $\alpha$, of the total sample current which was emitted into vacuum depended on the sample voltage and current, as well as the sample construction details, and was as high as 0.01. Similar experiments with Al-$Al_2O_3$-(Al or Pt) samples were reported by Cohen.[19] These early experiments demonstrated that emission currents could be drawn from such thin film devices, but the fraction of the total sample current that was emitted was small. Instabilities and breakdown effects were observed which severely limited the total current obtainable.

Mead[20] reported more extensive studies in 1962 using Be-BeO-Au devices, in which the emitted fraction, $\alpha$, of the sample current was measured as a function of Au overlayer film thickness. The results indicated strong attenuation of the hot electrons in the metal overlayer films, and gave evidence of elastic interactions of the injected electrons in the insulating film. Kanter and Feibelman[21] studied Al-$Al_2O_3$-Au devices with results that were in general agreement with the previous results.

Using Mead's results for attenuation in the Au films, an estimate of the importance of inelastic interactions in the $Al_2O_3$ film was obtained. Collins and Davies[22] and Savoye and Anderson[12] also concluded that strong attenuation of the hot electrons occurred in both the insulating film and metal overlayer.

The simple energy-band picture, originally proposed by Mead,[1] allows one to distinguish three stages in the hot electron emission process: injection of electrons into the insulator; transport of the electrons through the insulating film; and transfer through the metal overlayer region into vacuum.

The electron injection process has been analyzed theoretically by several observers.[5,6,8-16,23-25] The conclusion arrived at is that both thermal and field effect currents can occur with the barrier height determining which mechanism is dominant. The simple band picture was used by Simmons[11,23] to analyze the electron injection process in terms of tunnelling, where the insulator presents a potential barrier to the electrons. An approximate multiple-image correction to the potential profile was included in the analysis. The experiments of Nelson and Anderson[26] with

$Al-Al_2O_3-$(Al and Au) devices were found to be in good agreement with Simmon's potential profile model.

A major difficulty in the studies of thin film emission diodes is that the mechanisms of importance at the various stages of the hot electron transport process are not readily separable on an experimental basis. Although the work of Savoye and Anderson[12] allowed a partial decoupling of the hot electron interactions at the various stages of the electron transport process a number of uncertainties still exist. A large number of impurities are inevitable in the oxide film and at the oxide-metal overlayer interface when the films are moved from the vacuum system into an aqueous anodizing solution and back into another vacuum system. There is the possibility of an oxide gradient in the insulating film resulting in rectification effects, as seen by Nelson,[27] the insulator must be the oxide of the underlayer metal, and the metal and insulator films are amorphous.

The number of impurities in the devices can be greatly reduced if the device is never removed from the vacuum system during fabrication and study. This could be accomplished by plasma anodization[28,29] of a vacuum deposited underlayer metal and subsequent deposition of

an overlayer. The possibility of an oxide gradient and the condition that the insulator must be the oxide of the metal underlayer can be removed by vacuum deposition of the insulating layer. This can be accomplished by rf sputtering of the insulator[30,31] or reactive sputtering[32] of a metal or semiconductor in an active gas by dc methods. Another method of deposition is to evaporate the insulator at a controlled deposition rate by use of a high energy electron beam as first proposed by O'Bryan.[33] General design principles of this method are discussed by Holland.[32]

A major problem with amorphous devices is that the mean free path of hot electrons may be dominated by scattering from imperfections, while in an ordered device the electron scattering may be reduced to that characteristic of the ordered crystal. Another problem is that the simple band picture may not give a true description of the barrier profile, as a consequence of the spatial variations. The influence of structural effects in the thin insulating film was considered by Harris,[34] who presented strong evidence of preferential conduction associated with localized defects in the insulator. The existence of preferential electron emission through holes in the overlayer metal film was

discussed by Savoye and Anderson.[12] Thus, structural effects of both insulator and metal overlayer films play an important part in the emission of hot electrons into vacuum. McColl and Mead,[35] in their studies of electron current through single crystal mica films, found that tunnelling theory provides a self-consistent quantiative description for smaller voltages, but was completely inadequate for use with voltages larger than the barrier height. This is another indication that ordered devices may differ. Ordered devices can be fabricated by epitaxial growth[36] of each layer on a single crystal substrate.

In the present work it was found to be essential for a detailed interpretation of the emission results that certain other experiments be conducted on a given sample in order to gain information not directly obtainable from the I-V characteristics and simple emission results. The I-V characteristics must be measured to determine if the injection mechanism is field or thermally dominated emission. The simple emission measurements yield information on the attenuation of the hot electrons.

The experiments were designed to permit complete fabrication and study of the devices <u>in situ</u>, and hence

the information provided by these experiments was made for a given sample known to be free from impurities. A number of samples were prepared during one evacuation of the system and so measurements were made over a range of insulator thicknesses.

Evaporation of the MgO dielectric layer was done at a pressure of $10^{-8}$ Torr with no $O_2$ gas admitted during fabrication as well as with various background pressures of oxygen admitted in an attempt to produce stoichiometric MgO and thus vary the barrier presented to the flow of electrons by the dielectric layer. All measurements of device I-V characteristics were done at a number of different temperatures in order to determine the effect of temperature on the device characteristics. The results were then combined into a comprehensive model for the hot electron emission process for vacuum deposited Au-MgO-Au sandwich devices.

## II. THIN FILM SAMPLE FABRICATION AND MEASUREMENT TECHNIQUES

### A. General Considerations

In any experiment involving thin film devices the utmost care is required at all stages of sample fabrication and measurement to avoid contamination by trace amounts of impurities. These considerations are of particular importance in the present work, where films on the order of 100 Å thickness are required to be uniform in composition and thickness and free from localized defects.

It is necessary to carry out all stages of sample preparation and measurement without breaking vacuum. This requires means for producing the various films and making the various measurements with the sample *in situ*. In addition to measurement of sample transport properties, electron diffraction studies[37] must be made to determine film order.

The original choice of materials to be used was a device made of Au-MgO-Au thin films deposited on a cleaved single crystal substrate. The reason for this choice is that Au and MgO are quite similar in crystal structure and size, and the fact that Savoye and Anderson[12] had discovered preferential emission of electrons through holes in a gold overlayer. MgO was a good insulator because a considerable amount of information has been

obtained on MgO, particularly in these labs,[38] and the properties of MgO are thus quite well known.

B. Preliminary Studies

The major problem of concern is whether vacuum deposited MgO films are free from pinholes and breakdown. This problem was thought to be solved by a few preliminary investigations of MgO films rf sputter deposited on two types of substrates. The first attempt was a series of MgO films sputtered onto an unpolished nickel substrate. The resistance of the film was measured using a Triplett multimeter with a fine wire attached to one lead. The fine wire was moved around on the film to check uniformity and to discover any pinholes which might be present. These films were found to have many pinholes but had a high resistance in places free from pinholes. The next series of tests were run on MgO films sputtered onto a thin film of gold which was deposited on a clean microscope glass slide. These films were relatively free from pinholes and also had a high resistance as determined with an ohmmeter. It was assumed from the results of these studies that sputter deposited MgO would make a good insulator for metal-insulator-metal diode devices.

## 1. Initial Vacuum System

In order to fabricate and study the ordered metal-insulator-metal diode devices without breaking vacuum a number of items must be incorporated into the vacuuum system. These include an electron diffraction system, a means to electrically measure the devices, and means of depositing the underlayer, insulator, and overlayer into a given pattern. The first attempt at a vacuum system which would incorporate all these systems is shown in Fig. 1. The LEED apparatus had been incorporated into the top half of the bell jar. The LEED apparatus was shielded from the sputtering chamber by a stainless steel disk 5" in diameter with a 2" hole in the center. In this hole was a rotating substrate holder which was turned by means of a chain drive. On each side of the substrate holder was a cleaved single crystal MgO substrate. When the substrate was facing down the Au and MgO layers could be deposited; when it was facing up it could be studied with the LEED apparatus. The substrate had leads attached to it for the purpose of heating, temperature monitoring, and measurement of the diode characteristics. The insulating substrate holder carried these leads which had to be easily detachable. A pressure contact system was built for this purpose. It consisted of 13 stainless

steel washers which rotated on tungsten ribbons imbedded in another insulator.

The sputtering half of the bell jar included Kovar feedthroughs for use as rf sputtering electrodes. One electrode was shielded by a ceramic MgO disk. The other electrode had a Kovar disk attached to it which held a high purity MgO ceramic disk, used as the sputtering target. The metal layers for these devices were to be formed by dc sputtering of a high purity gold disk. The gold disk was mounted on an insulating disk which could be rotated so that the sputtering of gold was to be done directly above the MgO disk, as can be seen in Fig. 1. When MgO was to be sputtered the gold was rotated out of the plasma area. Initially the gold was to be sputtered using a triode configuration with a nickelate cathode[39] as the electron source. However, difficulty was encountered in providing sufficient filament power for conversion of the cathode. Thus, a tungsten filament was used.

The resulting diode was to have the geometrical configuration shown in Fig. 2b. This design could be accomplished by means of a single mask which consisted of two stainless steel plates as shown in Fig. 2a. These plates were attached to a threaded stainless steel rod by means of square nuts. One half of the rod had left-hand threads,

while the other half had right hand threads, so that both plates moved in and out from the substrate center at the same time and speed. This threaded rod was to be rotated by means of a chain drive. The method to be used in producing a diode configuration shown in Fig. 2b was as follows. When sputtering was to be initiated the edges A of the sheets would just overlap so that no deposit could be made while the target was sputter cleaned. The sheets were then to be separated so that edges A were 0.1" apart and a gold film deposited. The sheets were then to be moved in so that they overlapped while the MgO target was sputter cleaned. Then the sheets were to be moved out so that edges A were 0.2" apart and MgO deposited so that it completely covered the Au underlayer. The sheets were then moved so that edges B would just overlap and the Au overlayer deposited crosswise over the MgO layer producing the desired Au-MgO-Au diode device.

A bell-jar collar was used between the baseplate and the bell jar in order to allow an adequate number of electrical feedthroughs into the vacuum. The completed system had three moving parts; the substrate holder, the mask, and the gold target. Many components were mounted partially on the baseplate and partially on the collar. The result of this configuration was that any changes

that were necessary were extremely difficult to make as a consequence of the many moving parts and the close spacing involved in a 5" I.D. bell jar.

The initial pumpdown of this system was made and a number of baseplate feedthroughs were found to leak in the $10^{-1}$ Torr range. Rather than remount the components on a new baseplate, a new vacuum system configuration was used, still employing a 5" I.D. bell jar.

The vacuum system also included a Ti getter[40] to aid in pumpdown and to obtain a lower ultimate pressure; two sputter ion pumps,[41] one was a diode pump and the other a triode pump;[42] two gas admission systems, one to admit Ar gas for sputtering, this system included a cataphoresis tube[43] for cleaning the Ar gas, and one to admit $O_2$ gas for reactive sputtering in case the MgO films contained excess magnesium.

2. Second Vacuum System

The second vacuum system developed for these studies is shown in Fig. 3. The upper half of this system also contained the LEED apparatus. The electrical leads for the LEED apparatus, which are not shown, were run through an insulator attached to the stainless steel shield and attached to electrical feedthroughs in the bell-jar baseplate and collar which is described below. Removal of the

LEED apparatus was necessary in order to replace the substrates, which were otherwise inaccessible. Therefore, the LEED system was also mounted on this shield which in turn was easily demountable.

The bell-jar collar consisted of a stainless steel cylinder 0.1" thick with large flanges on top and bottom for attachement to bell jar and bell-jar baseplate respectively. Six smaller flanges were welded to the side of the cylinder. The collar was necessary in order to mount a magnetic feedthrough to rotate the substrate holder in a vertical plane. Additional electrical feedthroughs were needed so a five lead press and a six lead press mounted on flanges were attached to the collar. There was also a Pyrex glass window to enable visual indexing of the substrates behind the substrate masks.

The substrates were single crystals of MgO and were held on the rotating substrate holder by small tabs. The substrate holder had room for three substrates and a blank which was to face the target during sputter cleaning of the target. Inside the cylindrical substrate holder four small stationary heater filaments were mounted. The substrates were to be heated during deposition of Au and MgO in order to increase the probability of epitaxial growth of the film. The substrate could also be heated

during LEED investigations in order to minimize the charging of the dielectric substrate. A stationary insulator containing electrical contacts to electrical feedthroughs on the collar were also mounted inside the rotating substrate holder. The electrical contacts to the diodes were thus able to make pressure contact to the stationary leads when the substrate was in position in the LEED chamber.

Mounted on each side of the substrate holder were dc sputtering assemblies with Au targets directly in line with the substrates and 1.3" away. The MgO target was mounted on a Kovar rf feedthrough directly below the substrate and 1" away. A substrate mask was mounted between the substrate and each target resulting in a Au-MgO-Au diode as in Fig. 2.

Although this system had only one moving part, the substrate holder, the close spacing in the 5" I.D. bell jar resulted in some unsolvable problems. The main problem was the heat radiated by the filament used for dc support of the plasma. The heat caused cracking of the quartz crystal,[44,45] used to determine deposition rates, before any rates could be determined. In addition the heat opened up leaks in the baseplate feedthroughs when the filament was on, the leaks sealed when the filament was cooled but would open again when the filament was

again heated. The filament was then placed inside a heat shield with five metal layers separated by approximately 0.1". This did not help. It was decided that the close spacing involved in a 5" I.D. bell jar could not be tolerated. Rather than build a larger vacuum system a new approach was attempted.

The vacuum system included the same pumping and gas admission systems as included in the initial vacuum system.

3. Six Port Vacuum System

The six port vacuum system consisted of the standard bell-jar baseplate and collar with a special top shown in Fig. 4. The six holes on the 2.674 DIA.B.C. had bellows welded into them to move six different substrates, mounted on rods, from port to port and into each port for that particular part of the experiment. The system with push rods is shown schematically in Fig. 5. In this system six separate, related experiments could be carried out in the six different ports labeled A-F in Fig. 5, with the intention of fabricating and testing in situ ordered layer metal-oxide-metal diode devices. The six ports will be described in detail below. Port A was used to deposit the metal overlayer and port B to deposit the metal underlayer. Port C was used to rf sputter deposit the insulating layer. Port D contained the LEED system

used to determine the order of the film growth. Port E was the measurements port and port F was used to sputter clean the substrate. This vacuum system included the same pumping and gas admission system as the two previous systems with the exception that it contained two diode pumps as well as one triode pump.

The part of the system within the bell-jar collar contained the six substrates mounted on six different push rods labeled I-VI in Fig. 5. These push rods had holes drilled through them every 1/4 in. so that they could be pushed out into a particular port with a pick attached to a bellows and subsequently removed from this port. Each push rod ran through a guide rigidly attached to a rotating ring. Rotational motion could be achieved by pushing on the side of two of the push rods with the same picks used for linear motion. In this manner any given substrate attached to a push rod could be rotated and aligned with any given port.

The geometry that allowed six push rods and thus six substrates was that which had two push rods I and II in Fig. 5, that could move into ports 180° apart, above the others and aligned in a horizontal plane. Push rods III and IV were just beneath I and II, and V and VI were beneath these. Figure 5 also shows push rod VI pushed

out into port D, the LEED system. The size of the collar limited the system to six substrates.

A complete experiment on a single substrate was to be accomplished by the following succession of events. The substrate was to be inserted into port F and sputter cleaned, it was then to be moved to port D and the surface was to be examined with LEED. The substrate would then be moved to port B and a metal underlayer sputter deposited and the film order then studied with LEED. The substrate was then to be moved to port C and an insulating layer rf sputter deposited and the film order again studied with LEED. The substrate would then be moved to port A and a metal overlayer sputter deposited onto it with a study of film order again made. Finally the substrate was to be moved to port E and measurements made on the completed device. The following is a short description of each tube.

a. Metal Overlayer Tube

The purpose of this tube was to deposit the metal overlayer, which was always gold. The inside of the tube contained a filament, two anode rings, and a virtual cathode to produce a dc supported plasma. The plasma was confined to a beam with this geometry and the aid of an external magnet producing a field parallel to the filament-anode-virtual cathode center line. The gold target was

mounted in such a position that it was just on the edge of the plasma and in the same plane as the center of the substrate mask. The mask was mounted outside the plasma area and directly opposite the Au target, 3" from it. The mask allowed deposition of a 0.1" wide vertical strip of metal as the overlayer.

A filament enclosed in a Ta heat shield was mounted on the mask for the purpose of heating the substrate while deposition was taking place, in order to increase the probability of epitaxial growth. The filament was a 0.020" diameter advance wire wound into a spiral which then encircled the substrate mask. The heating of the substrate was found to be quite uniform with this geometry. Using this filament the substrate could be heated to a temperature of 500°C with a filament power of 50 watts.

The sputter deposition rates for this tube were very uniform from run to run at a given target current and voltage regardless of the other parameters. The deposition rate vs. target current curve was very close to the straight line predicted by Bell and Anderson[46] assuming a hemispherical distribution of sputtered atoms.

### b. Metal Underlayer Tube

This tube was designed exactly the same as the metal overlayer tube with the exception of the mask.

This mask allowed deposition of a 0.1" wide horizontal strip of metal for the underlayer film.

The sputter deposition rates for this tube were nearly exactly the same as for the overlayer tube.

c. MgO Insulator Tube

This tube employed rf sputtering to deposit the insulating layer of the devices. The major difficulties encountered in the six port vacuum system occurred in this tube. These difficulties and changes in tube design will be explained in section II-B-3-g.

d. LEED Tube

The LEED tube was used to determine whether the films grown were single crystal, polycrystalline, or amorphous. The unit consisted of a 2 1/2" diameter display chamber and a three element electron gun as shown in Fig. 6. Except for the gun, the main metal parts were #304 stainless steel.

The screen of the display chamber was a Pyrex hemisphere coated on the inner surface with conducting tin oxide over which was a thin layer of phosphor. Electrical connection was made between the conductive coating and the mounting plate via spring-loaded tungsten point contacts.

Inside the display screen and concentric to it were two hemispherical grids (2 3/32" and 1 7/8" in diameter) which were fabricated by chrome plating a tungsten mesh.[47] The flat end of the smaller grid was closed to prevent penetration of external fields into the display chamber.

The only LEED pattern ever observed in this tube was of the substrate, single crystal MgO, after sputter cleaning. This pattern was observed at a pressure of $10^{-3}$ Torr of Ar gas. No problems were encountered while the pressure was so high. The fact that the surface could be studied at so high a pressure made the experiment possible since the background pressure of the system was never below $10^{-8}$ Torr and the pumpdown time from $10^{-3}$ Torr to this level was about 6 hours.

e. Measurements Tube

This tube contained a Supramica 500* disk with four spring contacts attached to it for electrical contact to the underlayer and overlayer films. The I-V characteristics of the device could then be measured without removing it from the vacuum.

---

*Supramica 500 is the trade name of the Mycalex Corporation of America for their synthetic mica.

The end of the tube was made of a quartz window for which the light transmission versus photon energy had been measured. The center of the Supramica had a hole in it so that the light would be incident on the diode itself. The purpose of this arrangement was to measure the potential barrier presented to the electrons by the insulator.[26,27] The arrangement also allowed for photoemission measurements to be made, since a grid was present for collection of photoemitted electrons.

A swinging phosphor screen was also present so that the emission density patterns from the device as well as the total emission could be measured. This screen could be swung into a position in front of the diode while these measurements were to be made and then swung out of the line of sight to the diode when the photomeasurements were made.

f. Sputter Cleaning Tube

The purpose of this tube was to clean the substrate surface by $Ar^+$ ion bombardment. The design of the tube was identical to the overlayer and underlayer tubes except that no target was present. The plasma was a dc supported plasma with an rf potential applied between the substrate and the filament. RF sputter cleaning of the substrate was believed to be necessary in order to obtain an

atomically clean substrate surface, since Au will not grow epitaxially on a dirty MgO substrate.[48]

g. Methods Used in the Fabrication of Sputtered Metal-MgO-Au Devices

The six port vacuum system had many problems. The size of the system prevented pressures below $5 \times 10^{-9}$ Torr with the small ion pumps. This pressure could be attained only after a substantial bake at 250°C. Movement of the bellows after a bake always led to a leak in one or more of the bellows. Without a bake the ultimate pressure was $5 \times 10^{-8}$ Torr. The bellows would last for two or three pumpdowns before a leak would open up in one, if the system was not baked. Each time a bellows was replaced the shutdown time of the vacuum system was one week.

The first attempts to produce a sandwich device were done with Ag on an MgO substrate. Silver was used in the hope that silver might grow epitaxially on MgO somewhat easier than gold does. In every attempt at device fabrication the underlayer and overlayer presented no difficulty and the deposition of an MgO insulating layer was never achieved.

The first tube to be used to rf sputter deposit MgO consisted of two Kovar rf feedthroughs at right

angles to each other with no line of sight between the two MgO targets. One MgO target directly faced the substrate. This tube geometry was discarded after attempting to determine sputter deposition rates as a function of the rf potential between the two rf feedthroughs. The rates were extremely low and the films were very non-stoichiometric with an excess of Mg. This was determined by the brown-dusty film deposited on the glass walls of the tube.

The next tube used to deposit MgO was designed the same as the metal overlayer and underlayer tubes. The plasma was a dc supported plasma with the rf potential placed between the MgO target and the filament. The metal parts of the tube sputtered quite rapidly so the tube was redesigned to keep all metal parts of the tube out of the line of sight to the substrate. The first conclusive evidence of MgO dissociating into Mg and O was found with this tube. When the filament was on for a dc supported plasma the filament would burn out quite rapidly. If the plasma was an rf supported plasma with no hot filament in the tube all the metal parts in the tube became oxidized.

Deposition rates were determined using a quartz crystal monitor in this tube. Rates as high as

45 Å/min. were determined. The films again appeared to be non-stoichiometric, but not as bad as with the previous tube, so device fabrication was attempted using this tube. The first three devices were all shorts between underlayer and overlayer. After the substrates were removed from the vacuum system it was discovered that the metal mask had sputtered onto the substrate. When a positive potential was applied to the mask with respect to the filament, which was rf ground, no improvement was noted.

The same tube was used for the next six devices. The changes that were made were to replace the metal mask by an MgO mask and the plasma was an rf plasma with the rf applied between two MgO targets. In each case the underlayer was sputtered from the substrate in a circle corresponding to the hole in the MgO mask. The part of the silver underlayer that remained was definitely oxidized. It was thus decided to return to a gold underlayer since it does not have a stable oxide.

The next three devices attempted using this tube were also unsuccessful. No mask was used and in each case the underlayer was completely removed from the substrate.

A new rf sputter deposition tube was designed patterned after the Varian Plasma Peak[49] sputtering unit. Sputter deposition rates as high as 10 Å/min. were determined using this tube. The quartz crystal was removed and the MgO film studied using a microprobe.[50] The microprobe used* did not have the capability of detecting oxygen but the films were non-conducting and contained Mg. No other metals could be detected. The films, however, did appear to be Mg rich.

When the quartz cyrstal was removed and the next series of device fabrication attempts were made the metal underlayer was again removed from the substrate. Evidently the field configuration inside the tube was greatly changed when the insulating substrate replaced the metal quartz crystal holder and sputtering of the surface again occurred.

A final attempt was made to use this tube with a metal mask. The approach was to attempt to have the same electrode geometry present as when the quartz crystal was in the tube. This meant that the substrate had to be in contact with the mask. As a consequence of the

---

*The microprobe used was operated by Dr. Paul Weiblen, Geology Department, University of Minnesota.

many alignment problems present in this vacuum system the close spacing of substrate to mask could not be achieved and the mask again sputtered onto the substrate.

The next approach to the problem was to attempt a dc glow discharge in an oxygen atmosphere to reactively sputter Mg. A glow discharge could not be maintained at a pressure below $3 \times 10^{-2}$ Torr. At this pressure the Mg sputtered quite rapidly producing MgO films but the deposition rate was so low that it could not be measured. This was a consequence of the short mean free path at a pressure of $3 \times 10^{-2}$ Torr. The target to substrate spacing was approximately 10 cm. and the mean free path at this pressure is approximately 0.15 cm, resulting in many collisions occurring before the molecules could reach the substrate. A thick deposit of MgO was noted on the glass tube to a distance of about 1 cm from the target but no deposit could be detected beyond this point.

It was decided that a large bell jar type vacuum system would be necessary to fabricate and study ordered metal-insulator-metal tunnel devices <u>in situ</u>. A Varian ultra high vacuum system was obtained. This system is described below.

## C. Experimental Vacuum System and Techniques Used in Final Approach

### 1. Description of Vacuum System

The vacuum system used in the final approach was constructed by Varian Vacuum Division and was custom built for the University of Minnesota.

The base chamber is the standard Varian base chamber for vacuum system V1-221 and includes a 110 liter/sec. noble ion pump, Varian number 912-7006. The base chamber also contains 10 feedthrough ports and titanium sublimation cartridge number 916-0017 to aid in pumpdown and also to attain a lower base pressure. The outside diameter of the base chamber is 12".

The work area of the vacuum system is a stainless steel bell jar, 12" O.D. and 12" high. The system has 8 flanges mounted on it with centers 4 1/2" from the top and one flange on the top of the system concentric with the system. A schematic diagram of the bell jar work area is shown in Fig. 7. Two ports are 6" I.D. One of these ports admits the LEED system and the other port is a window, Varian number 954-5129, to view the LEED pattern and for visual alignment of the substrates with the various ports. Two of the ports are 4" I.D. and 90° from each 6" port. One of the ports

admits the manipulator, Varian number 954-5031, on which five substrates are mounted. The manipulator has rotational motion, lateral motion in two axes and linear motion in one, and it tilts in any direction. Thus, each substrate can be placed in a variety of positions within the work chamber. The other 4" I.D. port holds the sputter cleaning apparatus. The four 1 1/2" I.D. flanges are located 45° from a 6" I.D. flange and a 4" I.D. flange. Two of these ports contain filaments, one to heat the substrate during deposition and one to heat the completed device during measurements. One of these ports holds a Pt-Pt10%Rh thermocouple to monitor substrate temperature during deposition. The final 1 1/2" I.D. port contains a UHV gauge, Varian number 971-5008. This gauge is a Bayard-Alpert[51] type ion gauge which will measure pressures from $10^{-4}$ Torr down to $2 \times 10^{-11}$ Torr. The flange port on the top of the system contains the measurements apparatus.

A Varian number 971-5009 MilliTorr gauge is mounted on one of the ten ports on the base chamber. This gauge measures pressures from 1 Torr to $10^{-5}$ Torr and is thus an effective gauge to use for pumpdown of the system as well as for measuring the pressure of gas admitted for

sputtering. Connected to another one of these ports is an Ar and/or $O_2$ admission system as on the previous vacuum systems.

A stainless steel plate 1/4" thick x 10.8" in diameter separates the base chamber from the bell jar. This plate is used as a shield to prevent sputtered and evaporated material from depositing on the measuring apparatus in the bell jar. A mask, shown in Fig. 8a is mounted on the center of this shield. Deposition of materials through this mask onto a substrate will result in a metal-oxide-metal device shown in Fig. 8b. As can be seen from this figure each substrate contains three devices. Since there are five substrates present, 15 devices can be fabricated in one pumpdown.

A shutter is mounted on a linear motion feedthrough, Varian number 954-5049, which in turn is mounted on one of the 10 ports on the base chamber. The shutter prevents deposition of material onto the substrate until the source is clean and is releasing material at the chosen rate.

## 2. Description of Experimental Apparatus and Preliminary Results

The first attempts to deposit films were by sputtering. The sputtering apparatus was similar to

that previously described except that the discharge support system consisted of a filament and an anode at opposite sides of the base chamber. The targets, gold, aluminum, and MgO, were near the center of the base chamber and shielded from each other. Although high discharge currents were drawn, 4 amps, the target currents were always small. This was a consequence of the diffuse plasma which seemed to fill the entire base chamber. As a consequence of the large gap, 12" O.D., permanent magnets did not afford much assistance in increasing the sputtering rate. The sputter deposition rates were all very low. The rf sputtering was attempted with a dc supported plasma and with a straight rf plasma. In either case the deposition rates were extremely low and all metal parts, including the base chamber, were also sputtered. Sputtering was therefore determined to be an unsatisfactory deposition method.

Since some success had been attained in producing metal-oxide-metal devices by evaporation of the oxide,[52] an electron beam evaporator was mounted on the base chamber and the sputtering apparatus was removed. The electron beam evaporator is a 2 kw e-gun evaporation source with three crucibles, Varian number 920-0003.

The underlayer, insulator, and overlayer can be deposited using this source and the underlayer and overlayer can be of different materials.

The LEED apparatus is similar to that used in the 6 port vacuum system with the exception that it is larger, the hemispherical collector is 4" in diameter and there are four grids. The electron gun is the same type as used in the 6 port system except that it is made from stainless steel.

The sputter cleaning apparatus is a tantalum can with a hole on one end, 0.6" x 0.9", and a filament and anode within the can. This apparatus is similar to that used by Weber[53] except that it is somewhat larger. The principle of this system is that a plasma is supported within the can and ions drawn through the focusing hole to a target which is at a negative potential with respect to the anode. This type of apparatus is necessary to sputter clean the substrate since rf sputtering of the substrate cannot be done. The apparatus was placed in another vacuum system and tested on a $Ta_2O_5$ film grown on Ta by aqueous anodization of a Ta sheet to determine the uniformity of the sputtered area. The cleaned area was uniform to within about 5 Å after about 200 Å of $Ta_2O_5$ had been removed.

Since the substrates are insulators and will charge up when bombarded by ions, sputter cleaning of an insulator was tried next. In order to prevent charging of the insulator a filament was placed between the sputtering can and a substrate with a 1000 Å thick silver film and a 200 Å thick gold film on it. Within 30 minutes the 200 Å thick Au film was completely removed and within 2 hours most of the 1000 Å thick silver film was removed. From these results it was decided that this method for sputter cleaning of the substrate surface would be satisfactory.

The measurements system consists of a supramica disk on which are mounted 8 pressure contacts to make electrical contact to the underlayer film and the three overlayer films. A planar grid is mounted on the supramica on the side opposite the pressure contacts. The supramica is 1/8" thick and so the sample to grid spacing is about 0.2". Immediately beyond the grid is an anode, which has a hole 0.055" in diameter and beyond this is a Faraday cage[54] with a hole 0.055" in diameter. The two holes are aligned with the center of the center device of the three devices. This device can thus be studied with edge effects being avoided, while the other two devices on a substrate must include the edge effects.

The deposition rates for the electron beam evaporator were determined. The deposition rate for gold varied from 23 Å/min. at 1.4 kw to 800 Å/min. at 2 kw of beam power while for MgO it varied from 4 Å/min. at 40 watts to 90 Å/min. at 120 watts.

### 3. Sample Preparation

For these studies, diode samples consisting of a common Au underlayer film and a common oxide film were formed, and three Au overlayer films were deposited to produce three active units.

#### a. Glass Substrates

The substrates were cut from microscope slide glass, 1" x 0.6". They were then mounted in the substrate holder and the entire assembly was cleaned thoroughly by ultrasonic agitation in Freon TWD, a detergent solution, and rinsed thoroughly with tap water and finally, methanol. After drying, the assembly was placed in another ultrasonic agitator and first boiled in Freon and then ultrasonically agitated in Freon. The assembly was then immediately placed in the UHV system. The vacuum system was then evacuated and baked to 150°C which brought the pressure to a typical value of $6 \times 10^{-11}$ Torr. The substrates were then heated to a temperature of 400°C by means of a W filament to further

clean the surface. With the shutter in position to prevent deposition on the substrates, each source was thoroughly outgassed. The vacuum was again allowed to reach its base pressure, $6 \times 10^{-11}$ Torr, before sample fabrication was begun. During deposition of the metal layers the pressure rose to $10^{-9}$ Torr and to $10^{-8}$ Torr during deposition of the oxide layer. The entire fabrication process took less than 30 minutes.

b. MgO Substrates

As stated in section II-B-3-f, gold will not grow epitaxially on a dirty MgO substrate. Since the MgO single crystal could not be cleaved in vacuum, other methods to obtain a clean surface were attempted. The MgO substrates were cleaned in the same manner as the glass substrates and then cleaved immediately prior to insertion into the vacuum system. The cleaving was done on a laminar flow bench to minimize the collection of dust on the surface. Some substrates were sputter cleaned in vacuum, some were heated to 500°C before deposition began, and some were immediately deposited onto after baking of the system.

c. $CaF_2$ Substrates

The single crystal $CaF_2$ substrates were cleaned in the same manner as the MgO substrates with the

exception that they were not cleaved. A proper cleavage plane could not be achieved with the $CaF_2$ substrates. Some $CaF_2$ substrates were not cleaned before insertion into the vacuum system.

4. Millisecond-Pulse Measurement of I-V Characteristics

The $I_s$-$V_s$ characteristics of the thin film samples were measured using a millisecond pulse technique developed by Savoye[55] to minimize sample breakdown effects during measurement and to enable extension to the high current densities necessary to measure the emission into vacuum. The circuit permitted pulse measurements using a four-terminal method, and is shown schematically in Fig. 9. A voltage ramp of the desired time duration was generated by the time-base plug-in unit of oscilloscope I. (Both oscilloscopes employed in these measurements were Tektronix 536 X-Y, with appropriate plug-in units on X and Y channels.) This signal, amplitude modulated by the operational amplifier, Philbrick P45AL inserted in a model MP solid state manifold, used with a gain of 2, was applied to the sample under test. A signal proportional to the instantaneous current ($I_s$) through the sample was obtained across the resistor $R_s$ and applied to one channel

of a dual-channel plug-in unit on the vertical amplifier of oscilloscope II. The instantaneous voltage ($V_s$) across the sample, given by the difference in voltage between points A and B, was determined by a differential amplifier on the vertical input of oscilloscope I. The resulting difference voltage was applied to the horizontal amplifier of oscilloscope II. This arrangement allowed the display of $V_s$ versus time on oscilloscope I while the measurement was in progress, and hence provided a valuable check on the measurement.

A signal proportional to the emission current ($I_e$) was obtained across the resistor $R_e$ and applied through a low-level pre-amp to the second channel of the dual-channel amplifier on the vertical side of oscilloscope II. The resulting display on oscilloscope II thus consisted of a simultaneous plot of $I_s$ vs. $V_s$ and $I_e$ vs. $V_s$, on a single-pulse basis. Scope unblanking was accomplished by modulation of the gate signal generated by the time-base unit.

A direct tracing of a photograph of some typical I-V characteristics obtained from a thin-film emission diode using this pulse technique is shown in Fig. 10, where the various curves are labeled on the figure. During each pulse, the two signals, $I_e$ and $I_s$, were

displayed alternately by means of a multivibrator chopper, internal to the dual-channel plug-in unit of scope II, which switched the CRT beam from $I_s$ to $I_e$ at the rate of 100 kHz.

The results of a measurement are shown in the photograph. In the measurement two pulses were applied to the sample, the first pulse was used to display the entire $I_e$ and $I_s$ vs. $V_s$ characteristics and the second pulse to present the expanded-scale characteristics. As is seen from the photograph, the I-V characteristics obtained are nonlinear. The region of more rapid current change was displayed on an expanded voltage scale with a suppressed zero by means of the Tektronix type Z plug-in unit on the horizontal channel of oscilloscope II. This Z-unit allows display of the difference between a desired signal and an internally-generated, highly accurate, variable dc voltage. The input circuits have a large dynamic range so that saturation effects do not occur, thus allowing display of small variations in large signals on the most sensitivie scales. As an example, in Fig. 10 the I-V characteristics are shown expanded by a factor of 10 on the horizontal scale. It is seen that good agreement is obtained between the "normal" and the "expanded" traces, and that much

more accurate readout of the expanded trace characteristic is possible.

Measurements obtained on a pulse basis have been extended to sample current densities as high as 0.2 amperes/$cm^2$, without causing breakdown. In comparison, similar samples measured on a slowly-varying dc basis were found to suffer breakdown at current levels of the order of $10^{-2}$ amps/$cm^2$. Evidently the breakdown process in these devices is not a simple function of current density or applied field, but depends also upon the length of time that the bias is applied. This observation suggests that processes similar to those which have been designated Impulse-Thermal Breakdown[56] are of importance in these devices.

### 5. Pulse Techniques Applied to Emission Measurements

Measurements of hot electron emission into vacuum were made using the millisecond pulse technique previously discussed. No noticeable emission differences were noted with the samples in the position aligned with the hole in the Faraday cage and those not aligned with this hole. Thereafter the grid, anode, and Faraday cage were all biased at 22.5 volts with respect to the underlayer film.

Measurements were carried out starting at the lowest emission current levels commensurate with the sensitivity of the apparatus ($\sim 10^{-10}$ amperes). Data were taken at successively higher current levels, to the maximum output of the operational amplifier ($\sim 10^{-2}$ amps), and then repeated for successively lower current levels to the lower limit. In this manner irreversible changes occurring in the sample during a measurement sequence could be detected, and a check on the reproducibility of the data was provided.

### 6. DC Measurements of I-V Characteristics

A study of the current-voltage characteristics of thin film metal-oxide-metal diodes reveals considerable information concerning the nature of the oxide. As well as the current flow mechanism, temperature effects, rectification effects, and time-dependent changes can be investigated.

Measurements were made using a 4-terminal connection to the sample *in situ*. In each case the slowly varying dc bias was applied to the devices after the pulse measurements had been completed. The I-V characteristics of the samples did not change. A schematic of the circuit is shown in Fig. 11. The bias was applied using batteries and a motor driven potentiometer and the current was

monitored by measuring the voltage developed across a series sampling resistor with a Keithley 602 electrometer voltmeter whose output was recorded on the Y channel of a Hewlett Packard Mosley 135M X-Y recorder. The applied voltage was measured with a Keithley 603 electrometer amplifier with the output applied to the X channel of the recorder for low level voltages, less than 1 volt. For the higher voltages the applied bias was monitored directly by the X channel of the X-Y recorder.

The current-voltage characteristics were measured on a dc basis as well as on a pulse basis in order to monitor the I-V characteristics to lower levels than could be obtained on a pulse basis as well as for easier read-out of the characteristics.

Easier read-out of data was necessary in order to plot the data obtained as a function of the temperature of the device. A filament was placed in the vacuum system at a location 10" from the device in the measurements position. The filament current was varied and the temperature of the device was allowed to come to equilibrium. The temperature was monitored by a Pt-Pt10%Rh thermocouple which was located beneath the pressure contact to the center overlayer.

# III. RESULTS OF EXPERIMENTAL STUDIES OF HOT ELECTRON TRANSPORT IN THIN-FILM EMISSION DIODES

## A. Introduction

As stated in section I, the electron process of importance in these devices is in some doubt. A number of investigators[12,13,57-59] have discussed the situation when the transport mechanism appears to be a combination of thermal and field effects. There appears to be a range of barrier heights in which the thermal effects dominate the mechanism, small barriers, a range in which both effects are seen, and a range, large barriers, in which the field effects overshadow the thermal effects. The I-V characteristics of the device must be measured to determine which mechanism is of importance. If the I-V characteristics are measured as a function of the temperature of the device a better understanding of the mechanism involved can be achieved. The emission into vacuum of hot electrons from the diodes lends an insight into the scattering mechanism taking place in the oxide.

The experimental techniques which have been developed for these studies were discussed in some detail in previous sections. These investigations have involved

fabrication and testing of 60 thin film sample sets. The MgO film thicknesses ranged from 60 Å to 680 Å.

B. High Level I-V Characteristics of Thin Film Emission Diodes

The I-V characteristics of the thin film samples were measured using the millisecond-pulse technique discussed in section II-C-4 and also by the slowly varying dc technique discussed in section II-C-6. The level of measurements was restricted to avoid damage to the samples. In the simple band theory of solids, neglecting image forces, the barrier $\varphi_R$ is given by $\varphi_m - \chi_I$, where $\varphi_m$ is the work function of the metal and $\chi_I$ is the electron affinity of the insulator. If $\varphi_R$ is a low value, $\lesssim$ 1 eV, the Schottky mechanism will dominate and no tunnel electrons will be seen. At the higher barrier heights the electrons will not have enough thermal energy to surmount the barrier and tunnel current will be the dominant mechanism. Nelson[26] measured the barrier for Al-$Al_2O_3$-Al devices and found that it was 2.2 eV with no applied bias. For the same type of device, Savoye[12] found that field effects were dominant and that thermal effects were also present, but insignificant. It was believed that a Au-MgO-Au device would exhibit strictly field effects because the

simple barrier picture indicated that a barrier of 4.65 eV would be present at room temperature. This value was obtained from the work of Holscher,[79] $\varphi_{Au} = 5.45$ and Kemp and Neeley,[60] $\chi = 0.8$ eV. If the I-V characteristic was strictly tunnelling, the Fowler-Nordheim equation as applied to solids would indicate the dependence of current on voltage. This equation can be written in the form:

$$J = J_o(F/F_o)^2 e^{-(F_o/F)}$$

where $J_o$ and $F_o$ are parameters of the insulator. Assuming the free electron mass,

$$J_o = 7.2 \times 10^9 \varphi_o^2 A/cm^2 \qquad F_o = 6.8 \times 10^7 \varphi_o^{3/2} V/cm,$$

where $\varphi_o$ is the potential barrier height in electron volts presented by the oxide modified by the image forces. For $\varphi_o = 4.65$ eV,

$$J_o = 1.36 \times 10^{11} A/cm^2 \qquad F_o = 6.16 \times 10^8 V/cm,$$

then:

$$J = 1.36 \times 10^{11} (F/6.16 \times 10^8)^2 e^{-(\frac{6.16 \times 10^8}{F})} A/cm^2$$

if F is the field present in the insulator. Since the area of each device is $6.45 \times 10^{-2}$ $cm^2$,

$$I = 8.77 \times 10^9 (F/6.16 \times 10^8)^2 e^{-(\frac{6.16 \times 10^8}{F})} \text{ amps.}$$

For an insulating film 89 Å thick the device characteristic should look like that shown in Fig. 12, where the currents are labeled in amps per division. Two features

of these characteristics are immediately noticeable, the high voltage necessary before any measurable current can be drawn and the extremely high slope of the curves.

The first evaporated Au-MgO-Au device that was measured in any great detail was PY-G-11(1). This device had an 89 Å thick oxide layer and its I-V characteristic is shown in Fig. 13. In contrast to the theoretical tunnel curves, current is drawn at very low voltages and the slope of the curves is much less than those in Fig. 12. However, the curves are definitely nonlinear.

The Fowler-Nordheim equation can be written as:

$$I = aJ_o(V/sF_o)^2 e^{-F_o s/V}$$

or

$$I/V^2 = aJ_o(1/sF_o)^2 e^{-F_o s/V}$$

where a is the device area and s is the oxide thickness. If one takes the logarithm of each side the expression becomes:

$$\ln(I/V^2) = \ln\left[aJ_o(1/sF_o)^2\right] - F_o s/V$$

so that a plot of $\ln(I/V^2)$ vs. $1/V$ should yield a straight line. The I-V characteristics of device PY-G-11(1) is shown plotted on this Fowler-Nordheim plot in

Fig. 14. It can be seen that the Fowler-Nordheim expression does not hold for this device.

The Richardson-Schottky equation which may be applied to a metal-oxide-metal device, as explained by the simple band theory, is given by van der Ziel:[61]

$$J = AT^2 \, e^{-\varphi_R/kT} \, e^{bV^{1/2}}$$

where

$$b = (q^3/4\pi\epsilon_r\epsilon_o s)^{1/2}(kT)^{-1}$$

In these expressions:

A = Richardson's constant, 120 $A/cm^2$ $°K^2$

q = charge of the electron

$\epsilon_r$ = relative dielectric constant of the oxide

$\epsilon_o$ = permittivity of free space

k = Boltzmann's constant

T = temperature in °K.

This expression can also be written as:

$$\ln I = \ln \beta + b \, V^{1/2}$$

so that a plot of ln I vs. $V^{1/2}$ should yield a straight line, if the Schottky mechanism is the dominant mechanism. Such a plot of the I-V characteristics of device PY-G-11(1) is shown in Fig. 15. As can be seen from this figure the Schottky mechanism explains the characteristics quite well.

At this point, however, one must be careful not to assume Schottky emission just because the plot of log I vs. $V^{1/2}$ is a straight line. As pointed out by Hartman,[62] the Pool-Frenkel effect has a similar I-V characteristic. This equation is written as:

$$J = G_o V e^{(2bV^{1/2} - \psi/kT)}$$

where $G_o$ is a constant with the dimensions of a conductivity, $\psi$ is the energy difference between the trap level and the bottom of the conduction band, and all other symbols have already been defined. As can be seen this mechanism would also plot as a straight line on a log I vs. $V^{1/2}$ plot. Furthermore, a bulk-limited conduction mechanism discussed by Mead[63] also plots as a straight line on this type of plot. O'Dwyer[64] has recently machine calculated the voltage-current characteristics for films of a few hundred to a few thousand angstroms thickness with the help of a dielectric model originally proposed by Frolich.[65] His result is also a straight line on a ln I vs. $V^{1/2}$ plot. Jonscher[15] points out that the bulk limitation as proposed above probably does not arise for very thin dielectrics, 150 Å or less, but probably holds for the thicker films.

A number of checks can be made to determine if the Schottky mechanism is involved or if one of the other mechanisms is present. Hartman[62] noted that the dielectric constant, as determined by the slope of the log I vs. $V^{1/2}$ plots, was too high for SiO films if the Schottky or Pool-Frenkel mechanism is the dominant mechanism. He also noted that the zero field intercept of this curve varied as a function of the dielectric thickness, with the intercept becoming higher for thicker films. This should not happen for the Schottky or Pool-Frenkel mechanisms. This intercept gave a much different barrier height than the slope of the $\ln I_o$ vs. $\frac{1}{T}$ plots, and it should be the same for the Schottky mechanism.

If one assumes the Schottky mechanism to be the controlling mechanism for these devices, the slope of the curve in Fig. 15 is b, which can be written as:

$$b = \gamma\, \epsilon_r^{-1/2}\, s^{-1/2}\, T^{-1} .$$

Assuming the low frequency dielectric constant of MgO, which is 9.8,[4] and an oxide thickness of 80 Å, the slope gives a temperature of 330°K. The actual device temperature during measurement was 313°K, as measured by the Pt-Pt10%Rh thermocouple. A calculation of the temperature change of the device, during measurement,

was made. The heat equation for this problem was solved by Savoye[55] and he arrives at the expression:

$$\Delta T = \frac{2}{K}\sqrt{\frac{k}{\pi}}\, J_s\, V_s \sqrt{t}$$

where

$$k = \frac{K}{c\delta} = 3.92 \times 10^{-3}\ \frac{cm^2}{sec} \text{ for glass}$$

K = thermal conductivity = $8.0 \times 10^{-3}$ watts/cm°K

t = pulse length in seconds.

Using these values the expression becomes:

$$\Delta T = 8.9\, J_s\, V_s \sqrt{t}$$

and for a 10 millisecond pulse, with $J_s = 0.126\ A/cm^2$, $V_s = 2.9$ volts,

$$\Delta T = 0.325°K\ .$$

It can be seen that the device did not heat up much during pulse measurements. If the temperature is thus assumed to be 313°K, the relative dielectric constant of the oxide is calculated to be 10.9, which is fairly close to the assumed value of 9.8. Alternatively if the relative dielectric constant is 9.8 and the temperature is 313°K the oxide thickness must be 89 Å instead of the calculated 80 Å. This variation is well within the bounds of the experimental error involved in a deposition rate calibration of evaporated material. Since there is no a priori reason for assuming the high frequency dielectric constant for the Schottky mechanism,

as there is in the Pool-Frenkel[14] or Fowler-Nordheim[12] mechanisms, the Schottky mechanism cannot be ruled out. However, if one assumes the Pool-Frenkel mechanism, the plot of $\ln(I/V)$ vs. $V^{1/2}$ should be straight line with a slope of 2b. Such a plot of the I-V characteristics of device PY-G-11(1) is shown in Fig. 16. Although it is not a straight line over the entire plot, a straight line is drawn on the figure. Assuming an oxide thickness of 89 Å, the slope of this line gives a dielectric constant of $\epsilon_r = 3.17$, which is in good agreement with the high frequency dielectric constant of MgO, which is 2.95[4]. Therefore the Pool-Frenkel mechanism cannot be ruled out on this basis either. However, the curved line on Fig. 16, which is in extremely good agreement with the data points, is a plot of the Schottky equation. It thus appears that the Pool-Frenkel mechanism does not hold.

Devices were studied with oxide thicknesses in the range of 69 Å to 680 Å. In all cases, in which no oxygen gas was admitted during the deposition of the MgO film, the I-V characteristics plotted as a straight line on a $\ln I$ vs. $V^{1/2}$ plot and similar to the curve in Fig. 14 a $\ln \frac{I}{V^2}$ vs. $\frac{1}{V}$ plot and also similar to Fig. 16 for a $\ln \frac{I}{V}$ vs. $V^{1/2}$ plot. Figure 17 presents a summary of

data obtained from the thin samples studied in detail in which the MgO layer was deposited with no oxygen gas admitted during deposition. As can be seen from this curve there is essentially no change in the zero field intercept as a function of oxide thickness, another indication that the current flow mechanism is not bulk dominated.

From the Richardson-Schottky equation with zero field:

$$I_o = aAT^2 e^{-\varphi_R/kT}$$

where a is the area of the device. It can be seen from this expression that $\varphi_R$ can be obtained;

$$\varphi_R = kT \ln \frac{aAT^2}{I_o} .$$

The barriers obtained in this manner are given in Table I. It can be seen that the barriers are in remarkably good agreement. This determination of the barrier height may not be accurate because of the questionable value of the Richardson constant. However, as Hartman[62] pointed out, a change in this constant by an order of magnitude would only change the barrier determined in this manner by about 10%.

Figure 18 shows the Schottky plot of the devices with the thicker (680 Å) insulating films. Although the intercept is not the same, as a consequence of

Table I

BARRIERS FOR DIFFERENT DEVICES AS OBTAINED FROM THE ZERO FIELD INTERCEPT OF THE SCHOTTKY PLOT

| DEVICE NO. | S(Å) | $\phi_R$ (eV) |
|---|---|---|
| PY-G-19(2) | 79 | 0.710 |
| PY-G-11(1) | 89 | 0.714 |
| PY-G-18(2) | 109 | 0.700 |
| PY-G-17(1) | 159 | 0.721 |
| PY-G-20(1) | 680 | 0.695 |
| PY-G-20(3) | 680 | 0.695 |

measuring these devices at a lower temperature the barriers obtained in this manner are nearly the same. The difference in current at a given voltage, and consequently the different intercepts, is caused by a slight difference in device area. The overlayers for these two devices were deposited through a different mask than for the other devices. These barriers are much lower than that predicted by the simple model, so other measurements were necessary in order to determine what the conduction mechanism is. These measurements are described in the following sections but a number of other features of the I-V characteristics became evident during the measurements on these devices.

The forward, overlayer positive, and reverse, overlayer negative, characteristics of each of these devices were identical. This indicates that the barrier is symmetrical, which is not the case for devices fabricated by oxidation of the underlayer metal film. Rectification effects have been seen[27,66] for devices with identical metal electrodes which indicated a non-symmetrical barrier, probably due to an oxide gradient in the oxidized film.

Another feature that was noted was that the I-V characteristics, as measured by the slowly varying dc technique, were the same with the voltage decreasing as with the voltage increasing. Other authors[27,29,59,67] have seen a hysteresis effect, where the retrace differed from the original trace. If the current on the retrace is higher, at the same voltage, than on the original trace, it is probably due to Joule heating. However, to change the current by a noticeable amount the current must be left at the maximum value for about one minute. In the present experiment the voltage was always lowered after less than 30 seconds for measurements to the upper limits and heating was negligible. If the current

on the retrace is lower, at the same voltage, than on the original trace, it is due to the filling of traps[68,69] while the voltage is applied. This in turn increases the effective barrier at the underlayer-oxide interface. As the voltage is decreased, the finite lifetime associated with the trapping sites causes the effective barrier to remain higher and thus the current is lower for the same applied voltage. These traps arise from impurities introduced into the oxide film during oxidation. The impurities are not present in the evaporated MgO films. The results also cast doubt on the Pool-Frenkel and other trap limited mechanisms.

The I-V characteristics of the devices indicate that three problems involved in the oxidized underlayer type device have been removed. These problems were; the oxide must be that of the metal underlayer, the oxide gradient present in oxidized films, and the impurities introduced as a result of oxidizing the underlayer.

## C. Temperature Measurements of the I-V Characteristics of Thin Film Emission Diodes

The I-V characteristics of the devices indicate that the Schottky mechanism is probably the dominant mechanism in the transport of electrons through the oxide film. Since this mechanism is very temperature dependent and the tunnelling mechanism has very little temperature dependence it was decided to measure the I-V characteristics of the devices as a function of temperature. The method for this measurement is described in section II-C-6.

The I-V characteristics of device PY-G-11(1), as a function of temperature, are shown in Fig. 19. It can be seen that there is a large dependence of the I-V characteristics on temperature with a change of less than 100°K giving rise to an increase of current, at a given voltage, of an order of magnitude. This effect is also seen if some of the other mechanisms proposed are present. However, if a plot of the zero field intercepts, of the ln I vs. $V^{1/2}$ plots, is made on a $\ln(I_o/T^2)$ vs. 1/T plot, the slope of this plot should again give $\varphi_R$, as can be seen below:

$$I_o = aAT^2 e^{-\varphi_R/kT}$$

$$I_o/T^2 = aAe^{-\varphi_R/kT}$$

$$\ln(I_o/T^2) = \ln aA - \varphi_R/kT$$

If this slope gives $\varphi_R$ as the same value as $\varphi_R$ obtained from the zero field intercept calculations the mechanism of importance is the Schottky mechanism. A ln I vs. $V^{1/2}$ plot for different temperatures for device PY-G-11(1) is shown in Fig. 20. The intercepts, $I_o$, are plotted on a $\ln(I_o/T^2)$ vs. $10^3/T$ in Fig. 21. The barrier height, $\varphi_R$, obtained in this manner is 0.33 eV as compared to 0.71 eV by the zero field intercept method. This result casts some doubt on the Schottky mechanism. Table II shows the comparison of the barrier heights obtained using the two methods for the devices listed in Table I.

Table II

BARRIER HEIGHTS FOR DIFFERENT DEVICES AS OBTAINED BY THE ZERO FIELD INTERCEPT AND THE SLOPE OF THE $\ln(I_o/T^2)$ vs. 1/T PLOT

| DEVICE NO. | S (A) | $\varphi_R$ (eV) (Zero Field) | $\varphi_R$ (eV) (Slope) |
|---|---|---|---|
| PY-G-19(2) | 79 | .71 | .33 |
| PY-G-11(1) | 89 | .71 | .33 |
| PY-G-18(2) | 109 | .70 | .35 |
| PY-G-17(1) | 159 | .72 | .33 |

As can be seen from this table the results are quite consistent and cannot be explained by a simple Schottky mechanism.

D. Measurements Made on Devices Fabricated with Oxygen Gas Present During Deposition of the Oxide Film

The results on the above devices indicated that the oxide films were not pure MgO. The MgO probably dissociates to some degree during evaporation and probably does not re-combine at the substrate surface to give a stoichiometric film. The result is a film with an excess of magnesium atoms. It was decided to attempt to grow a more stoichiometric film by admitting oxygen gas during the deposition of the MgO film.

Since the pressure in the vacuum system is on the order of $10^{-8}$ Torr during deposition of the MgO films the first attempt to produce stoichiometric films was done with oxygen gas admitted to the system to a pressure of $1 \times 10^{-8}$ Torr, and this device, PY-G-22(2), was measured. Oxygen gas was admitted to a pressure of $10^{-7}$ Torr during fabrication of the next device, PY-G-25(3). A summary of these two devices and one fabricated with no oxygen admitted is shown in Fig. 22. It will be noted that although the I-V characteristics

still plot as a straight line on a ln I vs. $V^{1/2}$ plot, the zero field interecepts are no longer the same. The zero field interecept values of $\varphi_R$ are .780 eV for device PY-G-22(2) fabricated with $10^{-8}$ Torr of oxygen gas and 0.823 eV for device PY-G-25(3) fabricated with $10^{-7}$ Torr of oxygen. It is evident from these curves that something is changing in the MgO film when deposition of the MgO is done with oxygen present in the system.

The plots of $\ln(I_o/T^2)$ vs. $10^3/T$ for these two devices and PY-G-11(1) are shown in Fig. 23. It will be noted that the slopes of the plots decrease with increasing amounts of oxygen present during the MgO deposition. This would indicate a lower barrier, if the mechanism was strictly a Schottky mechanism, for increasing amounts of oxygen, while the zero field intercept indicated a higher barrier. The barriers measured in this manner give $\varphi_R$ of 0.21 eV for PY-G-22(2) and 0.11 eV for PY-G-25(3).

A number of devices were fabricated with the deposition of MgO done in an atmosphere of $10^{-6}$ Torr of oxygen. None of these devices could be measured. These devices either broke down before any current was drawn or they were initially shorts. The devices with MgO thicknesses greater than about 70 Å always

broke down when about 12 volts were applied and those with thinner oxides were all initially shorts. It is believed that the devices with thicknesses less than about 70 Å were shorted due to pinholes.

A number of devices were fabricated in which the MgO was deposited with $10^{-5}$ Torr of oxygen gas present for a short time and then the film was completed after the oxygen had been pumped from the system. The first device fabricated in this manner showed definite rectification effects with higher currents drawn for the overlayer negative than for the overlayer positive, as expected. This device had an MgO film that was 120 Å thick with oxygen present during deposition of the first 30 Å. The oxide layer was again too thick because the device broke down before any appreciable current could be drawn. All subsequent devices fabricated in this manner were either initially shorted or they were also unstable and broke down before any quantitative measurements could be made.

One device, however, was stable long enough for some measurements to be made. The I-V characteristics of this device, PY-G-38(1), are shown in Fig. 24. The curves are labeled in amps per division and + signifies that the overlayer is positive. It can be seen that

the device broke down at about 17.6 volts. The interesting features of these characteristics are the difference in current for the two biases, the characteristics are ohmic to about 6.5 volts, and the sharp rise in current beyond this bias. Figure 25 is a plot of these characteristics on a Fowler-Nordheim plot, $\ln(I_c/V^2)$ vs. $1/V$, where $I_c$ is the actual current minus the ohmic current. As can be seen from these curves the I-V characteristics of this device can be explained quite satisfactorily by the Fowler-Nordheim tunnel equation. The barrier, $\varphi_o$, can be obtained from the slopes of these curves. They are: 1.9 eV for the overlayer positive and 1.74 eV for the overlayer negative. The fact that the barrier is higher for the overlayer positive is expected since the more stoichiometric part of the oxide film is near the underlayer. These results are consistent with the hypothesis that the MgO films are magnesium rich and that admitting oxygen gas during deposition of the MgO film increases the stoichiometry as seen by an increased barrier height. The other devices plotted in this manner still plotted as in Fig. 14.

## E. Low Level I-V Characteristics of Thin Film Emission Devices

It was noted during the study of the I-V characteristics of these devices that at low fields, $\simeq 10^4$ V/cm, the I-V characteristics were ohmic. It was decided to study the I-V characteristics at these low levels in order to get a better understanding of the conduction mechanism.

The first device measured in this manner *in situ* was device PY-G-21(3). The I-V characteristics were linear up to a field of $\gtrsim 10^4$ V/cm and the resistance of the device was $1.3 \times 10^5$ Ω at a temperature of 312°K. The resistance was measured as a function of temperature and is plotted vs. $10^3/T$ in Fig. 26. A similar plot for devices PY-G-22(2), $10^{-8}$ Torr oxygen, and PY-G-25(3), $10^{-7}$ Torr oxygen, are also shown on this figure. Two features of the device resistance are noticeable in this figure. One of these features is that the resistance increases as the amount of oxygen gas increases during MgO deposition, even though the oxide thicknesses are not all the same. PY-G-21(3) and PY-G-22(2) both have an MgO layer of about 90 Å thickness and PY-G-25(3) has an oxide thickness of about 60 Å. The other feature is that the temperature dependence of the resistance is not linear on a plot of this type.

## F. Measurements of Electron Emission into Vacuum from Thin Film Diodes

The present experiment was designed to permit simultaneous measurements of the I-V characteristics of the device and the emission into vacuum from the device. Data was obtained using the millisecond-pulse technique discussed in section II-C-5. Although the experiment was designed to permit measurements on a given emission diode over a range of overlayer film thicknesses, this was never accomplished. After measurements were made on a given device and more gold was deposited to increase the overlayer thickness the devices were always shorted. Consequently the measurements were made on each device with only one overlayer thickness. The overlayer thickness for each device was calculated from the resistivity of the film. The resistance per square of a thin metallic film is typically higher than that predicted by the bulk resistivity.[32] The resistance of a given metal film also depends on the substrate. Thus, although this method is not an accurate method for determining the exact thickness, the ratio of thicknesses can be accurately determined. All films were deposited to a calibrated thickness of 200 Å, except where noted,

see section II-C-2. The thickness of the overlayer for device PY-G-11(1) will be assumed to be 200 Å and the rest of the overlayer thicknesses calculated with respect to this overlayer. The calculations will be based on the assumption that $S_o = K R_s^{-1/2}$, where $R_s$ is the sheet resistance in Ω/square, $S_o$ is the overlayer film thickness, and K is a constant. This emperical relationship has been observed by a number of workers.[20,32,55] The sheet resistance of device PY-G-11(1) is 1.5 Ω/square and a thickness of 200 Å for this value is not unreasonable (see reference 55, Fig. 8) since it lies between the value calculated from the bulk resistivity and Savoye's results for gold on $Al_2O_3$. Table III lists the devices previously

Table III

OVERLAYER THICKNESSES FOR MEASURED DEVICES

| DEVICE NO. | $R_s$ (Ω/square) | $S_o$ (A) |
|---|---|---|
| PY-G-11(1) | 1.50 | 200 |
| PY-G-17(1) | 1.60 | 194 |
| PY-G-18(2) | 1.22 | 222 |
| PY-G-19(2) | 3.39 | 133* |
| PY-G-22(2) | 1.38 | 209 |
| PY-G-25(3) | 1.50 | 200 |

*Deposited to a thickness of 150 Å.

discussed with their sheet resistance and calculated overlayer thicknesses.

The overlayer film thicknesses are of importance because attenuation of the hot electrons occurs in the overlayer film as well as in the oxide film.[12,20,70] The emission transfer ratio, $\alpha$, for device PY-G-11(1) is plotted vs. sample voltage, $V_s$, in Fig. 27. The immediate feature that is seen is that the emission transfer ratio, $\alpha$, decreases with increasing $V_s$, in contrast to the results seen by other investigators.[12,71] Savoye,[12] for example, was able to explain the increase of $\alpha$ with increasing $V_s$ on strong inelastic electron-phonon interactions. His results indicated a mean-free-path of about 7 Å with an energy loss of 0.1 eV per interaction. In this case only a fraction of the electrons would arrive at the overlayer metal with sufficient energy to escape over the vacuum work function barrier. This fraction would be expected to increase with increasing $V_s$ and, depending upon the details of the electron energy distribution, could in principle increase sufficiently rapidly with sample bias to give rise to a net increase in $\alpha$ with $V_s$. However, if these interactions did not occur, or if the interactions were elastic, one would expect that $\alpha$ would decrease with increasing

$V_s$, since injection into the overlayer would then occur at higher energies and the mean-free-path for hot electrons in the metal overlayer is expected to decrease for increasing electron energy.[72,73,74] This effect is seen here experimentally.

Figure 28 is a comparison of emission results for the devices previously discussed in which no oxygen was admitted during the deposition of MgO. Figure 29 is a comparison of emission results for devices fabricated with different amounts of oxygen present during the MgO deposition. The results for device PY-G-11(1) are also plotted on this figure for comparison purposes since it has the oxide thickness closest to that of device PY-G-22(2).

From the data presented in these figures the following observations can be made:

1) The magnitude of the emission transfer ratio, $\alpha$, is seen to decrease with increasing $V_s$ for each MgO thickness regardless of the amount of oxygen gas present during deposition of the MgO.

2) The general shape of the log $\alpha$ vs. $V_s$ curves is similar for all devices except at the low voltage levels where the measurements are not as accurate. Strangely, the main effect of increasing the MgO

thickness is to increase the transfer ratio at a given voltage.

3) The effect of increasing the oxygen pressure during MgO deposition is also to increase the transfer ratio at a given voltage.

G. Attempts to Fabricate a Device with a Single Crystal Oxide

As stated in section I an attempt was to be made to grow an epitaxial device, at least a device with a single crystal MgO film. A number of attempts were made on different substrates but in no case was a single crystal device achieved.

The devices fabricated on the MgO substrates appeared to have highly disoriented layers. These results were true regardless of the method of substrate preparation. Each device was a short circuit between underlayer and overlayer. Ten sample sets, thirty devices, were fabricated with no success.

The devices fabricated on the $CaF_2$ substrates appeared to be slightly more ordered than on the MgO substrates. The MgO film for two of these devices exhibited a ring pattern when studied with LEED. Each device was a short circuit between underlayer and

overlayer. Five sample sets, fifteen devices, were fabricated with no success.

The devices fabricated on the single crystal substrates were done with the substrate temperature at 400°C during deposition of the various layers. The deposition rates were then varied to attempt to achieve epitaxy.

Since a perfect cleavage plane was not achieved with any of these substrates the surfaces were never nearly atomically smooth. The devices had MgO films of about 100 Å thickness, about 15 molecule layers, so it can be seen that the substrate must be very smooth in order to achieve a device with no pinholes.

Another problem that is involved is that during epitaxial growth of a thin film, the film must nucleate[36] so that single crystal growth can occur. This nucleation leads to pinholes in the film until the film has reached a certain thickness. Since these devices must have thin oxide layers it appears that epitaxial growth and non-shorted devices are two competing mechanisms.

Epitaxial growth may be inhibited by the fact that the MgO films are non-stoichiometric with an excess of Mg atoms. In order to achieve stoichiometry and still

have a measurable device the MgO layer must be on the order of 40 Å thick. Thus again, epitaxy and a measurable device are incompatible. The conclusion arrived at is that the epitaxial growth of a measurable device with a stoichiometric film of MgO between two metals may not be impossible, but is surely extremely difficult. Time did not permit the pursuit of this topic any further.

Table IV is a summary of the results of all devices studied extensively.

Table IV

SUMMARY OF DEVICE DATA

| DEVICE NO. | S | $S_o$ | $\varphi_1$ | $\varphi_2$ | R | $P_{O_2}$ |
|---|---|---|---|---|---|---|
| PY-G-11(1) | 89 | 200 | .714 | .33 | - | - |
| PY-G-16(3) | 106 | - | .741 | - | - | - |
| PY-G-17(1) | 159 | 194 | .721 | .33 | - | - |
| PY-G-18(1) | 106 | - | .694 | .34 | - | - |
| PY-G-18(2) | 109 | 222 | .700 | .35 | - | - |
| PY-G-19(2) | 79 | 133 | .710 | .33 | - | - |
| PY-G-20(1) | 680 | - | .695 | - | - | - |
| PY-G-20(3) | 680 | - | .695 | - | - | - |
| PY-G-21(3) | 90 | - | .732 | .34 | $1.3\times10^5$ | - |
| PY-G-22(2) | 90 | 209 | .780 | .21 | $4.25\times10^5$ | $10^{-8}$ |
| PY-G-25(3) | 60 | 200 | .823 | .11 | $7.4\times10^5$ | $10^{-7}$ |
| PY-G-38(1) | 90 | - | 1.9,1.74 | - | $4.35\times10^5$ | $10^{-5}$,- |

In this table:

S = oxide thickness, in Å

$S_o$ = overlayer thickness, in Å

$\varphi_1$ = barrier obtained by zero field intercept method, in eV

$\varphi_2$ = barrier obtained by slope of Arrhenius plot, in eV

R = resistance of device for ohmic part of characteristic, in Ω, at about room temperature

$P_{O_2}$ = pressure of $O_2$ gas admitted during MgO deposition, in Torr

# IV. ANALYSIS OF HOT ELECTRON TRANSPORT PROCESSES IN VACUUM DEPOSITED THIN-FILM EMISSION DIODES

## A. Introduction

The transport of hot electrons in thin film emission diodes can be viewed as involving three stages, which are in principle separable: 1) a process by means of which electrons are injected into the thin oxide film, 2) transport through the oxide film, and 3) transmission of electrons through the overlayer metal film region, with emission into vacuum. A major difficulty in studies of such devices lies in the fact that these processes are not readily separable on an experimental basis.

In preceding sections of this thesis, a series of experiments was discussed which involved the study of the transport of hot electrons through these devices fabricated under a variety of conditions and the subsequent emission into vacuum of these electrons. These efforts were directed toward providing as complete an experimental description of the film properties and the transport processes as possible in order to determine the properties of vacuum deposited thin oxide films.

The present section first presents a brief summary of the important experimental observations of these studies. Analysis of the experimental results is separated into two stages: electron injection into the oxide film, and transmission of a fraction of the injected electrons into vacuum. The processes of importance at each stage are thus as nearly as possible subjected to analysis separately, and the results combined to formulate the complete model for the hot electron transport process in vacuum deposited thin-film emission diodes.

## B. Summary of Experimental Observations

These studies have involved investigations of Au-MgO-Au thin film emission diodes with the MgO film deposited with different amounts of oxygen gas present in the vacuum system and to different thicknesses. The properties of the MgO films changed as the amount of oxygen present in the vacuum system changed during deposition of the MgO film. This change was to higher biases necessary for the same sample current. These observations are consistent with an increase in barrier height with an increase in the amount of oxygen present. This might be expected if the films

are more stoichiometric with more oxygen present during deposition.

The thin film sample I-V characteristics were plotted on a ln I vs. $V^{1/2}$ plot for direct comparison between samples. The data for each sample plotted in this way were fit by straight lines, in qualitative agreement with the simple Richardson-Schottky or Pool-Frenkel equations. The data was plotted on a $\ln(I_o/T^2)$ vs. $1/T$ plot for each device. The data for each sample plotted in this manner were fit by straight lines. However, the data plotted in these two manners gave different barrier heights, if one assumes the Schottky equation, or different trap levels, if one assumes a Pool-Frenkel equation. Thus the data is inconsistent with either of these mechanisms applied in a simple manner to these devices. The data were also inconsistent with the simple Fowler-Nordheim equation adapted for internal field emission since it did not plot as a straight line on $\ln(I/V^2)$ vs. $1/V$ plot.

An emission current into vacuum was observed for all sample types, which was stable and reproducible and free from breakdown effects. The magnitude of the emission transfer ratio, $\alpha$, decreased with increasing sample voltage, $V_s$, and increased for thicker oxide films.

The indications are that the barrier presented to the flow of electrons by the oxide film increases with increasing amounts of oxygen present during the deposition of the MgO. Since no devices could be measured which were fabricated with an oxygen pressure of $10^{-6}$ Torr or greater present during MgO deposition, an attempt was made to produce a device with an oxide layer consisting of two regions with a different composition near either of the metal-oxide interfaces. Although the results indicated that these devices show rectification effects, since the barrier at either interface was different, no devices fabricated in this manner were stable over a large current range and no extensive quantitative results were obtained.

All devices fabricated on single crystal substrates were initially shorted and could not be repaired. The conclusion arrived at is that the epitaxial growth of a measurable device with a stoichiometric film of MgO between two metals may not be impossible, but is extremely improbable.

### C. Discussion of a Model for Injection of Electrons into the Oxide Film

Experimental results have been presented for the I-V characteristics of vacuum deposited thin film

emission diodes which are in agreement with an expression in which $I_s$ is directly proportional to $V_s$ at low fields and in which $\ln I_s$ is proportional to $V_s^{1/2}$ at high fields. However the results are not consistent with a field-controlled emission-limited Pool-Frenkel mechanism whereby electrons are emitted from a discrete trap level into the conduction band over the Coulomb potential barrier under the attendant lowering by the applied electric field. The origin of this equation was in connection with conduction processes in bulk insulators or semiconductors[14] in which the effects of the electron image force on the interface barrier are of less importance in conduction than for very thin films.

The results were also not consistent with the simple Richardson-Schottky equation used for emission into vacuum, modified for emission into the conduction band of the dielectric by multiplying $\epsilon_o$ by $\epsilon_r$. The origin of the Richardson-Schottky equation was in connection with thermionic emission of electrons into vacuum from metals of high work function in which the work function is lowered by the electric field because of image force modification of the metal - vacuum interfacial barrier. These results are not directly applicable to the case of internal electron emission from a metal into an oxide,

since a detailed analysis must consider the influence of the oxide dielectric constant in modifying the electron image force. Emtage and Tantraporn[5] and Pollack[6] obtained results which they attributed to a Schottky emission mechanism. The problem as applied to these devices needs some modification since the multiple image force corrections to the barrier must be made. This problem is solved in Appendix I. The result is:

$$I = aAT^2 e^{-\varphi_R/kT} e^{\frac{.148\ V}{kT}^{.484}}, \qquad (1)$$

for the equation that applies to Schottky type emission into the conduction band of the insulator for high fields. It can be seen that the current dependence on voltage is not exactly the same as for emission into vacuum from a thermionic cathode. However, the zero field intercept of the plot of ln I vs. $V^{.484}$ should still give the barrier height, $\varphi_R$. A plot of ln I vs. $V^{.484}$ for device PY-G-11(1) is shown in Fig. 32 for the various temperatures. As expected the device characteristics plotted as a straight line on this curve. The only difference between this plot and a plot of ln I vs. $V^{1/2}$ is that the zero field intercept is slightly lower for T = 313°K. The value of $\varphi_R$ obtained from the zero field intercept in Fig. 32 is .722 eV as compared

to .714 eV from the zero field intercept of the ln I vs. $V^{1/2}$ plot.

Figure 33 is a plot of $\ln(I_o/T^2)$ vs. $10^3/T$ for $I_o$ obtained from the ln I vs. $V^{.484}$ plots at different temperatures. It can be seen from this figure that the plot is not a "straight line" as it is in Fig. 21. The plot should be a straight line according to Eq. (1) if the barrier is independent of temperature. However, as stated in section III-B, the barrier was expected to be much higher than that measured in these devices. The barrier, however, could be lowered if impurities were introduced into the MgO film allowing energy states in the forbidden gap in the bulk material or at the surface. Since these devices were fabricated and studied in ultra-high-vacuum the probability of introducing foreign impurities into the device is slight. The impurity atoms must then be excess Mg giving rise to a localized energy level. Depending on the number of excess Mg atoms, or oxygen vacancies, and the location of this level in the energy band structure, the barrier could be temperature dependent. Thus the barrier picture as shown in Fig. 30 is complicated by the presence of donors. Calculations of the effective Debye length[80] shows that the square barrier, modified

by the electron image force, is the correct shape for this barrier. The emission data indicates that a height of $\varphi_R \approx .72$ eV is the correct height.

Since the dependence of the barrier height on applied voltage deviates from the ln I vs. $V^{.484}$ law for lower voltages, expression (1) does not hold for low voltages. This expression should thus be written as:

$$I = aAT^2 e^{-\varphi_R/kT} e^{f(V)/kT} \qquad (2)$$

where f(V) is a function of applied voltage and is plotted in Fig. 31. This expression shows that there should be a current at zero applied voltage. However no current is observed at zero applied voltage. Consider that the overlayer is biased positively. This expression then gives the value of the current from the overlayer to the underlayer, or the electron flow from the underlayer to the overlayer. However, at zero applied voltage there is an electron flow from underlayer to overlayer due to thermal agitation which allows electrons to flow over the barrier from underlayer to overlayer. However, since the barrier is symmetrical and the overlayer and underlayer are the same material, gold, at zero applied voltage the same number of electrons should have thermal energy to flow over the barrier from

overlayer to underlayer. In equilibrium this gives rise to equal and opposite currents, so that the measured current at V = 0 is I = 0. As the barrier is lowered for electron flow from underlayer to overlayer it is raised for electron flow from overlayer to underlayer. Thus the correct expression for current from a Schottky type mechanism is:

$$I = aAT^2 e^{-\varphi_R/kT} \left[ e^{f(V)/kT} - e^{g(V)/kT} \right], \qquad (3)$$

where,

$$g(V) = f(V) - eV \; . \qquad (4)$$

From this expression it can be seen that at V = 0

$$g(o) = f(o) \qquad (5)$$

and

$$I = 0 \; .$$

Figure 34 is a comparison between the data for device PY-G-21(3) and Eq. (3). The data points are circled and the solid line is Eq. (3). It can be seen from this figure that there is extremely good agreement between the data and Eq. (3) over 6 orders of magnitude of current and 5 orders of magnitude of voltage. Furthermore, Eq. (3) predicts a linear relationship between I and V for low voltages. The bracketed expression in Eq. (3) can be written as:

$$e^{f(V)}(1 - e^{-eV/kT}) \quad . \tag{6}$$

For fields $\lesssim 10^4$ V/cm, $f(V) \approx K$, thus (6) becomes:

$$e^{K/kT}(1 - e^{-eV/kT}), \tag{7}$$

where K is a constant and $\varphi_R - K = \varphi_o$, the actual barrier height. Expanding $e^{-eV/kT}$ in a Maclaurin's series the bracketed expression becomes:

$$1-\left[1 - \frac{eV}{kT} + \frac{1}{2}\left(\frac{eV}{kT}\right)^2 - \frac{1}{6}\left(\frac{eV}{kT}\right)^3 + \cdots\right] \quad . \tag{8}$$

For voltages on the order of $5 \times 10^{-3}$ volts, which is where the I-V characteristics of the this device, PY-G-21(3), start to deviate from linearity, $\frac{eV}{kT} = 0.186$ and $\frac{1}{2}\left(\frac{eV}{kT}\right)^2 = 0.017$. So it can be seen that below this value of voltage, (3) can be written as:

$$I_o \cong aAT^2 e^{-\varphi_o/kT}\left(\frac{eV}{kT}\right), \tag{9}$$

or,

$$V = IR, \tag{10}$$

where R is given by

$$R = \frac{kTe^{\varphi_o/kT}}{eaAT^2} \quad . \tag{11}$$

For this device at T = 312°K this resistance is $8 \times 10^4$ Ω while the measured resistance was $1.3 \times 10^5$ Ω, which is remarkably good agreement considering that the Richardson constant is involved in this expression.

The data for devices PY-G-17(1), 18(2), and 19(2), which were measured at high voltages only, are shown

in Fig. 35 where ln I is plotted vs. $V^{.484}$. As for device PY-G-11(1) the barriers calculated from the zero field intercept do not change substantially from those calculated from the zero field intercept of the ln I vs. $V^{1/2}$ plots. Figure 36 shows a comparison between the devices fabricated with varying amounts of oxygen present during deposition of the MgO on a ln I vs. $V^{.484}$ plot. The barriers obtained from these plots are given in Table V along with the barriers found for device PY-G-38(1) from the Fowler-Nordheim plots.

Table V

BARRIER HEIGHTS FOR A NUMBER OF DEVICES

WITH DIFFERENT PARAMETERS

| DEVICE NO. | S (Å) | $\varphi_R$ (eV) | $P_{O_2}$ (Torr) |
|---|---|---|---|
| PY-G-11(1) | 89 | .722 | $< 10^{-8}$ |
| PY-G-17(1) | 159 | .724 | $< 10^{-8}$ |
| PY-G-18(2) | 109 | .701 | $< 10^{-8}$ |
| PY-G-19(2) | 79 | .711 | $< 10^{-8}$ |
| PY-G-22(2) | 90 | .792 | $10^{-8}$ |
| PY-G-25(3) | 60 | .833 | $10^{-7}$ |
| PY-G-38(1) | 90 | 1.90, 1.74 | $10^{-5}$, $< 10^{-8}$ |

This table illustrates the fact that the barrier height does not change with oxide thickness but that the barrier height increases with increased oxygen pressure

present during deposition of the MgO film. Figure 37 is a plot of the data for devices PY-G-22(2), MgO deposited at $10^{-8}$ Torr $O_2$, and PY-G-25(3), MgO deposited at $10^{-7}$ Torr $O_2$, on log-log paper. The solid lines drawn on the curves are expression (3) with the appropriate values of $\varphi_R$ for these two devices. Again there is strikingly good agreement between the experimental points and the theoretical curves over six orders of magnitude of current. The values of resistance calculated and experimentally found were again in extremely good agreement. For device PY-G-22(2) the calculated value is $3.9 \times 10^5$ Ω while experimentally it was determined to be $4.3 \times 10^5$ Ω. For device PY-G-25(3) the numbers are $7.1 \times 10^5$ Ω and $7.5 \times 10^5$ Ω respectively.

The remarkably good agreement between Eq. (3) and the data indicates that the Schottky type mechanism, modified for these devices, is the dominant mechanism for injection of electrons into the oxide film. The data also indicate that the barrier presented to the flow of electrons by the oxide is much lower than that predicted by the simple band theory. If the barrier was $\varphi_M - \chi_I$, the barrier would be 4.65 eV regardless of the number of excess Mg atoms or oxygen vacancies. However the barrier is much lower than this and also

depends on the number of excess Mg atoms in a manner such that the barrier is lower for more excess Mg. The fact that the barrier seen is lower than that expected is not altoghether unreasonable. Other authors have seen this same effect[81,82,83] for metal-semiconductor interfaces. Mead[84] gives a semi-emperical analysis in which he characterizes the barrier as $\varphi_M - \chi_S$ for semiconductors of ionic character and independent of metal electrode for semiconductors of covalent bonding.

A brief resume of this analysis is given below, not as a statement to determine the barrier height but as a statement that it could be much lower than $\varphi_M - \chi_I$. Figure 38 is a reproduction of a figure in a classic paper on surface states by Shockley.[85] This figure shows the traditional splitting of atomic energy levels as the wave functions of the atoms overlap. In addition it shows the energy of the surface states as a function of lattice spacing. One fact is evident, that is that there are two distinct regions of surface state behavior. At large separations, the wave functions overlap only slightly and the surface states lie at the band edges. At small separations the wave functions overlap strongly and the surface states are near the center of the gap. This provides a valuable clue to

the behavior of different types of semiconductors with respect to surface states. In essentially ionic materials, the wave functions are atomic in nature and the overlap is small. Surface states are formed by the two types of atoms at the surface of the crystal and their energies lie close to the valence and conduction band edges. The upper surface states are unoccupied and the lower surface states are occupied. Thus the Fermi level at the surface may move from near the conduction band edge to near the valence band edge without creating any surface charge. This behavior is quite consistent with the oversimplified picture of the ionic crystal and it does explain the results for many materials. Until the wave function overlap reaches a critical value the surface states lie at the band edges. A small increase in overlap above this critical value causes the surface states to move rapidly to a region near the center of the forbidden gap.

The above analysis holds for intrinsic semiconductors and insulators. However when impurity atoms are added to the crystal the location of the Fermi level may change. If these atoms give rise to donor levels near the conduction band the Fermi level may be closer to the conduction band than the valence band. If the

impurities occupy interstitial positions in the lattice the wave function overlap would be greater than in the original material. A large density of donor like surface states near the conduction band could exist at the surface.

How do these surface states affect the barrier? The surface states are distributed in energy somewhere in the forbidden gap of the oxide, and when the free surface is charge neutral they are filled to some energy, $E_o$, below the conduction band. This will then locate the Fermi level at the surface. If an electric field is applied at the surface this field will induce charge in the oxide, primarily in the surface states if their density is large, and the Fermi level at the surface will shift from this value. However, the larger the number of surface states per unit energy interval, the smaller the movement of the Fermi level for a given induced charge. The same argument may be applied to the energies of a metal-oxide interface. In the limit of very high surface state density, the Fermi level at the surface is fixed by $E_o$, and the barrier energy is just the difference between the band edge and this Fermi level independent of the contact potential difference between metal and oxide.

Bardeen[87] discusses the behavior of the barrier as a function of surface state density. The conclusion arrived at is that for a high density of surface states the barrier height is nearly independent of the work function of the metal and is about the same as for a free surface. The height of the barrier is thus determined by the location of the surface states and their density.

There is some experimental evidence that excess Mg in MgO gives rise to a localized energy level near the bottom of the forbidden gap or possibly in the valence band.[88,89] These states are low lying donor states and when the crystal is irradiated with UV a current is carried by holes. The donor level in their samples is the ground state of an F center and when irradiated by UV the electron enters the excited state. An electron from the valence band can then be thermally excited into the ground state of the F center giving rise to a hole in the valence band. The current under these conditions is then carried by holes. Other results of Yamaka and Sawamoto[90] found that the current in MgO with an excess of Mg was carried by electrons. Their conclusion comes from the results of measurements of the thermo-electromotive

force at a temperature range of 650°C to 1000°C. These results indicated a donor level in the forbidden gap nearer the bottom of the conduction band.

It can be seen that there is some doubt as to the location of the donor levels in MgO with an excess of Mg. The explanation given by Olson[89] for a low lying donor level can be summarized as follows: The MgO crystal is heated in a magnesium vapor pressure. The excess magnesium thus arrives at the surface and reacts with the crystal. Rather than a diffusion of magnesium atoms into the crystal into interstitial positions this reaction causes diffusion of oxygen to the surface, creating an oxygen vacancy. This oxygen vacancy becomes the site of tightly bound electrons or a low lying donor level. Their analysis excluded Mg atoms in intersititial positions because the crystal cannot accommodate them.

An excess magnesium atom in an interstitial type position would probably give rise to a donor level nearer the conduction band. Since the films studied here are not single crystal films, the excess magnesium could very well occupy positions which are of an interstitial type. The experimental evidence indicated that this must be the case since the barrier is so low.

Thus, there must exist localized donor levels near the conduction band and donor like surface states also near the conduction band.

According to Fig. 33 the barrier height changes as a function of temperature. Figure 39 is a plot of $\ln(I_o/T^2)$ vs. $10^3/T$ for the two devices fabricated with $O_2$ gas present during the deposition of MgO. The results from device PY-G-11(1) are repeated here for comparison. It can be seen that none of these curves plot as straight lines. The zero field intercept of the ln I vs. $V^{.484}$ gives a value of $I_o$ as:

$$I_o = aAT^2 e^{-\varphi_R/kT} \tag{12}$$

Thus

$$I_o/T^2 = aAe^{-\varphi_R/kT} \tag{13}$$

or

$$\ln(I_o/T^2) = \ln aA - \varphi_R/kT \quad . \tag{14}$$

Therefore it can be seen that if $\varphi_R \neq \varphi_R(T)$ the slope of the $\ln(I_o/T^2)$ vs. 1/T plot should be a straight line:

$$d\ln(I_o/T^2)/d(1/T) = -\varphi_R/k \quad . \tag{15}$$

However if $\varphi_R$ is a function of temperature this becomes:

$$d\ln(I_o/T^2)/d(1/T) = -\varphi_R(T)/k - (1/kT)\, d\varphi_R(T)/d(1/T) \tag{16}$$

Thus the slope of these plots will not be proportional to the barrier height, which may explain the difference seen between the barriers found by the two methods in

section III-C since the barriers were found from the slope of the best straight line fit to the data for the $\ln(I_o/T^2)$ vs. $10^3/T$ plots. If $d\varphi_R(T)/dT$ is positive, i.e. if the barrier increases with increasing temperature, then $d\varphi_R(T)/d(1/T)$ is negative and the slope of the $\ln(I_o/T^2)$ vs. $1/T$ plots will give a number which is smaller than the actual barrier. The barrier heights obtained for these three devices from the ln I vs. $V^{.484}$ plots are plotted in Fig. 40 as a function of temperature. It can be seen from this figure that the barrier heights do increase with increasing temperature. Thus the slope of the Arrhenius plot will give a value for the barrier height which is actually less than the real barrier height, as seen in these experiments.

The barrier is the distance, in energy, between the location of the Fermi level and the bottom of the conduction band at the surface. In a bulk n-type semiconductor the Fermi level does move farther from the conduction band with increasing temperature. A similar process must exist for these devices. A discussion of this problem is given in Appendix II.

After oversimplification of the problem a qualitative result was obtained for the barrier height as a

function of temperature and donor concentration. The result is:

$$\varphi = kT\ln\left[(1/2)\left\{N_c/N_d+\left[(N_c/N_d)^2+8N_c e^{\psi/kT}/N_d\right]^{1/2}\right\}\right] \quad (17)$$

This simple calculation shows that the barrier increases for increasing temperature, increases for decreasing donor concentration, and increases faster for increasing temperature as the donor concentration decreases. These results are all consistent with the experimental results. This expression is plotted as the dashed curves in Fig. 40 and it can be seen that the agreement with the experimental results is fairly good on a qualitative basis.

The model developed here for the barrier height depends on the existence of surface states. As previously stated the barrier under these conditions should be nearly independent of the work function of the metal. Savoye[55] found a contact potential difference of $\varphi_{Au}-\varphi_{Al} = .8$ eV in his Al-$Al_2O_3$-Au samples. If the surface state model holds, the barrier should be nearly the same for current flow in either direction, if it does not hold the barrier will be modified by the contact potential difference between the metals. A number of Au-MgO-Al devices were fabricated. These devices were very unstable and usually broke down

before any extensive measurements could be made. One device, PY-A-1(1), was stable long enough to measure the I-V characteristics at T = 313°K. The results of this measurement are shown in Fig. 41 on a ln I vs. $V^{.484}$ plot. The barriers obtained from these plots are: for the Au-MgO interface, $\varphi_{RAu}$ = .702 eV, and for the Al-MgO interface, $\varphi_{RAl}$ = .643 eV. It can be seen that there is some difference between the two electrodes, $\varphi_{RAu}-\varphi_{RAl}$ = .059 eV, but this value is much smaller than the difference in work functions between gold and aluminum. This difference in barriers is about the same value as the difference noted by Mead[83] for different metals on CdSe. Thus the model incorporating surface states to lower the expected barrier is consistent with the observed results even though no quantitative results could be obtained.

We conclude that the current transfer process of importance in these thin film emission diodes is that of field-controlled emission-limited Schottky emission mechanism whereby electrons are emitted from the metal electrode into the conduction band of the insulating film over the image force interfacial barrier under the attendant lowering by the electric field. The simple Schottky equation does not hold but the equation

derived by taking into account the multiple image corrections to the barrier profile give excellent agreement with experimental results. The effective height of the energy barrier at the Au-MgO interface deduced from this analysis is about .7 eV. This value can only be explained if a large density of interface states exist. The barrier height is temperature dependent and also depends on the excess magnesium concentration. This model implies that a large density of surface states, which are all ionized, allows the barrier to be much smaller than initially expected and that the effect of increasing the temperature is to ionize more donors allowing more electrons to enter the conduction band of the MgO. This results in a higher barrier for higher temperatures.

In this model the electrons injected by the Schottky emission process appear in the conduction band of the insulating film, where they are accelerated by the strong electric field toward the positively biased electrode. The processes by means of which the injected electrons are transported through the insulating film are discussed in the next section.

## D. Discussion of Emission into Vacuum

The electron injection process in these thin film emission diodes has thus been characterized as a Schottky emission process. The subsequent transport of the injected electrons through the insulator under the influence of the strong electric field can be expected to involve some energy loss.

Figures 27, 28, and 29 show the emission transfer ratio, $\alpha = I_e/(I_e+I_s)$ as a function of sample bias. Two features of these plots are very striking. One is that the transfer ratio decreases with increasing sample bias and the other is that for only one device, PY-G-25(3), is the sample bias greater than 5.45 volts. Figure 44a shows the energy band diagram for these devices under an applied sample voltage of 4 volts, which is higher than most sample biases reached in these experiments. The straight line with the arrow shows the trajectory of an electron which loses no energy in traversing the oxide and metal overlayer. It can be seen that the electron should not be emitted into vacuum since it does not have enough energy to surmount the metal-vacuum interfacial potential barrier.

The anode-overlayer spacing is large enough so that Schottky emission should not occur from the metal

overlayer into vacuum. The resolution of the measurements was such that emission currents on the order of $10^{-10}$ amps could be measured. For current of $10^{-10}$ amps due to "thermionic" emission a sample bias of $\approx 4.45$ volts would be necessary. Therefore there should be no electrons emitted into vacuum until the sample bias is $\approx 4.45$ volts.

Savoye and Anderson[12] discuss the possibility of preferential emission of electrons through holes in the gold overlayer film. In order for electrons to be emitted from these Au-MgO-Au devices the electrons must be emitted through holes in the gold overlayer film. The energy band diagram appropriate to the fraction of electrons which arrive at the oxide-overlayer interface in the vicinity of a hole is shown in Fig. 44b for a 4 volt sample bias.

In the case of large holes, the field at the underlayer beneath the hole might be expected to decrease fairly rapidly with distance from the edge, and hence the current density would also decrease beneath a hole. In consequence only a fraction of the area of a particular hole would be expected to contribute appreciable emission current.

Electron micrographs of thin gold films deposited on cold substrates indicate that such films consist of a large number of agglomerates, separated by relatively narrow open regions resembling slots, which are characterized by a fairly well defined width.[93,94] We therefore assume that in the present case the holes in the Au overlayer films can be represented by slots of characteristic width d.

The width of the slots for a typical case is difficult to estimate from the electron micrographs, but is on the order of 20-200 Å for a film of about 100 Å thickness.[55] In the present experiments with MgO films varying from 60 Å to 160 Å thickness, the electric field strength at the underlayer beneath a slot might therefore be expected to decrease rapidly with distance from the slot edge. The electron current emitted into the oxide film beneath a slot can be estimated using a solution to the electrostatic problem for the field beneath a slot as a function of the distance from the slot edge.

A solution to the electrostatic problem simplified by neglecting the dielectric discontinuity at the surface has been obtained, and is presented in Appendix III. From this solution, numerical calculations for the

field strength, F(y), as a function of the distance, y, from one edge of the slot were carried out for the ratios of oxide thickness to slot width of interest, assuming all slots are 100 Å wide. Results of these calculations are presented in Fig. 45, where relative field strength, $F/F_o$, is plotted versus y. Notice that the ordinate scale is an expanded scale extending only from 75% to 100%.

The magnitude of $F/F_o$ is seen to decrease rapidly with distance and at a rate strongly dependent on the oxide thickness, as expected.

The relative electron current, $j_{rel}(y)$ resulting from the field F at y is:

$$j_{rel}(y) = \frac{j(y)}{j(-\infty)} = \frac{AT^2 e^{-\varphi_R/kT} e^{\beta[F(y)]^{1/2}}}{AT^2 e^{-\varphi_R/kT} e^{\beta F_o^{1/2}}}$$

$$= e^{\beta F_o^{1/2}\left[(F/F_o)^{1/2}-1\right]} . \qquad (19)$$

We have assumed the simplified form for the Schottky equation since it is nearly correct for the fields of interest. The constant $\beta$ has the value, $\beta = 4.5 \times 10^{-3}$ $(cm/volt)^{1/2}$, for T = 313°K, the temperature at which emission data was taken.

Let there be N such slots per unit area and of length $\ell$. If $\gamma$ is the ratio of overlayer hole area to total overlayer area

$$\gamma = N\ell d \ . \qquad (20)$$

An estimate to the current emitted into the oxide beneath a hole in the overlayer film can thus be made.

The sample current, $I_s$, can be viewed as consisting of two contributions; 1) a contribution from Schottky current density $j_s$ from regions of Au lying beneath the gold overlayer, and 2) a contribution from regions of Au lying beneath holes in the gold overlayer, which is written as $j_{rel}(y)j_s$. This second contribution will depend upon the position, y, under the slot of width d, with $0 \leq j_{rel}(y) \leq 1$. Assuming that $j_s$ is constant, and determined by the magnitude of the applied field at the Au underlayer beneath the Au overlayer, we write for the sample current:

$$I_s = j_s a(1-\gamma) + j_s N\ell a \int_o^d j_{rel}(y)\,dy - I_e \ , \qquad (21)$$

or

$$I_s = j_s a\left[(1-\gamma) + \gamma \frac{1}{d}\int_o^d j_{rel}(y)\,dy\right] - I_e \ , \qquad (22)$$

where a is the sample area and the integration is over a single slot of width d.

A similar expression can be written for the emission current, $I_e$:

$$I_e = j_s a\left[(1-\gamma)P_{oo}\alpha_t + \gamma\frac{1}{d}\int_o^d j_{rel}(y)P_{os}\alpha_H(y)\,dy\right], \quad (23)$$

where $\alpha_t$ is the attenuation factor for the Au film, $P_{oo}$ is the fraction of the electrons which arrive at the overlayer film energetically capable of emission, $P_{os}$ is the fraction of the electrons which arrive at a slot energetically capable of emission, and $\alpha_H(y)$ expresses the transfer ratio through a slot of width d, as a function of position y. For the biases, $V_s$, used in these experiments, $P_{oo} = 0$. Since the sample current beneath a slot is less than the sample current beneath the overlayer and $1-\gamma \approx 1$, $I_s$ and $I_e$ can be written as:

$$I_s = j_s a - I_e \quad (24)$$

$$I_e = j_s a\gamma\frac{1}{d}\int_o^d j_{rel}(y)P_{os}\alpha_H(y)\,dy\,. \quad (25)$$

On this model the measured transfer ratio $\alpha_M$ is:

$$\alpha_M = \frac{I_e}{I_e+I_s} = \gamma\frac{1}{d}\int_o^d j_{rel}(y)P_{os}\alpha_H(y)\,dy\,, \quad (26)$$

or

$$\alpha_M = \gamma\frac{1}{d}\int_o^d P_{os}\alpha_H(y)\,e^{\beta F_o^{1/2}\left\{\left[F(y)/F_o\right]^{1/2}-1\right\}}dy. \quad (27)$$

For an applied field of $F_o = 2.5 \times 10^6$ volts/cm (27) becomes

$$\alpha_M = \gamma\frac{1}{d}\int_o^d P_{os}\alpha_H(y)\,e^{7.1\left\{\left[F(y)/F_o\right]^{1/2}-1\right\}}dy\,. \quad (28)$$

If no energy loss occurred in the oxide all electrons arriving at a slot would be energetically capable of escape, for $F_o = 2.5 \times 10^6$ volts/cm, and a good approximation under these conditions would be $\alpha_H(y) = 1$ for $0 \leq y \leq d$. In this case,

$$\alpha_M = \gamma \frac{1}{d} \int_o^d e^{7.1\left\{\left[F(y)/F_o\right]^{1/2}-1\right\}} dy \quad . \qquad (29)$$

This expression for $\alpha_M$ can be integrated numerically for each oxide thickness of interest. This has been done and $\alpha_M$ is plotted vs. S, the oxide thickness, in Fig. 46. This shows that $\alpha$, on the basis of field alone, should go up for thicker oxides. Also shown on this figure are the actual emission ratios, for $F_o = 2.5 \times 10^6$ volts, divided by a suitable $\gamma$. The $\gamma$ used here is not the actual $\gamma$ since the emission transfer ratio drops off as a function of voltage. The $\gamma$ used was one in which the data would then fit the theoretical curve for s = 159 Å. It can be seen in this figure that the other data points fit the curve quite well.

An examination of Fig. 29 shows that an extension of the data to V = 0 leads to values of $\gamma$ on the order of $2 \times 10^{-3}$. This would put a lower bound on $\gamma$ of $2 \times 10^{-3}$. The reason for saying that this value is a lower bound on $\gamma$ is that the term $\alpha_H(y)$ in Eq. (23)

is not a constant of value 1.0 since the electrons arriving near the edge of a slot have a greater probability of being trapped than those arriving at the center of a slot with the same value of $v_x$. This is a consequence of the fringing field at the slot. This value for $\gamma$ is quite reasonable. A comparison with the results of Savoye (see reference 55, Fig. 40) shows that for an overlayer thickness of 200 Å, $\gamma$ has a value of $\approx 6 \times 10^{-3}$ for gold on $Al_2O_3$. As noted in section III-F of this thesis, the sheet resistance of a gold film on MgO is lower than for a gold film on $Al_2O_3$, indicating a more continuous film of gold on MgO, i.e., fewer pin-holes in the gold. This would lead to a smaller value of $\gamma$ for Au on MgO than for Au on $Al_2O_3$, as seen here.

Possible energy loss mechanisms in the MgO film include impurity scattering, impact ionization of valence electrons, and electron-phonon interactions.

Impact ionization of valence electrons can only occur if the energetic electron has kinetic energy $E \geq E_g$, where $E_g$ is the band-gap energy. Because there is a potential barrier of magnitude $\varphi_o$ between the overlayer Fermi level and the bottom of the oxide conduction band and the energy distribution of electrons

in the metal drops off quite rapidly above this level, the maximum kinetic energy available for $V_s$ volts applied is approximately $E_m = eV_s - \varphi_o$. From this the threshold voltage for impact ionization to be possible is $eV_s \geq E_g + \varphi_o$. The band-gap energy, $E_g$, of MgO is 8.7 eV and $\varphi_o \approx .7$ eV. These values show an estimate of the threshold voltage for impact ionization of about 9.4 volts. In the present experiments the maximum applied voltage is always less than 9 volts, hence impact ionization of valence electrons can be ignored.

Electron-phonon interactions, in particular the creation of optical phonons, can be expected to result in a loss in energy. The creation of optical phonons can be expected to result in an energy loss on the order[98] of 0.1 eV per interaction. The mean distance, $\lambda$, required for an electron of energy E to create an optical phonon can be crudely estimated[12] on the basis of the theories of intrinsic breakdown of insulators

$$\lambda \sim \frac{\hbar\omega}{dE/dx} \quad , \tag{30}$$

where $\hbar\omega$ is the optical phonon energy and dE/dx is the rate of energy loss to the lattice with distance x. O'Dwyer[56] gives an expression for dE/dt, for energies less than the valence-band ionization energy, which is

$$dE/dt = \left[\hbar\omega \log(4E/\hbar\omega)\right]/2\tau_o(E) \quad , \tag{31}$$

with

$$1/\tau_o(E) = \sqrt{\frac{m}{2}}\ \frac{e^2\omega}{2}\ \left(\frac{1}{\epsilon_{rh}} - \frac{1}{\epsilon_{r\ell}}\right) E^{-1/2} \quad , \tag{32}$$

in esu, with $\epsilon_{rh}$ and $\epsilon_{r\ell}$ the high and low frequency dielectric constants respectively. Using $dE/dx \sim dE/vdt$ with $E = \frac{1}{2}\,mv^2$, $\lambda$ can be written as

$$\lambda \sim \frac{4\hbar^2}{me^2 \log(4E/\hbar\omega)}\ \left(\frac{E}{\hbar\omega}\right)\ \frac{\epsilon_{rh}\epsilon_{r\ell}}{\epsilon_{r\ell} - \epsilon_{rh}} \quad . \tag{33}$$

For electron energies on the order of the phonon energy and $\epsilon_{r\ell} \simeq 10$, $\epsilon_{rh} \simeq 3$, $\lambda \sim 6.2 \times 10^{-8}$ cm = 6.2 Å. This can be compared with some results obtained from studies of secondary electron emission from MgO, in which a mean free path of about 5 Å is found to be appropriate for describing the internal secondary escape mechanism.[98]

On the basis of this estimate it can be seen that electron-phonon interactions alone cannot explain the results depicted in Figs. 27, 28, and 29. There are two reasons for this: 1) an electron would only lose about 2.6 eV in energy in traversing the thickest of these oxides and most of the electrons incident on a hole in the gold overlayer would escape, at an applied voltage of 4 volts, and 2) the mean free path should increase with increasing electron energy. Therefore on the basis of electron-phonon interactions the

ratio, $\alpha$, would be expected to go up with increasing sample voltage contrary to experimental results.

The term impurity scattering used here included two distinct types of events. In one case the scattering center does contain a weakly bound electron and in the other case it does not.

In the case in which the scattering center does not contain a weakly bound electron the mean free path is equal to the average distance between impurity atoms and can be given by:[99]

$$\lambda \sim \frac{2\epsilon_r^2 E^2}{\pi m^* N_i e^2 \log\left(1 + \frac{\epsilon_r^2 E^2}{e^2 N_i^{2/3}}\right)} . \qquad (34)$$

This again will not explain the experimental results since $\lambda$ again increases with increasing bias and it would be essentially elastic scattering.

For the case in which the impurity does contain a weakly bound electron there exists the possibility of appreciable energy loss per interaction if the scattering site, such as a donor or trap, contains an electron which can be excited into the conduction band of the insulator. Furthermore the mean free path in this case would decrease with increasing sample bias. This can be seen on the basis of the following analysis.

As the electron is accelerated in the conduction band of the oxide it gains energy and when it has gained energy greater than the energy difference between the conduction band minimum in the oxide and the donor level it could lose this energy to the donor electron which is then excited into the conduction band of the oxide. The greater the applied bias the more of these interactions that could occur.

This, however, leads to avalanche phenomena so that for each interaction there are two electrons in the conduction band for each initial electron. This would greatly increase the sample current if a great number of these interactions took place. However this effect is not noted in the sample I-V characteristics which can be completely explained on the basis of a Schottky type mechanism. If the total number of these interactions was small, then the transmission ratio $\alpha$ should increase or at least stay nearly constant with applied voltage.

As can be seen by this qualitative analysis none of the possible energy loss mechanisms can explain the observed behavior for these devices. The most probable explanation is that the oxide emitting surface becomes charged. When a sample current is first drawn, electrons arrive at the slot and those with enough energy are

emitted into vacuum. The remaining portion are not collected by the overlayer immediately but lead to a space charge at the slot. Thus the emitted current is dependent on sample current and time and in this manner indirectly dependent on the sample voltage. This is shown quite dramatically in Fig. 47.

Figure 47a shows the actual scope trace of $I_s$ and $I_e$ vs. $V_s$ for device PY-G-17(1). The pulse amplifier saturates at a given output power and the voltage is then constant beyond this point. The actual $V_s$ vs. time is observed on oscilloscope I (see section II-C-4). The applied voltage was allowed to saturate in this particular measurement and the actual pulse is shown in Fig. 47b. $I_s$ and $I_e$ were not observed as a function of time but were seen on oscilloscope II plotted vs. $V_s$. $I_s$ was seen to reach a maximum value when $V_s$ reached its maximum and remained at that current as evidenced by a bright spot at that point. $I_s$ vs. time can then be inferred from this curve and is shown in Fig. 47b as a constant current of $6.7 \times 10^{-3}$ amps for 6.75 msec. $\leq t \leq$ 10 msec. $I_e$ however was seen to drop to $4.6 \times 10^{-8}$ amps from its maximum of $7.6 \times 10^{-8}$ amps. This drop is shown as a linear drop as a function of time in Fig. 47b but may very well have another time dependence. This is

direct evidence that the oxide in the neighborhood of a slot does become negatively charged by the electrons that are not emitted into vacuum. The total charged area is so slight, however, that it does not affect the sample current.

Thus, although $\alpha$ is a function of applied sample voltage it is actually indirectly dependent upon voltage through the voltage dependence upon current and time. A better functional dependence for $\alpha$ would be $\alpha = \alpha(I,t)$. However, since $I = dQ/dt$ an even better functional dependence would be $\alpha = \alpha(Q,t)$. The total charge, Q, that has arrived at the overlayer is given by:

$$Q = \int_o^t I(\tau)\,d\tau \quad . \tag{35}$$

Again assuming the simple Schottly equation:

$$I = I_o e^{\beta V^{1/2}} \quad , \tag{36}$$

and since V is linearly dependent on time, $V = n^2\tau$:

$$I = I_o\, e^{\beta n \tau^{1/2}} \quad , \tag{37}$$

thus;

$$Q = I_o \int_o^t e^{\beta n \tau^{1/2}}\, d\tau \quad . \tag{38}$$

Integration yields:

$$Q = \frac{2I_o}{\beta^2 n^2}\left[(\beta n t^{1/2} - 1)\, e^{\beta n t^{1/2}} + 1\right]. \tag{39}$$

The results previously mentioned have been obtained on the assumption that $F(y)/F_o$ is a constant value for each device. However since the insulator is charging

up at the emitting slot, $F(y)/F_o$ is actually decreasing as $F_o$ increases. This means that the ratio $j_{rel}(y)$ is actually decreasing as $F_o$ increases so that relatively fewer electrons arrive at the slot as $F_o$ increases, or $\alpha_M$ from Eq. (27) decreases as $F_o$ increases.

Further evidence that the charging of the slot area is the determining factor in the emission results is shown in Fig. 48. In Fig. 48a, $\alpha$ of device PY-G-11(1), at $V_s$ = 2 volts, is plotted vs. the time it took for the voltage ramp to reach 2 volts, i.e., $dV/dt$ is different for each plotted point. Figure 48b is a plot of $\alpha$ with the same parameters, plotted vs. Q, the total charge passed through the insulator as found from Eq. (39). As can be seen from these figures $\alpha$ decreases as a function of time, or total charge, even though the sample current and sample voltage are the same. Similar results were obtained for each device, however on only one other device were the measurements extensive enough to determine a charging "time constant", this was device PY-G-17(1). The results of these two devices are plotted on a log$\alpha$ vs. t plot in Fig. 49. If $\alpha$ can be described as $\alpha = \alpha_o e^{-t/\tau}$ this "time constant", $\tau$, is 2 msec for PY-G-11(1) and 2.4 msec for PY-G-17(1). The decay of the charge is fairly rapid since a succeeding pulse,

on the order of one second later, gave identical results to the first pulse. The electrons are apparently being trapped in surface states which exist in the vicinity of the slots and have a time constant on the order of a millisecond which is in reasonable agreement with the time constants found for slow surface states.[80]

A further note of evidence that the emission current is controlled by charging of the insulator at the slot is given by the fact that no emission into vacuum was observed when the devices were studied using the slowly varying dc method.

The following section presents a brief summary of the important experimental results obtained and a discussion of the conclusions which can be drawn in terms of the preceding analyses.

## V. SUMMARY

This investigation was primarily concerned with the transport of hot electrons through vacuum deposited thin film emission diodes with subsequent emission into vacuum. The studies were specifically carried out on the evaporated Au-MgO-Au system.

The possible mechanisms for current flow from metal electrode to metal electrode are the following: 1) ohmic, 2) space charge limited, 3) tunnelling of electrons into the conduction band of the oxide and subsequent flow to the other electrode, 4) a Poole-Frenkel effect in which the electrons are thermally emitted from traps into the conduction band of the oxide by field enhancement, 5) mechanisms whereby electrons travel through the oxide by jumping from trap to trap, and 6) Schottky emission of electrons into the conduction band of the oxide.

The current-voltage characteristics were nonlinear which ruled out ohmic conduction except at very low field strengths and the current was not proportional to $V^2$ as it should be for space charge limited current.[16] Tunnelling could be ruled out since the functional dependence of I upon V was inconsistent with this mechanism (see Fig. 14). A Poole-Frenkel mechanism could also be ruled out on the same basis (see Fig. 16).

Furthermore when the MgO films were deposited in an oxygen atmosphere the term $\psi$ in the exponent in the equation $I = I_o e^{-\psi/kT} e^{\alpha V^{1/2}}$ becomes larger, which would indicate a lowering of the trap level by producing more stoichiometric films of MgO, if the Poole-Frenkel equation is assumed. It would indicate a higher barrier if the Schottky equation is assumed. It is much more reasonable to assume that the barrier is higher than a lowering of the trap level.

Some authors[15] have observed a power law dependence of current upon voltage in which $I \alpha V$ at low voltages, attributed to ohmic current flow, $I \alpha V^2$ for intermediate voltages, attributed to space charge limited current, and $I \alpha V^n$ where $n > 2$ for higher voltages. The term, n, in the exponent has varied from 4 all the way up to 16. This behavior has been attributed to the hopping of the electron between energy states in the forbidden gap of the insulator and eventual collection by the metal overlayer. Their analysis thus involved two or more changes in current flow mechanism as the voltage is increased. A look at Figs. 34 and 37 show a similar dependence of I upon V which can be completely explained by a Schottky type emission process in which the multiple image correction to the barrier profile has been made.

Using the multiple image correction to the potential barrier profile results in an I-V characteristic which is linear for low voltages and ultimately reaches a dependence such that ln $I \alpha V^{.484}$. The expressions derived using the multiple-image correction, Eq. (1)-(9), were plotted on log-log paper and fit the data over six orders of magnitude of current and four orders of magnitude of voltage. The conclusion drawn is that the electron flow in these devices is that of emission of electrons over the potential barrier into the conduction band of the oxide by a Schottky type process and subsequent acceleration by the strong electric field to the collection electrode.

A number of other features of these devices were brought to light during study of the I-V characteristics. There was no aging effect observed in these devices as noted by nearly every other author. The I-V characteristics were identical for the overlayer biased positively as for the overlayer biased negatively, indicating a symmetrical barrier, when gold was used as both electrodes. There was no hysteresis noted in dc measurement of the device characteristics and the pulse measurements were identical to the dc measurements. The barrier height did not change as the oxide thickness changed.

The barrier height did change as the amount of oxygen present in the vacuum system changed during deposition of the MgO film. The change was to a higher barrier as the oxygen pressure was made higher. Raising the oxygen pressure during deposition of the MgO film probably leads to a more stoichiometric film. The excess Mg present in these films gives rise to donor levels in the "bulk" and at the surface. These levels are near the conduction band so that the barrier is quite low. Decreasing the number of donors leads to a higher barrier since the Fermi level will be lower for fewer donors. The barrier height was also seen to change with temperature as noted by the results depicted in Figs. 39 and 40 and this change could be explained in a qualitative manner by assuming a high density of donor like interface states and "bulk" donors.

Another possible explanation for the nonlinear $\ln(I_o/T^2)$ vs. $1/T$ plots and the different barrier obtained by taking the slopes of these plots would be another current flow mechanism, which is nearly independent of temperature, such as tunnelling, superimposed on the Schottky current but of much smaller magnitude. It is impossible to determine which of these explanations hold or if both do.

The barrier height can be raised significantly by depositing the MgO in a high pressure of oxygen gas, on the order of $10^{-5}$ Torr, as evidenced by device PY-G-38(1). The barrier for this device was raised to about 2 eV and tunnelling became the dominant mechanism for current injection. The barrier to electron flow from overlayer to underlayer for this device was lower because the oxide near the overlayer was deposited after the oxygen had been pumped from the system resulting in a nonsymmetrical barrier. This is further evidence that the barrier goes up as the oxide film becomes more stoichiometric. None of the devices fabricated with a high pressure, $> 10^{-6}$ Torr, of oxygen present during deposition of the MgO were stable long enough to do extensive measurements.

In order to fabricate more stoichiometric devices, which can be measured, the oxide films must be very thin, $\lesssim$ 50 Å, and all devices made with such a thin oxide film were shorted between underlayer and overlayer due to pinholes. This led to the conclusion that single crystal devices may be impossible to attain. This would be especially true if the excess Mg in the films would in some way inhibit epitaxial growth of the oxide film. In this case the films would have to be stoichiometric

and very thin. Furthermore a perfect cleavage plane would have to be attained. None of the devices fabricated on single crystal substrates were single crystal devices, and all were shorts.

The low potential energy barrier is due to a high density of donor like interface states. If this is true the barrier should be nearly the same regardless of the metal used for the electrodes. One device, PY-A-1(1), which was a Au-MgO-Al device, was stable long enough to make one I-V characteristic run. The barrier to current flow from Au → Al was nearly the same as that from Al → Au. The difference between barriers to current flow was of the same order of magnitude as that seen for different metals on CdSe by Mead.[83] This is further evidence that the electron flow is controlled by the metal-oxide interfacial barrier.

Further evidence for Schottky emission is noted by the fact that emission into vacuum is seen from all the devices at very low sample voltages. The sample biases are never large enough to allow emission of electrons into vacuum through the gold overlayer film. Thus the electrons must be emitted through pinholes in the gold film, i.e., directly from the oxide film. The emitted electrons must still overcome a potential barrier at

the oxide-vacuum interface which is the electron affinity of the MgO. If the electrons were not coming over the underlayer-oxide interfacial barrier they would not have enough energy to be emitted into vacuum until the sample bias had reached about 1.0 volt or more. Emission into vacuum was noted from these devices at sample biases less than 0.5 volts. Thus, if the electron affinity of MgO is $\approx$ 0.8 eV, the emission current must be due to the electrons in the tail of the Fermi distribution above the energy level of the oxide conduction band. These electrons then have enough energy to be emitted into vacuum.

The emission ratio, $\alpha = \frac{I_e}{I_e+I_s}$, appears to be higher for the thicker oxide films at any given sample bias. It also appears to be slightly higher at the same field in the oxide. This can be explained on the basis of the electric field strength beneath a slot. The thicker the oxide the greater the electric field strength beneath a slot in the overlayer film. Thus for the thicker oxides more electrons are being emitted into the conduction band of the oxide beneath a slot in the overlayer film, and thus more electrons are arriving at the slot area for the same average field strength in the oxide.

This analysis is complicated by the fact that the oxide is charging negatively at the emitting slot. This is seen by the fact that the emission ratio goes down as the sample bias is increasing. None of the possible scattering mechanisms in the oxide film could account for this dependence of $\alpha$ on $V_s$ and still give sample I-V characteristics consistent with the Schottky mechanism observed here. Thus the emission transfer ratio is dependent on sample bias only to the extent that the bias depends on time or total charge passed through the oxide.

Evidence that $\alpha$ depends on the time is shown in Figs. 47, 48, and 49. Figure 47 shows that if the sample bias is left at the same value for any length of time the sample current remains constant but the emission current decreases rapidly. Thus $\alpha$ decreases as a function of time for a given sample bias. Figures 48 and 49 show that $\alpha$ decreases at a given sample bias as the time it takes to reach that bias increases. The dependence on the time taken to reach a given sample bias is such that $\alpha = \alpha_o e^{-t/\tau}$ where the "time constant" for charging is about 2 msec.

Further evidence that the oxide is charging in the vicinity of an emitting slot is the fact that no

emission into vacuum was observed when the devices were studied using the slowly varying dc technique.

Thus, although these devices are poor cold cathode electron emitters, a number of other uses may be possible. Since the metal-oxide interfacial potential barrier can be varied, depending upon deposition parameters, an array of these devices with different barriers could be used as light detectors such that a signal could be picked off at different points on this array, depending on the frequency of the light. The results obtained from device PY-G-38(1) indicates that these devices with different barrier heights at each interface could be designed as rectifiers. Much more work would be necessary to achieve either of these "practical" devices.

# APPENDIX I

## Application of the Schottky Emission Problem to a Metal-Insulator-Metal Diode

The following analysis for internal Schottky emission uses a physical model similar to that assumed for the case of emission into vacuum. The process of electron injection into the conduction band of the oxide film is analyzed in terms of the simple band theory of solids,[75] in which the metal overlayer and metal underlayer are idealized according to the Sommerfeld model. The oxide is assumed to present a barrier to electron conduction of height $\varphi_R$, modified by the electron image force. The energy level diagram appropriate for the potential barrier in this case shown in Fig. 30, drawn for a rectangular barrier height, $\varphi_R$, of 0.72 eV and an oxide thickness, S, of 100 Å with the zero of energy taken at the Fermi energy of the Au underlayer. The single image correction and the multiple image correction to this barrier are also shown.

The exact expression for the multiple-image correction to the potential energy of an electron in a medium with dielectric constant $\epsilon_r\epsilon_o$ between infinite parallel plane electrodes is derived by Savoye (see ref. 55, Appendix II). The result is:

$$eV_i = - \frac{e^2}{8\pi\epsilon_r\epsilon_o} \left\{ \frac{1}{2x} + \sum_{n=1}^{\infty} \left[ \frac{ns}{(ns)^2 - x^2} - \frac{1}{ns} \right] \right\} \quad \text{(I-1)}$$

This expression gives the image correction in joules. Using the appropriate values this expression becomes:

$$eV_i = - \frac{3.59}{\epsilon_r x} \left\{ 1 + \frac{2x}{s} \sum_{n=1}^{\infty} \frac{1}{n\left[ (s/x)^2 n^2 - 1 \right]} \right\} \text{(ev)}. \quad \text{(I-2)}$$

In this expression the distance, x, of the electron from one plate and the total dielectric thickness, S, are in Å. Assuming the low frequency dielectric constant of MgO the expression becomes:

$$eV_i = - \frac{.367}{x} \left\{ 1 + \frac{2x}{s} \sum_{n=1}^{\infty} \frac{1}{n\left[ (s/x)^2 n^2 - 1 \right]} \right\} . \quad \text{(I-3)}$$

This expression can be written as:

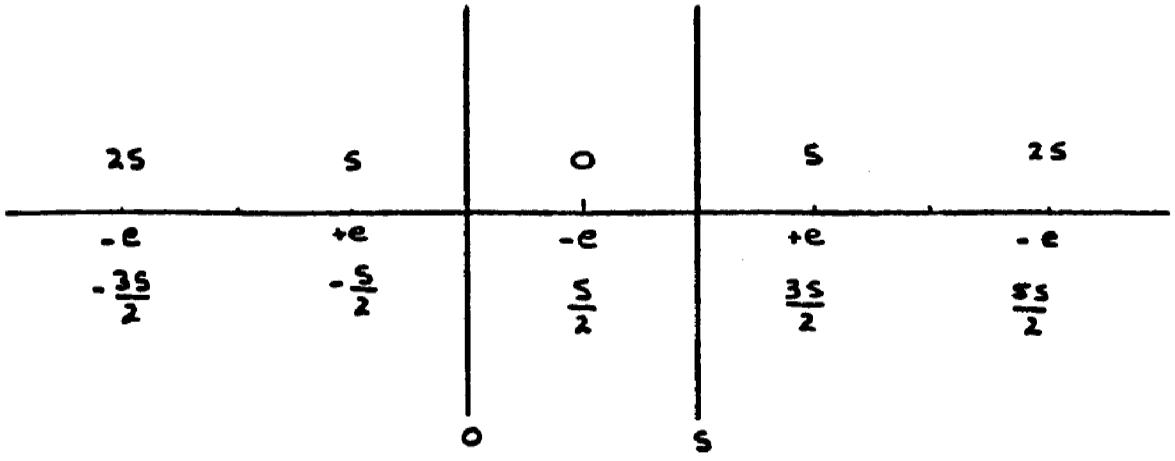
$$eV_i = - \frac{.367}{x} \left[ 1 + C\left(\frac{x}{s}\right) \right] , \quad \text{(I-4)}$$

where $- \frac{.367}{x}$ is the single image potential energy and $C(\frac{x}{s})$ is the multiple-image correction. Since this series has no closed form some approximations must be made. When x = s/2 expression (I-3) becomes:

$$eV_i = - \frac{.367}{x} \left\{ 1 + \sum_{n=1}^{\infty} \frac{1}{n(4n^2 - 1)} \right\} , \quad \text{(I-5)}$$

The easiest method for obtaining this expression in simpler form is to solve the porblem with the electron midway between the two electrodes. Since the force on the electron is zero in this case, a method differing from Savoye's must be used. In this case the coulomb

potential of all the image forces will be calculated at the center of the dielectric and the potential energy of the electron thus found by multiplying this expression by -e. Let the electrode spacing be S, with one electrode taken as the origin as shown in the diagram below. The positions and signs of the image charges are noted below the x axis with the distance from the electron noted above the x axis.




The total coulomb potential can be written by inspection:

$$V_i = \frac{e}{4\pi\epsilon_r\epsilon_o}\left\{\frac{2}{s} - \frac{2}{2s} + \frac{2}{3s} - \frac{2}{4s} + \frac{2}{5s} \cdots\right\} \qquad \text{(I-6)}$$

or

$$V_i = \frac{e}{2\pi\epsilon_r\epsilon_o s}\sum_{n=1}^{\infty}\frac{(-1)^{n+1}}{n} . \qquad \text{(I-7)}$$

Thus the potential energy of the electron at the midpoint between the electrodes is:

$$eV_i = -\frac{e^2}{2\pi\epsilon_r\epsilon_o s}\sum_{n=1}^{\infty}\frac{(-1)^{n+1}}{n} \qquad \text{(I-8)}$$

The series $\sum_{n=1}^{\infty} \frac{(-1)^{n+1}}{n}$ is convergent[76] and is the Taylor series for ln(x+1) evaluated at x = 1.[77,78]

The Taylor series expansion for f(x) is given by:

$$f(x) = \sum_{n=o}^{\infty} \frac{f^{(n)}(x_o)}{n!} (x-x_o)^n \quad , \tag{I-9}$$

thus:

$$\ln(x+1) = \sum_{n=1}^{\infty} \frac{x^n (-1)^{n+1}}{n} \quad . \tag{I-10}$$

For x = 1 this becomes:

$$\ln(2) = \sum_{n=1}^{\infty} \frac{(-1)^{n+1}}{n} \quad . \tag{I-11}$$

So we can write the potential energy of the electron as:

$$eV_i = - \frac{e^2 \ln 2}{2\pi \epsilon_r \epsilon_o s} \quad . \tag{I-12}$$

According to Simmons (see ref. 11, Eq. (33) and Fig. 4) an extremely good approximation to the multiple image correction is of the form:

$$eV_i = - \frac{Ks^2}{x(s-x)} \quad . \tag{I-13}$$

To find the value of K one must equate this expression to expression (I-12) at $x = \frac{s}{2}$, one gets:

$$K = \frac{e^2 \ln 2}{8\pi \epsilon_r \epsilon_o s} \quad . \tag{I-14}$$

Thus the expression

$$eV_i = - \frac{e^2 \ln 2}{8\pi \epsilon_r \epsilon_o} \left[\frac{s}{x(s-x)}\right] \tag{I-15}$$

is an extremely good approximation to the multiple image correction and this expression is plotted in Fig. 30. Putting in the appropriate values

$$eV_i = -.508\left[\frac{s}{x(s-x)}\right], \qquad \text{(I-16)}$$

where dimensions x and s are in Å.

From Eq. (I-18) it can be seen that the actual barrier $\varphi_o$ is given by

$$\varphi_o = \varphi_R - .508\left[\frac{s}{x(s-x)}\right](eV). \qquad \text{(I-17)}$$

Thus when an electric field is applied, the barrier to electron flow becomes

$$\varphi(x) = \varphi_o - eV\frac{x}{s} \qquad \text{(I-18)}$$

or

$$\varphi(x) = \varphi_R - .508\left[\frac{s}{x(s-x)}\right] - eV\frac{x}{s}. \qquad \text{(I-19)}$$

The resulting barriers for a field of $3 \times 10^6$ V/cm, which corresponds to an applied voltage of 3 volts across the 100 Å thick oxide film, is also shown in Fig. 30. Even though Eq. (I-19) is a simplified approximation to the true multiple image modification it is still extremely difficult to work with. To apply this expression to the Schottky equation the maximum of the potential energy of the electron when a field is applied must be found. Let $eV_i|_F$ be the potential energy of an electron in an applied field.

$$eV_i|_F = -.508\left[\frac{s}{x(s-x)}\right] - eV\frac{x}{s} \qquad \text{(I-20)}$$

$eV_i|_{F_{max}}$ is found when $\frac{d(eV_i|_F)}{dx} = 0$ or

$$.508\left[\frac{s-2x}{x^2(s-x)^2}\right] - \frac{eV}{s} = 0 \; . \qquad \text{(I-21)}$$

The solution to (I-23) cannot be found for general values of s and V. Thus the problem will be solved numerically for an oxide thickness of 100 Å and compared to the solutions found for the single image problem. The values of $-eV_i|_{F_{max}}$ are plotted against F in Fig. 31. As can be seen from this figure the dependence of the potential maximum on applied electric field deviates from a straight line on a $\ln(eV_i|_{F_{max}})$ vs. $\ln(F)$ plot for fields less than about $10^5$ V/cm. At the fields where the curve is linear the dependence is not proportional to $V^{1/2}$ but to $V^{.484}$, using Simmon's multiple image approximation. Since the barrier height is $\varphi_R + eV_i|_{F_{max}}$ it can be seen that the barrier is lower for the multiple image correction than for the single image correction for all applied fields of interest.

Thus $eV_i|_{F_{max}}$ can be written as

$$eV_i|_{F_{max}} = -DV^{.484} \; . \qquad \text{(I-22)}$$

Therefore, if Richardson's equation is written

$$J = AT^2 e^{-\Phi/kT} \qquad \text{(I-23)}$$

$$\Phi = \varphi_R - DV^{.484} \quad . \qquad \text{(I-24)}$$

So the Schottky equation for a dielectric sandwiched between two metal electrodes beoomes

$$J = AT^2 \, e^{-\varphi_R/kT} \, e^{DV^{.484}/kT} \quad . \qquad \text{(I-25)}$$

Using the values obtained in this manner this equation becomes

$$J = AT^2 \, e^{-\varphi_R/kT} \, e^{.148V^{.484}/kT} \quad . \qquad \text{(I-26)}$$

# APPENDIX II

## Barrier Height as a Function of Temperature and Excess Mg Concentration

The barrier height is defined as the energy difference between the bottom of the conduction band and the Fermi level at the interface. In a bulk semiconductor this difference, in the bulk, increases for an increase in temperature for an n-type semiconductor. The location of the Fermi level as a function of temperature is found by the condition of charge neutrality in equilibrium, the total positive charge is set equal to the total negative charge. If surface states are present the charge involved with these must also be taken into account. For a device of this type however, the condition of charge neutrality must be imposed on the entire device and not just for the oxide.

Figure 42 is a schematic energy band diagram for a metal showing how the barrier changes under different conditions. Figure 42a shows the barrier presented to the flow of electrons out of the metal when the interface is a gold-vacuum interface. In these devices the MgO films deposited have an excess of Mg atoms which give rise to a donor level quite a distance from the conduction band.[88,89,90] If no surface states were present the

barrier presented to the flow of electrons from the metal, Au, to the oxide, MgO, would be $\varphi_R = \varphi_M - \chi_I$ as previously stated. The energy band diagram for this problem is shown in Fig. 42b. This picture shows that the donors near the interface must be ionized in order to get a barrier of this height. The distribution of ionized donors is schematically shown on this figure by the separation between signs. The result is a sheet of negative charge just within the metal. Thus it can be seen that to lower the barrier from $\varphi_M$ to $\varphi_M - \chi_I$ a positive charge density must be set up in the oxide. To lower the barrier even further, more positive charge must reside in the oxide and therefore more negative charge in the metal. Since all the "bulk" donors are ionized near the surface this "extra" positive charge must come from ionized donor like interface states. The energy band picture for this situation is shown in Fig. 42c. Thus a large density of donor like interface states must exist at the Au-MgO interface.

This picture is somewhat misleading since it deals with a metal-bulk oxide contact. In reality there is another metal-oxide interface very near the one pictured here. To determine what the potential energy of an electron is the oxide looks like, Poisson's equation must

be solved using the proper boundary conditions. This problem has been solved by Geppert[91] for an intrinsic oxide and he found that the depression of the potential energy profile at the mid-point between the two metal interfaces was $2.74 \times 10^{-19}$ eV using the following parameters, $\varphi_R = 1$ eV, $\epsilon_r = 9$, $s = 100$ Å and $T = 300$°K. Thus, for an intrinsic oxide the barrier is essentially flat. Roberts[92] found a potential energy depression at the mid-point between electrodes of $5 \times 10^{-13}$ eV for an n-type semiconductor with the following parameters, $N_d = 10^{16}/cm^3$, $\varphi_R = 0.7$ eV, $E_c - E_d = 1.2$ eV, $\epsilon_r = 10$, $s = 100$ Å, and $T = 300$°K. The parameters used in this problem are nearly the same as those involved in a Au-MgO-Au device and the mid-point potential energy depression is again negligible. Thus Figs. 42b and 42c would show flat bands terminating on another electrode for a device of this type.

The above analysis did not include image forces and when these are included the potential barrier will have the shape shown in Fig. 30, as calculated in Appendix I.

The charge neutrality condition for the device is a very complicated expression since it must include all charges. Since the oxide film is not a single crystal,

the energy band diagram does not strictly hold. In this case there is probably no single discrete donor level, there may be traps at various levels due to lattice inperfections which apparently do not affect the conduction mechanism, the surface states probably have a band of discrete allowed energy levels, and there may very well be acceptor levels at the interface and in the oxide. The charge neutrality condition can be written as:

$$P_t + N_d^+ + p = n + N + N_t' + N_a^- + n_t \qquad \text{(II-1)}$$

where: $P_t$ = number of unoccupied donor like surface states

$N_d^+$ = number of ionized "bulk" donors

$P$ = number of holes in the valence band

$n$ = number of electrons in the conduction band

$N$ = negative charge just inside the metal electrodes

$N_t'$ = number of filled "bulk" traps

$N_a^-$ = number of ionized donors

$n_t$ = number of occupied acceptor like surface states.

Since the Fermi level at the surface is near the conduction band and the band gap is so large, coupled with the fact that the bands are flat,[91,92] the number of holes in the

valence band and the number of ionized acceptors can be ignored if they are low lying in the forbidden gap. The acceptor like surface states can also be ignored. Thus (II-1) can be written as

$$P_t + N_d^+ = n + N + N_t' \quad . \tag{II-2}$$

If the further assumptions are made that at the temperature involved in these studies all the donor like surface states are ionized and $N = P_t$ this expression can be written as

$$N_d^+ = n + N_t' \quad . \tag{II-3}$$

Each of the terms in (II-3) are expressed by either a series or an integral. If one more assumption is made that the donors and traps have a single discrete level this becomes:

$$\frac{N_d}{2e^{\frac{E_f - E_d}{kT}} + 1} = N_c e^{(E_f - E_c)/kT} + \frac{N_t}{2e^{\frac{E_t - E_f}{kT}} + 1} \tag{II-4}$$

This expression is very simplified but is still extremely difficult to handle because there are four unknowns. If one ignores the traps a qualitative solution can be made for the barrier as a function of temperature.

This extremely simplified solution then becomes:

$$\frac{N_d}{2e^{\frac{E_f - E_d}{kT}} + 1} = N_c e^{(E_f - E_c)/kT} \tag{II-5}$$

Let

$$E_c - E_f = \varphi_R$$

$$E_f - E_d = E_c - E_d - (E_c - E_f) = \psi - \varphi_R \qquad \text{(II-6)}$$

Then the expression becomes

$$N_d/(2e^{\psi/kT} + e^{\varphi_R/kT}) = N_c/e^{2\varphi_R/kT} \qquad \text{(II-7)}$$

which can be solved for $\varphi_R$. This solution is:

$$\varphi_R = kT \ln \frac{1}{2}\left\{N_c/N_d + \left[(N_c/N_d)^2 + 8N_c e^{\psi/kT}/N_d\right]^{1/2}\right\} \qquad \text{(II-8)}$$

So it can be seen that $\varphi_R$ increases for increasing T, increases for decreasing $N_d$, and increases faster with T for smaller $N_d$.

# APPENDIX III

## Calculation of the Fringing Field, F, at a Plane Electrode, Beneath a Slot in an Opposing Plane - Parallel Electrode

The variation of field F(x) at the underlayer, which determines $j_s(x)$ as a function of position, x, under a slot of width, d, in the overlayer can be obtained approximately by the following method:* Fig. 43a shows the geometry assumed; the insulating film thickness is s with dielectric constant $\epsilon_r\epsilon_o$, the slot width is d. This problem is idealized in Fig. 43b, where an electrostatic problem is indicated in which we have assumed no dielectric discontinuity, and also that the slot is infinitely deep.

This electrostatic problem can be solved by a Schwarz-Christoffel transformation.[95,96] The z-plane representation is shown in Fig. 43b, and the transformation to the upper half of the w-plane shown in Fig. 43c is accomplished by:

$$dz/dw = K(w-a)^{1/2}(w-b)^{1/2}/w(w-1). \qquad \text{(III-1)}$$

---

*Note that in this appendix x is taken as the distance from the slot edge, while in the text it is the coordinate perpendicular to the overlayer plane.

To find the value of K and the relationship between a and b one must integrate in the complex plane. In these expressions $z = x+jy$ and $w = u+jv$.

$$\int_D^C dz = \int_D^C \frac{dz}{dw}\, dw \qquad \text{(III-2)}$$

In the z plane, $\int_D^C dz = js$, while in the w plane this integral can be taken along a semi-circle of very large radius, such that $w = Re^{j\theta}$, $dw = jRe^{j\theta}d\theta$, and $|Re^{j\theta}| = R \gg a$, $R \gg b$, and $R \gg 1$, then:

$$js \simeq \int_o^\pi K \frac{(Re^{j\theta})^{1/2}(Re^{j\theta})^{1/2}}{Re^{j\theta}Re^{j\theta}}\, jRe^{j\theta}d\theta$$

$$= \int_o^\pi jKd\theta = j\pi K \; . \qquad \text{(III-3)}$$

Therefore

$$K = s/\pi \; . \qquad \text{(III-4)}$$

Another integration that can be made is

$$\int_A^B dz = \int_A^B \frac{dz}{dw}\, dw \; . \qquad \text{(III-5)}$$

In this case $\int_A^B dz = js$, and now integrate along a small semi-circle in the w-plane such that $w = re^{j\theta}$, where $|re^{j\theta}| = r \ll a$, $r \ll 1$, $r \ll b$ so that

$$js \simeq \int_o^\pi K \frac{(ab)^{1/2}}{re^{j\theta}(-1)}\, jre^{j\theta}d\theta = -j\frac{s}{\pi}(ab)^{1/2}\pi \; . \qquad \text{(III-6)}$$

Therefore $ab = 1$. Thus (III-1) can be written as

$$dz/dw = (s/\pi)(w-a)^{1/2}(w-b)^{1/2}/w(w-1) \quad , \qquad \text{(III-7)}$$

which cannot be integrated easily. The substitution

$$p^2 = (w-b)/(w-a) \qquad \text{(III-8)}$$

yields:

$$z = \frac{2s}{\pi} \int \frac{(b-a)^2 p^2 dp}{a(1-a)(p^2-1)(p^2-b^2)(b+p^2)} \quad . \qquad \text{(III-9)}$$

Letting $a = \frac{1}{b}$ results in

$$z = \frac{2s}{\pi} \int \frac{(b+1)^2 (b-1) p^2 dp}{(1-p^2)(b^2-p^2)(b+p^2)} \qquad \text{(III-10)}$$

or

$$z = \frac{2s}{\pi}\left[ \int \frac{dp}{1-p^2} - \int \frac{b\,dp}{b^2-p^2} - \int \frac{(b-1)\,dp}{b+p^2} \right] \quad . \qquad \text{(III-11)}$$

Integration yields

$$z = \frac{s}{\pi}\left\{ \ln\left|\frac{1+p}{1-p}\right| - \ln\left|\frac{b+p}{b-p}\right| - \frac{2(b-1)}{\sqrt{b}} \tan^{-1}\left(\frac{p}{\sqrt{b}}\right) \right\} . \qquad \text{(III-12)}$$

The constants of integration have been set equal to zero and this fixes the origin of the z-plane. It is noted that when $p = 0$, $w = b$, and $z = 0$, this information is shown in Fig. 43b and c. As $w \to a$, $z \to -d$, but $p \to \infty$ so $z \to -s(b-1)/\sqrt{b}$ . Therefore

$$d/s = (b-1)/\sqrt{b} \quad . \qquad \text{(III-13)}$$

The transformation from the w-plane to the $\chi$-plane where the field is uniform is given[97] by

$$\chi = \frac{V_o}{\pi} \log w \quad . \qquad \text{(III-14)}$$

The field strength, F, is given by

$$F = \left|\frac{d\chi}{dz}\right| = \left|\frac{d\chi}{dw}\frac{dw}{dz}\right| , \qquad \text{(III-15)}$$

thus

$$F = \left(\frac{V_o}{s}\right)\frac{w-1}{(w-a)^{1/2}(w-b)^{1/2}} . \qquad \text{(III-16)}$$

Now as $w \to o$, $z \to -\infty$, and $F \to V_o/s$ as it should, therefore we write

$$F = F_o \frac{w-1}{(w-a)^{1/2}(w-b)^{1/2}} . \qquad \text{(III-17)}$$

For negative real w this gives the field at the underlayer and the calculations need only to be made for $-1 \leq w \leq 0$. At $w = -1$, $z = -d/2 + js$, and from symmetry the field will be the same on either side of the point on the underlayer beneath the center of the slot. A numerical calculation of F(z) at $z = x+js$ for $x \leq -d/2$ can be made choosing $-1 \leq w \leq 0$, evaluating $F/F_o$ from (III-17) and finding x from

$$x/s = \mathrm{Re}\left\{\frac{1}{\pi}\left[\ln\left(\frac{1+p}{1-p}\right) - \ln\left(\frac{b+p}{b-p}\right) - \frac{2(b-1)}{\sqrt{b}}\tan^{-1}\left(\frac{p}{\sqrt{b}}\right)\right]\right\} \qquad \text{(III-18)}$$

where $p^2$ is given in (III-18).

It will be assumed that d = 100 Å and the appropriate values for d/s for these devices will then be; 1.67, 1.28, 1.12, .92, and .63.

The calculations for the field strength at the underlayer metal beneath the slot in the overlayer were carried out numerically and the results are shown plotted as $F/F_o$ vs. distance from one edge of the slot in Fig. 45.

## BIBLIOGRAPHY


1. C. A. Mead, "The Tunnel-Emission Amplifier," Proc. IRE 48, 359 (1960).
2. C. A. Mead, "Operation of Tunnel-Emission Devices," J. Appl. Phys. 32, 646 (1961).
3. D. V. Geppert, "Internal Field Emission and Low Temperature Thermionic Emission into Vacuum," Proc. IRE 48, 9, 1644 (1960).
4. N. F. Mott and R. W. Gurney, Electronic Processes in Ionic Crystals, Oxford Clarendon Press (Oxford), 1940.
5. P. R. Emtage and W. Tantraporn, "Schottky Emission through Thin Insulating Films," Phys. Rev. Letters 8, 267 (1962).
6. S. R. Pollack, "Schottky Field Emission through Insulating Layers," J. Appl. Phys. 34, 877 (1963).
7. R. H. Fowler and L. Nordheim, "Electron Emission in Intense Electric Fields," Proc. Roy. Soc. (London) A199, 173 (1928).
8. P. S. Schnupp, "Kronig-Penny-Type Calculations for Electron Tunneling through Thin Dielectric Films," Phys. Stat. Sol. 21, 567 (1967).
9. T. E. Hartman, "Tunnelling of a Wave Packet," J. Appl. Phys. 33, 3427 (1962).

10. R. Stratton, "Voltage-Current Characteristics for Tunnelling through Insulating Films," J. Phys. Chem. Solids 23, 1177 (1962).

11. J. G. Simmons, "Generalized Formula for the Electric Tunnel Effect between Similar Electrodes Separated by a Thin Insulating Film," J. Appl. Phys. 34, 1793 (1963).

12. E. D. Savoye and D. E. Anderson, "Injection and Emission of Hot Electrons in Thin-Film Tunnel Emitters," J. Appl. Phys. 38, 3245 (1967).

13. W. Tantraporn, "Electron Current through Metal-Insulator-Metal Sandwiches," Solid State Elect. 7, 81 (1964).

14. J. Frenkel, "On Pre-Breakdown Phenomena in Insulators and Electronic Semiconductors," Phys. Rev. 54, 647 (1938).

15. A. K. Jonscher, "Electronic Properties of Amorphous Dielectric Films," Thin Solid Films 1, 213-234 (1967), Elsevier, Amsterdam.

16. M. A. Lampert, "Injection Currents in Insulators," Proc. IRE 50, 1781 (1962).

17. M. A. Lampert and F. Edelman, "Theory of One-Carrier Space-Charge-Limited Currents Including Diffusion and Trapping," J. Appl. Phys. 35, 2971 (1964).

18. J. Lindmayer, J. Reynold, and C. Wrigley, "One Carrier Space-Charge-Limited Currents in Solids," J. Appl. Phys. 34, 809 (1963).

19. J. Cohen, "Tunnel Emission into Vacuum," J. Appl. Phys. 33, 1999 (1962).

20. C. A. Mead, "Transport of Hot Electrons in Thin Gold Films," Phys. Rev. Letters 8, 56 (1962). Erratum, Phys. Rev. Letters 9, 46 (1962).

21. H. Kanter and W. A. Feibelman, "Electron Emission from Thin Al-$Al_2O_3$-Au Structures," J. Appl. Phys. 33, 3580 (1962).

22. R. E. Collins and L. W. Davis, "Electron Distribution of Hot Electrons in Al," Appl. Phys. Letters 2, 213 (1963), and "The Transport of Hot Electrons in Al-$Al_2O_3$-Al Tunnel Cathodes," Solid State Elect. 7, 445 (1964).

23. J. G. Simmons, "Intrinsic Fields in Thin Insulating Films between Dissimilar Electrodes," Phys. Rev. Letters 10, 10 (1963).

24. R. Holm, "The Electric Tunnel Effect Across Thin Insulator Films in Contacts," J. Appl. Phys. 22, 569 (1951).

25. T. Hartman, "Tunnelling through Asymmetric Barriers," J. Appl. Phys. 35, 3283 (1964).

26. O. L. Nelson and D. E. Anderson, "Potential Barrier Parameters in Thin-Film Al-$Al_2O_3$-Metal Diodes," J. Appl. Phys. 37, 77 (1966).

27. O. L. Nelson, Studies of Potential Barrier Parameters in Thin-Film Metal-Oxide-Metal Devices, Ph.D. Thesis, University of Minnesota, 1965.

28. J. L. Miles and P. H. Smith, "The Formation of Metal Oxide Films Using Gaseous and Solid Electrolytes," J. Electrochem. Soc. 110, 1240 (1963).

29. M. Scharfe, The Gaseous Anodization of Tantalum, M.S.E.E. Thesis, University of Minnesota, 1966.

30. G. S. Anderson, W. N. Meyer, and G. K. Wehner, "Sputtering of Dielectrics by High-Frequency Fields," J. Appl. Phys. 33, 2991 (1962).

31. P. D. Davidse and L. I. Maissel, "Dielectric Thin Films through R.F. Sputtering," J. Appl. Phys. 37, 574 (1966).

32. L. Holland, Vacuum Deposition of Thin Films, John Wiley and Sons, Inc., New York, 1956.

33. H. M. O'Bryan, "Evaporation Technique for Highly Refractory Substances," Rev. Sci. Instr. 5, 125 (1934).

34. L. A. Harris, "Structural Effects in Thin-Film Sandwich Emitters," J. Appl. Phys. 35, 268 (1964).

35. M. McColl and C. A. Mead, "Electron Current Through Thin Mica Films," Trans. Metall. Soc. AIME 233, 502 (1965).

36. D. W. Pashley, "Epitaxy in Thin Surface Films," Metall. Adv. Elect. Mat. 19, 175-207 (1962).

37. C. Davisson and L. H. Germer, "Diffraction of Electrons by a Crystal of Nickel," Phys. Rev. 30, 705-740 (1927).

38. D. E. Anderson, A. B. Laponsky, and W. T. Peria, Research in Physics of Electron Emission and Electron Tube Technology, Third Interim Report, Contract No. AF 33(657)-10475, University of Minnesota, Minneapolis, Minnesota, October 16, 1963 to April 15, 1964.

39. T. J. Szczech, Ph.D. Thesis, University of Minnesota, 1966.

40. T. Tom and C. F. Brothers, "The Role of Sublimation Pumping in Conjunction with Ion Pumping," Northern California Vacuum Society Meeting, October 1965.

41. L. D. Hall, "Electronic Ultra-high Vacuum Pump," Rev. Sci. Instr. 29, 367 (1958).

42. W. M. Brubaker, "A Method for Greatly Enhancing the Pumping Action of a Penning Discharge," Trans. 6th. Nat. Vac. Symp., 1959, 302, Pergamon Press, London, 1960.

43. R. Riesz and G. H. Dieke, "The Analysis and Purification of Rare Gases by Means of Electric Discharges," J. Appl. Phys. 25, 196 (1954).

44. K. H. Behrndt and R. W. Love, "Control of Deposition Rate and Film Thickness with the Crystal Oscillator," Vacuum Symposium Trans. 87, 1960.

45. S. J. Lins and H. S. Kukuk, "Resonance Frequency Shift Thin-Film Thickness Monitor," Vacuum Symposium Trans. 333, 1960.

46. D. E. Anderson, Studies of Thin Film Hard Superconductors, Report No. 2, Contract No. DA-44-009-AMC-812(T) University of Minnesota, Minneapolis, Minnesota, October 26, 1965-October 25, 1966.

47. P. W. Palmberg, D. C. Johnson, and H. J. Boll, "Construction of Hemispherical Grids," Rev. Sci. Instr. 35, 244 (1964).

48. P. W. Palmberg, North American Rockwell Science Center, Thousand Oaks, California, Private Communicatio

49. F. Kloss and L. Herte, "Advances in RF-Induced Plasma Sputtering," SCP and Solid State Tech., 45 (1967).

50. First International Conference on Electron and Ion Beam Science and Technology, John Wiley and Sons, Inc., 1965.

51. R. T. Bayard and D. Alpert, "Extension of the Low Pressure Range of the Ionization Gauge," Rev. Sci. Instr. 21, 571 (1950).

52. F. L. Schuermeyer and J. A. Crawford, "Interpretation of Low Voltage Photomeasurements in Metal-Insulator-Metal Films," Appl. Phys. Letters 9, 317 (1966).

53. R. E. Weber, Work Function and Structural Studies for Alkali-Covered Semiconductors, Tech. Report AFAL-TR-67-355, University of Minnesota, Minneapolis, Minnesota, February 1968.

54. W. R. Miller, Jr. and N. N. Axelrod, "Modified Faraday Cage," Rev. Sci. Instr. 37, 1096 (1966).

55. E. D. Savoye, Extraction and Injection of Hot Electrons in Thin Film Emission Diodes, Ph.D. Thesis, University of Minnesota, 1966.

56. J. J. O'Dwyer, "Dielectric Breakdown in Solids," Phil. Mag. Suppl. 1 (Adv. in Phys.) 1, 349 (1958).

57. W. W. Dolan and W. P. Dyke, "Temperature-and-Field Emission of Electrons from Metals," Phys. Rev. 95, 327 (1954).

58. R. H. Good, Jr. and E. W. Müller, "Field Emission," Encyclopedia of Physics 21, 176-231 (1956).

59. T. B. Linnerooth, Alkali Ion Doping of the Metal-Oxide Interface, M.S. Thesis, University of Minnesota, 1965.

60. J. C. Kemp and V. I. Neeley, "Wave Functions for F Centers in MgO," Phys. Rev. 132, 215 (1963).

61. A. van der Ziel, Solid State Physical Electronics, Second Edition, Prentice Hall, Englewood Cliffs, New Jersey, 1968, p. 149.

62. T. E. Hartman, J. C. Blair, and R. Bauer, "Electrical Conduction through SiO Films," J. Appl. Phys. 37, 2468 (1966).

63. C. A. Mead, "Electron Transport Mechanisms in Thin Insulating Films," Phys. Rev. 128, 2088 (1962).

64. J. J. O'Dwyer, "Current-Voltage Characteristics of Dielectric Films," J. Appl. Phys. 37, 599 (1966). "Electric Current in Thin Dielectric Films," Bull. Am. Phys. Soc. 10, 389 (1965).

65. H. Frolich, "On the Theory of Dielectric Breakdown in Solids," Proc. Roy. Soc. (London) A188, 521 (1947).

66. S. R. Pollack and C. E. Morris, "Electron Tunnelling through Asymmetric Films of Thermally Grown $Al_2O_3$," J. Appl. Phys. 35, 1503 (1964).

67. D. A. Lavrinets, Electron Scattering in $Ta_2O_5$ Thin Films, M.S.E.E. Thesis, University of Minnesota, 1969.

68. E. Pittrelli, "Tunnel Emission into an Insulating Film with Traps," Solid-State Electr. 6, 667 (1963).

69. D. Meyerhofer and S. A. Ochs, "Current Flow in Very Thin Films of $Al_2O_3$ and BeO," J. Appl. Phys. 34, 2535 (1963).

70. H. Kanter, "Slow Electron Transfer through Evaporated Au Films," J. Appl. Phys. 34, 3629 (1963).

71. I. W. Hickmott, "Anomalous Transmission of Low-energy Electrons through Thin Metal Films," J. Appl. Phys. 34, 1569 (1963).

72. S. M. Sze, J. L. Moll, and T. Sugano, "Range-Energy Relation of Hot Electrons in Gold," Solid State Electronics 7, 509 (1964).

73. J. J. Quinn, "The Range of Hot Electrons and Holes in Metals," Appl. Phys. Letters 2, 167 (1963).

74. K. Motizuki and M. Sparks, "Range of Excited Electrons and Holes in Metals and Semiconductors," J. Phys. Soc. Japan 19, 486 (1964).

75. A. J. Dekker, Solid State Physics, Prentice Hall, Inc., Englewood Cliffs, New Jersey, 1957, Chapter 11.

76. G. B. Thomas, Jr., Calculus and Analytic Geometry, Addison-Wesley Publishing Company, Inc., Reading, Massachusetts, 1953, p. 614.

77. E. Hille, Analytic Function Theory, Ginn and Company, 1959, Vol. I, p. 197.

78. A. E. Taylor, Advanced Calculus, Ginn and Gompany, 1955, p. 562.

79. A. A. Holscher, "A Field Emission Retarding Potential Method for Measuring Work Functions," Surface Science 4 (1966).

80. A. Many, Y. Goldstein, and N. B. Grover, Semiconductor Surfaces, John Wiley and Sons, Inc., New York, 1965, p. 138.

81. W. E. Meyerhof, "Contact Potential Differences in Silicon Crystal Rectifiers," Phys. Rev. 71, 727 (1947).

82. W. G. Spitzer and C. A. Mead, "Barrier Height Studies on Metal-Semiconductor Systems," J. Appl. Phys. 34, 3061 (1963).

83. C. A. Mead, "Surface States on Semiconductor Crystals; Barriers on the Cd (Se:S) System," Appl. Phys. Letters 6, 103 (1965).

84. C. A. Mead, "Metal-Semiconductor Surface Barriers," Solid-State Elect. 9, 1023 (1966).

85. W. Shockley, "On the Surface States Associated with a Periodic Potential," Phys. Rev. 56, 317 (1939).

86. L. Pauling, The Nature of the Chemical Bond, Cornell University Press, Ithaca, New York, 1960.

87. J. Bardeen, "Surface States and Rectification at a Metal Semiconductor Contact," Phys. Rev. 71, 717 (1947).

88. E. Yamaka and K. Sawamoto, "Photoinduced Hall Effect in MgO," Phys. Rev. 101, 565 (1956).

89. E. Olson, Radiation Induced Electrical Phenomenon in the Alkaline Earth Oxides, Ph.D. Thesis, University of Minnesota, 1969.

90. E. Yamaka and K. Sawamoto, "Electrical Conductivity and Thermo-electric Motive Force in MgO Single Crystals," J. Phys. Soc. Japan 10, 176 (1955).

91. D. V. Geppert, "Theoretical Shape of Metal-Insulator-Metal Potential Barriers," J. Appl. Phys. 34, 490 (1963).

92. G. G. Roberts, "Equilibrium Space Charge Distribution in Semiconductors," Brit. J. Appl. Phys. 18, 749 (1967).

93. K. L. Chopra, L. C. Bobb, and M. H. Francombe, "Electrical Resistivity of Thin Single-Crystal Gold Films," J. Appl. Phys. 34, 1699 (1963).

94. C. A. Neugebauer, Physics of Thin Films, Ed. by G. Hass and R. E. Thun, Academic Press, New York and London, 1964.

95. R. V. Churchill, Complex Variables and Applications, McGraw-Hill Book Company, Inc., New York, Toronto, and London, 1960.

96. S. Ramo and J. R. Whinnery, Fields and Waves in Modern Radio, Second Edition, John Wiley and Sons, Inc., New York and London, 1953.

97. W. J. Gibbs, Conformal Transformations in Electrical Engineering, Chapman and Hall, Ltd., London, 1958.

98. W. S. Khokley and K. M. van Vliet, "Escape Mechanism of Secondary Electrons in Polar Crystals," Phys. Rev. 128, 1123 (1962).

99. A. J. Dekker, Solid State Physics, Prentice Hall, Inc., Engelwood Cliffs, New Jersey, 1957, Chapter 13.

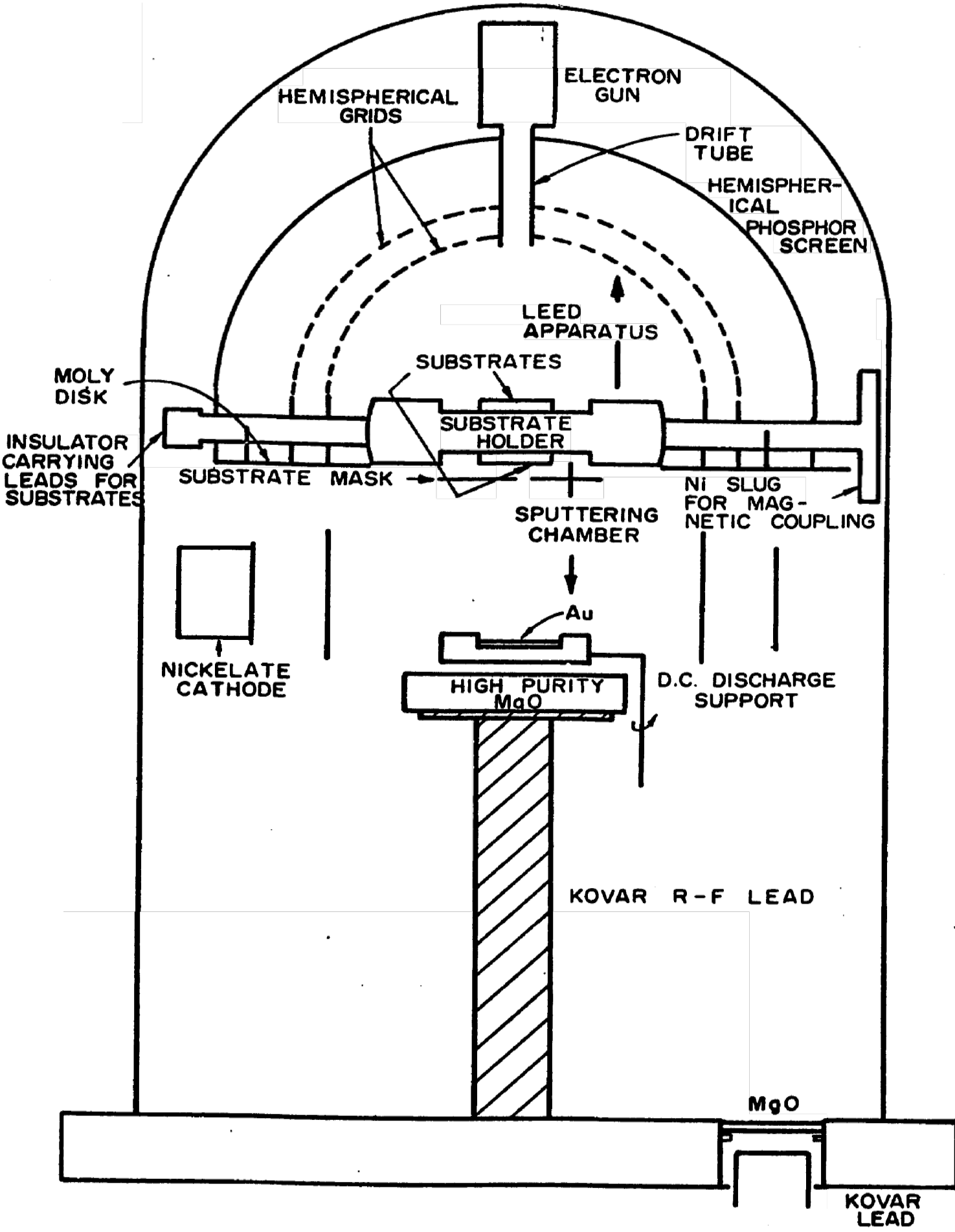
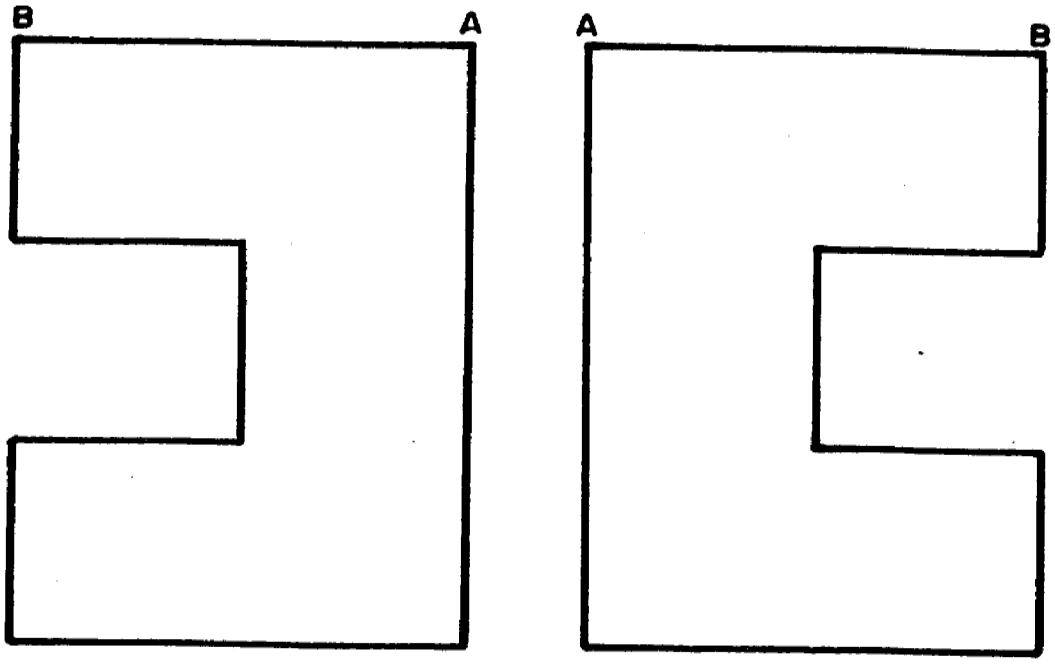
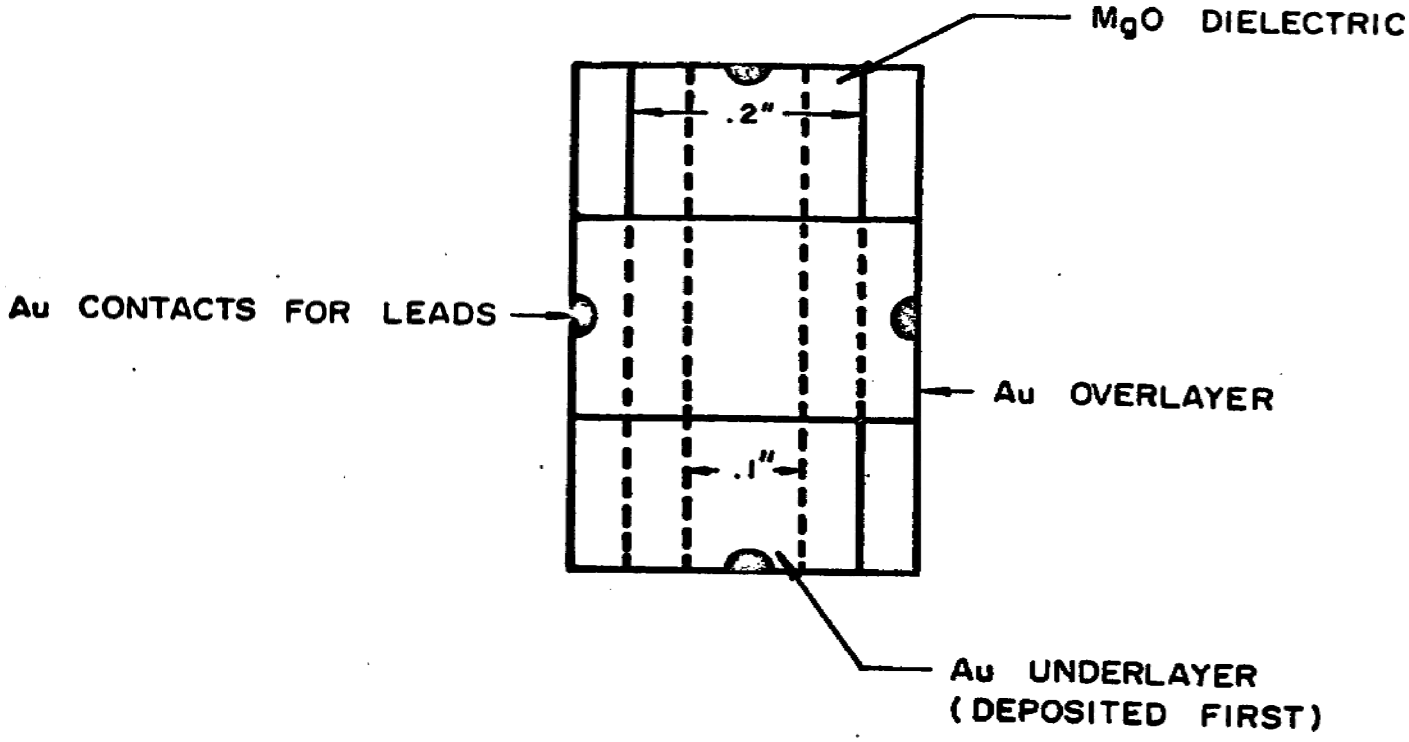



Figure 1. Schematic Representation of Initial Vacuum System Used for Depositing Ordered Au-MgO-Au Emission Diodes




2a. Substrate Masks




2b. Substrate with Au-MgO-Au Thin-Film Diode

Figure 2

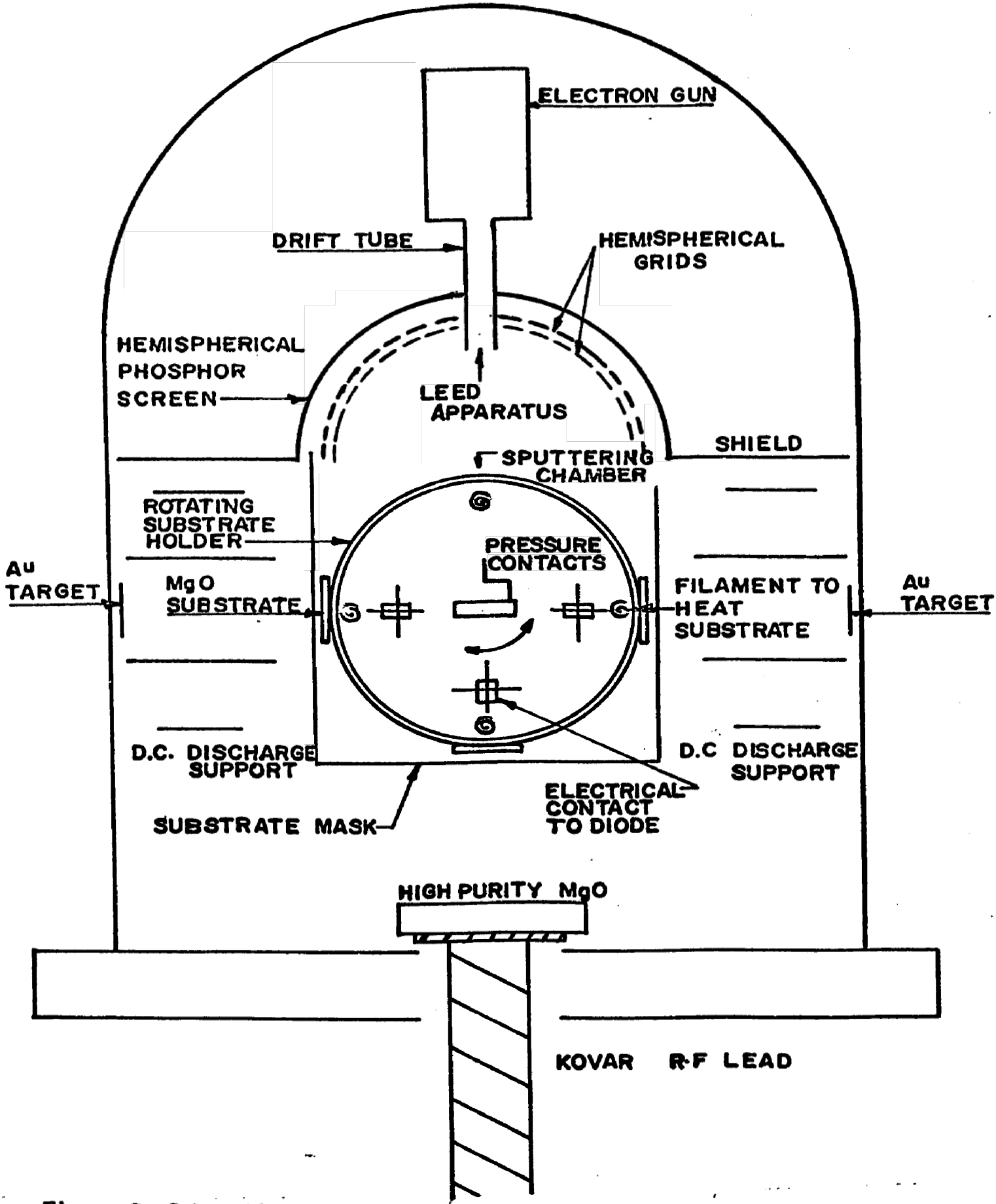



Figure 3. Schematic Representation of the Second Vacuum System Used for Depositing Ordered Au-MgO-Au Emission Diodes

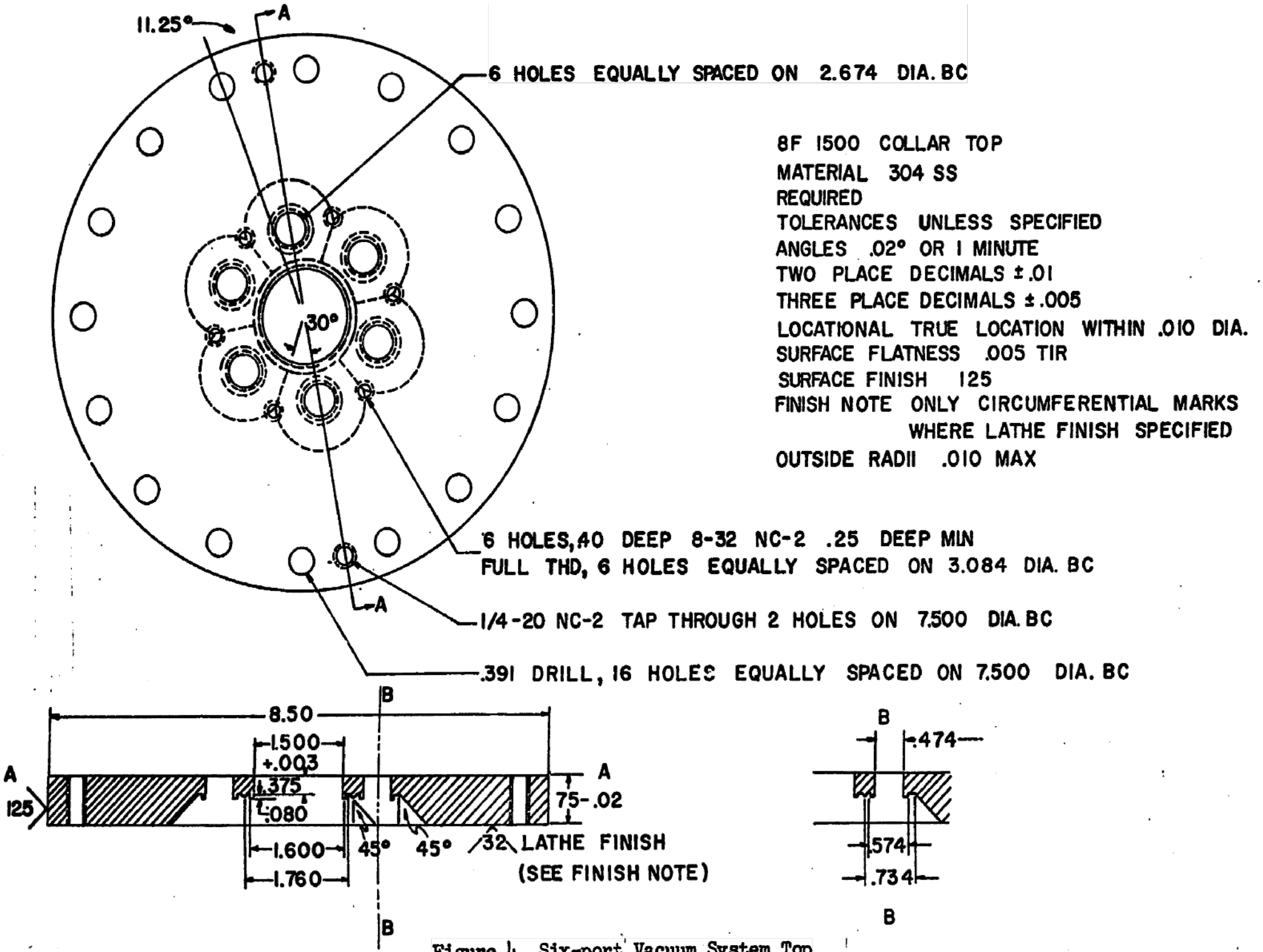



Figure 4. Six-port Vacuum System Top

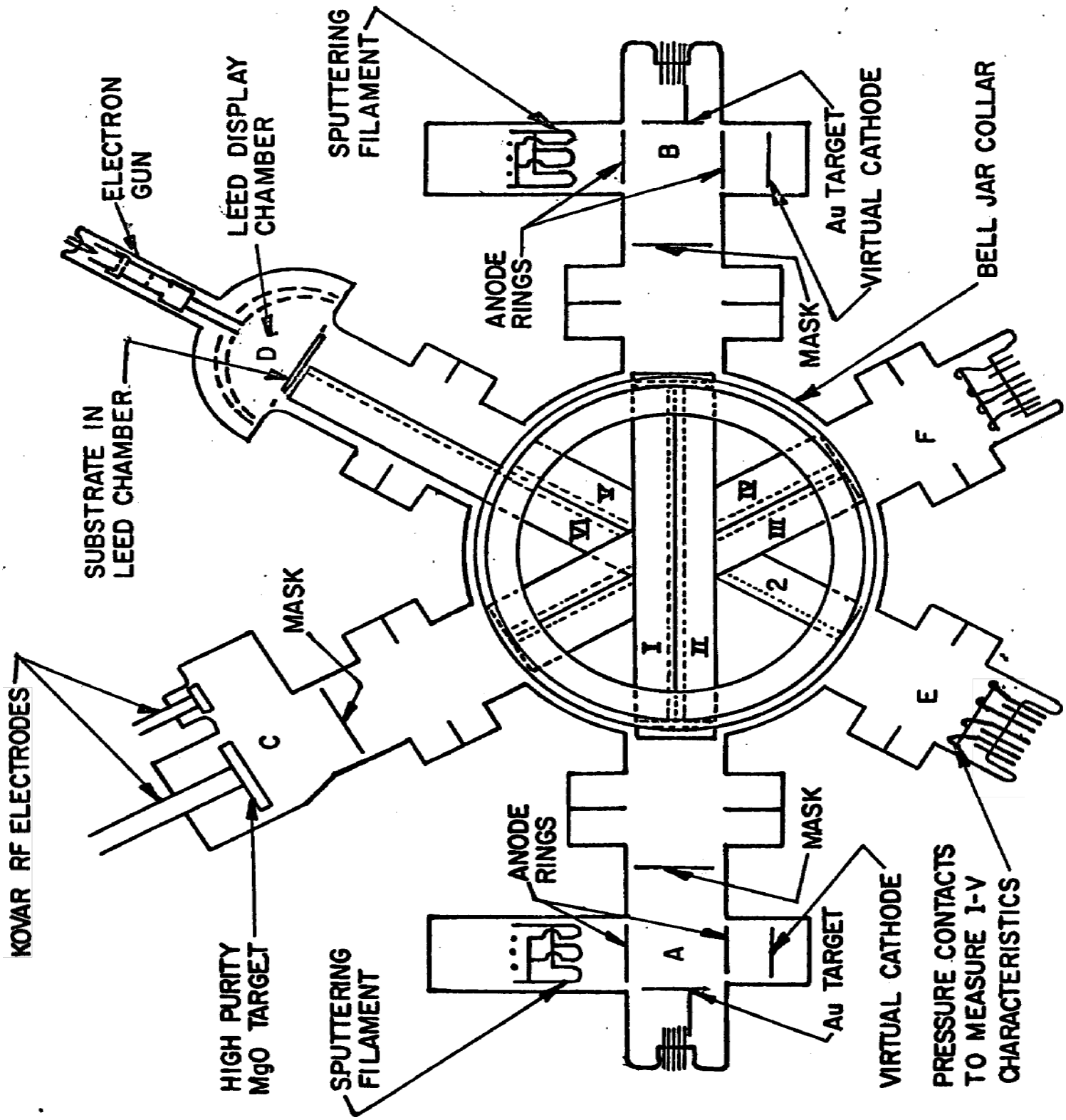



Figure 5. Schematic View of Six-port Vacuum System

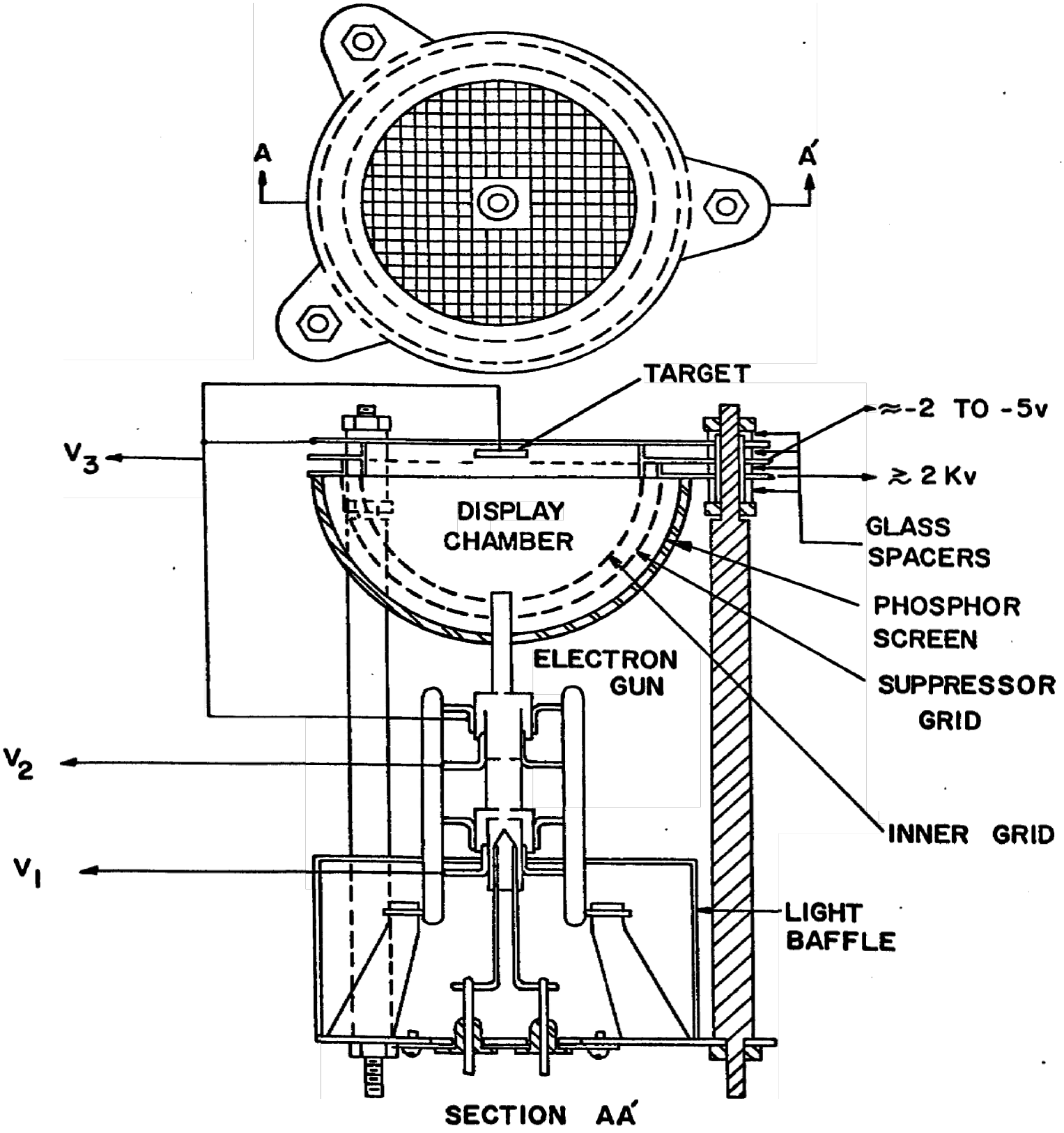



Figure 6. Detail of LEED Unit

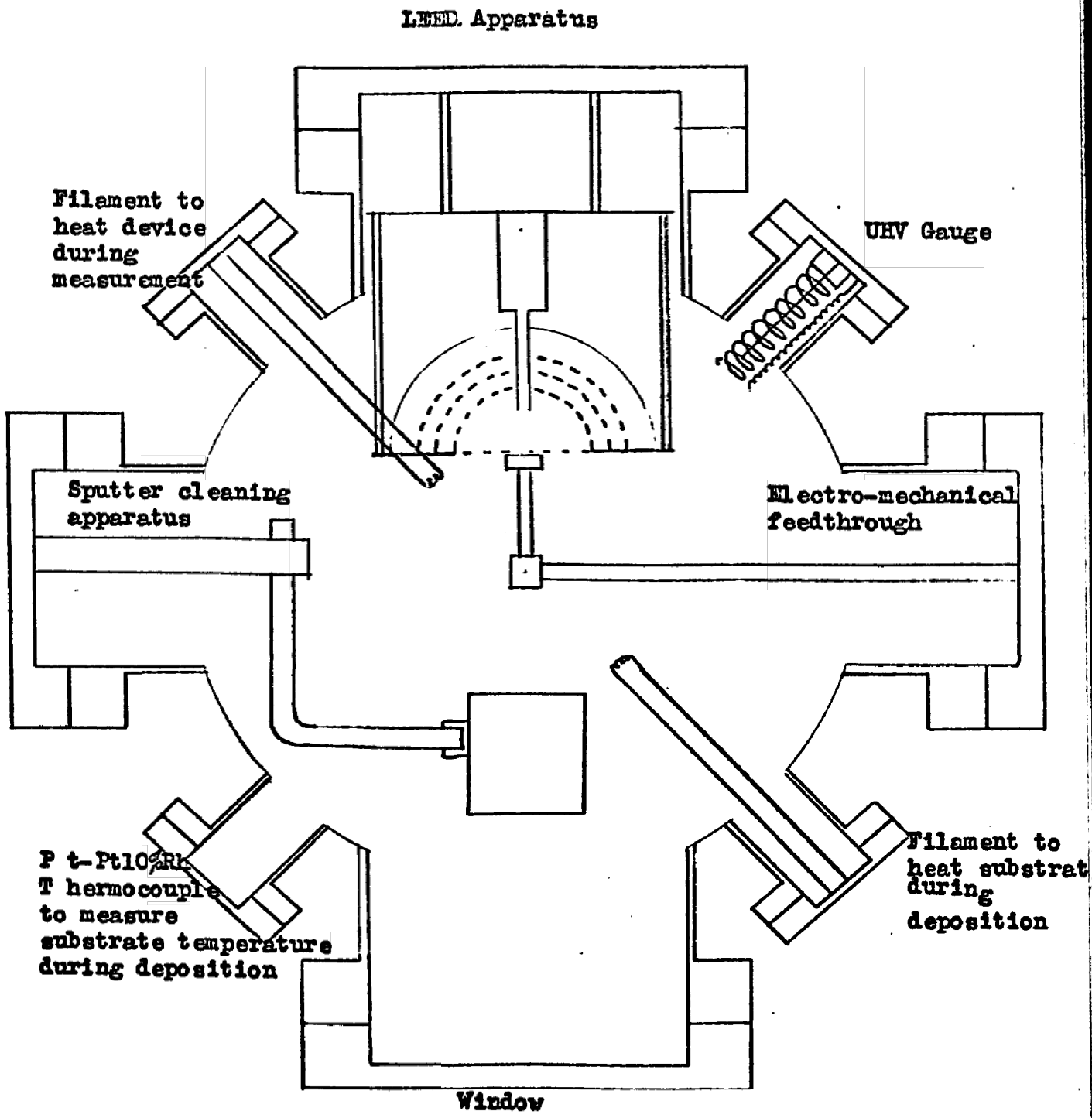
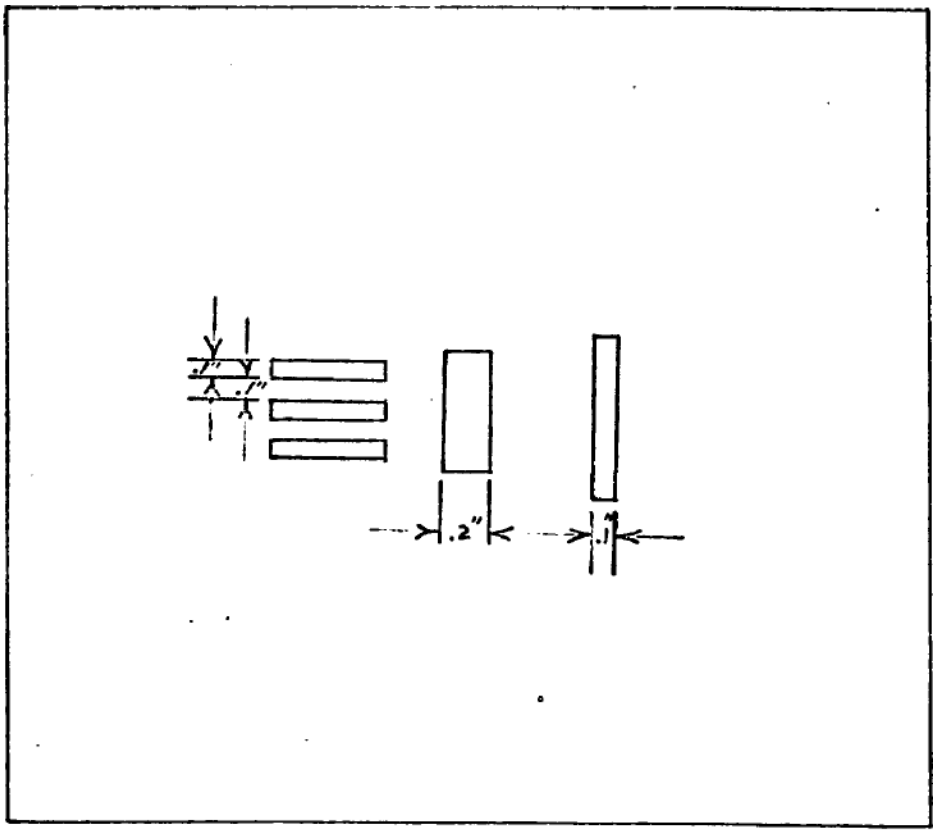
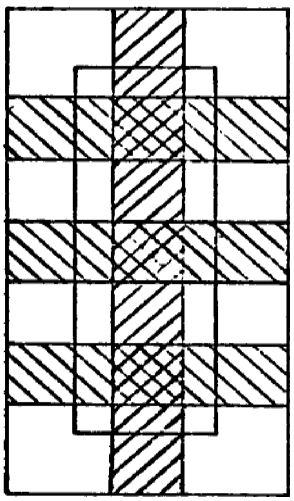



Figure7. Schematic Representation of Bell-jar Section of Final Vacuum System




8a. Mask for Final Vacuum System



8b. Substrate with 3 Metal-Insulator-Metal Emission Diodes

Figure8

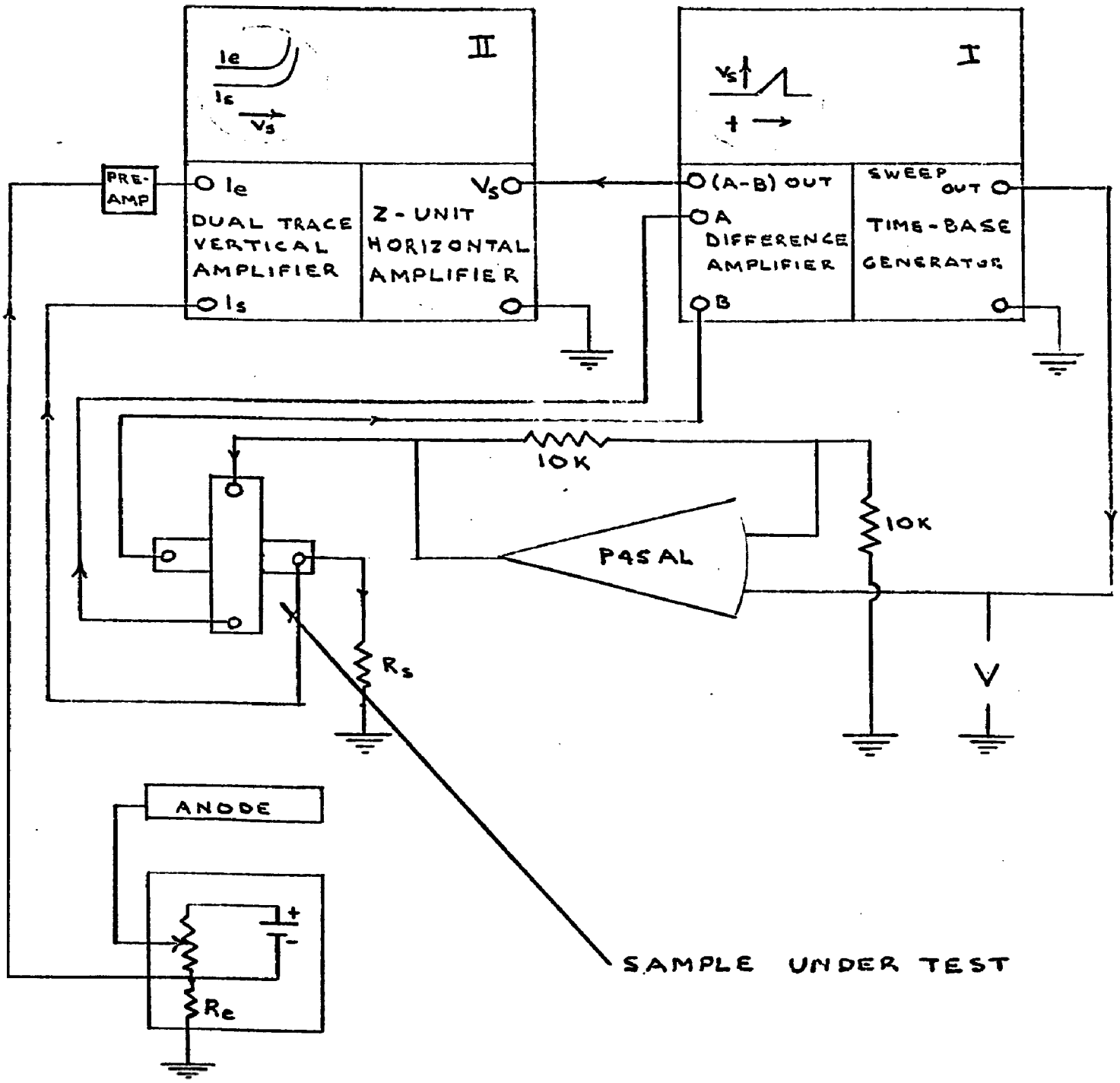


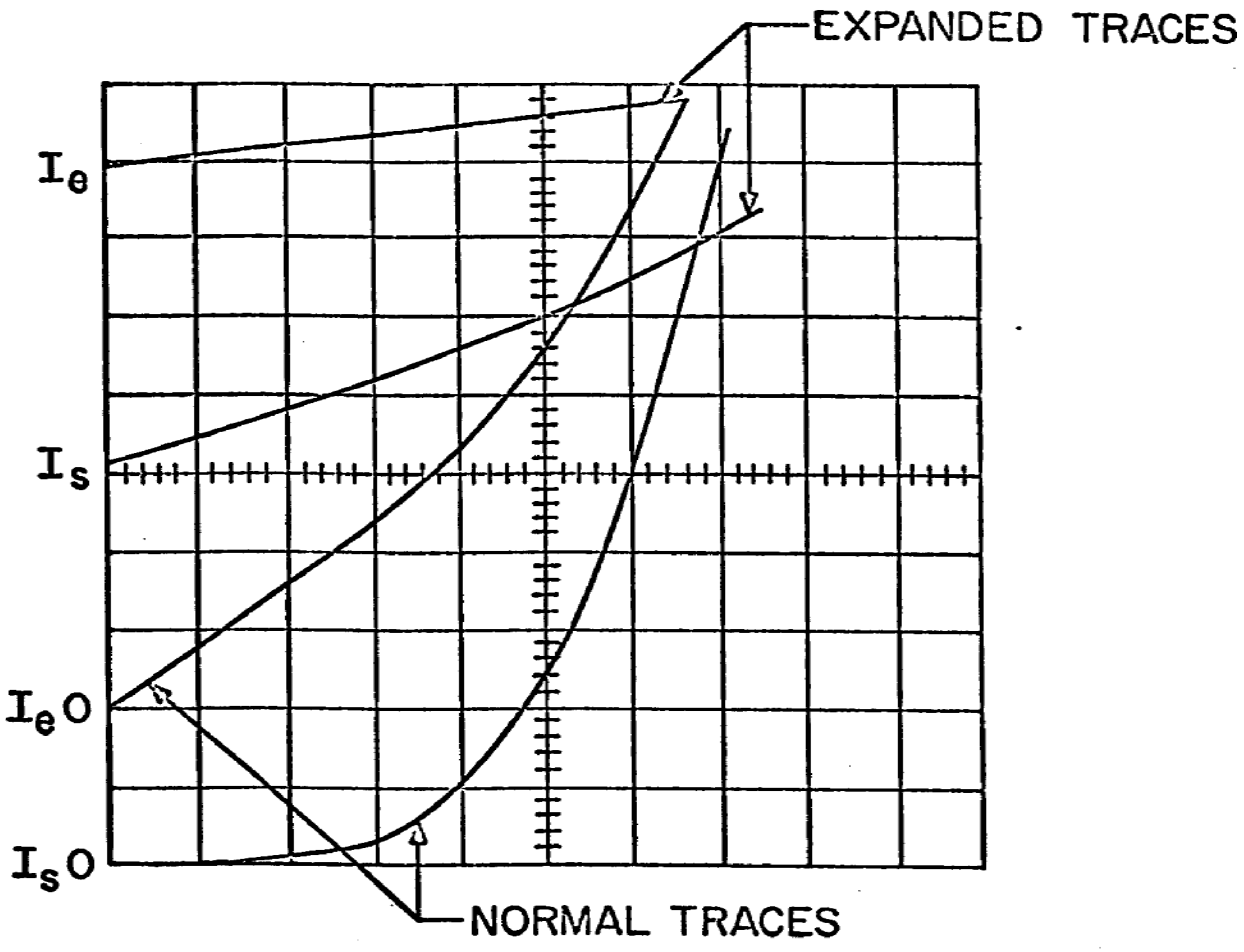

Figure 9. Circuit Used for Millisecond-Pulse Measurements of Thin-Film Hot Electron Emission Diodes

$I_s$ AND $I_e$ vs. $V_s$ FOR Au - MgO - Au

SAMPLE NO. PY-G-17

OVERLAYER NO. 1, 310° K

10 MILLISECOND PULSE




SCALES:

VERTICAL: $I_s$: 1 m A / DIVISION

$I_e$: $10^{-8}$ A / DIVISION

HORIZONTAL: $V_s$: 1.0 V / DIVISION

$V_s$: EXPANDED 0.1 VOLTS/DIVISION

ZERO SUPPRESSED 6.0 VOLTS

Figure 10. Results of Millisecond-Pulse Measurement Technique, Showing I-V Characteristics and Expanded Traces.

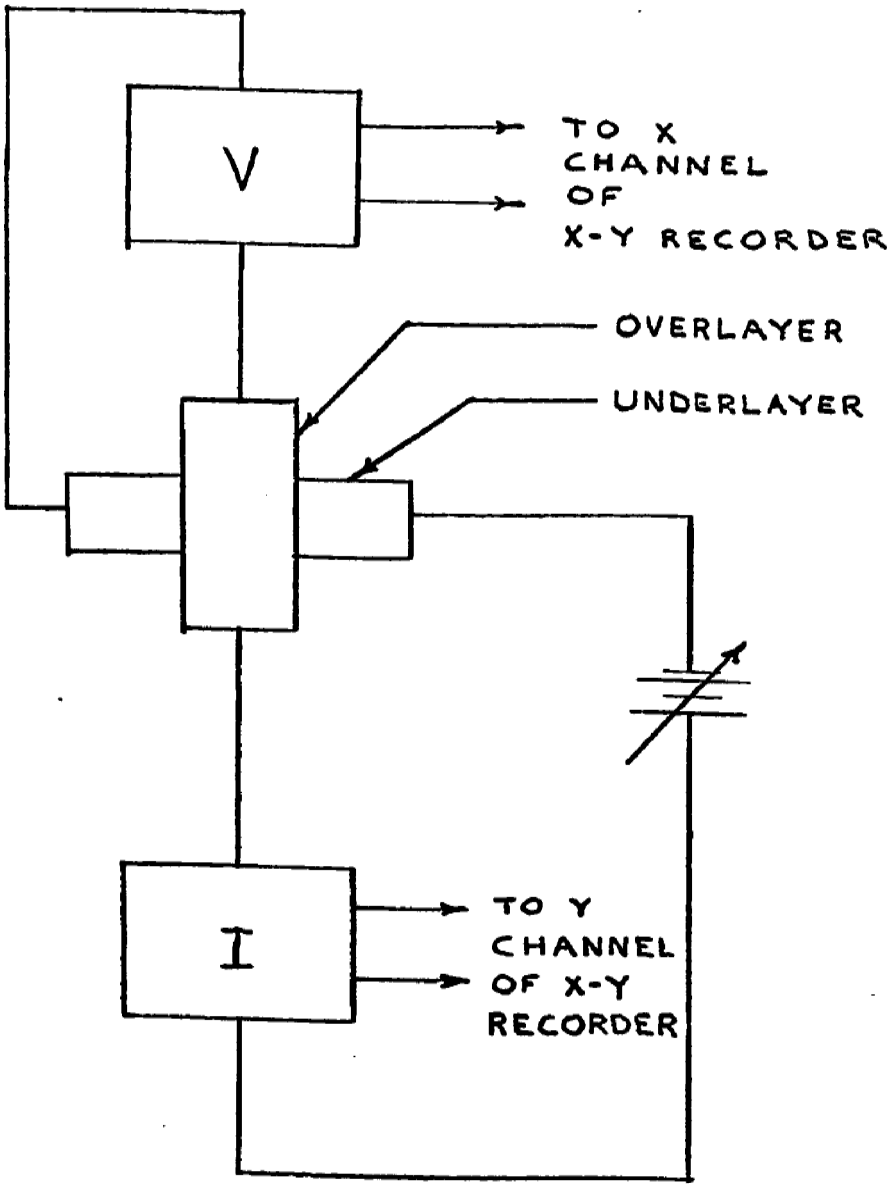



Figure 11. Schematic of DC Measurement Technique for Au-MgO-Au Emission Diodes

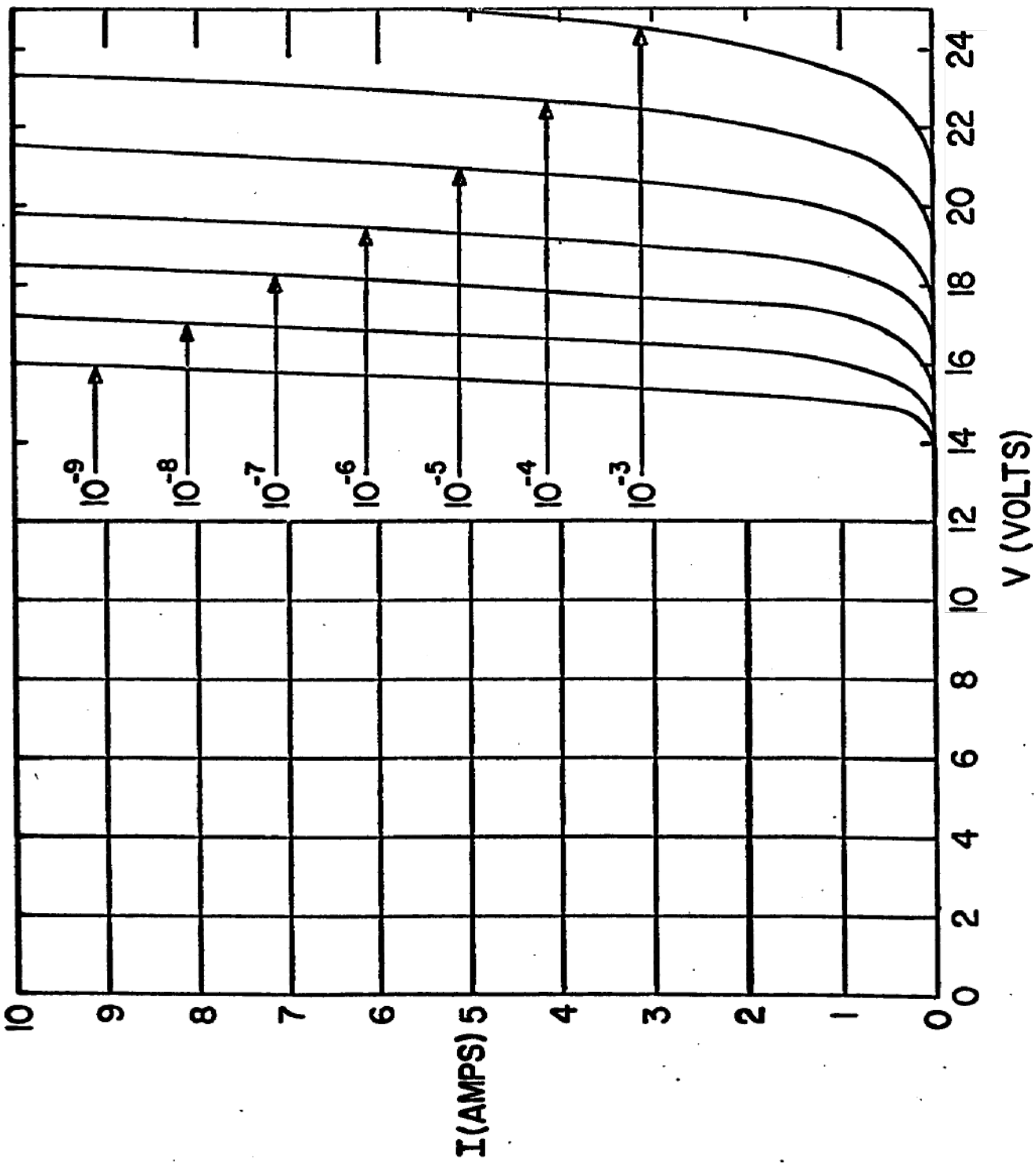



Figure 12. Tunnel I-V Characteristics of a Au-MgO-Au Device with an 89Å Thick Oxide

I-V CHARACTERISTICS FROM
DEVICE PY-G-II
OVERLAYER I 313°K
89 Å OXIDE

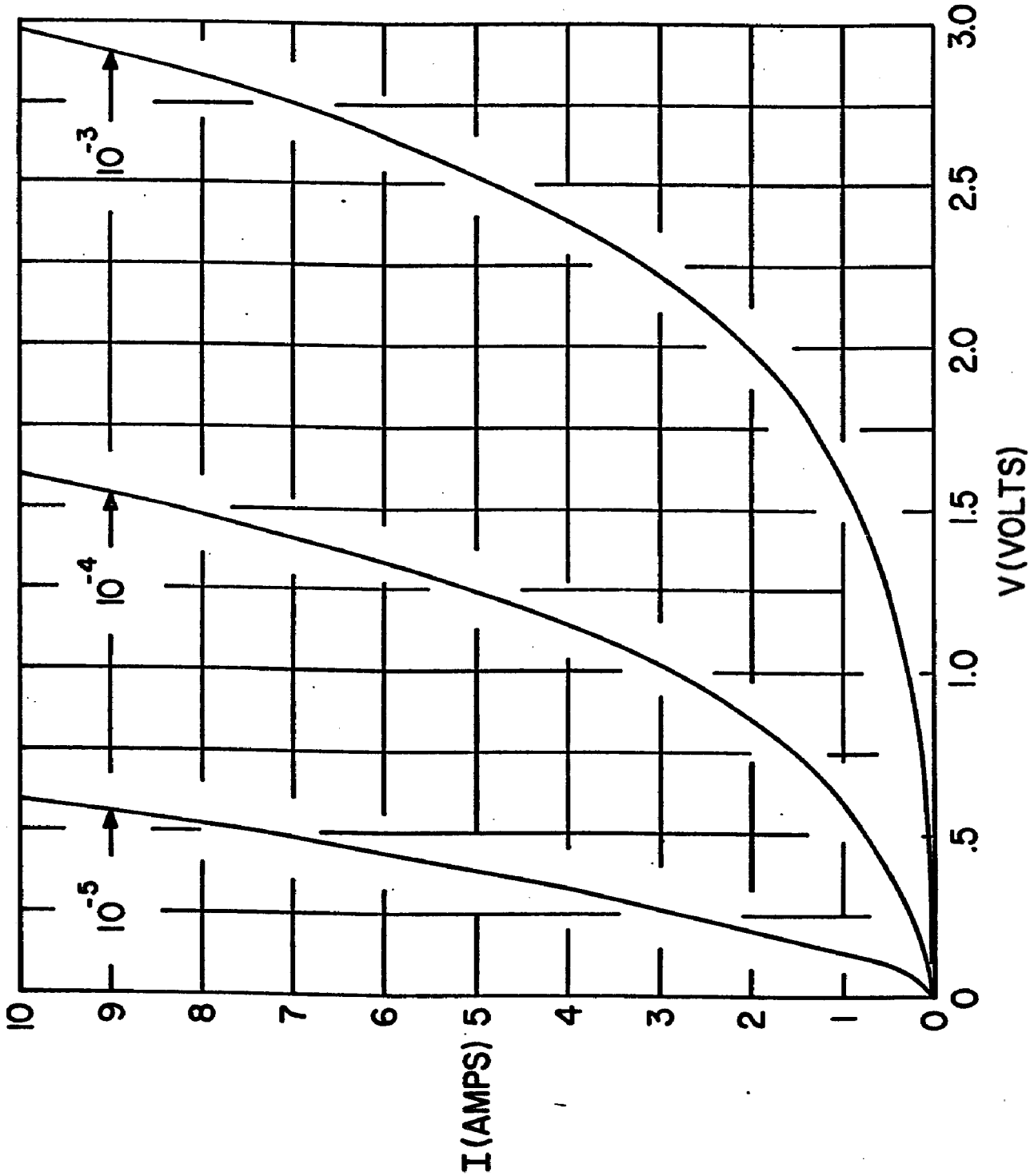



Figure 13

FOWLER-NORDHEIM PLOT OF I-V CHARACTERISTICS OF DEVICE PY-G-11 OVERLAYER 1

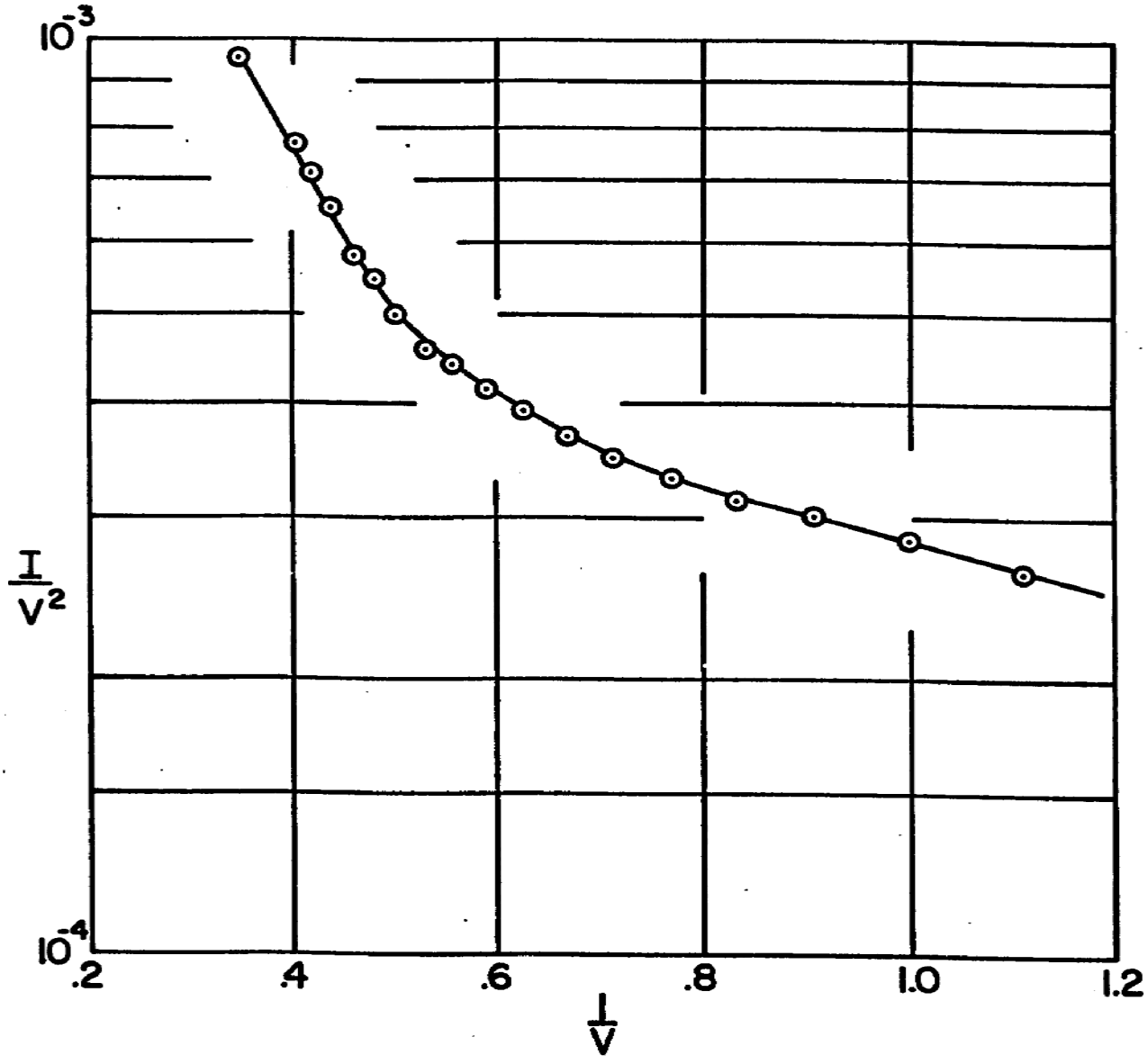



Figure 14

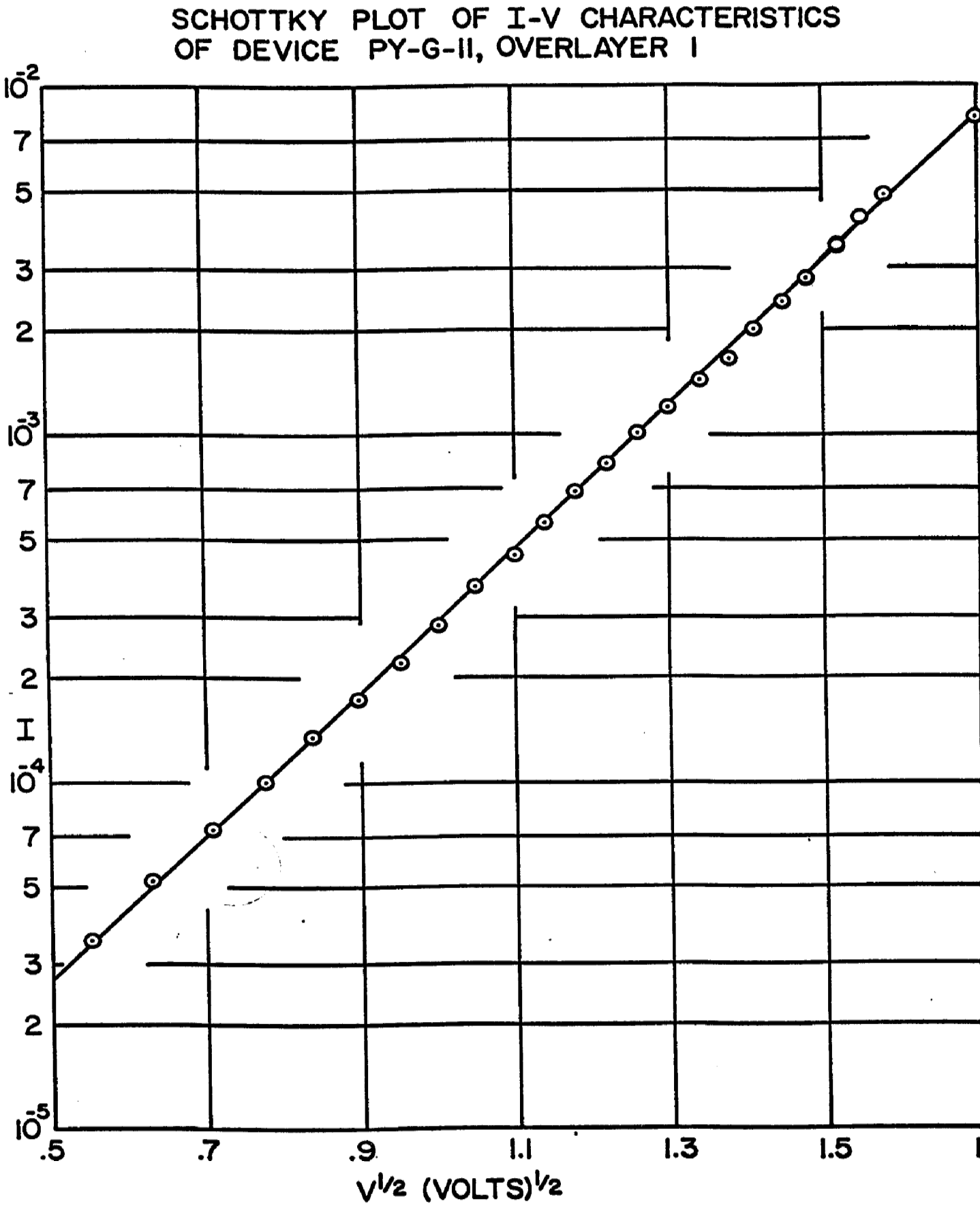

SCHOTTKY PLOT OF I-V CHARACTERISTICS
OF DEVICE PY-G-II, OVERLAYER I
$10^{-2}$
7
5
3
2
$10^{-3}$
7
5
3
2
I
$10^{-4}$
7
5
3
2
$10^{-5}$
.5
.7
.9
1.1
1.3
1.5
$V^{1/2}$ (VOLTS)$^{1/2}$

Figure 15

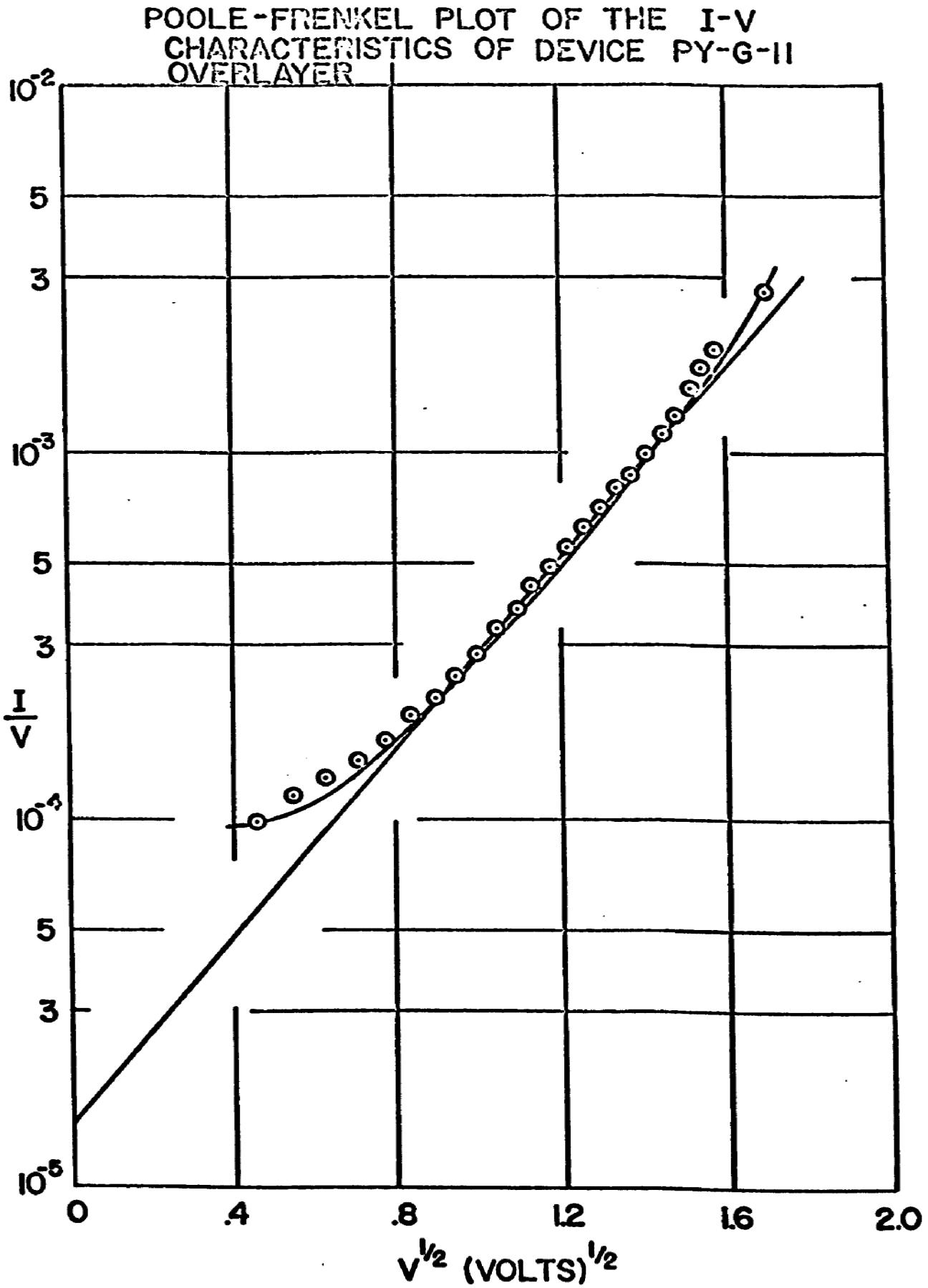

POOLE-FRENKEL PLOT OF THE I-V CHARACTERISTICS OF DEVICE PY-G-II OVERLAYER
10-2
5
3
10-3
5
3
I/V
10-4
5
3
10-5
0
.4
.8
1.2
1.6
2.0
V1/2 (VOLTS)1/2

Figure 16

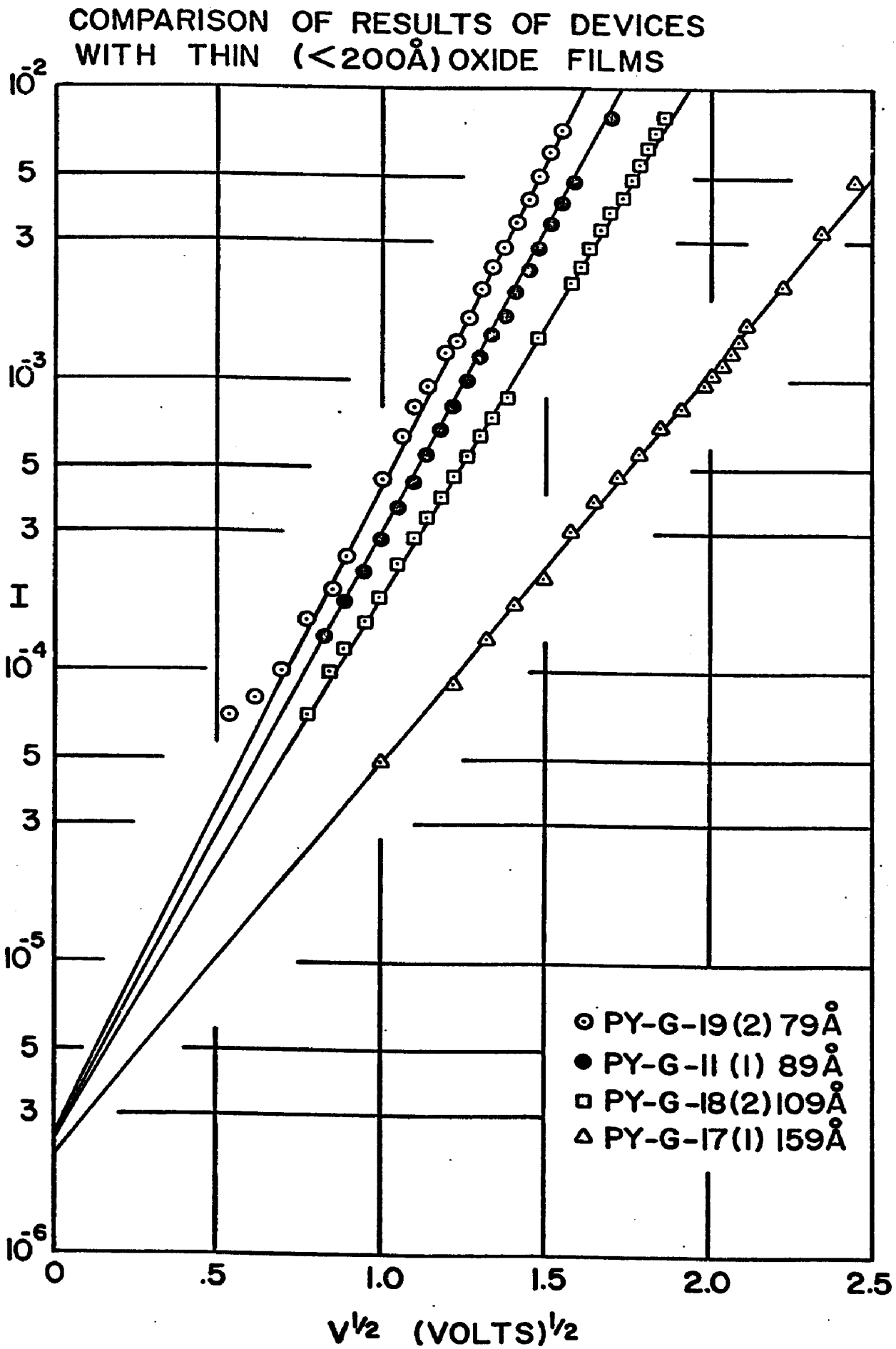

COMPARISON OF RESULTS OF DEVICES
WITH THIN (<200Å) OXIDE FILMS
10⁻²
5
3
10⁻³
5
3
I
10⁻⁴
5
3
10⁻⁵
5
3
10⁻⁶
0
.5
1.0
1.5
2.0
2.5
V½ (VOLTS)½
PY-G-19(2) 79Å
PY-G-11 (1) 89Å
PY-G-18(2)109Å
PY-G-17(1) 159Å

Figure 17

Ln I VS. $V^{1/2}$ PLOT FOR TWO DEVICES WITH THICKER OXIDE FILMS (680 Å)

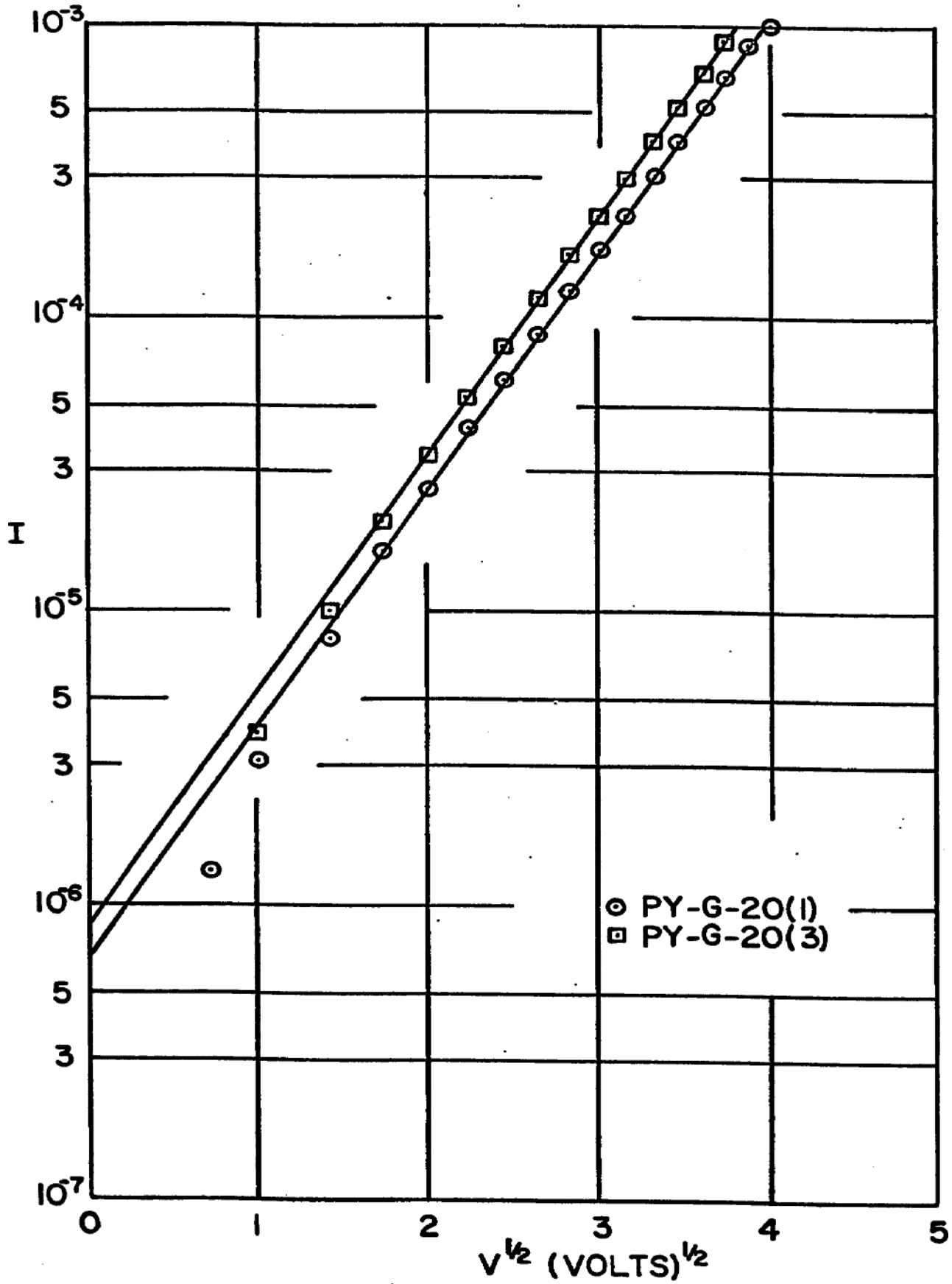



Figure 18

TEMPERATURE DEPENDENCE OF I-V CHARACTERISTICS OF DEVICE PY-G-II OVERLAYER I

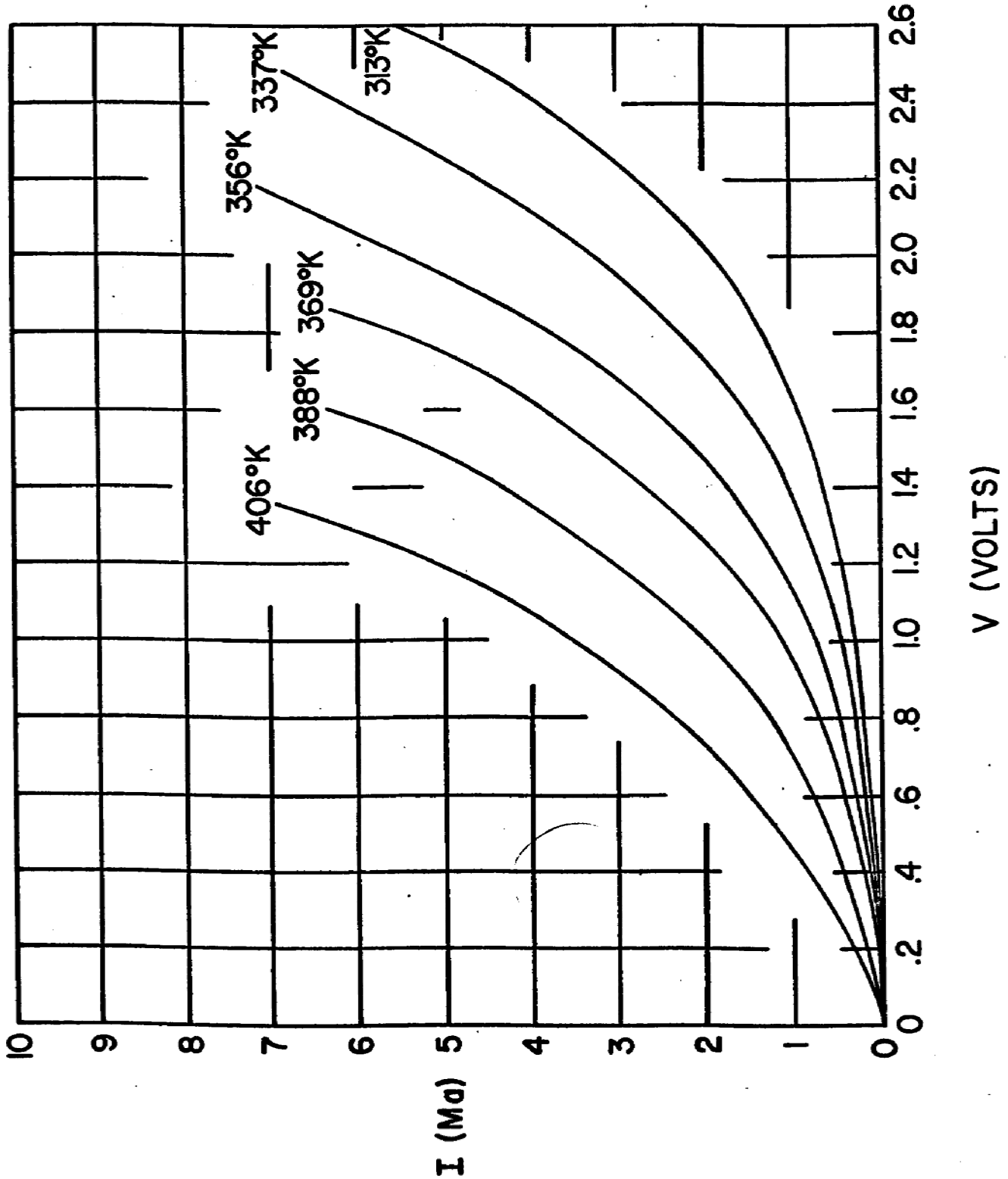



Figure 19

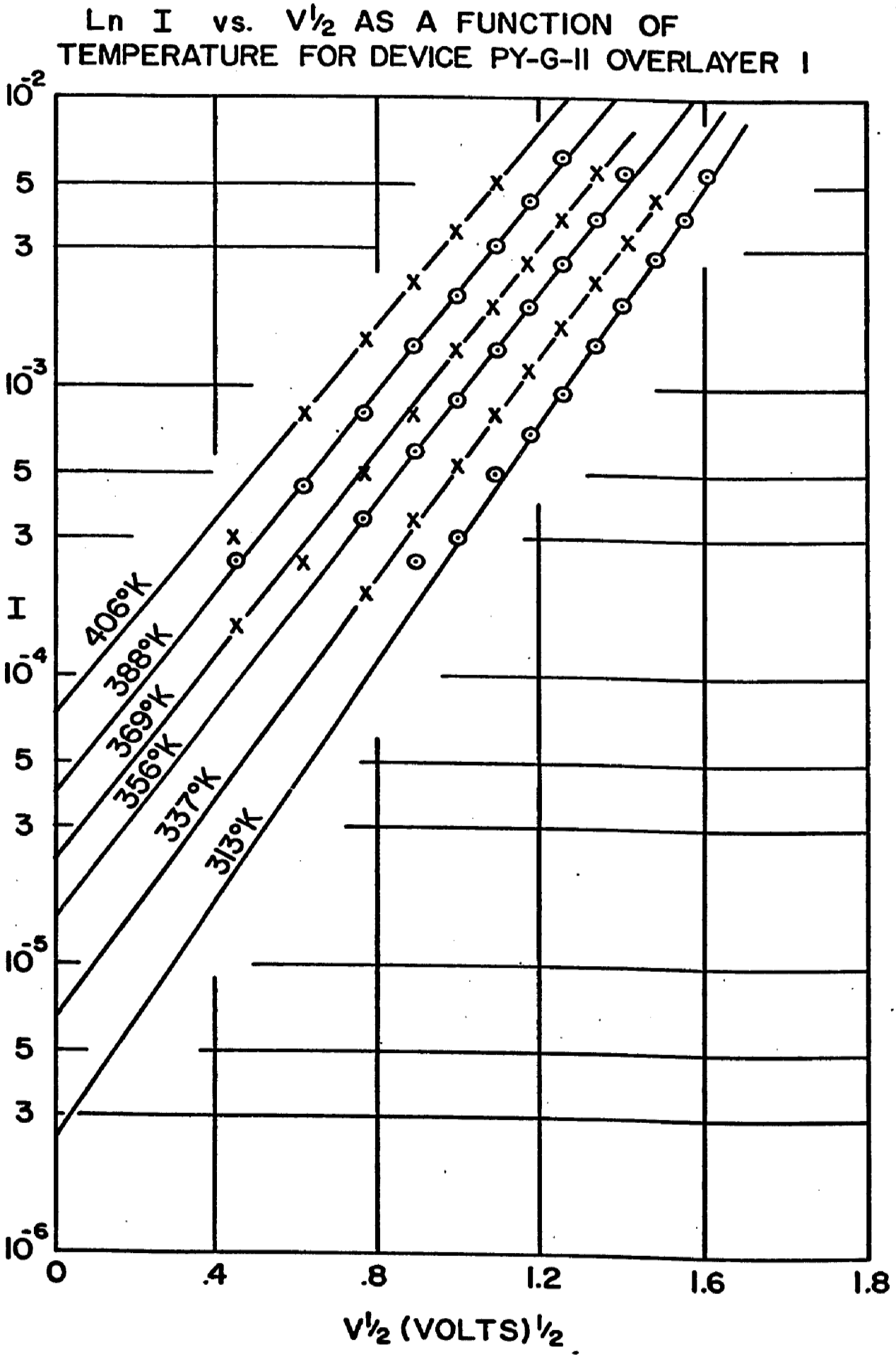

Ln I vs. V½ AS A FUNCTION OF
TEMPERATURE FOR DEVICE PY-G-II OVERLAYER I
10⁻²
5
3
10⁻³
5
3
I
10⁻⁴
5
3
10⁻⁵
5
3
10⁻⁶
406°K
388°K
369°K
356°K
337°K
313°K
0
.4
.8
1.2
1.6
1.8
V½ (VOLTS)½

Figure 20

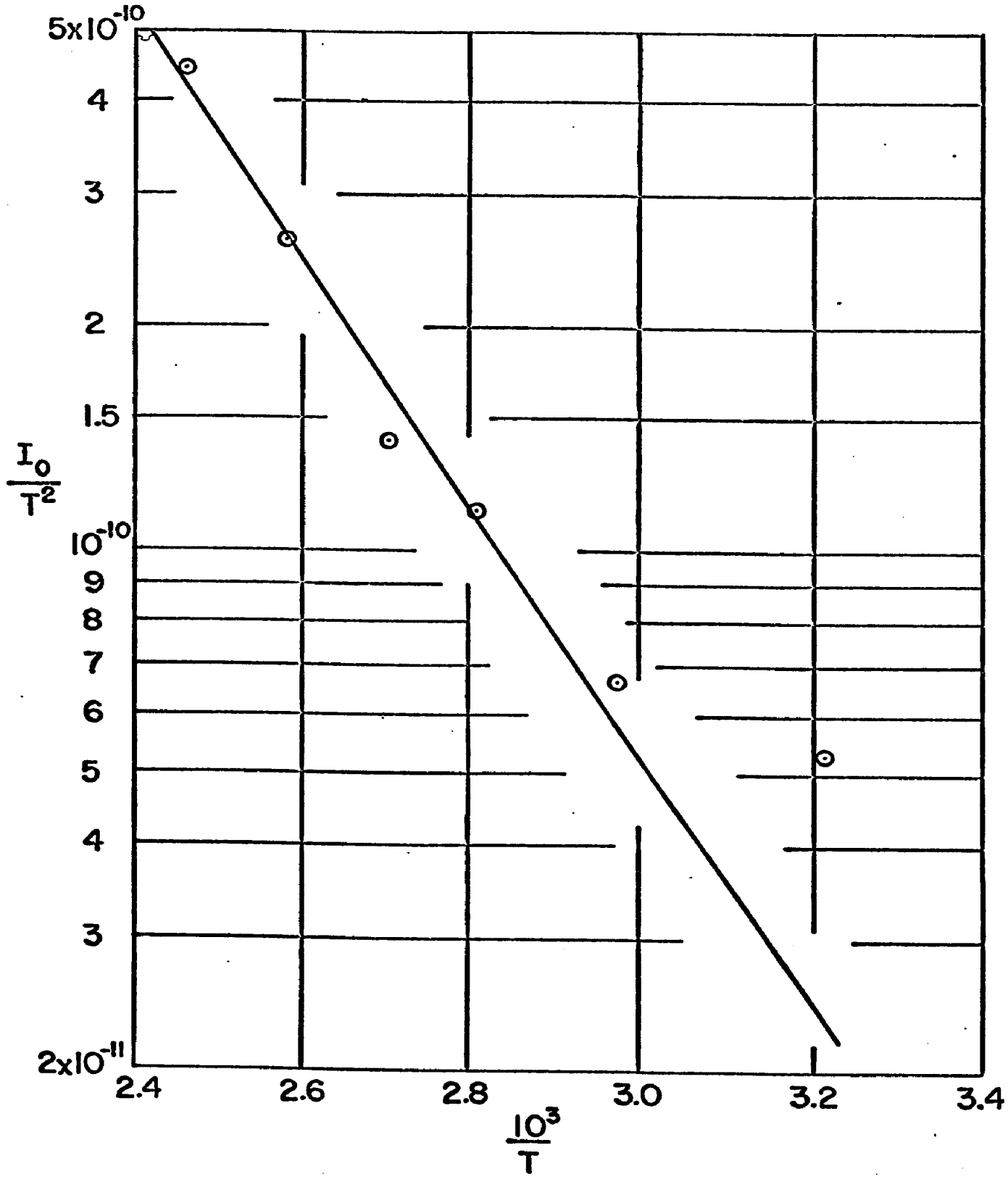

Ln ($I_0/T^2$) VS. $10^3/T$ FOR DEVICE PY-G-II, OVERLAYER I.
$5\times10^{-10}$
4
3
2
1.5
$10^{-10}$
9
8
7
6
5
4
3
$2\times10^{-11}$
$\frac{I_0}{T^2}$
2.4
2.6
2.8
3.0
3.2
3.4
$\frac{10^3}{T}$

Figure 21

COMPARISON OF RESULTS WITH DIFFERENT PRESSURES OF OXYGEN PRESENT DURING FABRICATION

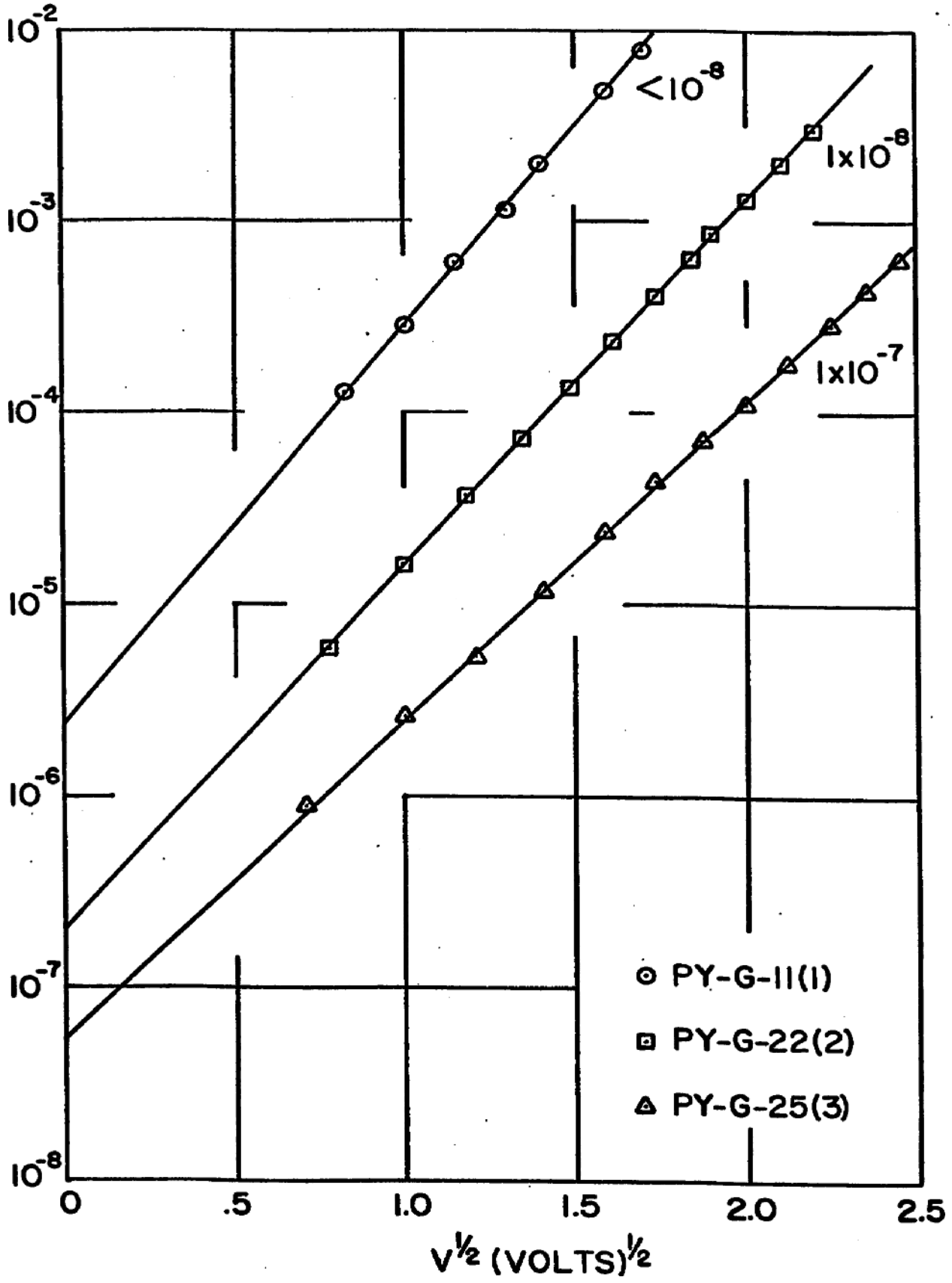



Figure 22

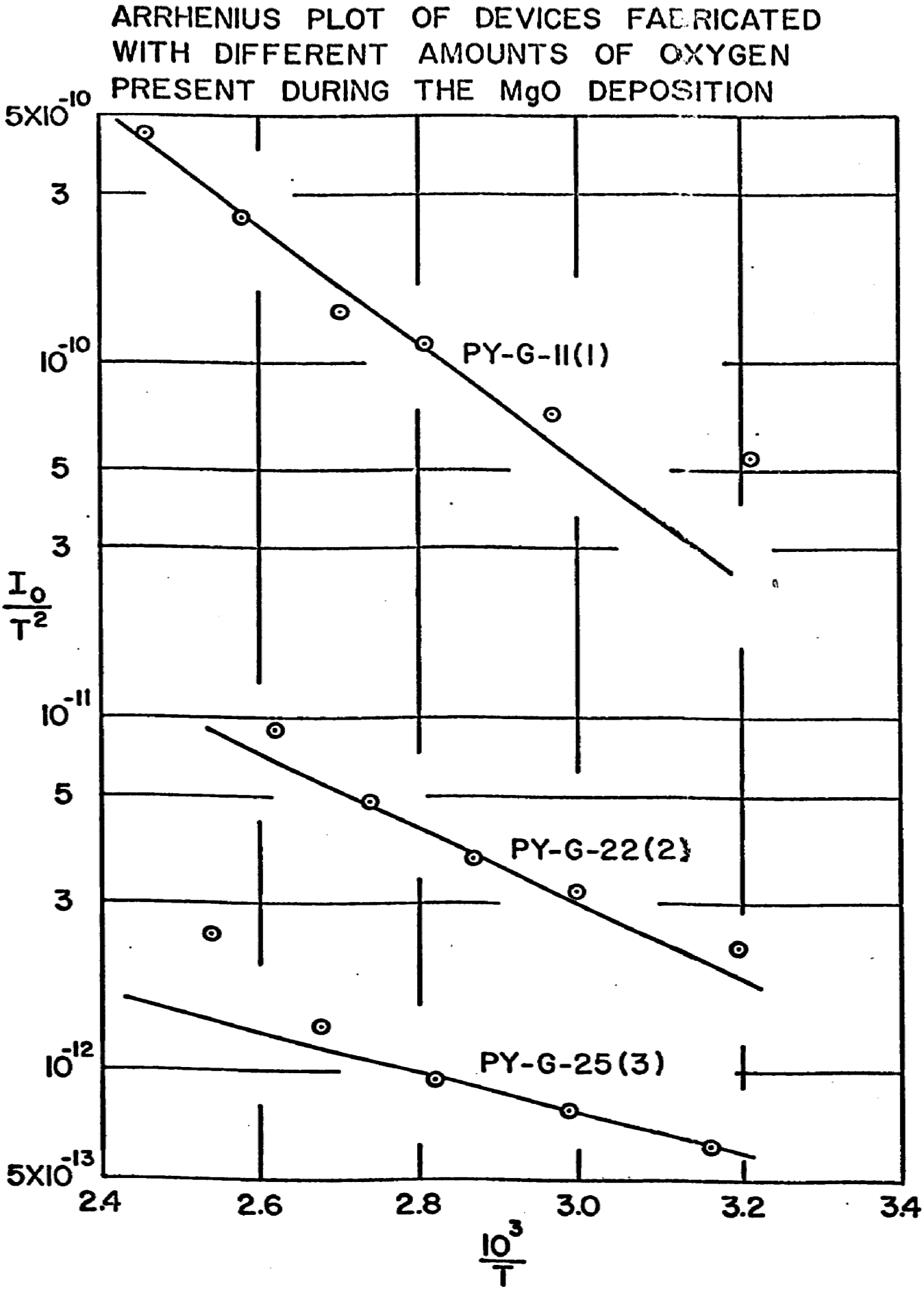
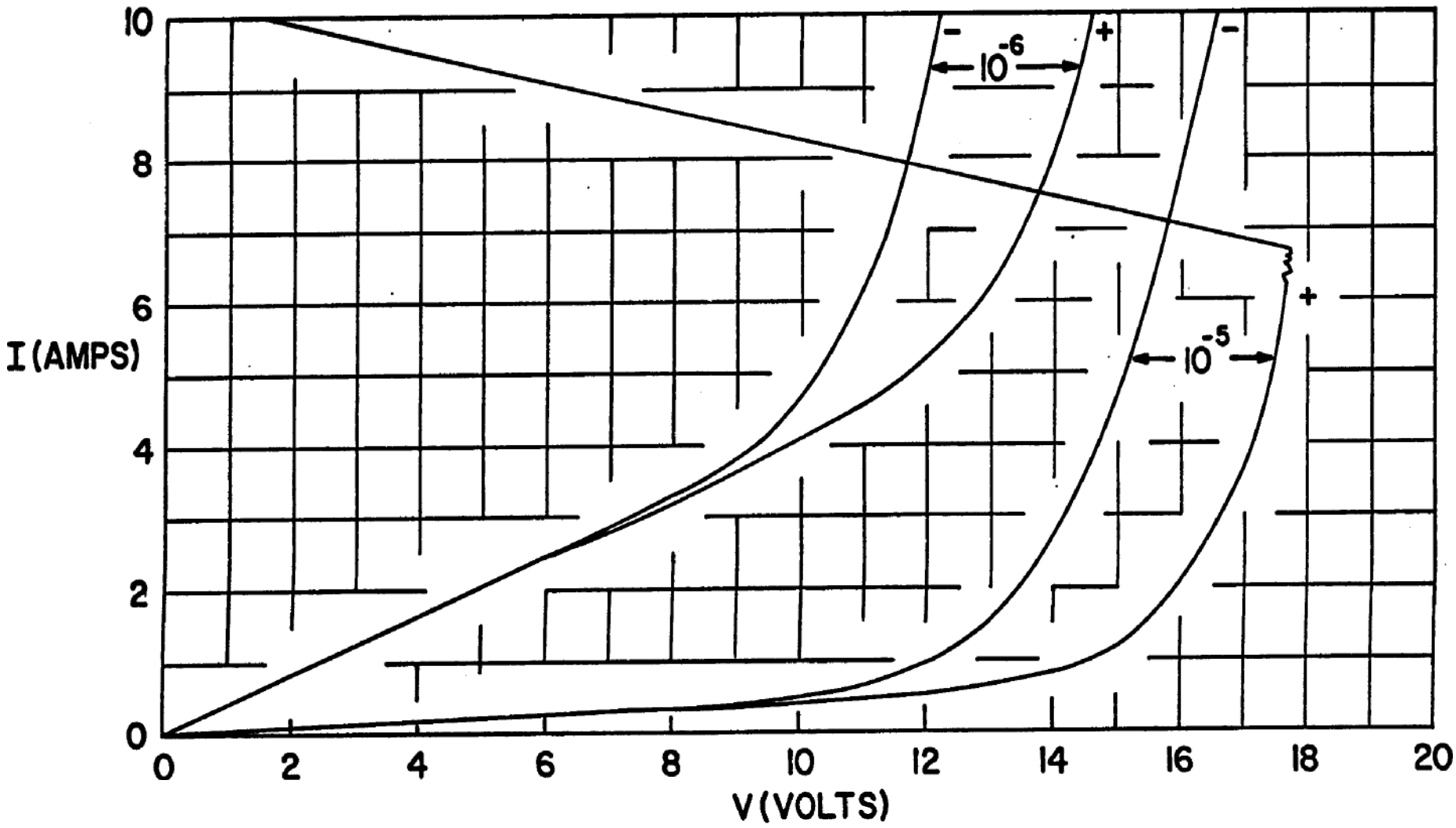

ARRHENIUS PLOT OF DEVICES FABRICATED WITH DIFFERENT AMOUNTS OF OXYGEN PRESENT DURING THE MgO DEPOSITION
5X10-10
3
10-10
5
3
10-11
5
3
10-12
5X10-13
I0/T2
PY-G-11(1)
PY-G-22(2)
PY-G-25(3)
2.4
2.6
2.8
3.0
3.2
3.4
10^3/T

Figure 23

# I - V CHARACTERISTICS OF DEVICE PY-G-38(1)



FOWLER-NORDHEIM PLOT OF I - V CHARACTERISTICS OF DEVICE PY-G-38(1)

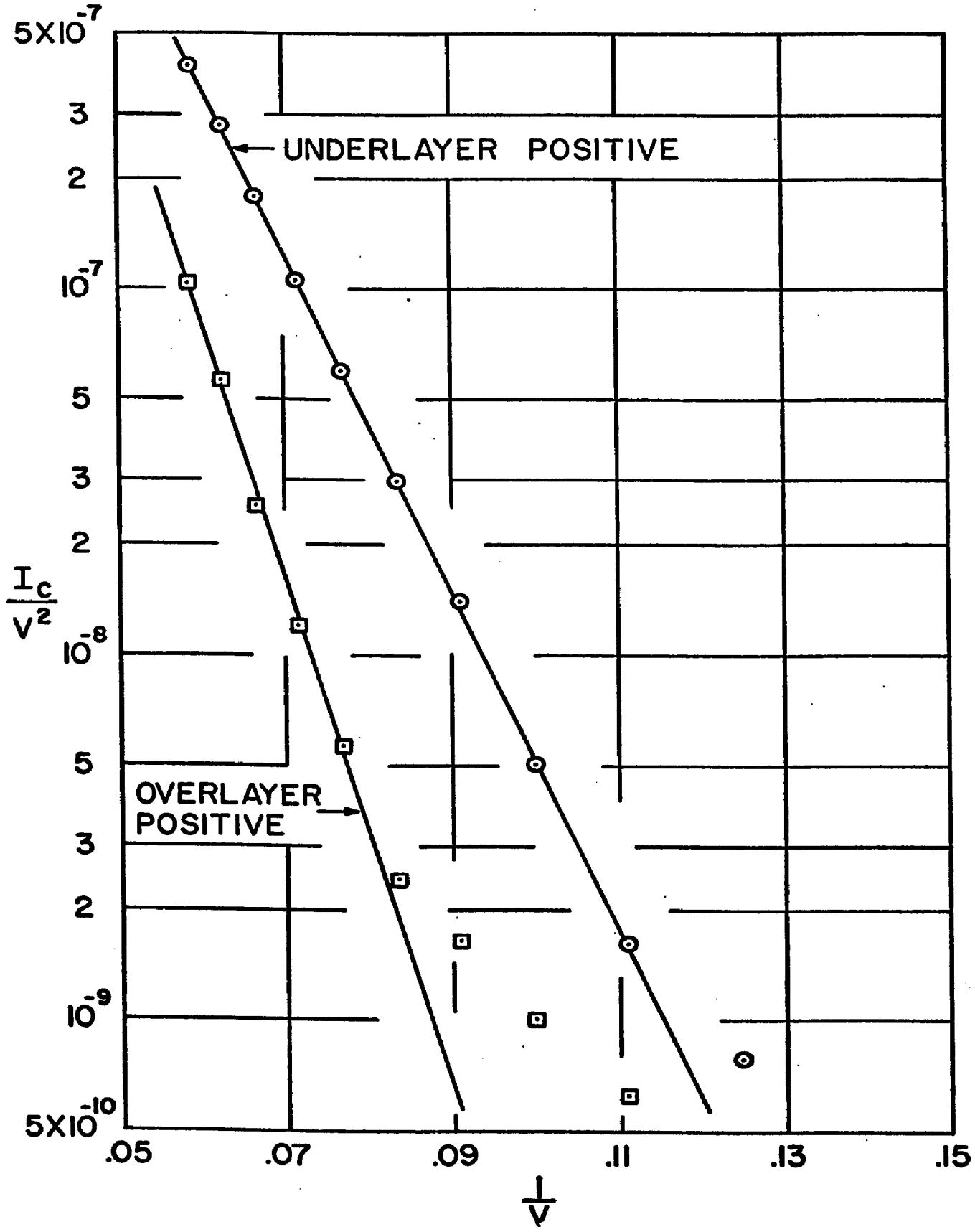



Figure 25

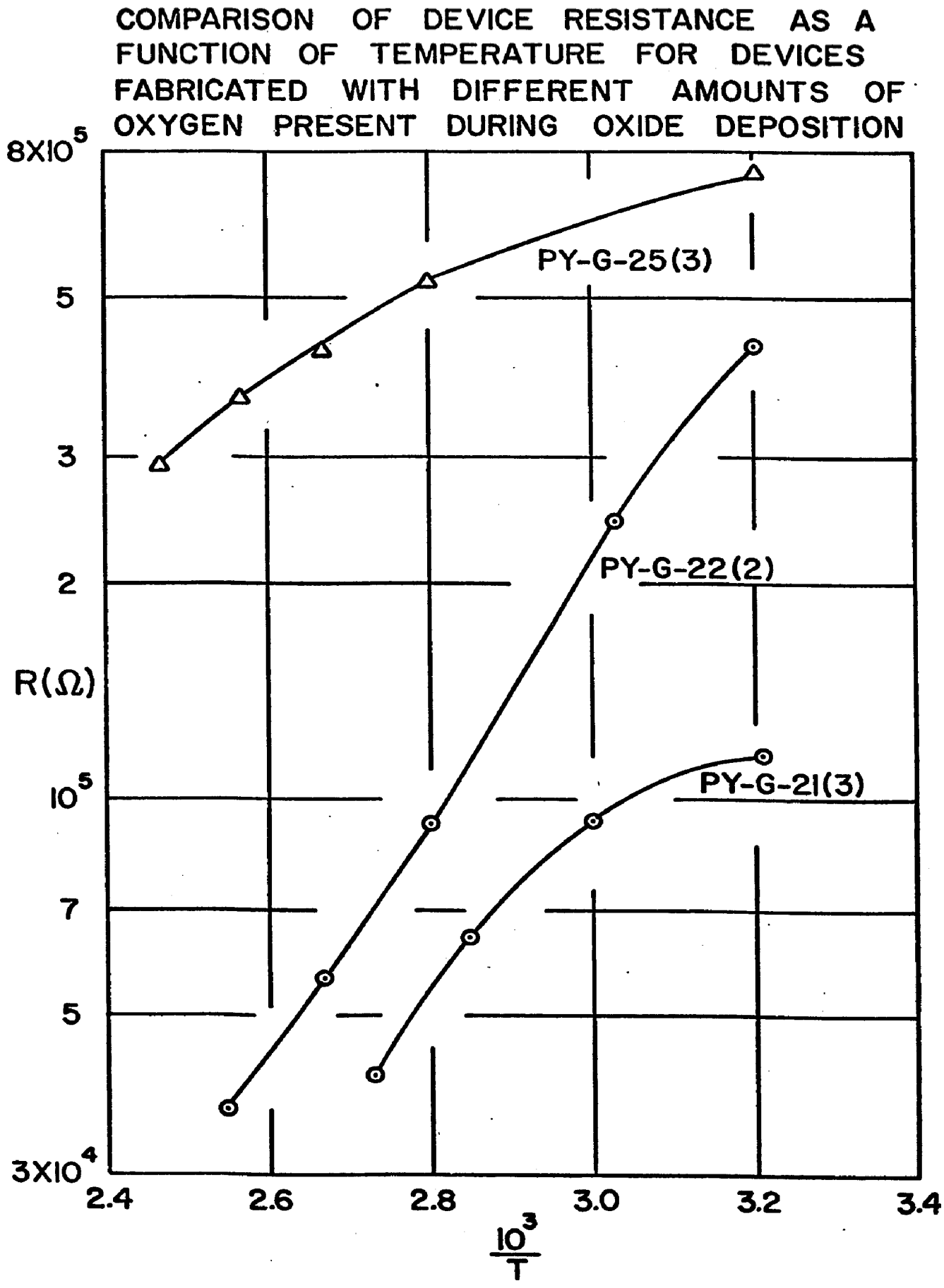

COMPARISON OF DEVICE RESISTANCE AS A FUNCTION OF TEMPERATURE FOR DEVICES FABRICATED WITH DIFFERENT AMOUNTS OF OXYGEN PRESENT DURING OXIDE DEPOSITION
8X10^5
5
3
2
R(Ω)
10^5
7
5
3X10^4
PY-G-25(3)
PY-G-22(2)
PY-G-21(3)
2.4
2.6
2.8
3.0
3.2
3.4
10^3/T

Figure 26

EMISSION TRANSFER RATIO, $\alpha$, VS. SAMPLE VOLTAGE, $V_s$, FOR DEVICE PY-G-11(1)

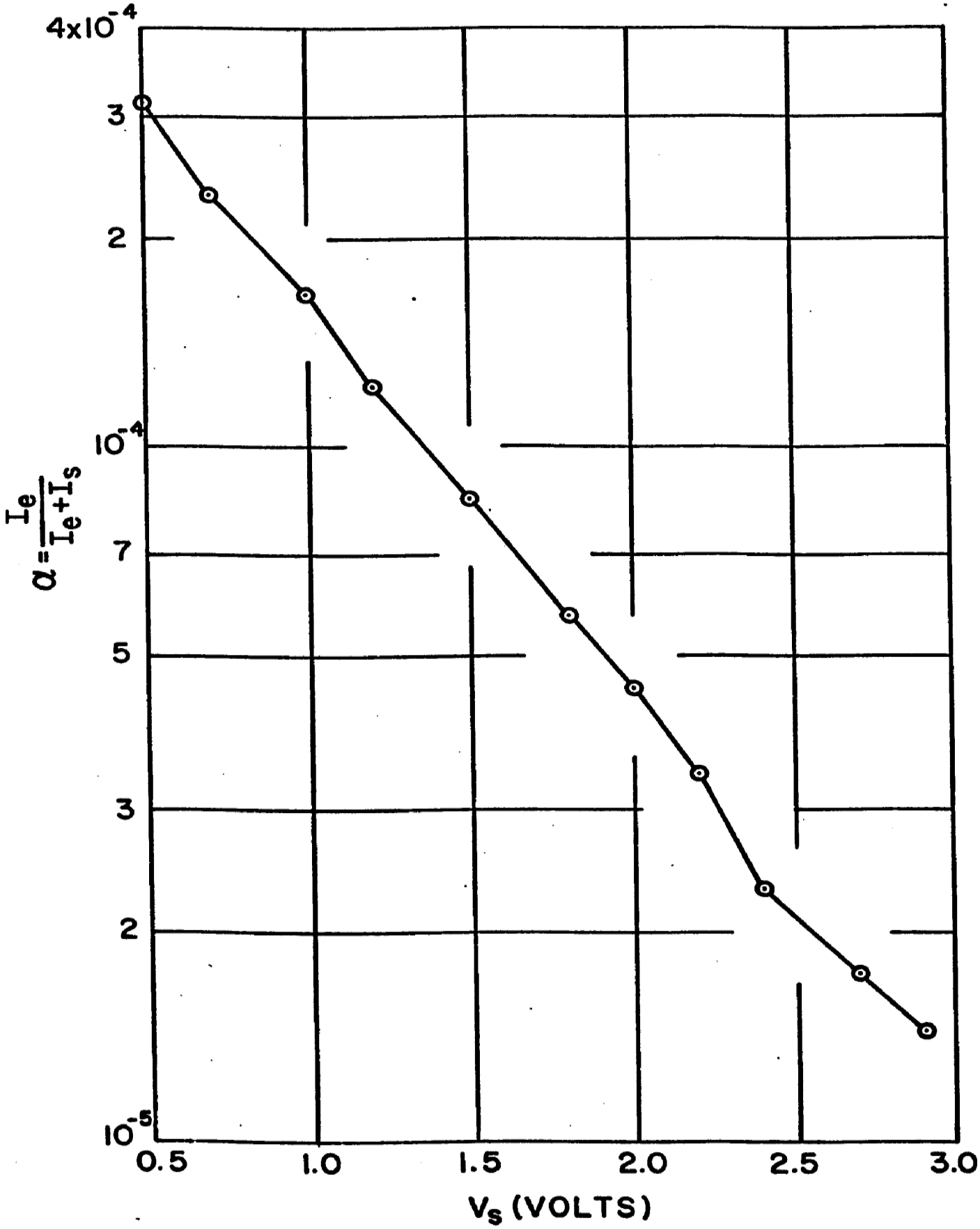



Figure 27

COMPARISON OF EMISSION TRANSFER RATIO FOR DEVICES WITH DIFFERENT OXIDE THICKNESSES

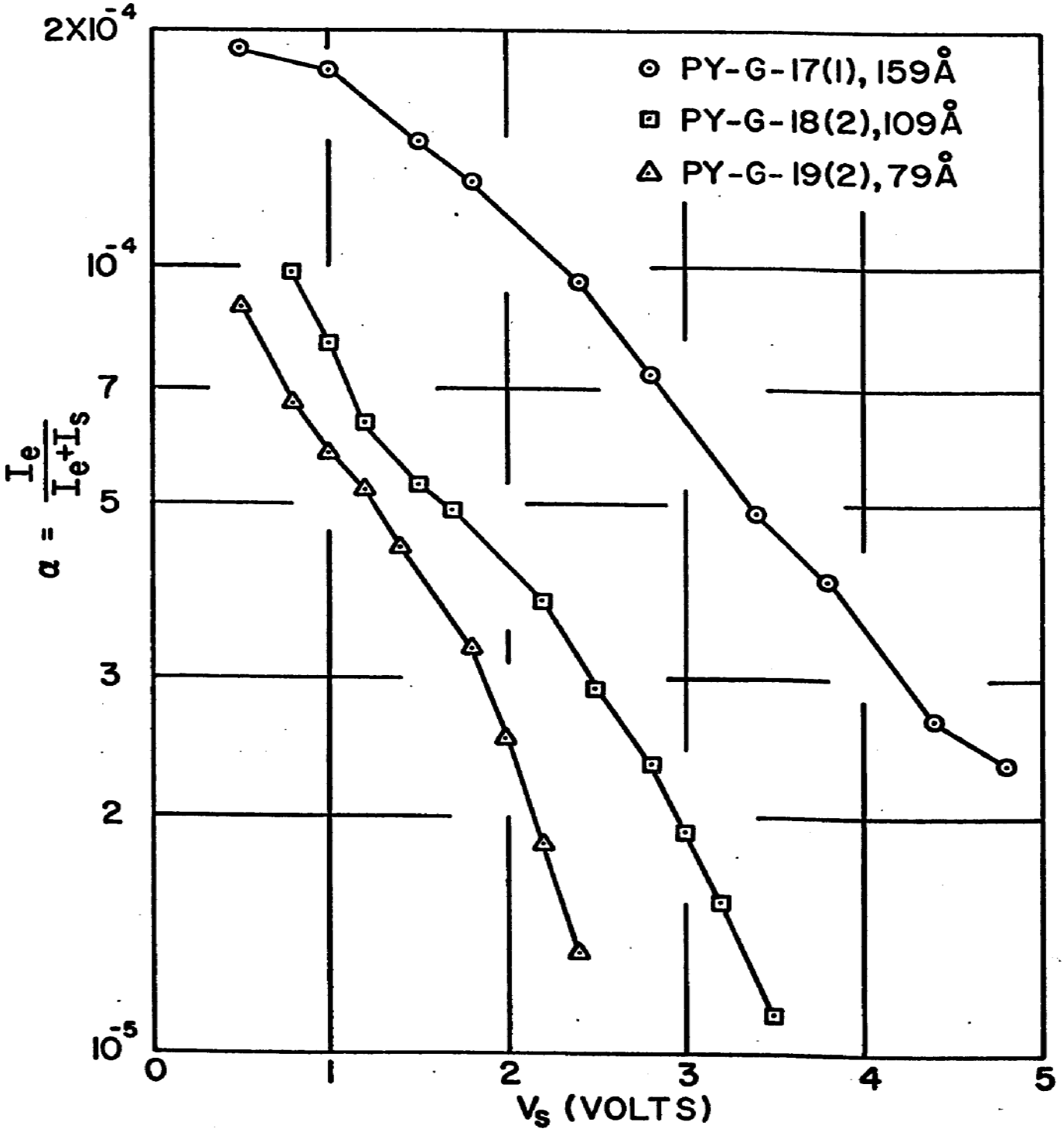



Figure 28

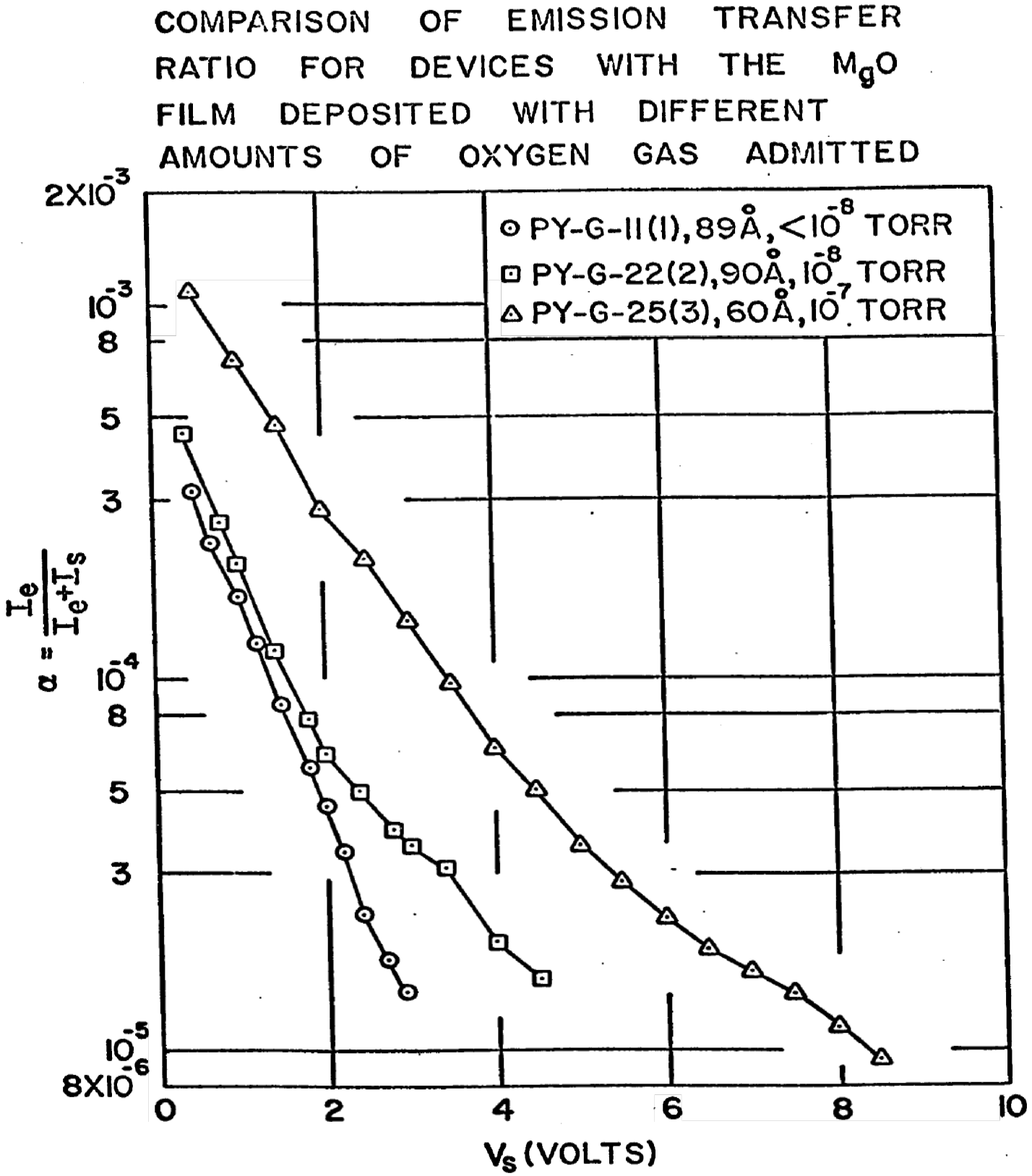

COMPARISON OF EMISSION TRANSFER RATIO FOR DEVICES WITH THE MgO FILM DEPOSITED WITH DIFFERENT AMOUNTS OF OXYGEN GAS ADMITTED
⊙ PY-G-11(1), 89Å, <10⁻⁸ TORR
⊡ PY-G-22(2), 90Å, 10⁻⁸ TORR
△ PY-G-25(3), 60Å, 10⁻⁷ TORR
α = Ie / (Ie+Is)
2X10⁻³
10⁻³
8
5
3
10⁻⁴
8
5
3
10⁻⁵
8X10⁻⁶
0
2
4
6
8
10
Vs (VOLTS)

Figure 29

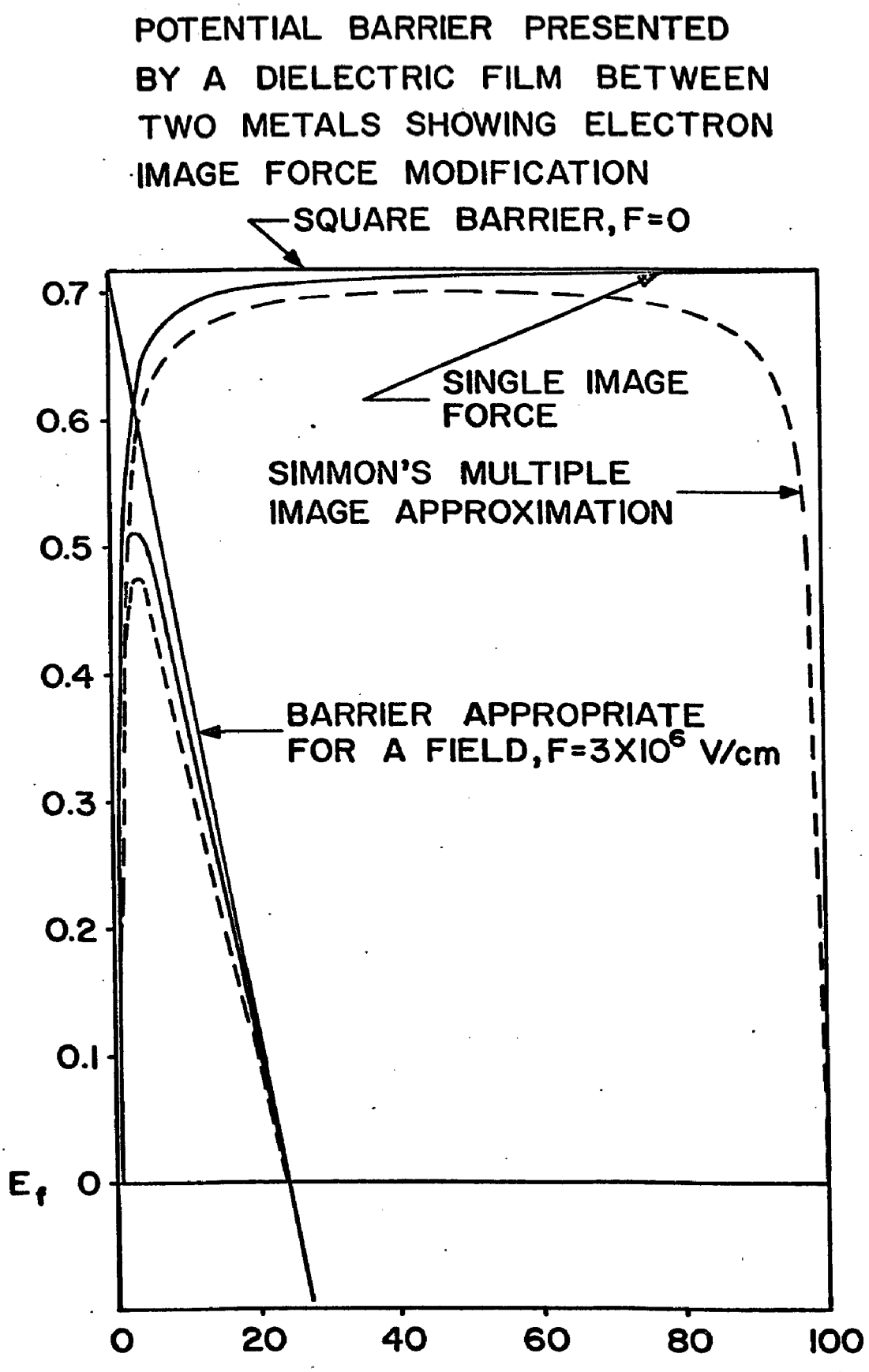

POTENTIAL BARRIER PRESENTED
BY A DIELECTRIC FILM BETWEEN
TWO METALS SHOWING ELECTRON
IMAGE FORCE MODIFICATION
SQUARE BARRIER, F=0
SINGLE IMAGE
FORCE
SIMMON'S MULTIPLE
IMAGE APPROXIMATION
BARRIER APPROPRIATE
FOR A FIELD, F=3X10^6 V/cm
0.7
0.6
0.5
0.4
0.3
0.2
0.1
E_f 0
0
20
40
60
80
100

Figure 30

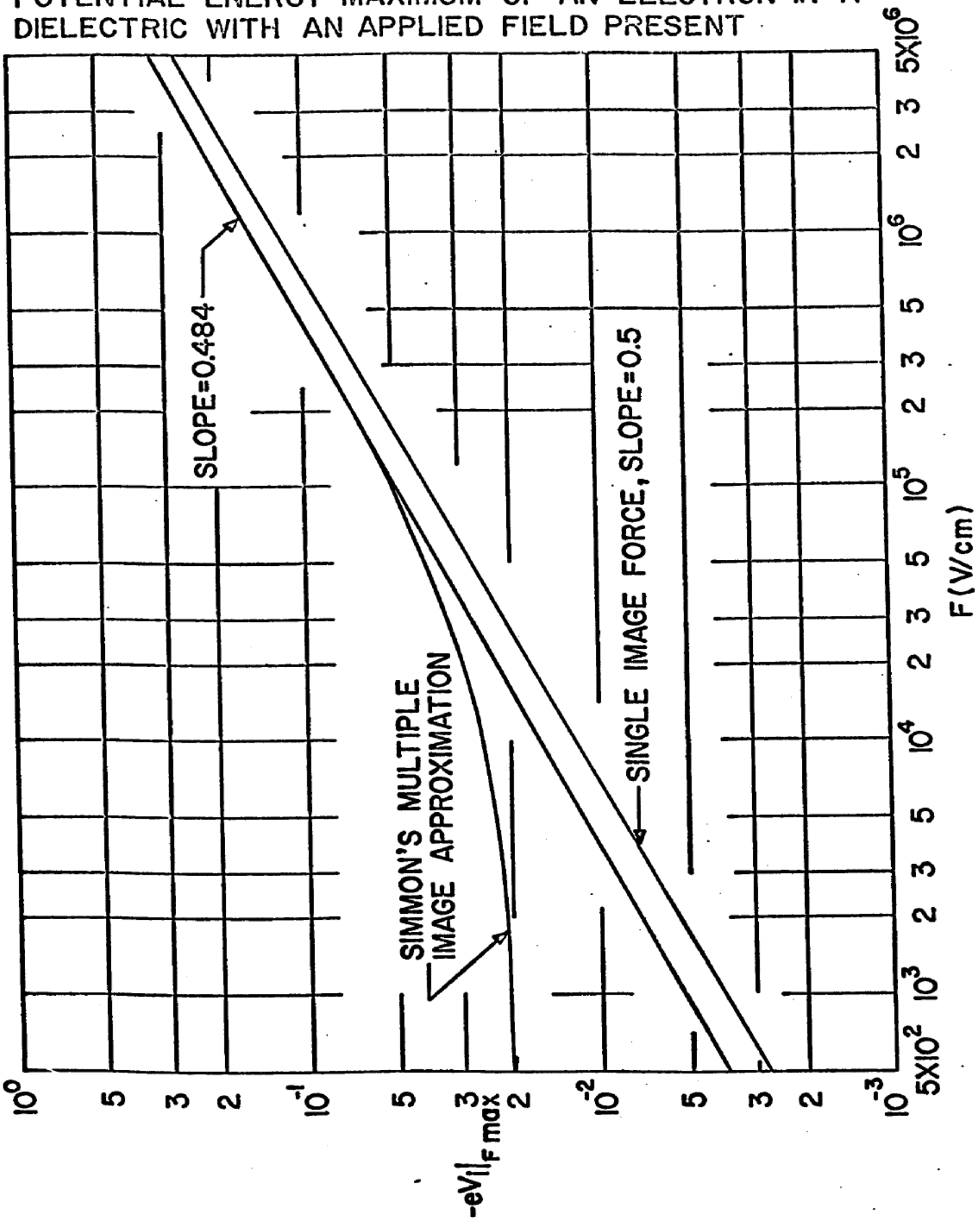

POTENTIAL ENERGY MAXIMUM OF AN ELECTRON IN A DIELECTRIC WITH AN APPLIED FIELD PRESENT
SLOPE=0.484
SINGLE IMAGE FORCE, SLOPE=0.5
SIMMON'S MULTIPLE IMAGE APPROXIMATION
F(V/cm)
$-eV|_{F\,max}$
$10^{0}$
5
3
2
$10^{-1}$
5
3
2
$10^{-2}$
5
3
2
$10^{-3}$
$5X10^{2}$
$10^{3}$
2
3
5
$10^{4}$
2
3
5
$10^{5}$
2
3
5
$10^{6}$
2
3
$5X10^{6}$

Figure 31

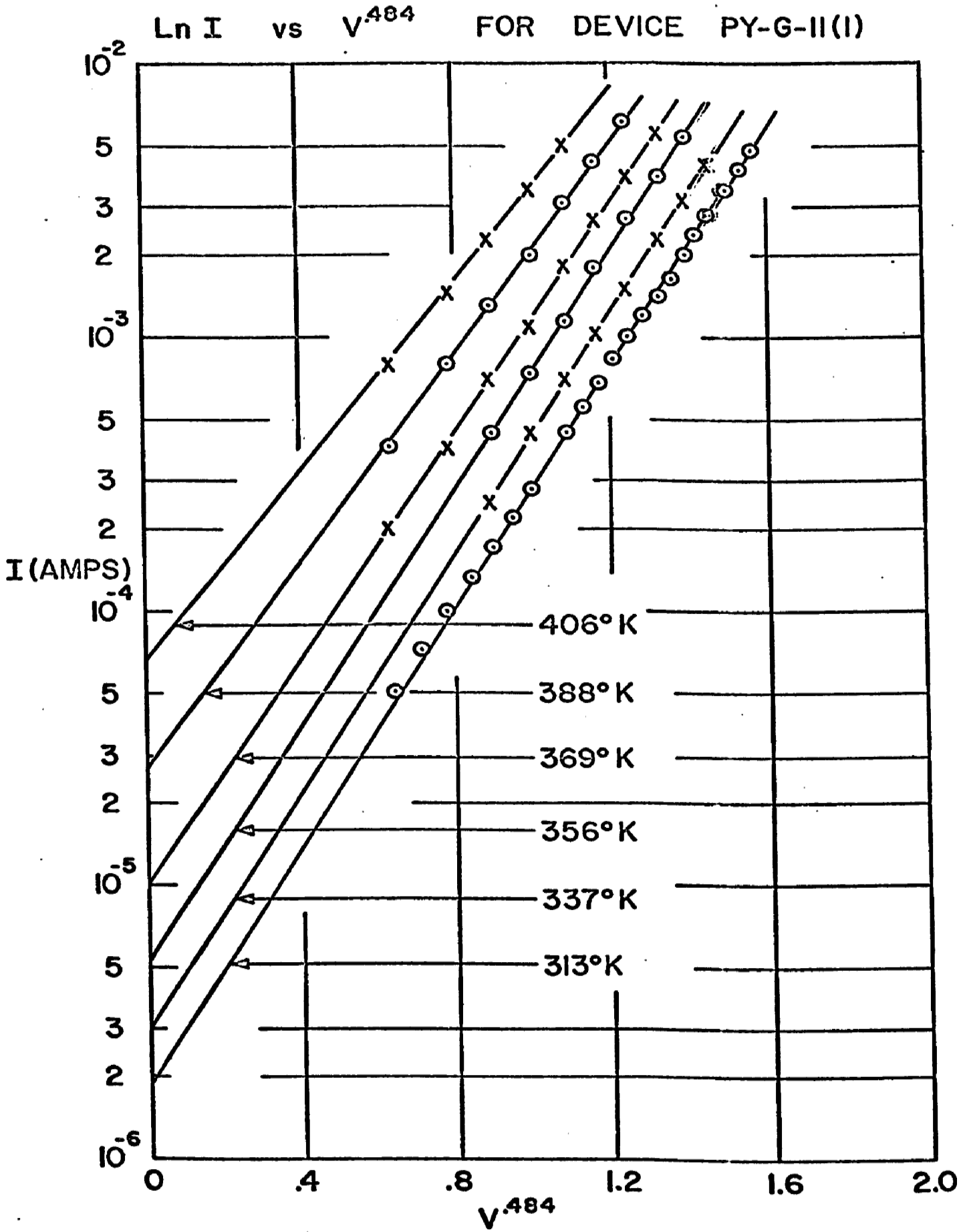

Ln I vs V.484 FOR DEVICE PY-G-II(I)
I(AMPS)
10-2
5
3
2
10-3
5
3
2
10-4
5
3
2
10-5
5
3
2
10-6
406° K
388° K
369° K
356° K
337° K
313° K
0
.4
.8
1.2
1.6
2.0
V.484

Figure 32

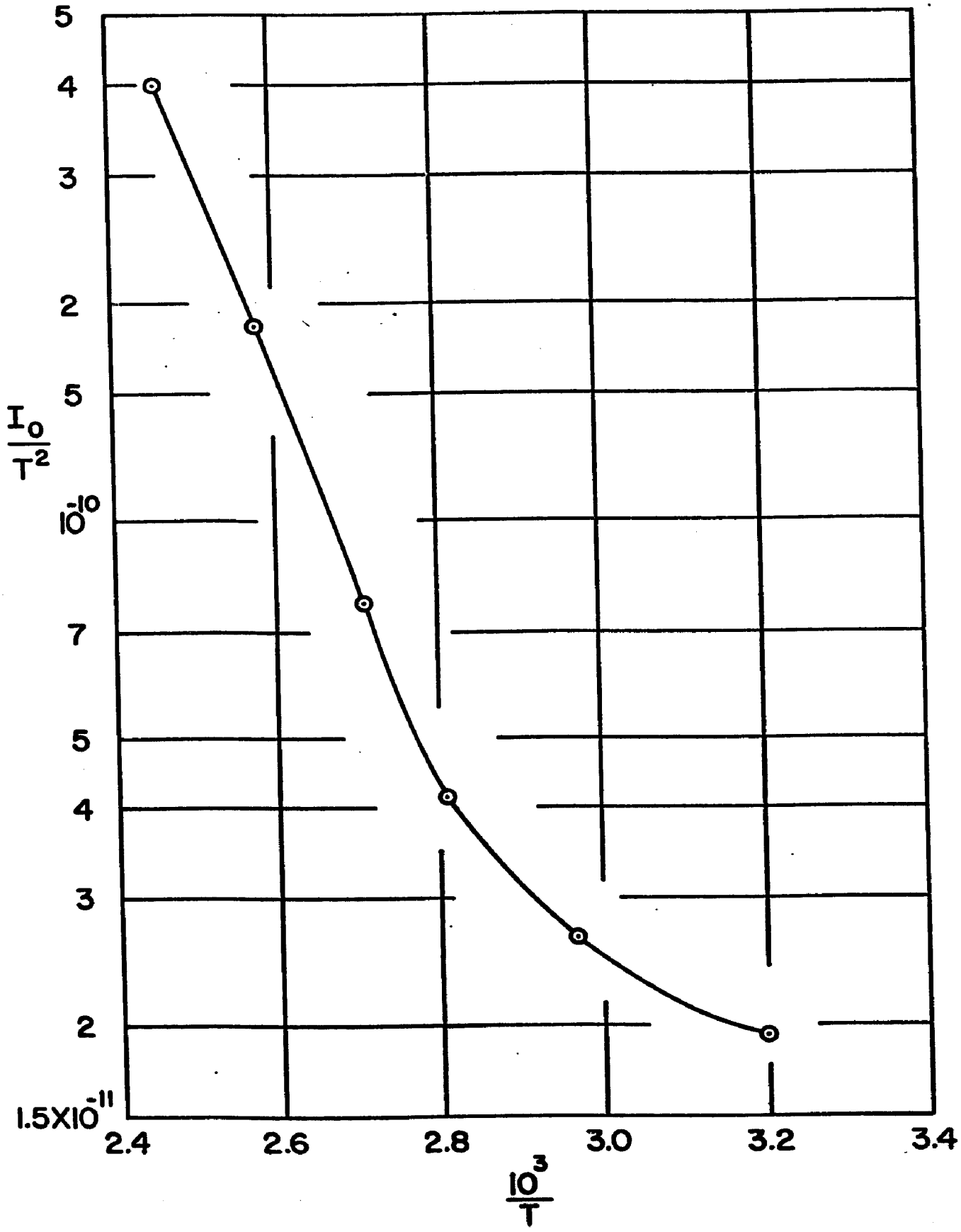

Ln $I_o/T^2$ VS. $10^3/T$ FOR DEVICE PY-G-11(1) WHERE $I_o$ IS FOUND FROM THE Ln I VS. $V^{.484}$ PLOTS
5
4
3
2
5
7
5
4
3
2
$10^{-10}$
$1.5X10^{-11}$
$\frac{I_o}{T^2}$
2.4
2.6
2.8
3.0
3.2
3.4
$\frac{10^3}{T}$

Figure 33

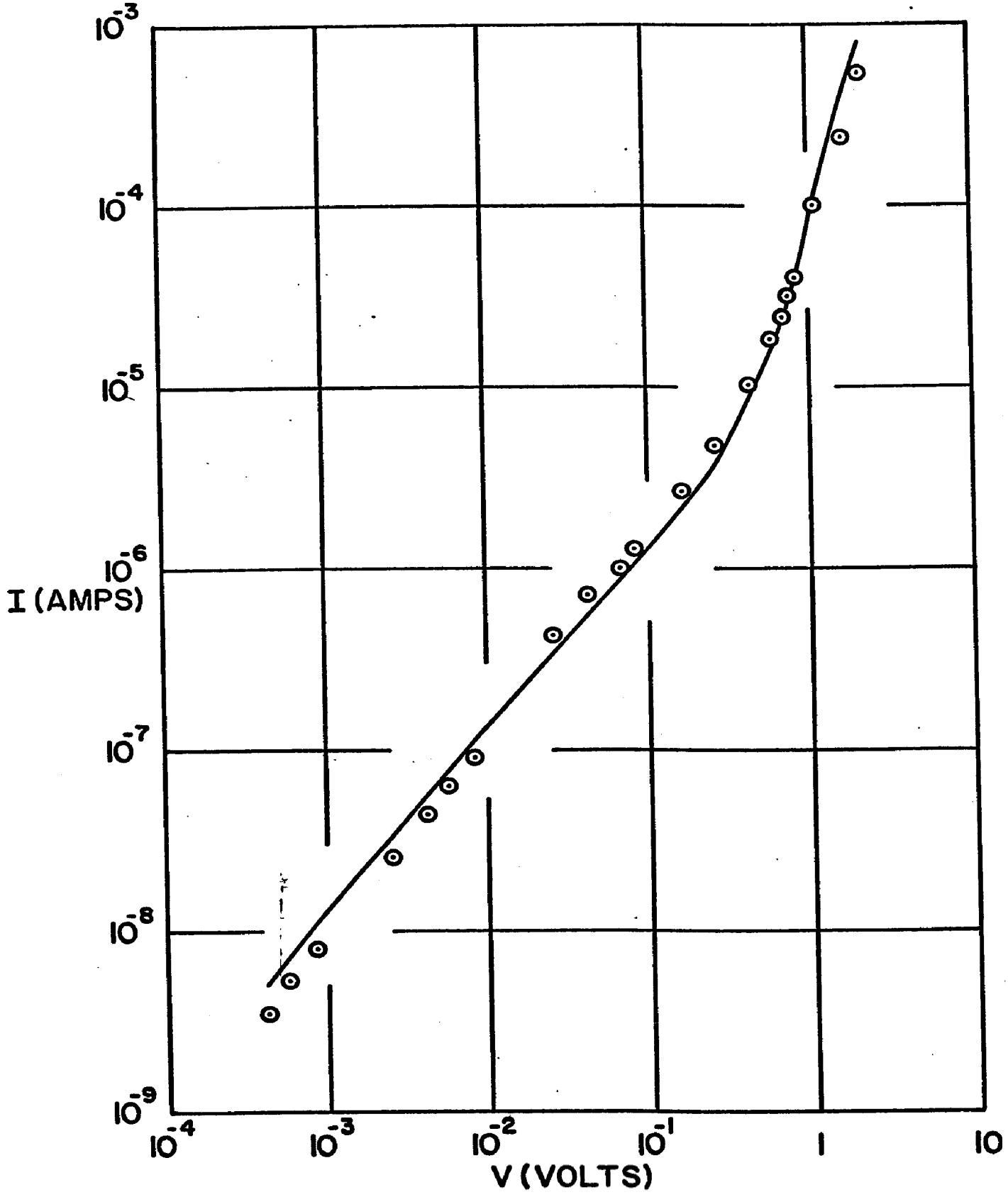

COMPARISON BETWEEN THE DATA FOR
DEVICE PY-G-21(3) AND EQUATION 3
$10^{-3}$
$10^{-4}$
$10^{-5}$
$10^{-6}$
$10^{-7}$
$10^{-8}$
$10^{-9}$
I (AMPS)
$10^{-4}$
$10^{-3}$
$10^{-2}$
$10^{-1}$
1
10
V (VOLTS)

Figure 34

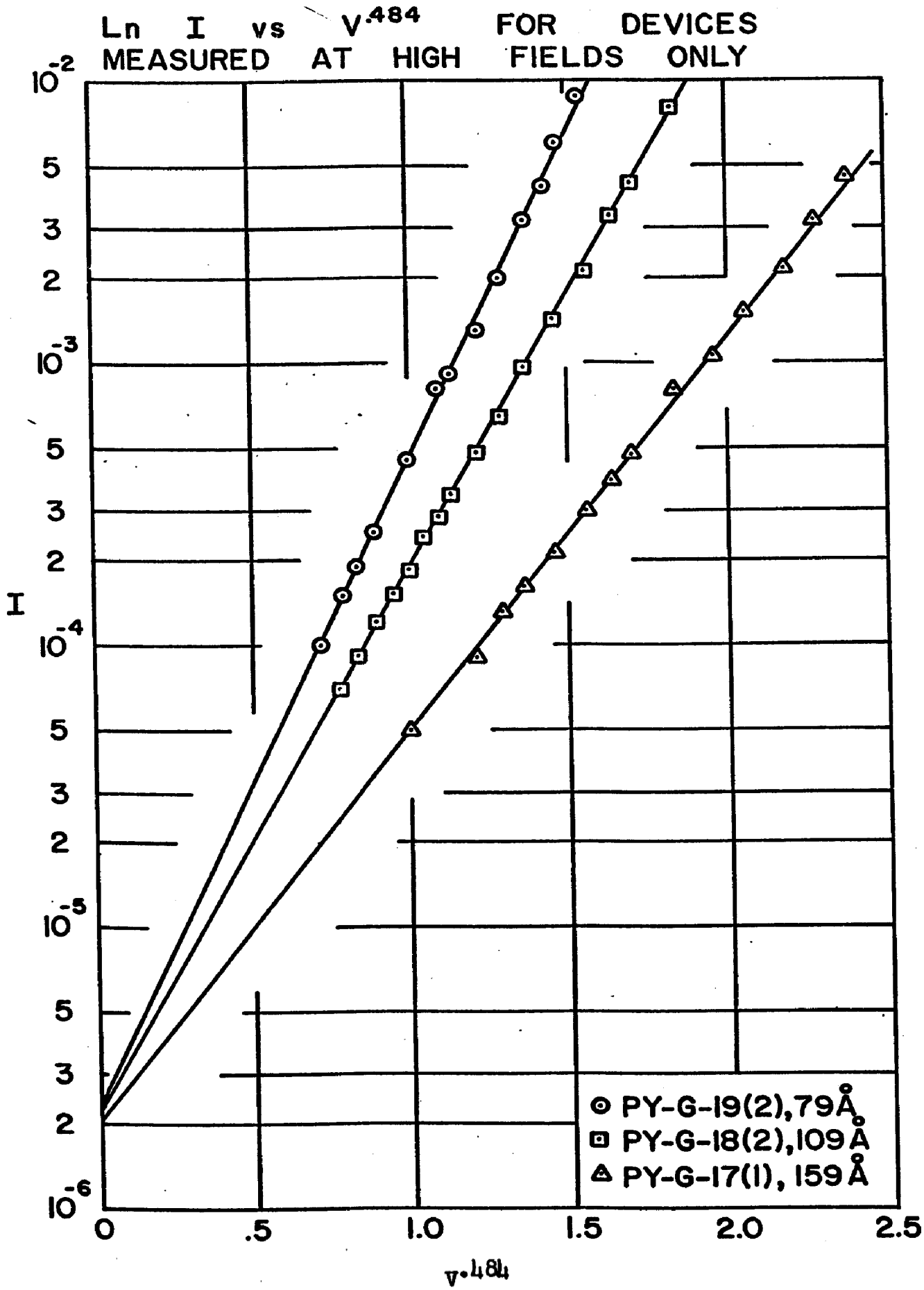

Ln I vs V.484 FOR DEVICES
MEASURED AT HIGH FIELDS ONLY
I
10-2
5
3
2
10-3
5
3
2
10-4
5
3
2
10-5
5
3
2
10-6
0
.5
1.0
1.5
2.0
2.5
V.484
PY-G-19(2),79Å
PY-G-18(2),109Å
PY-G-17(1), 159Å

Figure 35

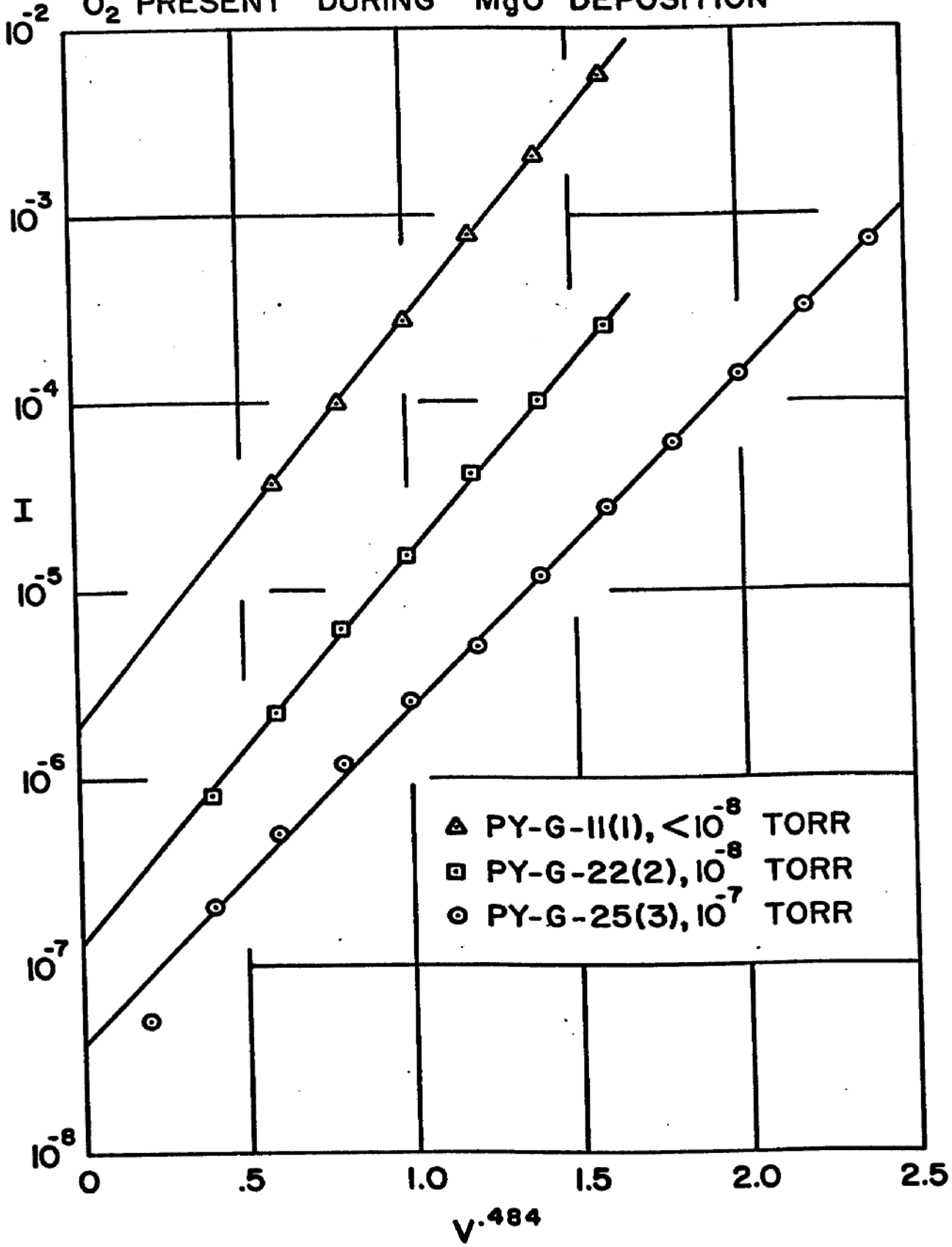

COMPARISON OF RESULTS FOR DEVICES FABRICATED WITH DIFFERENT AMOUNTS OF $O_2$ PRESENT DURING MgO DEPOSITION
$10^{-2}$
$10^{-3}$
$10^{-4}$
I
$10^{-5}$
$10^{-6}$
$10^{-7}$
$10^{-8}$
0
.5
1.0
1.5
2.0
2.5
$V^{.484}$
PY-G-11(1), $<10^{-8}$ TORR
PY-G-22(2), $10^{-8}$ TORR
PY-G-25(3), $10^{-7}$ TORR

Figure 36

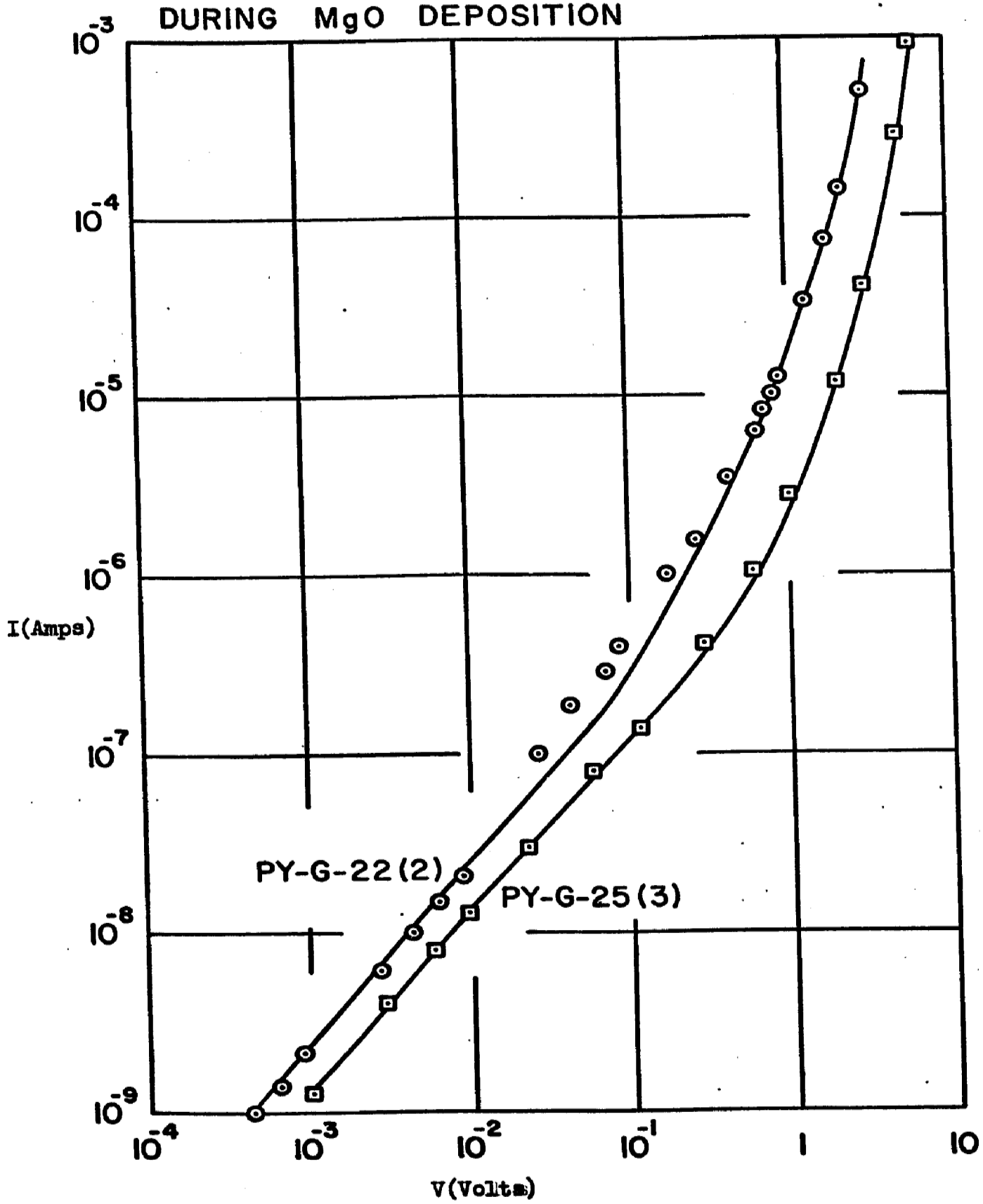

COMPARISON BETWEEN EXPERIMENTAL DATA AND EQUATION 3 FOR DEVICES FABRICATED WITH OXYGEN PRESENT DURING MgO DEPOSITION
$10^{-3}$
$10^{-4}$
$10^{-5}$
$10^{-6}$
$10^{-7}$
$10^{-8}$
$10^{-9}$
I(Amps)
PY-G-22(2)
PY-G-25(3)
$10^{-4}$
$10^{-3}$
$10^{-2}$
$10^{-1}$
1
10
V(Volts)

Figure 37

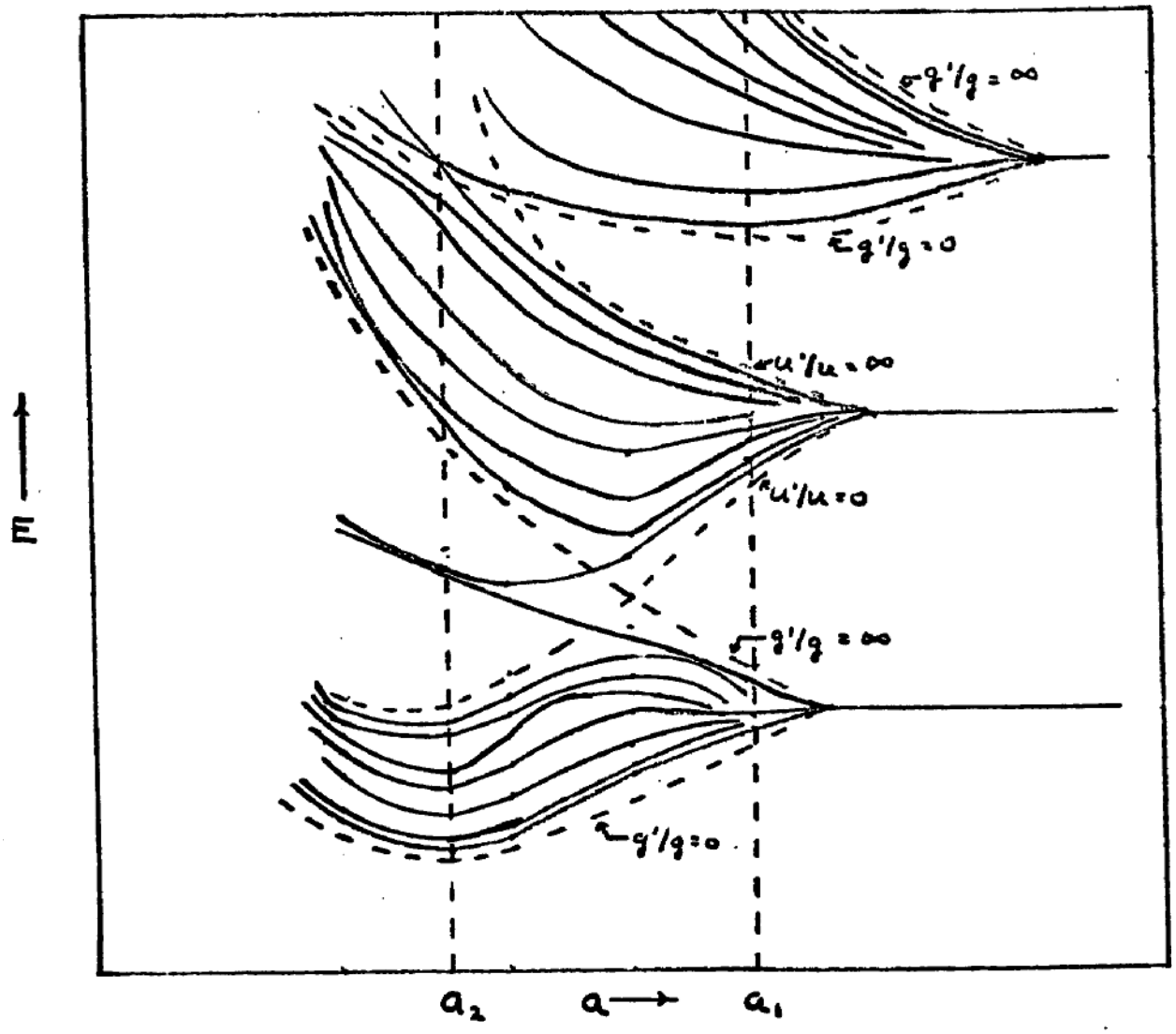



Figure 38. Energy Bands as a Function of Interatomic Spacing for a Simple Linear Chain

$Ln(I_o/T^2)$ VS $10^3/T$ FOR DEVICES FABRICATED WITH DIFFERERENT AMOUNTS OF OXYGEN PRESENT DURING MgO DEPOSITION

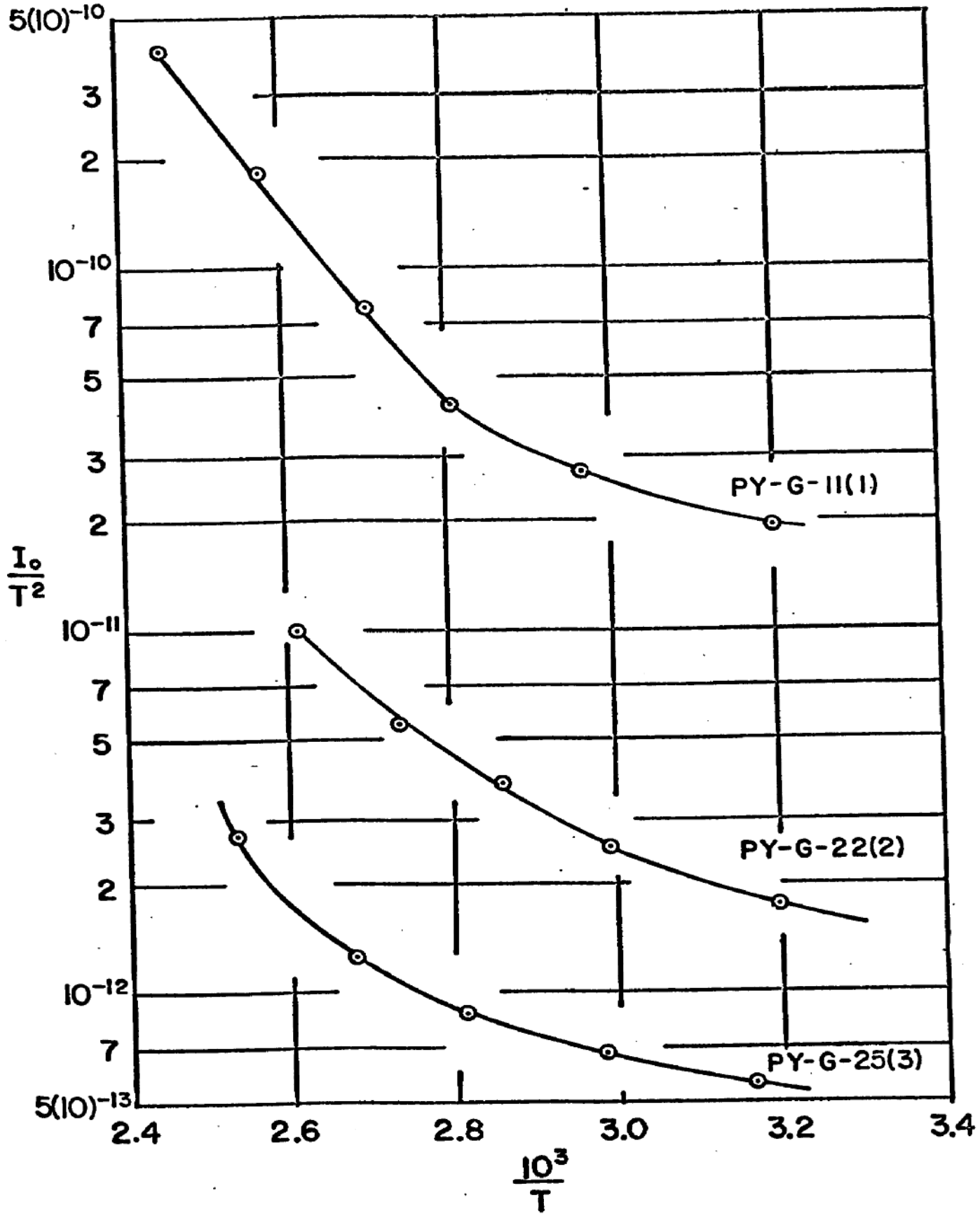



Figure 39

# BARRIER HEIGHTS AS A FUNCTION OF TEMPERATURE

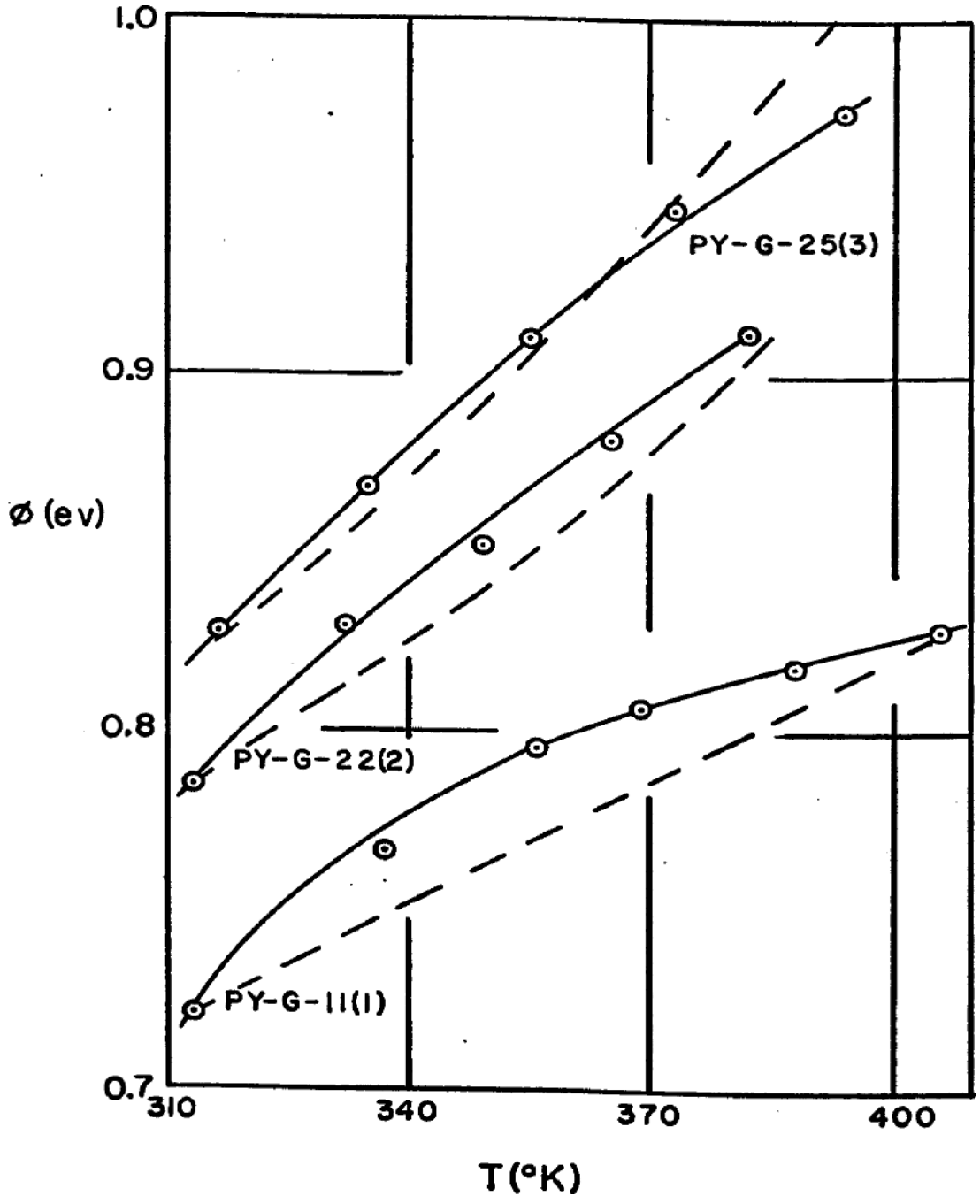



Figure 40

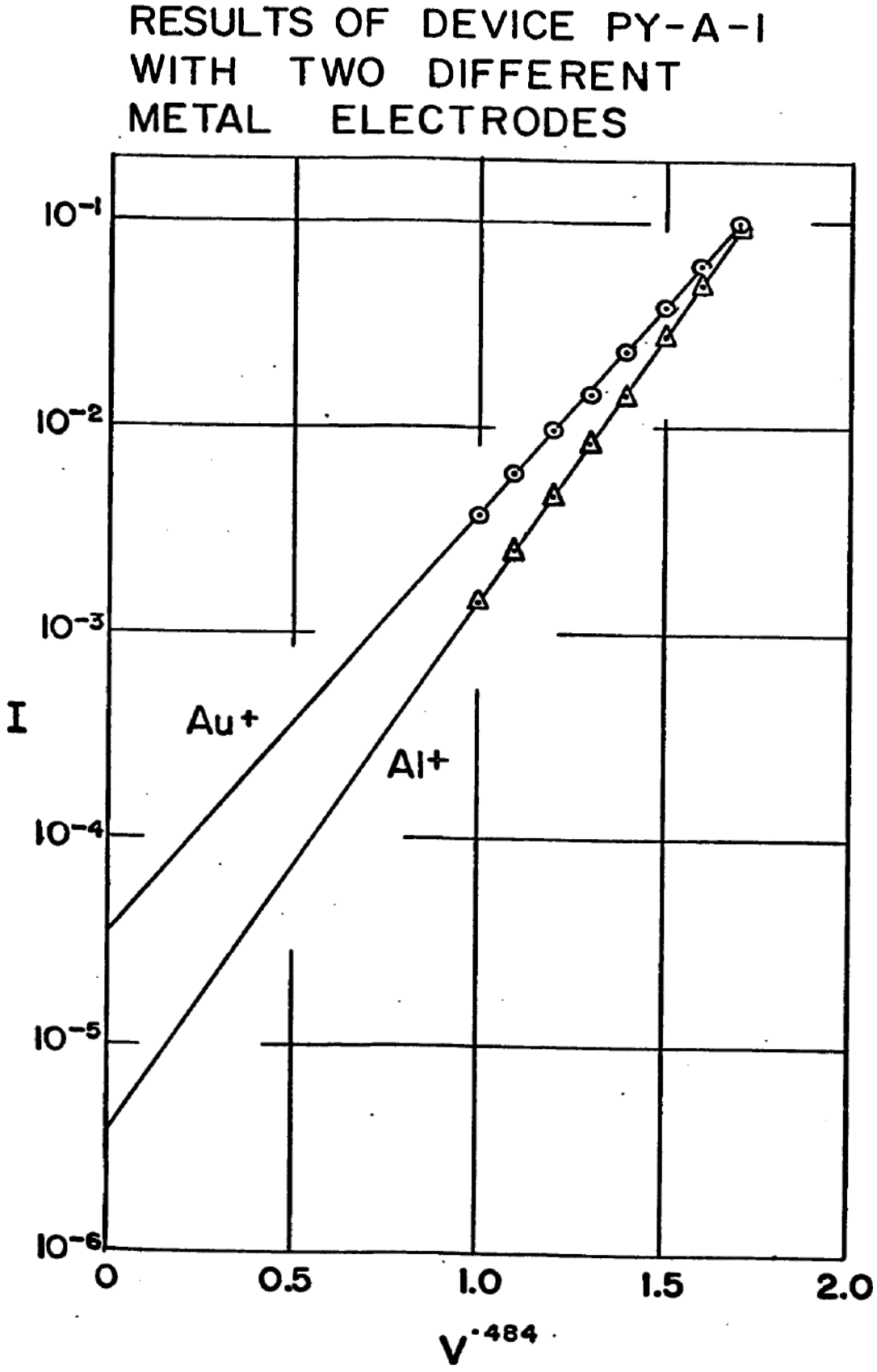
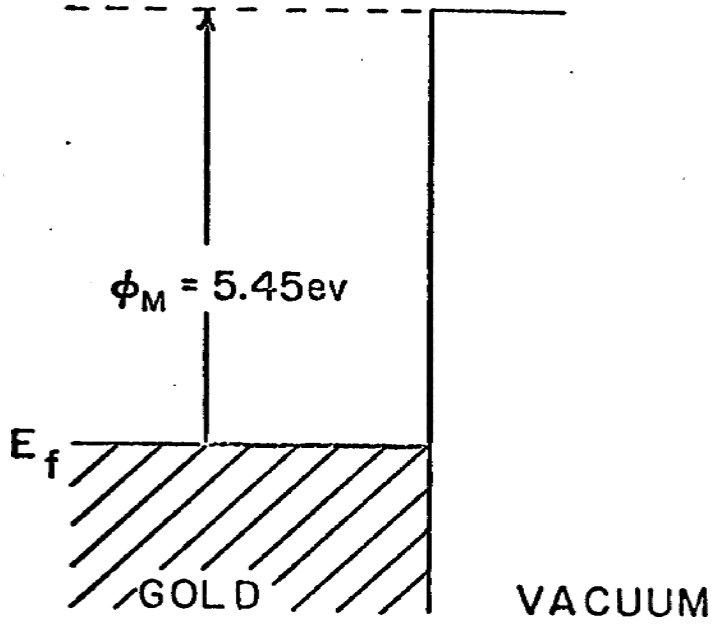
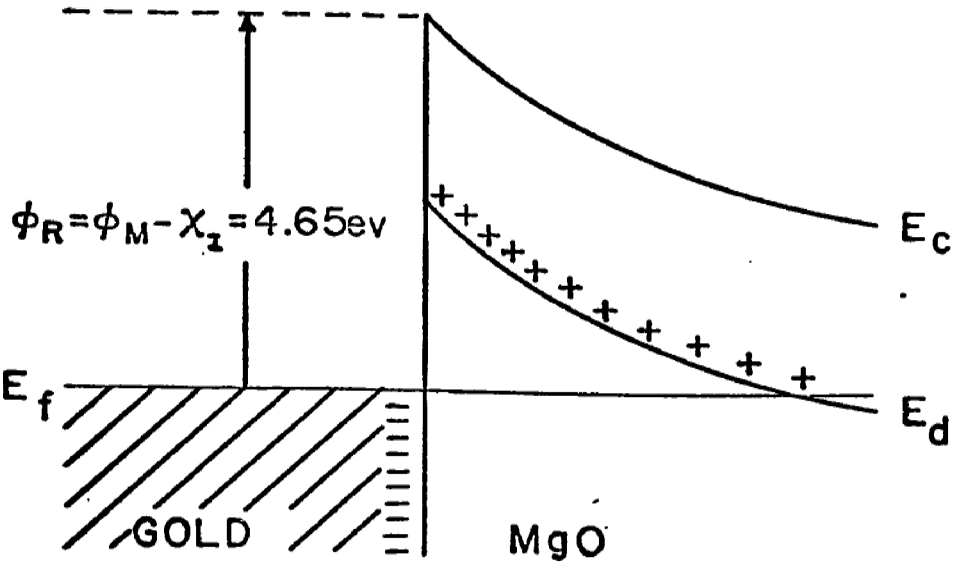

RESULTS OF DEVICE PY-A-1
WITH TWO DIFFERENT
METAL ELECTRODES
10⁻¹
10⁻²
10⁻³
10⁻⁴
10⁻⁵
10⁻⁶
I
Au+
Al+
0
0.5
1.0
1.5
2.0
V·484

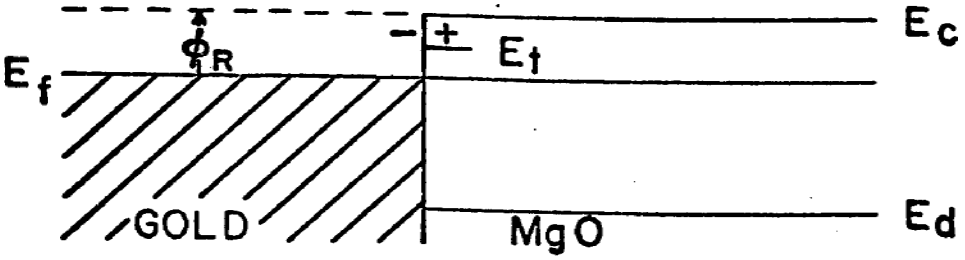
Figure 41




a. ENERGY BAND PICTURE FOR A GOLD–VACUUM INTERFACE

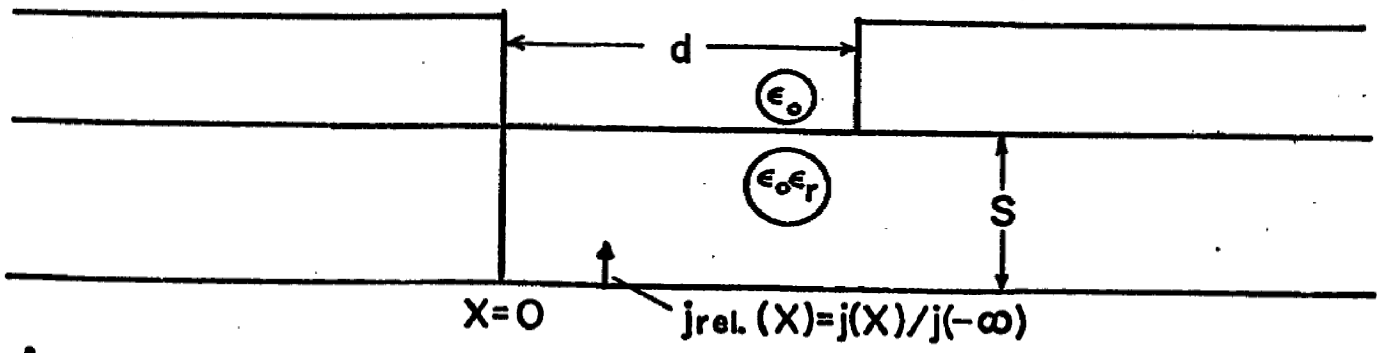



b. ENERGY BAND PICTURE FOR A GOLD–MgO INTERFACE IF NO INTERFACE STATES EXIST

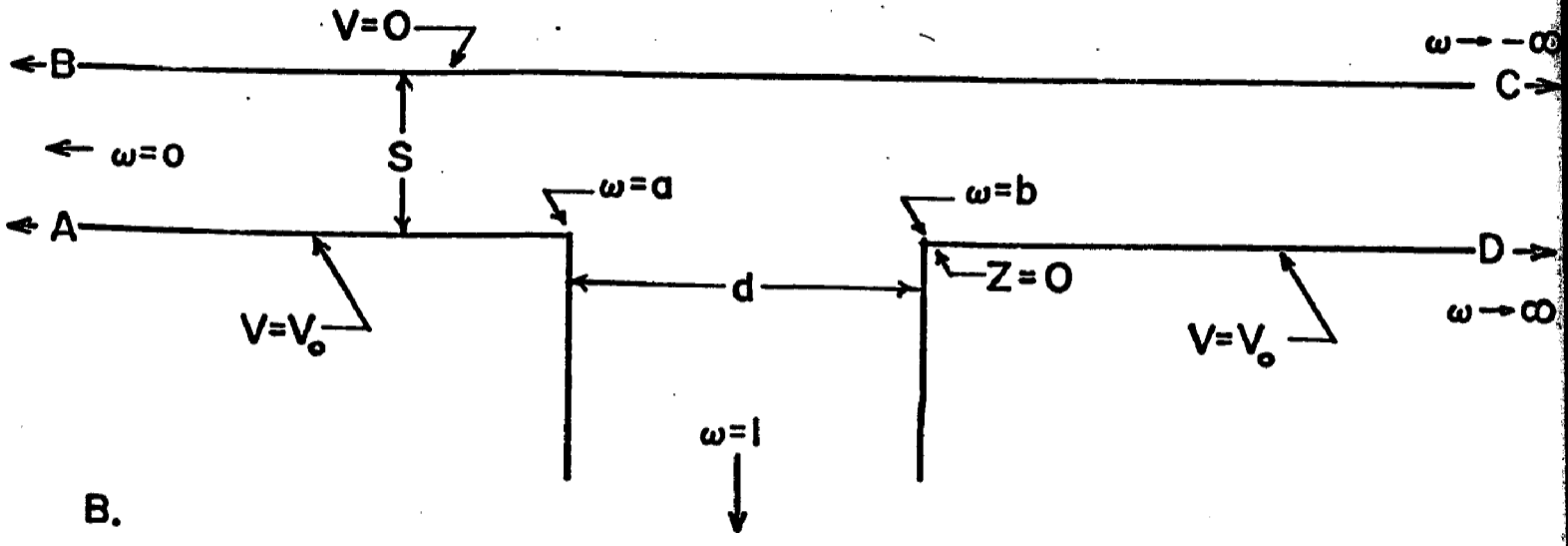



c. ENERGY BAND PICTURE FOR A GOLD-MgO INTERFACE WITH A HIGH DENSITY OF DONOR LIKE INTERFACE STATES

Figure 42




A.




B.

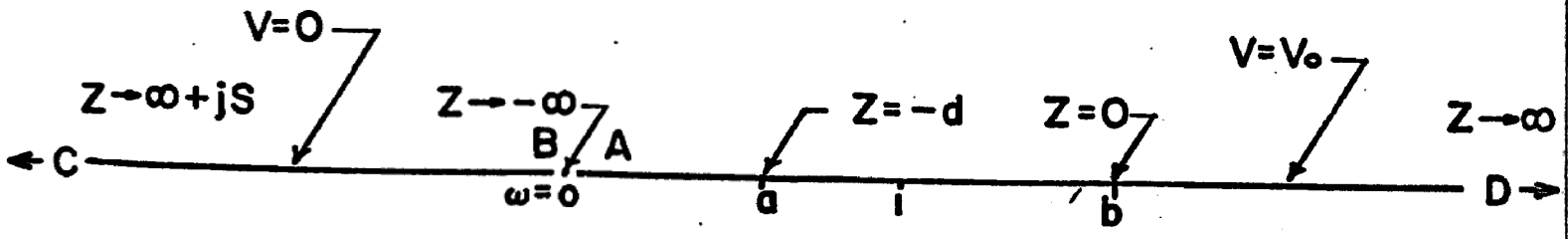
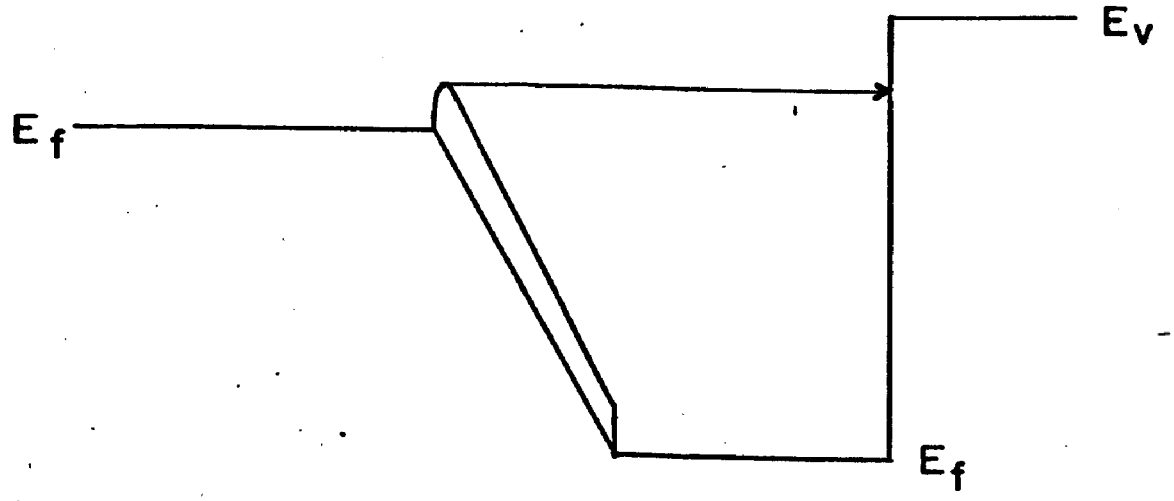
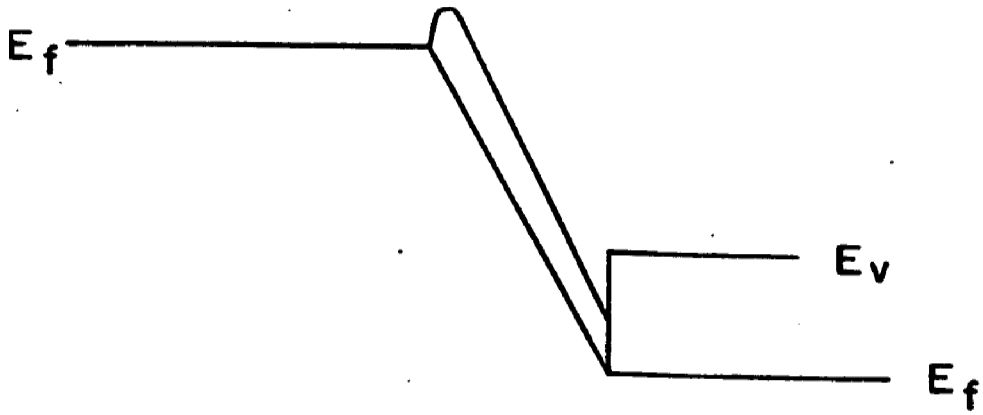



DIAGRAM INDICATING DETAILS OF THE CALCULATION OF ELECTRIC FIELD VARIATION AT A PLANE ELECTRODE OPPOSITE A SLOTTED ELECTRODE

Figure 43




44a. ENERGY LEVEL DIAGRAM FOR AN APPLIED SAMPLE BIAS OF 4 VOLTS SHOWING THAT NO ELECTRONS SHOULD BE EMITTED THROUGH THE OVERLAYER




44b. ENERGY LEVEL DIAGRAM APPROPRIATE FOR EMISSION THROUGH HOLES IN THE GOLD OVERLAYER FILM

Figure 44

FIELD STRENGTH AT THE UNDERLAYER
BENEATH A SLOT IN THE OVERLAYER

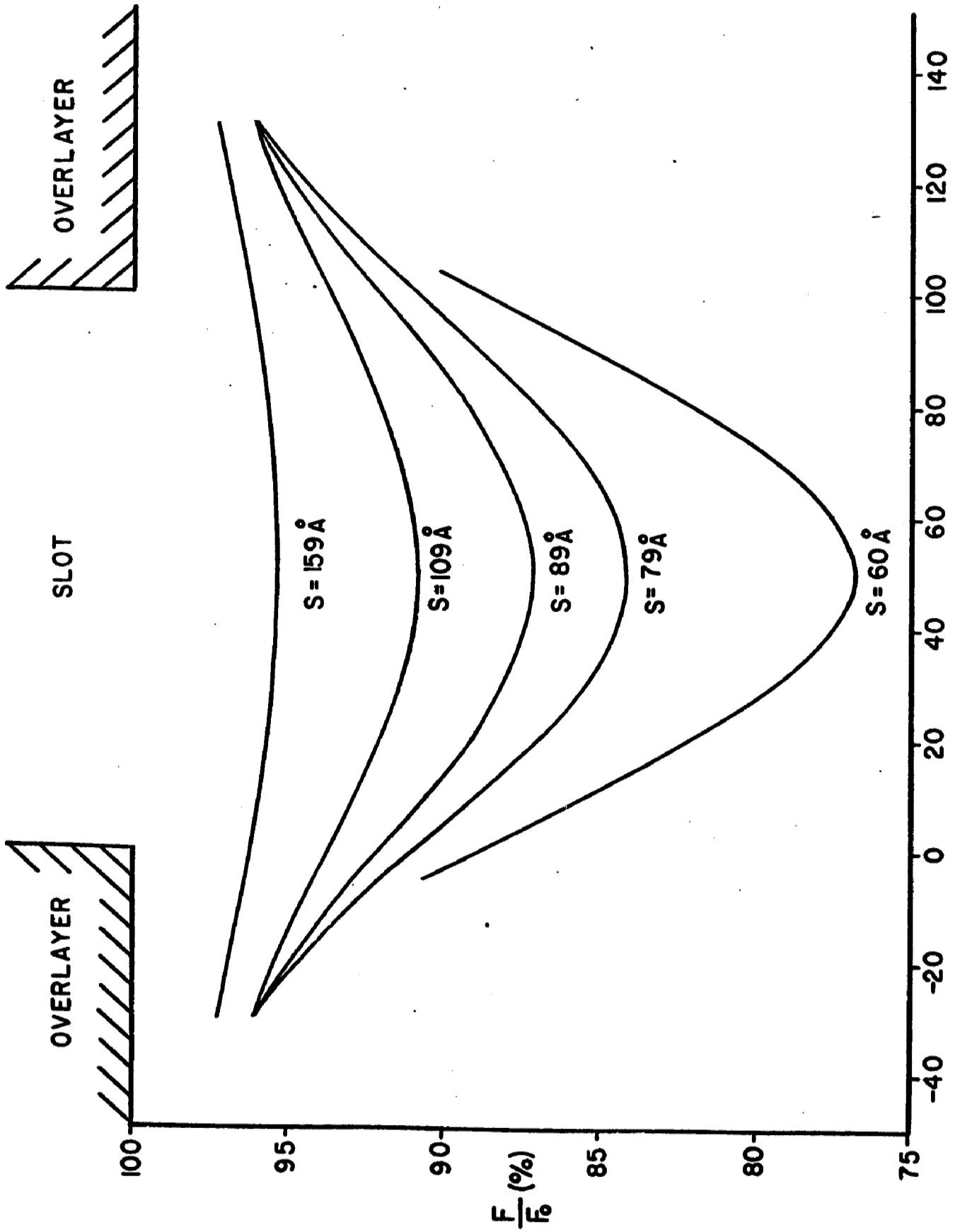



Figure 45

$\alpha = \frac{I_e}{I_e + I_s}$ AS A FUNCTION OF OXIDE THICKNESS

ASSUMING NO ENERGY LOSS IN THE OXIDE

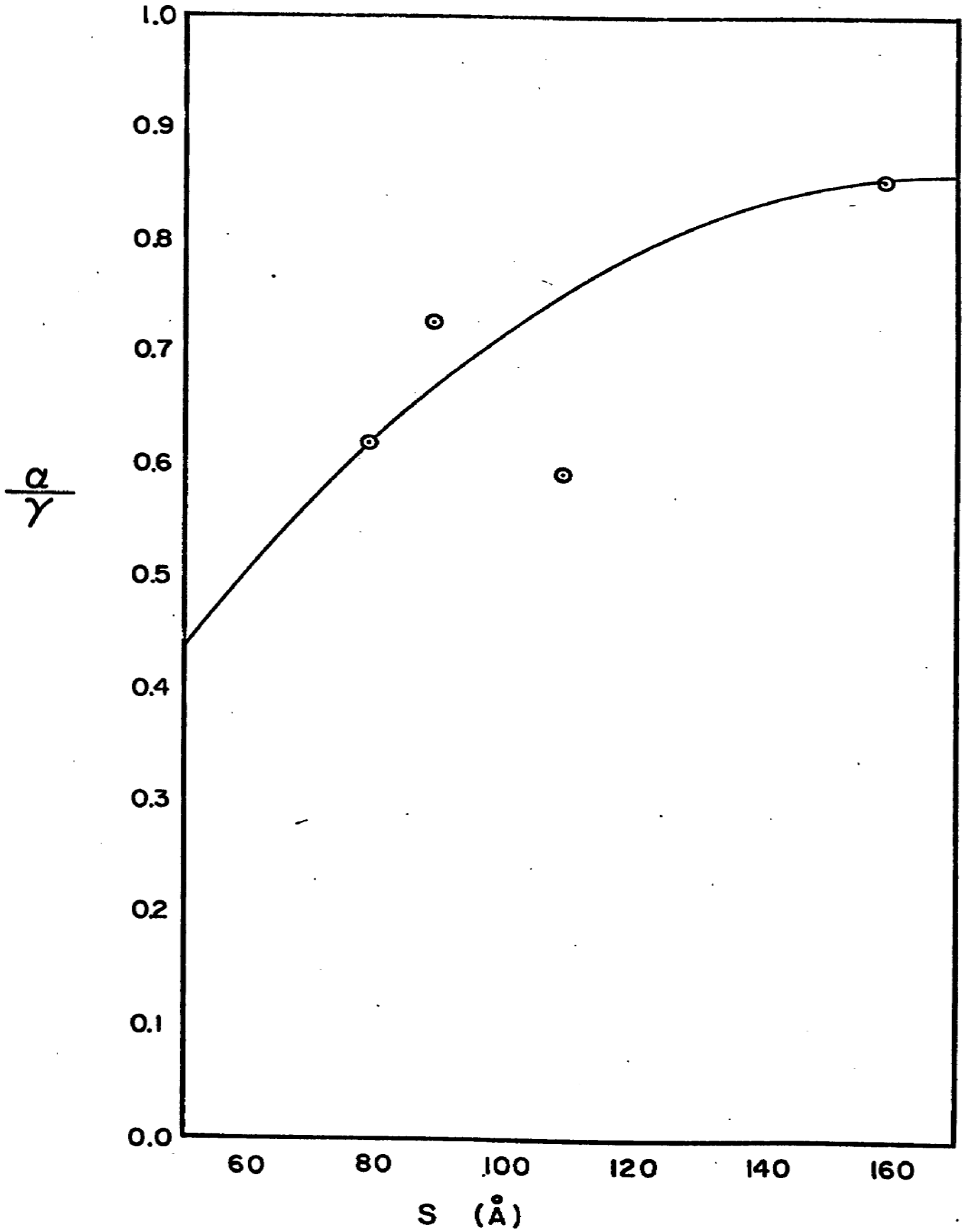
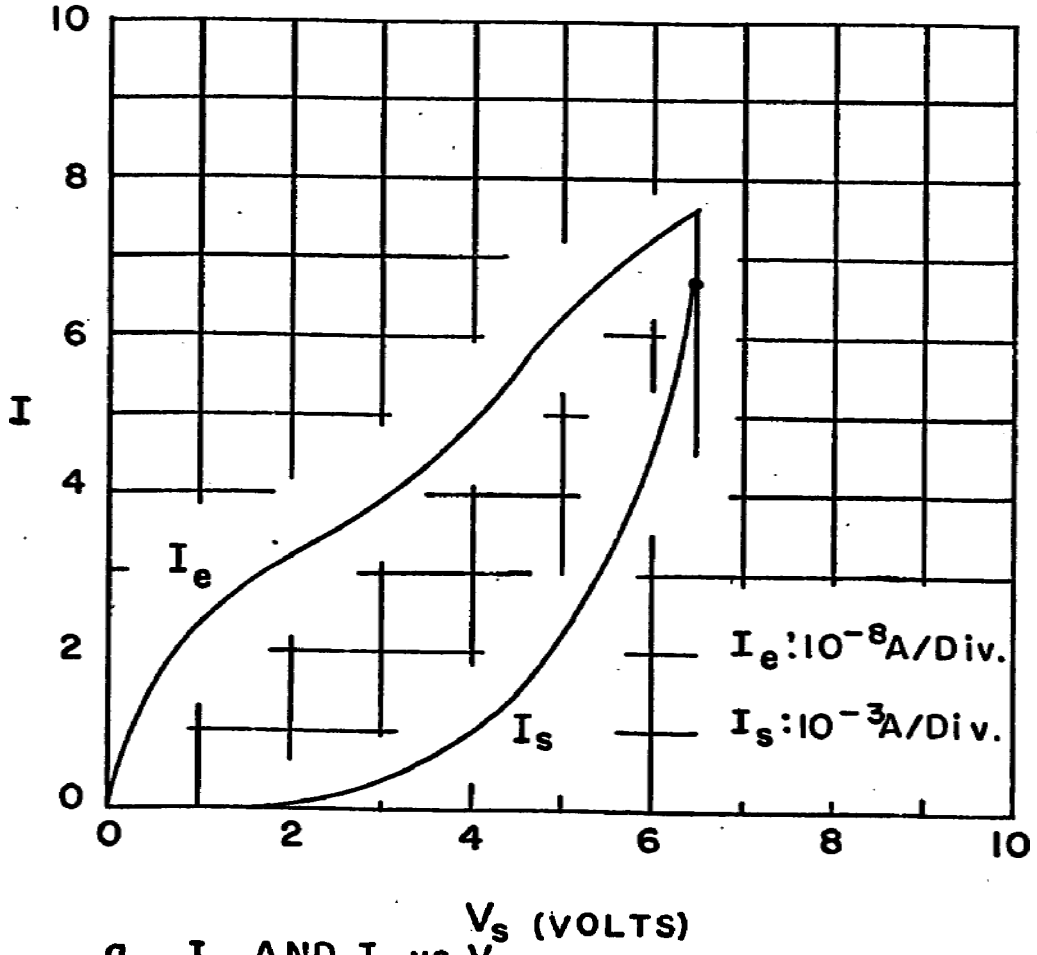
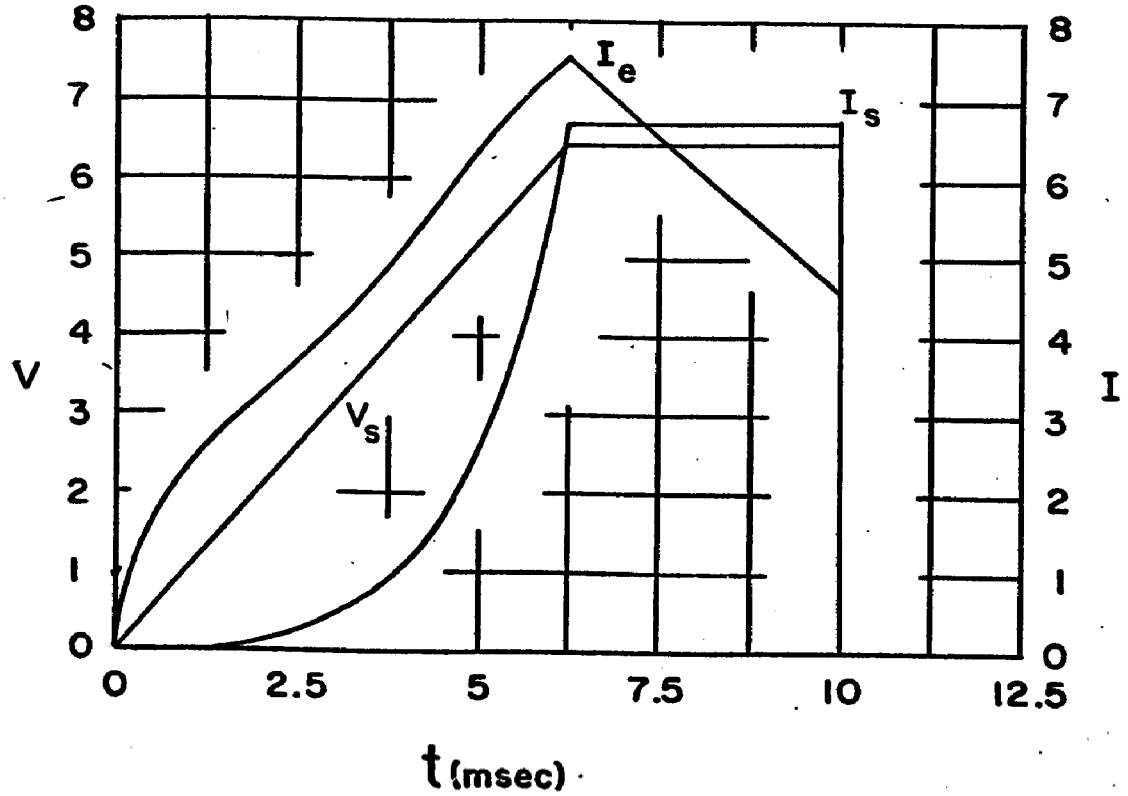



Figure 46

EVIDENCE OF CHARGING AT AN EMITTING SLOT, DEVICE PY-G-17(1)

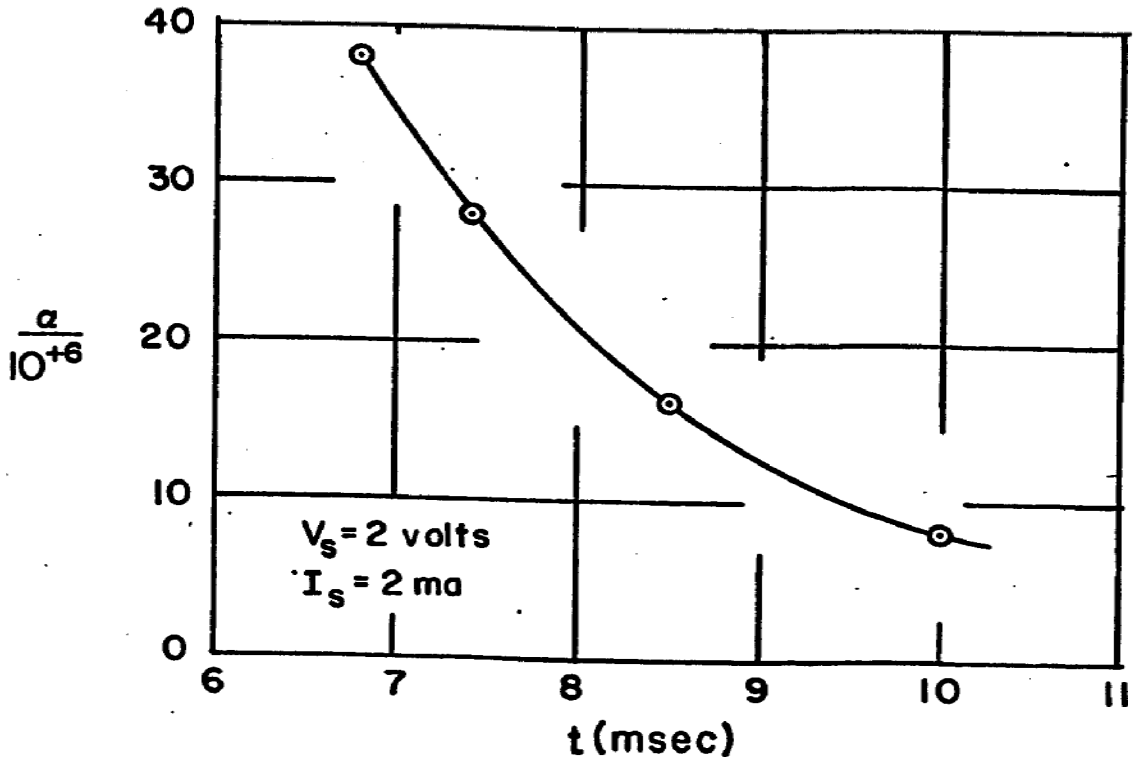



a. $I_e$ AND $I_s$ vs. $V_s$

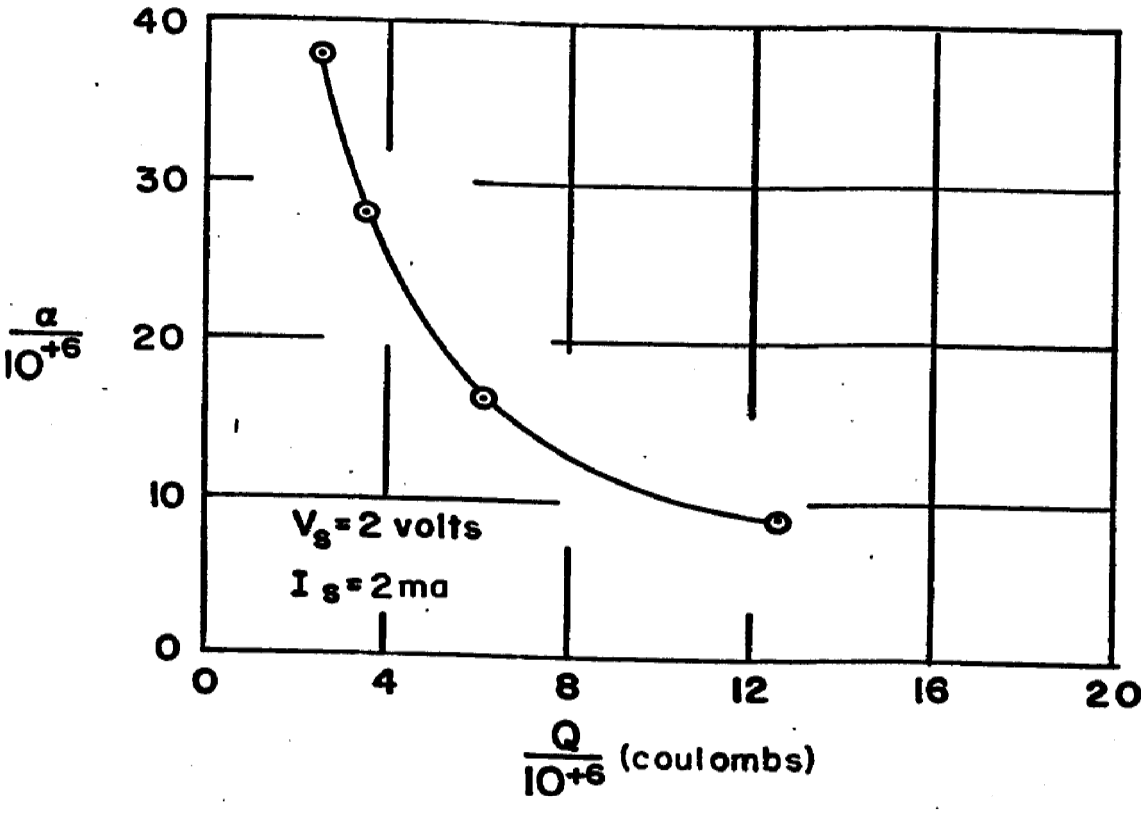



b. $I_e$, $I_s$, AND $V_s$ vs. TIME.

Figure 47




a. EMISSION TRANSFER RATIO VS. TIME REQUIRED TO REACH $V_s$ = 2 VOLTS




b. EMISSION TRANSFER RATIO VS. TOTAL CHARGE PASSED THROUGH THE DEVICE

Figure 8

TIME CONSTANTS FOR CHARGING
OF THE INSULATOR BENEATH A SLOT

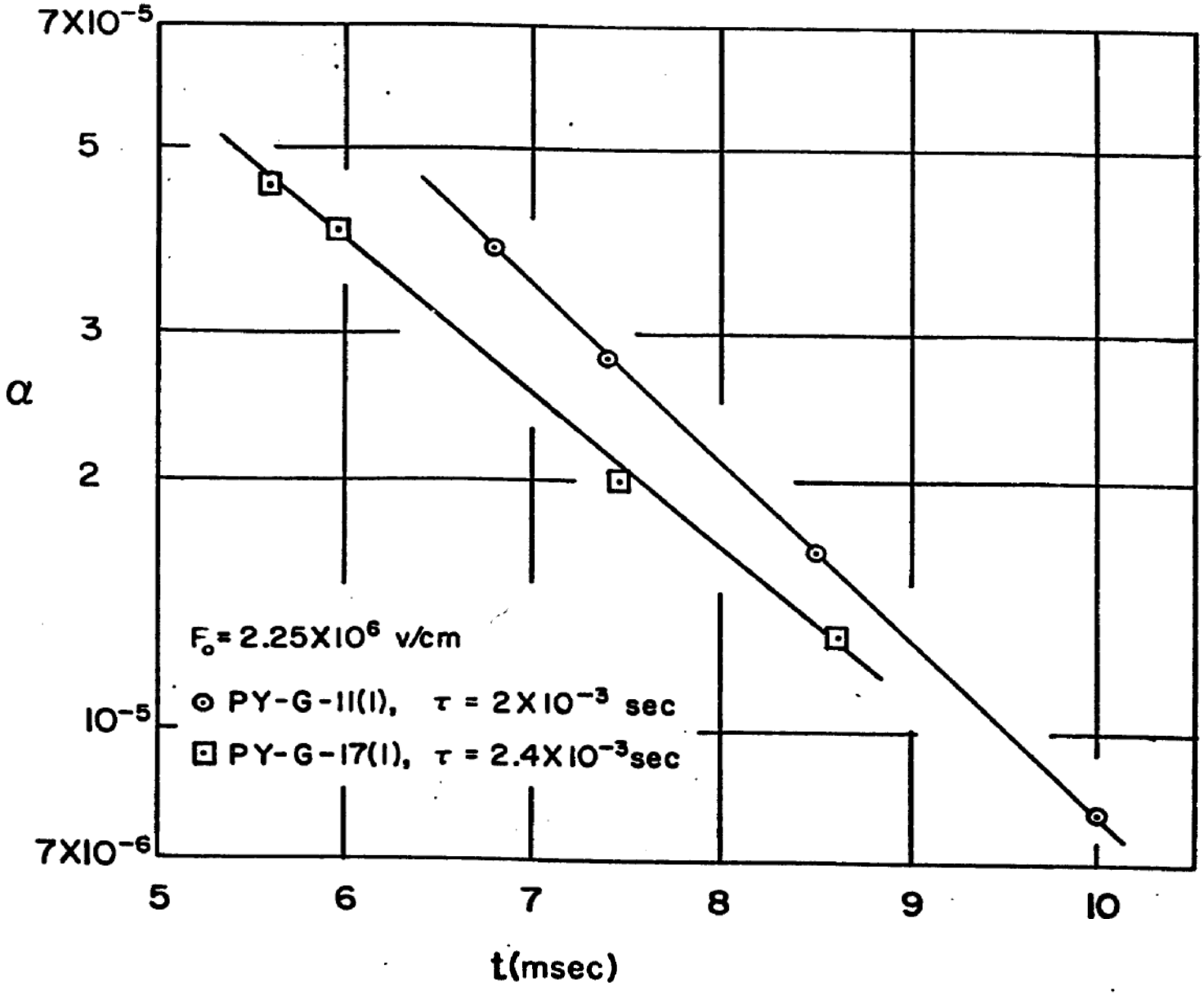



Figure 49

# Attachment A-3

PURDUE UNIVERSITY

Libraries and School of Information Studies

The following pages contain materials you requested from Interlibrary Loan via ILLiad.

As these are typically delivered without staff intervention, please report any problems with the copy to the Interlibrary Loan department as soon as possible. You may reply to the delivery email (ill@purdue.edu) or call us at 765-494-2800. In these cases, there is no need to re-request the article.

Need assistance with your research? Ask a Librarian

*Copyright Statement*

The copyright law of the United States (Title 17, United States Code) governs the making of photocopies or other reproductions of copyrighted materials. Under certain conditions specified in the law, libraries and archives are authorized to furnish a photocopy or other reproduction. One of these specified conditions is that the photocopy or reproduction is not to be "used for any purpose other than private study, scholarship, or research".

# Documents to U / MNU Lending

**University of Minnesota – Interlibrary Loan Lending**

**OCLC MNU * DOCLINE MNUMIN * RAPID MNU**

**University of Minnesota | 60 Wilson Library | 309 19th Avenue South**

**University of Minnesota**

**Minneapolis, MN 55455 USA**

**Phone: 612-624-4388, Fax: 612-624-4508, e-mail: docstou@umn.edu**

*This article is delivered directly from the collections of the University of Minnesota.*

*Thank you for using our service.*

**If you have problems with delivery, please contact us within 48 hours.**


---

MNU 1892495 / 228218805

Title: Hot electron transport in vacuum deposited thin film emission diodes.
Author: Soukup, Rodney Joseph. Rodney Joseph Soukup
ArticleTitle: [cover, inside front cover, title page, and the following ten pages including table of contents]
ArticleAuthor: Soukup, Rodney Joseph. Rodney Joseph Soukup
Date: 1969 Pages: (please see article title)
OCLC - 17923718;
Publisher: 1969.
Copyright: CCL

---


NOTICE CONCERNING COPYRIGHT RESTRICTIONS:

The copyright law of the United States [Title 17, United StatesCode] governs the making of photocopies or other reproductions of copyrighted materials.

Under certain conditions specified in the law, libraries and archives are authorized to furnish a photocopy or other reproduction. One of these specific conditions is that the photocopy is not to be "used for any purpose other than private study, scholarship, or research." If a user makes a request for, or later uses, a photocopy or reproduction for purposes in excess of "fair use," that user may be liable for copyright infringement.

This institution reserves the right to refuse to accept a copying order if, in its judgment, fulfillment of that order would involve violation of copyright law.

# HOT ELECTRON TRANSPORT IN VACUUM DEPOSITED THIN FILM EMISSION DIODES

A Thesis

Submitted to the Graduate Faculty

of the

University of Minnesota

by

Rodney Joseph Soukup

2

In Partial Fulfillment of the Requirements

for the

Degree of

Doctor of Philosophy

June, 1969

DEGREE GRANTED July 1969

Mat-D
69-109

## ACKNOWLEDGMENTS

I wish to extend my sincere appreciation to Dr. D. E. Speliotis for his advice and helpful discussions.

I also wish to thank Dr. D. E. Anderson for suggesting the topic of study and for his interest and suggestions. To all associated with the Physical Electronics Laboratory, I extend thanks for the loan of equipment and for helpful suggestions.

I wish to acknowledge the support of this work by Aeronautical Systems Division, Air Force Systems Command, United States Air Force, under Contract Number AF 33(657)-10475 and Air Force Avionics Laboratory, Research and Technology Division, Air Force Systems Command, United States Air Force under Contract Number AF 33(615)-3434.

I thank my wife, Therese, for her constant encouragement and considerable help in preparing this manuscript.

TABLE OF CONTENTS


| | | Page |
|---|---|---|
| I. | Introduction | 1 |
| II. | Thin Film Sample Fabrication and Measurement Techniques | 9 |
| | A. General Considerations | 9 |
| | B. Preliminary Studies | 10 |
| | 1. Initial Vacuum System | 11 |
| | 2. Second Vacuum System | 14 |
| | 3. Six Port Vacuum System | 17 |
| | a. Metal Overlayer Tube | 19 |
| | b. Metal Underlayer Tube | 20 |
| | c. MgO Insulator Tube | 21 |
| | d. LEED Tube | 21 |
| | e. Measurements Tube | 22 |
| | f. Sputter Cleaning Tube | 23 |
| | g. Methods Used in the Fabrication of Sputtered Metal-MgO-Au Devices | 24 |
| | C. Experimental Vacuum System and Techniques Used in Final Approach | 29 |
| | 1. Description of Vacuum System | 29 |
| | 2. Description of Experimental Apparatus and Preliminary Results | 31 |

TABLE OF CONTENTS (continued)


| | | Page |
|---|---|---|
| | 3. Sample Preparation | 35 |
| | a. Glass Substrates | 35 |
| | b. MgO Substrates | 36 |
| | c. $CaF_2$ Substrates | 36 |
| | 4. Millisecond-Pulse Measurements of I-V Characteristics | 37 |
| | 5. Pulse Techniques Applied to Emission Measurements | 40 |
| | 6. DC Measurements of I-V Characteristics | 41 |
| III. | Results of Experimental Studies of Hot Electron Transport in Thin-Film Emission Diodes | 43 |
| | A. Introduction | 43 |
| | B. High Level I-V Characteristics of Thin Film Emission Diodes | 44 |
| | C. Temperature Measurements of the I-V Characteristics of Thin Film Emission Diodes | 56 |
| | D. Measurements Made on Devices Fabricated with Oxygen Gas Present During Deposition of the Oxide Film | 58 |

TABLE OF CONTENTS (continued)


| | | Page |
|---|---|---|
| | E. Low Level I-V Characteristics of Thin Film Emission Devices | 62 |
| | F. Measurements of Electron Emission into Vacuum from Thin Film Diodes | 63 |
| | G. Attempts to Fabricate a Device with a Single Crystal Oxide | 67 |
| IV. | Analysis of Hot Electron Transport Processes in Vacuum Deposited Thin-Film Emission Diodes | 71 |
| | A. Introduction | 71 |
| | B. Summary of Experimental Observations | 72 |
| | C. Discussion of a Model for Injection of Electrons into the Oxide Film | 74 |
| | D. Discussion of Emission into Vacuum | 93 |
| V. | Summary | 109 |
| APPENDICES | | |
| I. | Application of the Schottky Emission Problem to a Metal-Insulator-Metal Diode | 118 |
| II. | Barrier Height as a Function of Temperature and Excess Mg Concentration | 126 |

TABLE OF CONTENTS (continued)

Page

III. Calculation of the Fringing Field, F, at a Plane Electrode Beneath a Slot in an Opposing Plane Parallel Electrode 132

BIBLIOGRAPHY 136

FIGURES

# LIST OF FIGURES


| Figure Number | |
|---|---|
| 1 | Schematic Representation of Initial Vacuum System Used for Depositing Ordered Au-MgO-Au Emission Diodes. |
| 2a | Substrate Masks. |
| 2b | Substrate with Au-MgO-Au Thin Film Diode. |
| 3 | Schematic Representation of the Second Vacuum System Used for Depositing Ordered Au-MgO-Au Emission Diodes. |
| 4 | Six Port Vacuum System Top. |
| 5 | Schematic View of Six Port Vacuum System. |
| 6 | Detail of LEED Unit. |
| 7 | Schematic Representation of Bell Jar Section of Final Vacuum System. |
| 8a | Mask for Final Vacuum System. |
| 8b | Substrate with 3 Metal-Insulator-Metal Emission Diodes. |
| 9 | Circuit Used for Millisecond-Pulse Measurements of Thin-Film Hot Electron Emission Diodes. |
| 10 | Results of Millisecond-Pulse Measurement Technique, Showing I-V Characteristics and Expanded Traces. |

LIST OF FIGURES (continued)


| Figure Number | |
|---|---|
| 11 | Schematic of DC Measurement Technique for Au-MgO-Au Emission Diodes. |
| 12 | Tunnel I-V Characteristics of a Au-MgO-Au Device with an 89 Å Thick Oxide. |
| 13 | I-V Characteristics from Device PY-G-11, Overlayer 1. |
| 14 | Fowler-Nordheim Plot of the I-V Characteristics of Device PY-G-11, Overlayer 1. |
| 15 | Schottky Plot of the I-V Characteristics of Device PY-G-11, Overlayer 1. |
| 16 | Poole-Frenkel Plot of the I-V Characteristics of Device PY-G-11, Overlayer 1. |
| 17 | Comparison of Results of Devices with Thin (< 200 Å) Oxide Films. |
| 18 | Ln I vs. $V^{1/2}$ Plot for Two Devices with Thicker Oxide Films (680 Å). |
| 19 | Temperature Dependence of the I-V Characteristics of Device PY-G-11, Overlayer 1. |
| 20 | Ln I vs. $V^{1/2}$ as a Function of Temperature for Device PY-G-11, Overlayer 1. |
| 21 | $Ln(I_o/T^2)$ vs. 1/T for Device PY-G-11, Overlayer 1. |

LIST OF FIGURES (continued)


| Figure Number | |
|---|---|
| 22 | Comparison of Results with Different Pressures of Oxygen Present During Fabrication. |
| 23 | Arrhenius Plot of Devices Fabricated with Different Amounts of Oxygen Present During the MgO Deposition. |
| 24 | I-V Characteristics of Device PY-G-38(1). |
| 25 | Fowler-Nordheim Plot of I-V Characteristics of Device PY-G-38(1). |
| 26 | Comparison of Device Resistance as a Function of Temperature for Devices Fabricated with Different Amounts of Oxygen Present During Oxide Deposition. |
| 27 | Emission Transfer Ratio, $\alpha$, vs. Sample Voltage, $V_s$, for Device PY-G-11(1). |
| 28 | Comparison of Emission Transfer Ratio for Devices with Different Oxide Thicknesses. |
| 29 | Comparison of Emission Transfer Ratio for Devices with the MgO Film Deposited with Different Amounts of Oxygen Gas Admitted. |
| 30 | Potential Barrier Presented by a Dielectric Film Between Two Metals, Showing Electron Image Force Modification. |

LIST OF FIGURES (continued)


| Figure Number | |
|---|---|
| 31 | Potential Energy Maximum of an Electron in a Dielectric with an Applied Field Present. |
| 32 | Ln I vs. $V^{.484}$ for Device PY-G-11(1). |
| 33 | $Ln(I_o/T^2)$ vs. $10^3/T$ for Device PY-G-11(1) where $I_o$ is Found from the Ln I vs. $V^{.484}$ Plots. |
| 34 | Comparison Between the Data for Device PY-G-21(3) and Equation (3). |
| 35 | Ln I vs. $V^{.484}$ for Devices Measured at High Fields Only. |
| 36 | Comparison of Results for Devices Fabricated with Different Amounts of $O_2$ Present During MgO Deposition. |
| 37 | Comparison Between Experimental Data and Equation (3) for Devices Fabricated with Oxygen Present During MgO Deposition. |
| 38 | Energy Bands as a Function of Interatomic Spacing for a Simple Linear Chain. |
| 39 | $Ln(I_o/T^2)$ vs. $10^3/T$ for Devices Fabricated with Different Amounts of Oxygen Present During MgO Deposition. |
| 40 | Barrier Heights as a Function of Temperature. |

LIST OF FIGURES (continued)


Figure Number

41 Results of Device PY-A-1 with Two Different Metal Electrodes.

42a Energy Band Picture for a Gold-Vacuum Interface.

42b Energy Band Picture for a Gold-MgO Interface if No Interface States Exist.

42c Energy Band Picture for a Gold-MgO Interface with a High Density of Donor Like Interface States.

43 Diagram Indicating Details of the Calculation of Electric Field Variation at a Plane Electrode Opposite a Slotted Electrode.

44a Energy Level Diagram for an Applied Sample Bias of 4 Volts Showing that No Electrons Should be Emitted through the Overlayer.

44b Energy Level Diagram Appropriate for Emission through Holes in the Gold Overlayer Film.

45 Field Strength at the Underlayer Beneath a Slot in the Overlayer.

46 $\alpha = \frac{I_e}{I_e+I_s}$ as a Function of Oxide Thickness Assuming No Energy Loss in the Oxide.

47 Evidence of Charging at an Emitting Slot, Device PY-G-17(1).

LIST OF FIGURES (continued)

Figure Number

48a Emission Transfer Ratio vs. Time Required to Reach $V_s$ = 2 Volts.

48b Emission Transfer Ratio vs. Total Charge Passed through the Device.

49 Time Constants for Charging of the Insulator Beneath a Slot.

# Attachment A-4

Screen capture created by J L Mullins from WorldCat on December 6, 2024 at URL:
https://search.worldcat.org/title/763139404

WorldCat®

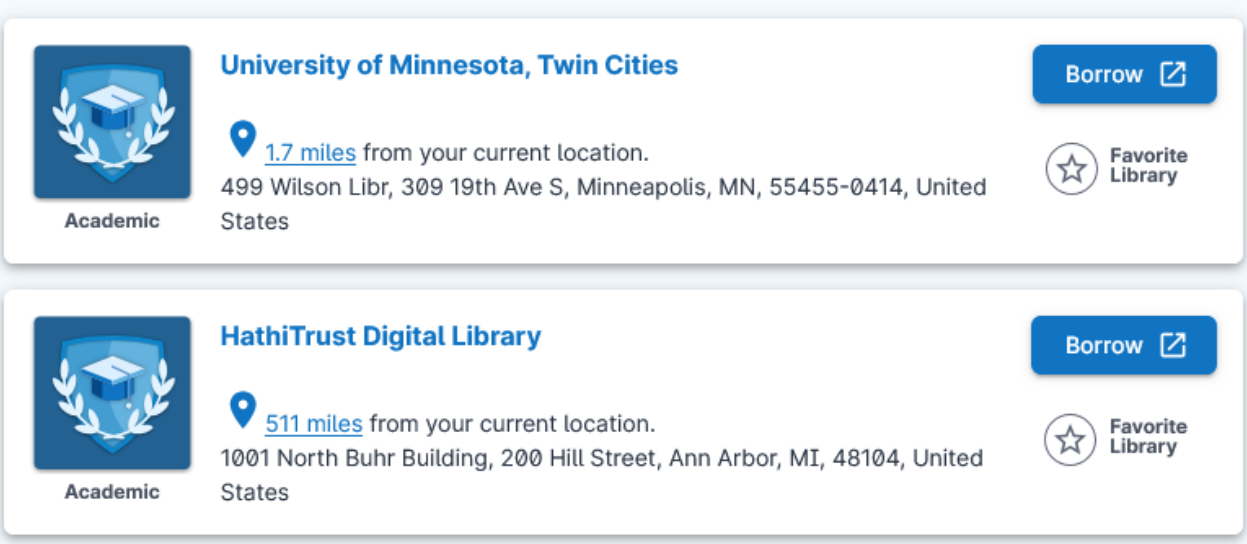
# Hot electron transport in vacuum deposited thin film emission diodes

**Author:** Rodney Joseph Soukup

**Thesis, Dissertation**, English, 1969
**Dissertation:** University of Minnesota

| | |
|---|---|
| **Genre:** | dissertations |
| **Physical Description:** | 1 online resource (xi, 146, [49] leaves) illustrations |
| **OCLC Number / Unique Identifier:** | 763139404 |
| **Subjects:** | Academic theses<br>Couches minces métalliques<br>Electrons Emission<br>Émission électronique<br>Metallic films<br>Thèses et écrits académiques<br>dissertations |
| **Additional Physical Form Entry:** | Print version:<br>Hot electron transport in vacuum deposited thin film emission diodes.<br>Soukup, Rodney Joseph.<br>17923718 |

Screen capture created by J L Mullins from WorldCat on December 6, 2024 at URL:
https://search.worldcat.org/title/763139404



# Attachment A-5

Screen capture created by J L Mullins from the University of Minnesota Libraries OPAC on December 6, 2024 at URL: https://primo.lib.umn.edu/discovery/fulldisplay?docid=alma9939979500001701&context=L&vid=01UMN_INST:TWINCITIES&lang=en&search_scope=TwinCitiesCampus_and_CI&adaptor=Local%20Search%20Engine&tab=Everything&query=any,contains,Hot%20Electron%20Transport%20in%20Vacuum%20Deposited%20Thin%20Film%20Emission%20Diodes.%20



THESIS / DISSERTATION

**Hot electron transport in vacuum deposited thin film emission diodes.**

Rodney Joseph Soukup

1969

Available at TC MN Library Access Center (Storage) U of M Twin Cities (MnU-D 69-109) >

Get It

Please sign in to see request options and to place requests. Sign in

< BACK TO LOCATIONS

LOCATION ITEMS

TC MN Library Access Center (Storage)
Available , U of M Twin Cities ; MnU-D 69-109
(1 copy, 1 available, 0 requests)

Item in place 319510019252833
Loanable

Details

| | |
|---|---|
| **Title** | Hot electron transport in vacuum deposited thin film emission diodes. |
| **Author/Creator** | Rodney Joseph Soukup > |
| **Date** | 1969 |
| **Thesis / Dissertation** | Ph.D. Univ. of Minnesota. |
| **Format** | xi, 146 pages, 49 unnumbered leaves : illustrations ; 29 cm |
| **Language** | English |
| **Description** | Bibliography: leaves 135-146. |
| **Subjects** | Electrons -- Emission > Metallic films > |
| **Identifier** | OCLC : 17923718 |
| **Source** | University of Minnesota Catalog 9939979500001701 |

# Attachment A-6

Screen capture created by J L Mullins from the University of Minnesota Libraries OPAC on December 6, 2024 at URL:
https://primo.lib.umn.edu/discovery/fulldisplay?docid=cdi_proquest_journals_302428580&context=PC&vid=01UMN_INST:TWINCITIES&lang=en&search_scope=TwinCitiesCampus_and_CI&adaptor=Primo%20Central&tab=Everything&query=any,contains,Hot%20Electron%20Transport%20in%20Vacuum%20Deposited%20Thin%20Film%20Emission%20Diodes.%20

LIBRARIES



THESIS / DISSERTATION

**HOT ELECTRON TRANSPORT IN VACUUM DEPOSITED THIN FILM EMISSION DIODES**

SOUKUP, RODNEY JOSEPH

ProQuest Dissertations & Theses; 1969

Download PDF › Read Article ›

Online access ›

## Online Access

**Access full text or digital resources**

Access in ProQuest

## Details

| | |
|---|---|
| **Title** | HOT ELECTRON TRANSPORT IN VACUUM DEPOSITED THIN FILM EMISSION DIODES |
| **Author/Creator** | SOUKUP, RODNEY JOSEPH › |
| **Publisher** | ProQuest Dissertations & Theses |
| **Date** | 1969 |
| **Language** | English |
| **Subjects** | Condensation › |
| **Identifier** | ISBN: 9798658445168 |
| **Source** | ProQuest Dissertations & Theses Global |

# Attachment A-7

Screen capture created by J L Mullins from the University of Minnesota Libraries OPAC on December 6, 2024 at URL:
https://primo.lib.umn.edu/discovery/fulldisplay?docid=alma9939979500001701&context=L&vid=01UMN_INST:TWINCITIES&lang=en&search_scope=TwinCitiesCampus_and_CI&adaptor=Local%20Search%20Engine&tab=Everything&query=any,contains,Hot%20Electron%20Transport%20in%20Vacuum%20Deposited%20Thin%20Film%20Emission%20Diodes.%20

```
leader  01104nam a22003611  4500
001     9939979500001701
005     20240223061650.0
008     871109s1969    mnua     b    000 0 eng d
035     ##$a(OCoLC)17923718
040     ##$aMnU $cMnU
100     1#$aSoukup, Rodney Joseph.
245     10$aHot electron transport in vacuum deposited thin film emission
diodes.
260     ##$c1969.
300     ##$axi, 146 pages, 49 unnumbered leaves : $billustrations ; $c29 cm
336     ##$atext $btxt $2rdacontent
337     ##$aunmediated $bn $2rdamedia
338     ##$avolume $bnc $2rdacarrier
502     ##$bPh.D. $cUniv. of Minnesota.
504     ##$aBibliography: leaves 135-146.
650     #0$aElectrons $xEmission
650     #0$aMetallic films
926     ##$aMARS
935     ##$a(MnU)notisAEH0411
935     ##$a(Aleph)000196246UMN01
945     ##$aCAT $b1987-12-21
967     ##$ascs20170325
967     ##$ascs20220128
968     ##$aRDA ENRICHED
999     99$aAEH0411 $bUL
998     ##$aLDR:01105nam#a22003611##4500
998     ##$b008:871109s1969####mnua#####b####000#0#eng#d
997     ##$a17923718
996     ##$bPh.D. $cUniv. of Minnesota.
```

Privacy Statement | Acceptable Use Policy

24/7 chat

# Attachment A-8

**JAMES L. MULLINS**

**From:** disspub@proquest.com
**Sent:** Monday, November 25, 2024 1:10 PM
**To:** JAMES L. MULLINS
**Subject:** Date of availability of a dissertation
**Attachments:** 7001819.pdf

You don't often get email from disspub@proquest.com. Learn why this is important

---- **External Email**: Use caution with attachments, links, or sharing data ----

Hello Jim,

Thanks for chatting in today and being so quick to call in for the affidavit fee.

I have sent over a request to our team to start working on the affidavit for publication #7001819. I have also attached the complimentary PDF copy to this email.

I will send the affidavit over to you once it's ready.

Let me know if you have any additional questions!

Kind regards,

Vicky Turner (she/her)
Author & School Relations

T +1 800 521 0600 press 2, then 1 (Time Zone: ET)

ProQuest | Part of Clarivate
about.proquest.com | clarivate.com

Visit our Knowledge Base<https://support.proquest.com> for additional information.
Visit our Status Page<https://status.proquest.com> to receive updates on planned/unplanned outages.

---------- Original Message ----------

**Subject**
Date of availability of a dissertation
**Description**
First Name: James
Last Name: Mullins
Email Address: jmullins@purdue.edu
Product: Dissertations & Theses
Subject: Date of availability of a dissertation
Case Number: 00000000

Brief Description: I need to know when the following dissertation was submitted to University Microfilms (pre ProQuest), when it would have been available for purchase, when an abstract would have been published in Dissertation Abstracts: Science and Engineering Soukup, Rodney Joseph. Hot Electron Transport in Vacuum Deposited Thin Film Emission Diodes. University of Minnesota, 1969.
Thank you.
Site: ASR
User Tech info: Mozilla/5.0 (Windows NT 10.0; Win64; x64) AppleWebKit/537.36 (KHTML, like Gecko) Chrome/131.0.0.0 Safari/537.36



ref:!00D300XOy.!500QO0MgQES:ref

# Attachment A-9

# DECLARATION

I, **Heather Stewart,** declare that the following statements are true and correct to the best of my knowledge, information and belief:

1. I am over 18 years of age and have personally reviewed the facts set forth in this declaration, based upon practices and training encountered in the course of my work overseeing a team of Technical Support Analysts, including my personal review and confirmation of available business records and documentation maintained by my employer, ProQuest LLC ("ProQuest").

2. I am a **Manager, Content Curation** employed by ProQuest in Ann Arbor, Michigan. I have worked for ProQuest since **1998** (+25 years). ProQuest is an information company that collects, organizes publishes and distributes for sale content from a wide range of sources, including dissertations and master's theses. I am familiar with ProQuest's sales and publication practices with respect to the publication of dissertations and master's theses as well as the related Abstract Database (defined in in paragraph 3).

3. ProQuest receives dissertations and master's theses from participating degree granting institutions. Shortly after these works are received, ProQuest makes them available for sale to the public, unless specifically restricted from sales by the dissertation author or the degree granting institution. Prior to 2013, a "Record" of each dissertation and each master's thesis submitted to ProQuest was published in ProQuest's print publication Dissertations Abstracts International or Master's Abstracts International, respectively (the print editions ceased being distributed in print as of volume 73-06 published in December 2012). Beginning in 1985, each Record is also published in the Dissertation Abstracts International Database ("Abstract Database").[1] A "Record" consists of an

[1] The Abstract Database has been maintained exclusively by ProQuest under various corporate names, including Bell & Howell Information and Learning Company, ProQuest Information and Learning Company, UMI Company and University Microfilms, Inc. and has been licensed to subscribers under various product names including "Dissertation Abstracts Online" and "ProQuest® Digital Dissertations."

abstract, index record, and citation information including title, author name, degree granting institution and degree date.

4. Prior to 1985, Records were published only in the print publications Dissertations Abstracts International and Master's Abstracts International. In 1985, the Records in these print publications were combined to create the Abstract Database which was made available online through third party vendors, such as Dialog, Data-Star, and OCLC. In 1987, ProQuest began to offer the Abstract Database on CD ROM. In 1997, ProQuest made available the contents of the Abstract Database in its ProQuest® Digital Dissertations and Theses database ("PQDT"), which is accessible via the world wide web to authenticated subscribers. The Abstract Database allows for text searching of the Records, including the title, author, index terms and the abstract.

5. The **PQDT** database includes the **Abstract Database** and is supplemented by the addition of certain select dissertations and master's theses in PDF format. Whether a dissertation is represented in full PDF format varies based on a number of factors, including the format in which the dissertation or theses was originally submitted for publication (digital, paper or microfiche) or whether the dissertation or theses was part of a retrospective digitization effort. PQDT allows for text searching of the Records as well as full text where the full PDF is properly formatted.

6. At the time of publication of the Dissertation (the full citation is provided in paragraph 9 below), ProQuest published in the **Abstract Database** a Record of each dissertation and each master's thesis that ProQuest offers for sale with new Records added on a **monthly** basis. Once a Record is published on the Abstract Database, the Record is available to the students, faculty, staff and/or patrons of any institutions that subscribe to the Abstract Database. At the time of publication the Abstract Database was available throughout the United States, through third party vendors as well as in CD-ROM format directly from ProQuest.

7. At the time of the Dissertation's publication, the Record and full PDF of the Dissertation was added to PQDT as specified below.

---

ProQuest LLC (and its predecessor entities) is and at all times has been a U.S. Company based in Ann Arbor, MI.

8. I have reviewed ProQuest's records regarding the Dissertation cited as:

| | |
|---|---|
| Dissertation No. | 7001819 |
| Title: | HOT ELECTRON TRANSPORT IN VACUUM DEPOSITED THIN FILM EMISSION DIODES |
| Author: | SOUKUP, RODNEY JOSEPH |
| Degree Date: | 1969 |
| University: | University of Minnesota |

**Full Text Availability**

| | |
|---|---|
| First Received by UMI/ProQuest: | n/a |
| First Made Available for Sale (print or electronic) | 01/1969 |
| DAI volume issue: | DAI-B 30/08, Dissertation Abstracts International |
| DAI publication month and year: | 01/1969 |
| Date full text is loaded into PQDT: | 01/1969 |
| Information available on restrictions: | no restrictions ever placed on document |

9. At the time of the Dissertation's publication, the Record of the Dissertation was made available directly from ProQuest in electronic format and online via third party vendors, including Dialog, as part of the Abstract Database which was made available via such vendors in the ordinary course of business.

10. The attached print copy of the Dissertation is a true and complete copy of the Record and the full Dissertation as originally published and kept by ProQuest in the ordinary course of its business.

I make this Declaration on personal knowledge and, if called as a witness at trial, I am competent to testify.

I declare under penalty of perjury that the forgoing is true and correct.

Executed on 11/26/2024

Heather Stewart

**Heather Stewart**
**Manager, Content Curation**

# Attachment A-10

This dissertation has been
microfilmed exactly as received

70-1819

SOUKUP, Rodney Joseph, 1939-

HOT ELECTRON TRANSPORT IN VACUUM DEPOSITED THIN FILM EMISSION DIODES.

University of Minnesota, Ph.D., 1969
Physics, solid state

University Microfilms, Inc., Ann Arbor, Michigan

# HOT ELECTRON TRANSPORT IN VACUUM DEPOSITED THIN FILM EMISSION DIODES

A Thesis

Submitted to the Graduate Faculty

of the

University of Minnesota

by

Rodney Joseph Soukup

In Partial Fulfillment of the Requirements

for the

Degree of

Doctor of Philosophy

June, 1969

## ACKNOWLEDGMENTS

I wish to extend my sincere appreciation to Dr. D. E. Speliotis for his advice and helpful discussions.

I also wish to thank Dr. D. E. Anderson for suggesting the topic of study and for his interest and suggestions. To all associated with the Physical Electronics Laboratory, I extend thanks for the loan of equipment and for helpful suggestions.

I wish to acknowledge the support of this work by Aeronautical Systems Division, Air Force Systems Command, United States Air Force, under Contract Number AF 33(657)-10475 and Air Force Avionics Laboratory, Research and Technology Division, Air Force Systems Command, United States Air Force under Contract Number AF 33(615)-3434.

I thank my wife, Therese, for her constant encouragement and considerable help in preparing this manuscript.

TABLE OF CONTENTS


| | | Page |
|---|---|---|
| I. | Introduction | 1 |
| II. | Thin Film Sample Fabrication and Measurement Techniques | 9 |
| | A. General Considerations | 9 |
| | B. Preliminary Studies | 10 |
| | 1. Initial Vacuum System | 11 |
| | 2. Second Vacuum System | 14 |
| | 3. Six Port Vacuum System | 17 |
| | a. Metal Overlayer Tube | 19 |
| | b. Metal Underlayer Tube | 20 |
| | c. MgO Insulator Tube | 21 |
| | d. LEED Tube | 21 |
| | e. Measurements Tube | 22 |
| | f. Sputter Cleaning Tube | 23 |
| | g. Methods Used in the Fabrication of Sputtered Metal-MgO-Au Devices | 24 |
| | C. Experimental Vacuum System and Techniques Used in Final Approach | 29 |
| | 1. Description of Vacuum System | 29 |
| | 2. Description of Experimental Apparatus and Preliminary Results | 31 |

TABLE OF CONTENTS (continued)


| | | Page |
|---|---|---|
| 3. | Sample Preparation | 35 |
| | a. Glass Substrates | 35 |
| | b. MgO Substrates | 36 |
| | c. $CaF_2$ Substrates | 36 |
| 4. | Millisecond-Pulse Measurements of I-V Characteristics | 37 |
| 5. | Pulse Techniques Applied to Emission Measurements | 40 |
| 6. | DC Measurements of I-V Characteristics | 41 |
| III. | Results of Experimental Studies of Hot Electron Transport in Thin-Film Emission Diodes | 43 |
| A. | Introduction | 43 |
| B. | High Level I-V Characteristics of Thin Film Emission Diodes | 44 |
| C. | Temperature Measurements of the I-V Characteristics of Thin Film Emission Diodes | 56 |
| D. | Measurements Made on Devices Fabricated with Oxygen Gas Present During Deposition of the Oxide Film | 58 |

TABLE OF CONTENTS (continued)


| | | Page |
|---|---|---|
| | E. Low Level I-V Characteristics of Thin Film Emission Devices | 62 |
| | F. Measurements of Electron Emission into Vacuum from Thin Film Diodes | 63 |
| | G. Attempts to Fabricate a Device with a Single Crystal Oxide | 67 |
| IV. | Analysis of Hot Electron Transport Processes in Vacuum Deposited Thin-Film Emission Diodes | 71 |
| | A. Introduction | 71 |
| | B. Summary of Experimental Observations | 72 |
| | C. Discussion of a Model for Injection of Electrons into the Oxide Film | 74 |
| | D. Discussion of Emission into Vacuum | 93 |
| V. | Summary | 109 |
| APPENDICES | | |
| I. | Application of the Schottky Emission Problem to a Metal-Insulator-Metal Diode | 118 |
| II. | Barrier Height as a Function of Temperature and Excess Mg Concentration | 126 |

TABLE OF CONTENTS (continued)


| | Page |
|---|---|
| III. Calculation of the Fringing Field, F, at a Plane Electrode Beneath a Slot in an Opposing Plane Parallel Electrode | 132 |
| BIBLIOGRAPHY | 136 |
| FIGURES | |

## LIST OF FIGURES


| Figure Number | |
|---|---|
| 1 | Schematic Representation of Initial Vacuum System Used for Depositing Ordered Au-MgO-Au Emission Diodes. |
| 2a | Substrate Masks. |
| 2b | Substrate with Au-MgO-Au Thin Film Diode. |
| 3 | Schematic Representation of the Second Vacuum System Used for Depositing Ordered Au-MgO-Au Emission Diodes. |
| 4 | Six Port Vacuum System Top. |
| 5 | Schematic View of Six Port Vacuum System. |
| 6 | Detail of LEED Unit. |
| 7 | Schematic Representation of Bell Jar Section of Final Vacuum System. |
| 8a | Mask for Final Vacuum System. |
| 8b | Substrate with 3 Metal-Insulator-Metal Emission Diodes. |
| 9 | Circuit Used for Millisecond-Pulse Measurements of Thin-Film Hot Electron Emission Diodes. |
| 10 | Results of Millisecond-Pulse Measurement Technique, Showing I-V Characteristics and Expanded Traces. |

LIST OF FIGURES (continued)


| Figure Number | |
|---|---|
| 11 | Schematic of DC Measurement Technique for Au-MgO-Au Emission Diodes. |
| 12 | Tunnel I-V Characteristics of a Au-MgO-Au Device with an 89 Å Thick Oxide. |
| 13 | I-V Characteristics from Device PY-G-11, Overlayer 1. |
| 14 | Fowler-Nordheim Plot of the I-V Characteristics of Device PY-G-11, Overlayer 1. |
| 15 | Schottky Plot of the I-V Characteristics of Device PY-G-11, Overlayer 1. |
| 16 | Poole-Frenkel Plot of the I-V Characteristics of Device PY-G-11, Overlayer 1. |
| 17 | Comparison of Results of Devices with Thin (< 200 Å) Oxide Films. |
| 18 | Ln I vs. $V^{1/2}$ Plot for Two Devices with Thicker Oxide Films (680 Å). |
| 19 | Temperature Dependence of the I-V Characteristics of Device PY-G-11, Overlayer 1. |
| 20 | Ln I vs. $V^{1/2}$ as a Function of Temperature for Device PY-G-11, Overlayer 1. |
| 21 | $Ln(I_o/T^2)$ vs. 1/T for Device PY-G-11, Overlayer 1. |

LIST OF FIGURES (continued)

Figure Number

22 Comparison of Results with Different Pressures of Oxygen Present During Fabrication.

23 Arrhenius Plot of Devices Fabricated with Different Amounts of Oxygen Present During the MgO Deposition.

24 I-V Characteristics of Device PY-G-38(1).

25 Fowler-Nordheim Plot of I-V Characteristics of Device PY-G-38(1).

26 Comparison of Device Resistance as a Function of Temperature for Devices Fabricated with Different Amounts of Oxygen Present During Oxide Deposition.

27 Emission Transfer Ratio, $\alpha$, vs. Sample Voltage, $V_s$, for Device PY-G-11(1).

28 Comparison of Emission Transfer Ratio for Devices with Different Oxide Thicknesses.

29 Comparison of Emission Transfer Ratio for Devices with the MgO Film Deposited with Different Amounts of Oxygen Gas Admitted.

30 Potential Barrier Presented by a Dielectric Film Between Two Metals, Showing Electron Image Force Modification.

LIST OF FIGURES (continued)


Figure Number

31 Potential Energy Maximum of an Electron in a Dielectric with an Applied Field Present.

32 Ln I vs. $V^{.484}$ for Device PY-G-11(1).

33 $Ln(I_o/T^2)$ vs. $10^3/T$ for Device PY-G-11(1) where $I_o$ is Found from the Ln I vs. $V^{.484}$ Plots.

34 Comparison Between the Data for Device PY-G-21(3) and Equation (3).

35 Ln I vs. $V^{.484}$ for Devices Measured at High Fields Only.

36 Comparison of Results for Devices Fabricated with Different Amounts of $O_2$ Present During MgO Deposition.

37 Comparison Between Experimental Data and Equation (3) for Devices Fabricated with Oxygen Present During MgO Deposition.

38 Energy Bands as a Function of Interatomic Spacing for a Simple Linear Chain.

39 $Ln(I_o/T^2)$ vs. $10^3/T$ for Devices Fabricated with Different Amounts of Oxygen Present During MgO Deposition.

40 Barrier Heights as a Function of Temperature.

## LIST OF FIGURES (continued)


Figure Number

41 Results of Device PY-A-1 with Two Different Metal Electrodes.

42a Energy Band Picture for a Gold-Vacuum Interface.

42b Energy Band Picture for a Gold-MgO Interface if No Interface States Exist.

42c Energy Band Picture for a Gold-MgO Interface with a High Density of Donor Like Interface States.

43 Diagram Indicating Details of the Calculation of Electric Field Variation at a Plane Electrode Opposite a Slotted Electrode.

44a Energy Level Diagram for an Applied Sample Bias of 4 Volts Showing that No Electrons Should be Emitted through the Overlayer.

44b Energy Level Diagram Appropriate for Emission through Holes in the Gold Overlayer Film.

45 Field Strength at the Underlayer Beneath a Slot in the Overlayer.

46 $\alpha = \frac{I_e}{I_e+I_s}$ as a Function of Oxide Thickness Assuming No Energy Loss in the Oxide.

47 Evidence of Charging at an Emitting Slot, Device PY-G-17(1).

LIST OF FIGURES (continued)

Figure Number

48a Emission Transfer Ratio vs. Time Required to Reach $V_s$ = 2 Volts.

48b Emission Transfer Ratio vs. Total Charge Passed through the Device.

49 Time Constants for Charging of the Insulator Beneath a Slot.

## LIST OF TABLES


| | | Page |
|---|---|---|
| Table I | Barriers for different devices as obtained from the zero field intercept of the Schottky plot. | 53 |
| Table II | Barrier heights for different devices as obtained by the zero field intercept and the slope of the ln $(I_o/T^2)$ vs. 1/T plot. | 57 |
| Table III | Overlayer thicknesses for measured devices. | 64 |
| Table IV | Summary of device data. | 70 |
| Table V | Barrier heights for a number of devices with different parameters. | 81 |

# I. INTRODUCTION

Thin film metal-insulator-metal diode devices have been investigated quite extensively in recent years. The interest in these devices has arisen, in part, from the possible application of such devices as active circuit elements or electron sources, as suggested by Mead[1,2] and Geppert.[3] Additional motivation has been provided by interest in the transport of "hot electrons" in the insulator and in the metal overlayer with subsequent emission into vacuum. The term "hot electrons" is used to describe a nonequilibrium situation in solids where a group of electronic energy levels above the Fermi energy is characterized by a greater electron population than that which coincides with the lattice temperature. Well-known examples of this phenomenon include photoemission and secondary emission, in which the internal secondary electrons and photoexcited electrons can be characterized as hot electrons.

When an insulator and a metal are placed in contact the insulator presents a barrier to electron motion, which is part of its forbidden energy gap. However, when an electric field on the order of $10^6$ V/cm. is applied to a thin insulating film on the order of 100 Å thick, sandwiched between two metal films, a current is

observed. This current could be ionic current,[4] but, if the metal and insulator are stable during the application of this field, ionic current can be ignored. The current must then be an electron current. The electrons must either surmount the barrier, Richardson-Schottky current,[5,6] or penetrate through it. This penetration of electrons through a barrier is known as tunnelling and was first described by Fowler and Nordheim[7] in 1928. It has specifically been applied to thin film devices by other authors.[2,8-11] A combination of the two processes is also possible.[12,13] Another mechanism that has been proposed to explain the current observed is the Pool-Frenkel effect.[14] In this effect the current is limited by the field enhanced thermal emission of electrons from a discreet trap level into the conduction band of the oxide. Other possible processes for the conduction mechanism in thin oxide films have been summarized by Jonscher.[15] These processes could all be modified by space charge.[16-18] Thus, the electron process of importance in these devices is in some doubt. Under appropriate conditions a fraction of these electrons, accelerated by the electric field and injected into the overlayer metal film as hot electrons, can penetrate the overlayer film and arrive at the vacuum

interface with sufficient energy to escape, thus constituting an emission current.

Hot electron emission from such devices was first reported by Mead[2] in 1961 using Al-$Al_2O_3$-Al thin film devices. The fraction, $\alpha$, of the total sample current which was emitted into vacuum depended on the sample voltage and current, as well as the sample construction details, and was as high as 0.01. Similar experiments with Al-$Al_2O_3$-(Al or Pt) samples were reported by Cohen.[19] These early experiments demonstrated that emission currents could be drawn from such thin film devices, but the fraction of the total sample current that was emitted was small. Instabilities and breakdown effects were observed which severely limited the total current obtainable.

Mead[20] reported more extensive studies in 1962 using Be-BeO-Au devices, in which the emitted fraction, $\alpha$, of the sample current was measured as a function of Au overlayer film thickness. The results indicated strong attenuation of the hot electrons in the metal overlayer films, and gave evidence of elastic interactions of the injected electrons in the insulating film. Kanter and Feibelman[21] studied Al-$Al_2O_3$-Au devices with results that were in general agreement with the previous results.

Using Mead's results for attenuation in the Au films, an estimate of the importance of inelastic interactions in the $Al_2O_3$ film was obtained. Collins and Davies[22] and Savoye and Anderson[12] also concluded that strong attenuation of the hot electrons occurred in both the insulating film and metal overlayer.

The simple energy-band picture, originally proposed by Mead,[1] allows one to distinguish three stages in the hot electron emission process: injection of electrons into the insulator; transport of the electrons through the insulating film; and transfer through the metal overlayer region into vacuum.

The electron injection process has been analyzed theoretically by several observers.[5,6,8-16,23-25] The conclusion arrived at is that both thermal and field effect currents can occur with the barrier height determining which mechanism is dominant. The simple band picture was used by Simmons[11,23] to analyze the electron injection process in terms of tunnelling, where the insulator presents a potential barrier to the electrons. An approximate multiple-image correction to the potential profile was included in the analysis. The experiments of Nelson and Anderson[26] with

$Al-Al_2O_3-$(Al and Au) devices were found to be in good agreement with Simmon's potential profile model.

A major difficulty in the studies of thin film emission diodes is that the mechanisms of importance at the various stages of the hot electron transport process are not readily separable on an experimental basis. Although the work of Savoye and Anderson[12] allowed a partial decoupling of the hot electron interactions at the various stages of the electron transport process a number of uncertainties still exist. A large number of impurities are inevitable in the oxide film and at the oxide-metal overlayer interface when the films are moved from the vacuum system into an aqueous anodizing solution and back into another vacuum system. There is the possibility of an oxide gradient in the insulating film resulting in rectification effects, as seen by Nelson,[27] the insulator must be the oxide of the underlayer metal, and the metal and insulator films are amorphous.

The number of impurities in the devices can be greatly reduced if the device is never removed from the vacuum system during fabrication and study. This could be accomplished by plasma anodization[28,29] of a vacuum deposited underlayer metal and subsequent deposition of

an overlayer. The possibility of an oxide gradient and the condition that the insulator must be the oxide of the metal underlayer can be removed by vacuum deposition of the insulating layer. This can be accomplished by rf sputtering of the insulator[30,31] or reactive sputtering[32] of a metal or semiconductor in an active gas by dc methods. Another method of deposition is to evaporate the insulator at a controlled deposition rate by use of a high energy electron beam as first proposed by O'Bryan.[33] General design principles of this method are discussed by Holland.[32]

A major problem with amorphous devices is that the mean free path of hot electrons may be dominated by scattering from imperfections, while in an ordered device the electron scattering may be reduced to that characteristic of the ordered crystal. Another problem is that the simple band picture may not give a true description of the barrier profile, as a consequence of the spatial variations. The influence of structural effects in the thin insulating film was considered by Harris,[34] who presented strong evidence of preferential conduction associated with localized defects in the insulator. The existence of preferential electron emission through holes in the overlayer metal film was

discussed by Savoye and Anderson.[12] Thus, structural effects of both insulator and metal overlayer films play an important part in the emission of hot electrons into vacuum. McColl and Mead,[35] in their studies of electron current through single crystal mica films, found that tunnelling theory provides a self-consistent quantiative description for smaller voltages, but was completely inadequate for use with voltages larger than the barrier height. This is another indication that ordered devices may differ. Ordered devices can be fabricated by epitaxial growth[36] of each layer on a single crystal substrate.

In the present work it was found to be essential for a detailed interpretation of the emission results that certain other experiments be conducted on a given sample in order to gain information not directly obtainable from the I-V characteristics and simple emission results. The I-V characteristics must be measured to determine if the injection mechanism is field or thermally dominated emission. The simple emission measurements yield information on the attenuation of the hot electrons.

The experiments were designed to permit complete fabrication and study of the devices <u>in situ</u>, and hence

the information provided by these experiments was made for a given sample known to be free from impurities. A number of samples were prepared during one evacuation of the system and so measurements were made over a range of insulator thicknesses.

Evaporation of the MgO dielectric layer was done at a pressure of $10^{-8}$ Torr with no $O_2$ gas admitted during fabrication as well as with various background pressures of oxygen admitted in an attempt to produce stoichiometric MgO and thus vary the barrier presented to the flow of electrons by the dielectric layer. All measurements of device I-V characteristics were done at a number of different temperatures in order to determine the effect of temperature on the device characteristics. The results were then combined into a comprehensive model for the hot electron emission process for vacuum deposited Au-MgO-Au sandwich devices.

# II. THIN FILM SAMPLE FABRICATION AND MEASUREMENT TECHNIQUES

## A. General Considerations

In any experiment involving thin film devices the utmost care is required at all stages of sample fabrication and measurement to avoid contamination by trace amounts of impurities. These considerations are of particular importance in the present work, where films on the order of 100 Å thickness are required to be uniform in composition and thickness and free from localized defects.

It is necessary to carry out all stages of sample preparation and measurement without breaking vacuum. This requires means for producing the various films and making the various measurements with the sample *in situ*. In addition to measurement of sample transport properties, electron diffraction studies[37] must be made to determine film order.

The original choice of materials to be used was a device made of Au-MgO-Au thin films deposited on a cleaved single crystal substrate. The reason for this choice is that Au and MgO are quite similar in crystal structure and size, and the fact that Savoye and Anderson[12] had discovered preferential emission of electrons through holes in a gold overlayer. MgO was a good insulator because a considerable amount of information has been

obtained on MgO, particularly in these labs,[38] and the properties of MgO are thus quite well known.

B. Preliminary Studies

The major problem of concern is whether vacuum deposited MgO films are free from pinholes and breakdown. This problem was thought to be solved by a few preliminary investigations of MgO films rf sputter deposited on two types of substrates. The first attempt was a series of MgO films sputtered onto an unpolished nickel substrate. The resistance of the film was measured using a Triplett multimeter with a fine wire attached to one lead. The fine wire was moved around on the film to check uniformity and to discover any pinholes which might be present. These films were found to have many pinholes but had a high resistance in places free from pinholes. The next series of tests were run on MgO films sputtered onto a thin film of gold which was deposited on a clean microscope glass slide. These films were relatively free from pinholes and also had a high resistance as determined with an ohmmeter. It was assumed from the results of these studies that sputter deposited MgO would make a good insulator for metal-insulator-metal diode devices.

## 1. Initial Vacuum System

In order to fabricate and study the ordered metal-insulator-metal diode devices without breaking vacuum a number of items must be incorporated into the vacuuum system. These include an electron diffraction system, a means to electrically measure the devices, and means of depositing the underlayer, insulator, and overlayer into a given pattern. The first attempt at a vacuum system which would incorporate all these systems is shown in Fig. 1. The LEED apparatus had been incorporated into the top half of the bell jar. The LEED apparatus was shielded from the sputtering chamber by a stainless steel disk 5" in diameter with a 2" hole in the center. In this hole was a rotating substrate holder which was turned by means of a chain drive. On each side of the substrate holder was a cleaved single crystal MgO substrate. When the substrate was facing down the Au and MgO layers could be deposited; when it was facing up it could be studied with the LEED apparatus. The substrate had leads attached to it for the purpose of heating, temperature monitoring, and measurement of the diode characteristics. The insulating substrate holder carried these leads which had to be easily detachable. A pressure contact system was built for this purpose. It consisted of 13 stainless

steel washers which rotated on tungsten ribbons imbedded in another insulator.

The sputtering half of the bell jar included Kovar feedthroughs for use as rf sputtering electrodes. One electrode was shielded by a ceramic MgO disk. The other electrode had a Kovar disk attached to it which held a high purity MgO ceramic disk, used as the sputtering target. The metal layers for these devices were to be formed by dc sputtering of a high purity gold disk. The gold disk was mounted on an insulating disk which could be rotated so that the sputtering of gold was to be done directly above the MgO disk, as can be seen in Fig. 1. When MgO was to be sputtered the gold was rotated out of the plasma area. Initially the gold was to be sputtered using a triode configuration with a nickelate cathode[39] as the electron source. However, difficulty was encountered in providing sufficient filament power for conversion of the cathode. Thus, a tungsten filament was used.

The resulting diode was to have the geometrical configuration shown in Fig. 2b. This design could be accomplished by means of a single mask which consisted of two stainless steel plates as shown in Fig. 2a. These plates were attached to a threaded stainless steel rod by means of square nuts. One half of the rod had left-hand threads,

while the other half had right hand threads, so that both plates moved in and out from the substrate center at the same time and speed. This threaded rod was to be rotated by means of a chain drive. The method to be used in producing a diode configuration shown in Fig. 2b was as follows. When sputtering was to be initiated the edges A of the sheets would just overlap so that no deposit could be made while the target was sputter cleaned. The sheets were then to be separated so that edges A were 0.1" apart and a gold film deposited. The sheets were then to be moved in so that they overlapped while the MgO target was sputter cleaned. Then the sheets were to be moved out so that edges A were 0.2" apart and MgO deposited so that it completely covered the Au underlayer. The sheets were then moved so that edges B would just overlap and the Au overlayer deposited crosswise over the MgO layer producing the desired Au-MgO-Au diode device.

A bell-jar collar was used between the baseplate and the bell jar in order to allow an adequate number of electrical feedthroughs into the vacuum. The completed system had three moving parts; the substrate holder, the mask, and the gold target. Many components were mounted partially on the baseplate and partially on the collar. The result of this configuration was that any changes

that were necessary were extremely difficult to make as a consequence of the many moving parts and the close spacing involved in a 5" I.D. bell jar.

The initial pumpdown of this system was made and a number of baseplate feedthroughs were found to leak in the $10^{-1}$ Torr range. Rather than remount the components on a new baseplate, a new vacuum system configuration was used, still employing a 5" I.D. bell jar.

The vacuum system also included a Ti getter[40] to aid in pumpdown and to obtain a lower ultimate pressure; two sputter ion pumps,[41] one was a diode pump and the other a triode pump;[42] two gas admission systems, one to admit Ar gas for sputtering, this system included a cataphoresis tube[43] for cleaning the Ar gas, and one to admit $O_2$ gas for reactive sputtering in case the MgO films contained excess magnesium.

## 2. Second Vacuum System

The second vacuum system developed for these studies is shown in Fig. 3. The upper half of this system also contained the LEED apparatus. The electrical leads for the LEED apparatus, which are not shown, were run through an insulator attached to the stainless steel shield and attached to electrical feedthroughs in the bell-jar baseplate and collar which is described below. Removal of the

LEED apparatus was necessary in order to replace the substrates, which were otherwise inaccessible. Therefore, the LEED system was also mounted on this shield which in turn was easily demountable.

The bell-jar collar consisted of a stainless steel cylinder 0.1" thick with large flanges on top and bottom for attachement to bell jar and bell-jar baseplate respectively. Six smaller flanges were welded to the side of the cylinder. The collar was necessary in order to mount a magnetic feedthrough to rotate the substrate holder in a vertical plane. Additional electrical feedthroughs were needed so a five lead press and a six lead press mounted on flanges were attached to the collar. There was also a Pyrex glass window to enable visual indexing of the substrates behind the substrate masks.

The substrates were single crystals of MgO and were held on the rotating substrate holder by small tabs. The substrate holder had room for three substrates and a blank which was to face the target during sputter cleaning of the target. Inside the cylindrical substrate holder four small stationary heater filaments were mounted. The substrates were to be heated during deposition of Au and MgO in order to increase the probability of epitaxial growth of the film. The substrate could also be heated

during LEED investigations in order to minimize the charging of the dielectric substrate. A stationary insulator containing electrical contacts to electrical feedthroughs on the collar were also mounted inside the rotating substrate holder. The electrical contacts to the diodes were thus able to make pressure contact to the stationary leads when the substrate was in position in the LEED chamber.

Mounted on each side of the substrate holder were dc sputtering assemblies with Au targets directly in line with the substrates and 1.3" away. The MgO target was mounted on a Kovar rf feedthrough directly below the substrate and 1" away. A substrate mask was mounted between the substrate and each target resulting in a Au-MgO-Au diode as in Fig. 2.

Although this system had only one moving part, the substrate holder, the close spacing in the 5" I.D. bell jar resulted in some unsolvable problems. The main problem was the heat radiated by the filament used for dc support of the plasma. The heat caused cracking of the quartz crystal,[44,45] used to determine deposition rates, before any rates could be determined. In addition the heat opened up leaks in the baseplate feedthroughs when the filament was on, the leaks sealed when the filament was cooled but would open again when the filament was

again heated. The filament was then placed inside a heat shield with five metal layers separated by approximately 0.1". This did not help. It was decided that the close spacing involved in a 5" I.D. bell jar could not be tolerated. Rather than build a larger vacuum system a new approach was attempted.

The vacuum system included the same pumping and gas admission systems as included in the initial vacuum system.

3. Six Port Vacuum System

The six port vacuum system consisted of the standard bell-jar baseplate and collar with a special top shown in Fig. 4. The six holes on the 2.674 DIA.B.C. had bellows welded into them to move six different substrates, mounted on rods, from port to port and into each port for that particular part of the experiment. The system with push rods is shown schematically in Fig. 5. In this system six separate, related experiments could be carried out in the six different ports labeled A-F in Fig. 5, with the intention of fabricating and testing in situ ordered layer metal-oxide-metal diode devices. The six ports will be described in detail below. Port A was used to deposit the metal overlayer and port B to deposit the metal underlayer. Port C was used to rf sputter deposit the insulating layer. Port D contained the LEED system

used to determine the order of the film growth. Port E was the measurements port and port F was used to sputter clean the substrate. This vacuum system included the same pumping and gas admission system as the two previous systems with the exception that it contained two diode pumps as well as one triode pump.

The part of the system within the bell-jar collar contained the six substrates mounted on six different push rods labeled I-VI in Fig. 5. These push rods had holes drilled through them every 1/4 in. so that they could be pushed out into a particular port with a pick attached to a bellows and subsequently removed from this port. Each push rod ran through a guide rigidly attached to a rotating ring. Rotational motion could be achieved by pushing on the side of two of the push rods with the same picks used for linear motion. In this manner any given substrate attached to a push rod could be rotated and aligned with any given port.

The geometry that allowed six push rods and thus six substrates was that which had two push rods I and II in Fig. 5, that could move into ports 180° apart, above the others and aligned in a horizontal plane. Push rods III and IV were just beneath I and II, and V and VI were beneath these. Figure 5 also shows push rod VI pushed

out into port D, the LEED system. The size of the collar limited the system to six substrates.

A complete experiment on a single substrate was to be accomplished by the following succession of events. The substrate was to be inserted into port F and sputter cleaned, it was then to be moved to port D and the surface was to be examined with LEED. The substrate would then be moved to port B and a metal underlayer sputter deposited and the film order then studied with LEED. The substrate was then to be moved to port C and an insulating layer rf sputter deposited and the film order again studied with LEED. The substrate would then be moved to port A and a metal overlayer sputter deposited onto it with a study of film order again made. Finally the substrate was to be moved to port E and measurements made on the completed device. The following is a short description of each tube.

a. Metal Overlayer Tube

The purpose of this tube was to deposit the metal overlayer, which was always gold. The inside of the tube contained a filament, two anode rings, and a virtual cathode to produce a dc supported plasma. The plasma was confined to a beam with this geometry and the aid of an external magnet producing a field parallel to the filament-anode-virtual cathode center line. The gold target was

mounted in such a position that it was just on the edge of the plasma and in the same plane as the center of the substrate mask. The mask was mounted outside the plasma area and directly opposite the Au target, 3" from it. The mask allowed deposition of a 0.1" wide vertical strip of metal as the overlayer.

A filament enclosed in a Ta heat shield was mounted on the mask for the purpose of heating the substrate while deposition was taking place, in order to increase the probability of epitaxial growth. The filament was a 0.020" diameter advance wire wound into a spiral which then encircled the substrate mask. The heating of the substrate was found to be quite uniform with this geometry. Using this filament the substrate could be heated to a temperature of 500°C with a filament power of 50 watts.

The sputter deposition rates for this tube were very uniform from run to run at a given target current and voltage regardless of the other parameters. The deposition rate vs. target current curve was very close to the straight line predicted by Bell and Anderson[46] assuming a hemispherical distribution of sputtered atoms.

### b. Metal Underlayer Tube

This tube was designed exactly the same as the metal overlayer tube with the exception of the mask.

This mask allowed deposition of a 0.1" wide horizontal strip of metal for the underlayer film.

The sputter deposition rates for this tube were nearly exactly the same as for the overlayer tube.

c. MgO Insulator Tube

This tube employed rf sputtering to deposit the insulating layer of the devices. The major difficulties encountered in the six port vacuum system occurred in this tube. These difficulties and changes in tube design will be explained in section II-B-3-g.

d. LEED Tube

The LEED tube was used to determine whether the films grown were single crystal, polycrystalline, or amorphous. The unit consisted of a 2 1/2" diameter display chamber and a three element electron gun as shown in Fig. 6. Except for the gun, the main metal parts were #304 stainless steel.

The screen of the display chamber was a Pyrex hemisphere coated on the inner surface with conducting tin oxide over which was a thin layer of phosphor. Electrical connection was made between the conductive coating and the mounting plate via spring-loaded tungsten point contacts.

Inside the display screen and concentric to it were two hemispherical grids (2 3/32" and 1 7/8" in diameter) which were fabricated by chrome plating a tungsten mesh.[47] The flat end of the smaller grid was closed to prevent penetration of external fields into the display chamber.

The only LEED pattern ever observed in this tube was of the substrate, single crystal MgO, after sputter cleaning. This pattern was observed at a pressure of $10^{-3}$ Torr of Ar gas. No problems were encountered while the pressure was so high. The fact that the surface could be studied at so high a pressure made the experiment possible since the background pressure of the system was never below $10^{-8}$ Torr and the pumpdown time from $10^{-3}$ Torr to this level was about 6 hours.

e. Measurements Tube

This tube contained a Supramica 500* disk with four spring contacts attached to it for electrical contact to the underlayer and overlayer films. The I-V characteristics of the device could then be measured without removing it from the vacuum.

---

*Supramica 500 is the trade name of the Mycalex Corporation of America for their synthetic mica.

The end of the tube was made of a quartz window for which the light transmission versus photon energy had been measured. The center of the Supramica had a hole in it so that the light would be incident on the diode itself. The purpose of this arrangement was to measure the potential barrier presented to the electrons by the insulator.[26,27] The arrangement also allowed for photoemission measurements to be made, since a grid was present for collection of photoemitted electrons.

A swinging phosphor screen was also present so that the emission density patterns from the device as well as the total emission could be measured. This screen could be swung into a position in front of the diode while these measurements were to be made and then swung out of the line of sight to the diode when the photomeasurements were made.

### f. Sputter Cleaning Tube

The purpose of this tube was to clean the substrate surface by $Ar^+$ ion bombardment. The design of the tube was identical to the overlayer and underlayer tubes except that no target was present. The plasma was a dc supported plasma with an rf potential applied between the substrate and the filament. RF sputter cleaning of the substrate was believed to be necessary in order to obtain an

atomically clean substrate surface, since Au will not grow epitaxially on a dirty MgO substrate.[48]

### g. Methods Used in the Fabrication of Sputtered Metal-MgO-Au Devices

The six port vacuum system had many problems. The size of the system prevented pressures below $5 \times 10^{-9}$ Torr with the small ion pumps. This pressure could be attained only after a substantial bake at 250°C. Movement of the bellows after a bake always led to a leak in one or more of the bellows. Without a bake the ultimate pressure was $5 \times 10^{-8}$ Torr. The bellows would last for two or three pumpdowns before a leak would open up in one, if the system was not baked. Each time a bellows was replaced the shutdown time of the vacuum system was one week.

The first attempts to produce a sandwich device were done with Ag on an MgO substrate. Silver was used in the hope that silver might grow epitaxially on MgO somewhat easier than gold does. In every attempt at device fabrication the underlayer and overlayer presented no difficulty and the deposition of an MgO insulating layer was never achieved.

The first tube to be used to rf sputter deposit MgO consisted of two Kovar rf feedthroughs at right

angles to each other with no line of sight between the two MgO targets. One MgO target directly faced the substrate. This tube geometry was discarded after attempting to determine sputter deposition rates as a function of the rf potential between the two rf feedthroughs. The rates were extremely low and the films were very non-stoichiometric with an excess of Mg. This was determined by the brown-dusty film deposited on the glass walls of the tube.

The next tube used to deposit MgO was designed the same as the metal overlayer and underlayer tubes. The plasma was a dc supported plasma with the rf potential placed between the MgO target and the filament. The metal parts of the tube sputtered quite rapidly so the tube was redesigned to keep all metal parts of the tube out of the line of sight to the substrate. The first conclusive evidence of MgO dissociating into Mg and O was found with this tube. When the filament was on for a dc supported plasma the filament would burn out quite rapidly. If the plasma was an rf supported plasma with no hot filament in the tube all the metal parts in the tube became oxidized.

Deposition rates were determined using a quartz crystal monitor in this tube. Rates as high as

45 Å/min. were determined. The films again appeared to be non-stoichiometric, but not as bad as with the previous tube, so device fabrication was attempted using this tube. The first three devices were all shorts between underlayer and overlayer. After the substrates were removed from the vacuum system it was discovered that the metal mask had sputtered onto the substrate. When a positive potential was applied to the mask with respect to the filament, which was rf ground, no improvement was noted.

The same tube was used for the next six devices. The changes that were made were to replace the metal mask by an MgO mask and the plasma was an rf plasma with the rf applied between two MgO targets. In each case the underlayer was sputtered from the substrate in a circle corresponding to the hole in the MgO mask. The part of the silver underlayer that remained was definitely oxidized. It was thus decided to return to a gold underlayer since it does not have a stable oxide.

The next three devices attempted using this tube were also unsuccessful. No mask was used and in each case the underlayer was completely removed from the substrate.

A new rf sputter deposition tube was designed patterned after the Varian Plasma Peak[49] sputtering unit. Sputter deposition rates as high as 10 Å/min. were determined using this tube. The quartz crystal was removed and the MgO film studied using a microprobe.[50] The microprobe used* did not have the capability of detecting oxygen but the films were non-conducting and contained Mg. No other metals could be detected. The films, however, did appear to be Mg rich.

When the quartz cyrstal was removed and the next series of device fabrication attempts were made the metal underlayer was again removed from the substrate. Evidently the field configuration inside the tube was greatly changed when the insulating substrate replaced the metal quartz crystal holder and sputtering of the surface again occurred.

A final attempt was made to use this tube with a metal mask. The approach was to attempt to have the same electrode geometry present as when the quartz crystal was in the tube. This meant that the substrate had to be in contact with the mask. As a consequence of the

---

*The microprobe used was operated by Dr. Paul Weiblen, Geology Department, University of Minnesota.

many alignment problems present in this vacuum system the close spacing of substrate to mask could not be achieved and the mask again sputtered onto the substrate.

The next approach to the problem was to attempt a dc glow discharge in an oxygen atmosphere to reactively sputter Mg. A glow discharge could not be maintained at a pressure below $3 \times 10^{-2}$ Torr. At this pressure the Mg sputtered quite rapidly producing MgO films but the deposition rate was so low that it could not be measured. This was a consequence of the short mean free path at a pressure of $3 \times 10^{-2}$ Torr. The target to substrate spacing was approximately 10 cm. and the mean free path at this pressure is approximately 0.15 cm, resulting in many collisions occurring before the molecules could reach the substrate. A thick deposit of MgO was noted on the glass tube to a distance of about 1 cm from the target but no deposit could be detected beyond this point.

It was decided that a large bell jar type vacuum system would be necessary to fabricate and study ordered metal-insulator-metal tunnel devices <u>in situ</u>. A Varian ultra high vacuum system was obtained. This system is described below.

## C. Experimental Vacuum System and Techniques Used in Final Approach

### 1. Description of Vacuum System

The vacuum system used in the final approach was constructed by Varian Vacuum Division and was custom built for the University of Minnesota.

The base chamber is the standard Varian base chamber for vacuum system V1-221 and includes a 110 liter/sec. noble ion pump, Varian number 912-7006. The base chamber also contains 10 feedthrough ports and titanium sublimation cartridge number 916-0017 to aid in pumpdown and also to attain a lower base pressure. The outside diameter of the base chamber is 12".

The work area of the vacuum system is a stainless steel bell jar, 12" O.D. and 12" high. The system has 8 flanges mounted on it with centers 4 1/2" from the top and one flange on the top of the system concentric with the system. A schematic diagram of the bell jar work area is shown in Fig. 7. Two ports are 6" I.D. One of these ports admits the LEED system and the other port is a window, Varian number 954-5129, to view the LEED pattern and for visual alignment of the substrates with the various ports. Two of the ports are 4" I.D. and 90° from each 6" port. One of the ports

admits the manipulator, Varian number 954-5031, on which five substrates are mounted. The manipulator has rotational motion, lateral motion in two axes and linear motion in one, and it tilts in any direction. Thus, each substrate can be placed in a variety of positions within the work chamber. The other 4" I.D. port holds the sputter cleaning apparatus. The four 1 1/2" I.D. flanges are located 45° from a 6" I.D. flange and a 4" I.D. flange. Two of these ports contain filaments, one to heat the substrate during deposition and one to heat the completed device during measurements. One of these ports holds a Pt-Pt10%Rh thermocouple to monitor substrate temperature during deposition. The final 1 1/2" I.D. port contains a UHV gauge, Varian number 971-5008. This gauge is a Bayard-Alpert[51] type ion gauge which will measure pressures from $10^{-4}$ Torr down to $2 \times 10^{-11}$ Torr. The flange port on the top of the system contains the measurements apparatus.

A Varian number 971-5009 MilliTorr gauge is mounted on one of the ten ports on the base chamber. This gauge measures pressures from 1 Torr to $10^{-5}$ Torr and is thus an effective gauge to use for pumpdown of the system as well as for measuring the pressure of gas admitted for

sputtering. Connected to another one of these ports is an Ar and/or $O_2$ admission system as on the previous vacuum systems.

A stainless steel plate 1/4" thick x 10.8" in diameter separates the base chamber from the bell jar. This plate is used as a shield to prevent sputtered and evaporated material from depositing on the measuring apparatus in the bell jar. A mask, shown in Fig. 8a is mounted on the center of this shield. Deposition of materials through this mask onto a substrate will result in a metal-oxide-metal device shown in Fig. 8b. As can be seen from this figure each substrate contains three devices. Since there are five substrates present, 15 devices can be fabricated in one pumpdown.

A shutter is mounted on a linear motion feedthrough, Varian number 954-5049, which in turn is mounted on one of the 10 ports on the base chamber. The shutter prevents deposition of material onto the substrate until the source is clean and is releasing material at the chosen rate.

## 2. Description of Experimental Apparatus and Preliminary Results

The first attempts to deposit films were by sputtering. The sputtering apparatus was similar to

that previously described except that the discharge support system consisted of a filament and an anode at opposite sides of the base chamber. The targets, gold, aluminum, and MgO, were near the center of the base chamber and shielded from each other. Although high discharge currents were drawn, 4 amps, the target currents were always small. This was a consequence of the diffuse plasma which seemed to fill the entire base chamber. As a consequence of the large gap, 12" O.D., permanent magnets did not afford much assistance in increasing the sputtering rate. The sputter deposition rates were all very low. The rf sputtering was attempted with a dc supported plasma and with a straight rf plasma. In either case the deposition rates were extremely low and all metal parts, including the base chamber, were also sputtered. Sputtering was therefore determined to be an unsatisfactory deposition method.

Since some success had been attained in producing metal-oxide-metal devices by evaporation of the oxide,[52] an electron beam evaporator was mounted on the base chamber and the sputtering apparatus was removed. The electron beam evaporator is a 2 kw e-gun evaporation source with three crucibles, Varian number 920-0003.

The underlayer, insulator, and overlayer can be deposited using this source and the underlayer and overlayer can be of different materials.

The LEED apparatus is similar to that used in the 6 port vacuum system with the exception that it is larger, the hemispherical collector is 4" in diameter and there are four grids. The electron gun is the same type as used in the 6 port system except that it is made from stainless steel.

The sputter cleaning apparatus is a tantalum can with a hole on one end, 0.6" x 0.9", and a filament and anode within the can. This apparatus is similar to that used by Weber[53] except that it is somewhat larger. The principle of this system is that a plasma is supported within the can and ions drawn through the focusing hole to a target which is at a negative potential with respect to the anode. This type of apparatus is necessary to sputter clean the substrate since rf sputtering of the substrate cannot be done. The apparatus was placed in another vacuum system and tested on a $Ta_2O_5$ film grown on Ta by aqueous anodization of a Ta sheet to determine the uniformity of the sputtered area. The cleaned area was uniform to within about 5 Å after about 200 Å of $Ta_2O_5$ had been removed.

Since the substrates are insulators and will charge up when bombarded by ions, sputter cleaning of an insulator was tried next. In order to prevent charging of the insulator a filament was placed between the sputtering can and a substrate with a 1000 Å thick silver film and a 200 Å thick gold film on it. Within 30 minutes the 200 Å thick Au film was completely removed and within 2 hours most of the 1000 Å thick silver film was removed. From these results it was decided that this method for sputter cleaning of the substrate surface would be satisfactory.

The measurements system consists of a supramica disk on which are mounted 8 pressure contacts to make electrical contact to the underlayer film and the three overlayer films. A planar grid is mounted on the supramica on the side opposite the pressure contacts. The supramica is 1/8" thick and so the sample to grid spacing is about 0.2". Immediately beyond the grid is an anode, which has a hole 0.055" in diameter and beyond this is a Faraday cage[54] with a hole 0.055" in diameter. The two holes are aligned with the center of the center device of the three devices. This device can thus be studied with edge effects being avoided, while the other two devices on a substrate must include the edge effects.

The deposition rates for the electron beam evaporator were determined. The deposition rate for gold varied from 23 Å/min. at 1.4 kw to 800 Å/min. at 2 kw of beam power while for MgO it varied from 4 Å/min. at 40 watts to 90 Å/min. at 120 watts.

### 3. Sample Preparation

For these studies, diode samples consisting of a common Au underlayer film and a common oxide film were formed, and three Au overlayer films were deposited to produce three active units.

#### a. Glass Substrates

The substrates were cut from microscope slide glass, 1" x 0.6". They were then mounted in the substrate holder and the entire assembly was cleaned thoroughly by ultrasonic agitation in Freon TWD, a detergent solution, and rinsed thoroughly with tap water and finally, methanol. After drying, the assembly was placed in another ultrasonic agitator and first boiled in Freon and then ultrasonically agitated in Freon. The assembly was then immediately placed in the UHV system. The vacuum system was then evacuated and baked to 150°C which brought the pressure to a typical value of $6 \times 10^{-11}$ Torr. The substrates were then heated to a temperature of 400°C by means of a W filament to further

clean the surface. With the shutter in position to prevent deposition on the substrates, each source was thoroughly outgassed. The vacuum was again allowed to reach its base pressure, $6 \times 10^{-11}$ Torr, before sample fabrication was begun. During deposition of the metal layers the pressure rose to $10^{-9}$ Torr and to $10^{-8}$ Torr during deposition of the oxide layer. The entire fabrication process took less than 30 minutes.

b. MgO Substrates

As stated in section II-B-3-f, gold will not grow epitaxially on a dirty MgO substrate. Since the MgO single crystal could not be cleaved in vacuum, other methods to obtain a clean surface were attempted. The MgO substrates were cleaned in the same manner as the glass substrates and then cleaved immediately prior to insertion into the vacuum system. The cleaving was done on a laminar flow bench to minimize the collection of dust on the surface. Some substrates were sputter cleaned in vacuum, some were heated to 500°C before deposition began, and some were immediately deposited onto after baking of the system.

c. $CaF_2$ Substrates

The single crystal $CaF_2$ substrates were cleaned in the same manner as the MgO substrates with the

exception that they were not cleaved. A proper cleavage plane could not be achieved with the $CaF_2$ substrates. Some $CaF_2$ substrates were not cleaned before insertion into the vacuum system.

4. Millisecond-Pulse Measurement of I-V Characteristics

The $I_s$-$V_s$ characteristics of the thin film samples were measured using a millisecond pulse technique developed by Savoye[55] to minimize sample breakdown effects during measurement and to enable extension to the high current densities necessary to measure the emission into vacuum. The circuit permitted pulse measurements using a four-terminal method, and is shown schematically in Fig. 9. A voltage ramp of the desired time duration was generated by the time-base plug-in unit of oscilloscope I. (Both oscilloscopes employed in these measurements were Tektronix 536 X-Y, with appropriate plug-in units on X and Y channels.) This signal, amplitude modulated by the operational amplifier, Philbrick P45AL inserted in a model MP solid state manifold, used with a gain of 2, was applied to the sample under test. A signal proportional to the instantaneous current ($I_s$) through the sample was obtained across the resistor $R_s$ and applied to one channel

of a dual-channel plug-in unit on the vertical amplifier of oscilloscope II. The instantaneous voltage ($V_s$) across the sample, given by the difference in voltage between points A and B, was determined by a differential amplifier on the vertical input of oscilloscope I. The resulting difference voltage was applied to the horizontal amplifier of oscilloscope II. This arrangement allowed the display of $V_s$ versus time on oscilloscope I while the measurement was in progress, and hence provided a valuable check on the measurement.

A signal proportional to the emission current ($I_e$) was obtained across the resistor $R_e$ and applied through a low-level pre-amp to the second channel of the dual-channel amplifier on the vertical side of oscilloscope II. The resulting display on oscilloscope II thus consisted of a simultaneous plot of $I_s$ vs. $V_s$ and $I_e$ vs. $V_s$, on a single-pulse basis. Scope unblanking was accomplished by modulation of the gate signal generated by the time-base unit.

A direct tracing of a photograph of some typical I-V characteristics obtained from a thin-film emission diode using this pulse technique is shown in Fig. 10, where the various curves are labeled on the figure. During each pulse, the two signals, $I_e$ and $I_s$, were

displayed alternately by means of a multivibrator chopper, internal to the dual-channel plug-in unit of scope II, which switched the CRT beam from $I_s$ to $I_e$ at the rate of 100 kHz.

The results of a measurement are shown in the photograph. In the measurement two pulses were applied to the sample, the first pulse was used to display the entire $I_e$ and $I_s$ vs. $V_s$ characteristics and the second pulse to present the expanded-scale characteristics. As is seen from the photograph, the I-V characteristics obtained are nonlinear. The region of more rapid current change was displayed on an expanded voltage scale with a suppressed zero by means of the Tektronix type Z plug-in unit on the horizontal channel of oscilloscope II. This Z-unit allows display of the difference between a desired signal and an internally-generated, highly accurate, variable dc voltage. The input circuits have a large dynamic range so that saturation effects do not occur, thus allowing display of small variations in large signals on the most sensitivie scales. As an example, in Fig. 10 the I-V characteristics are shown expanded by a factor of 10 on the horizontal scale. It is seen that good agreement is obtained between the "normal" and the "expanded" traces, and that much

more accurate readout of the expanded trace characteristic is possible.

Measurements obtained on a pulse basis have been extended to sample current densities as high as 0.2 amperes/$cm^2$, without causing breakdown. In comparison, similar samples measured on a slowly-varying dc basis were found to suffer breakdown at current levels of the order of $10^{-2}$ amps/$cm^2$. Evidently the breakdown process in these devices is not a simple function of current density or applied field, but depends also upon the length of time that the bias is applied. This observation suggests that processes similar to those which have been designated Impulse-Thermal Breakdown[56] are of importance in these devices.

### 5. Pulse Techniques Applied to Emission Measurements

Measurements of hot electron emission into vacuum were made using the millisecond pulse technique previously discussed. No noticeable emission differences were noted with the samples in the position aligned with the hole in the Faraday cage and those not aligned with this hole. Thereafter the grid, anode, and Faraday cage were all biased at 22.5 volts with respect to the underlayer film.

Measurements were carried out starting at the lowest emission current levels commensurate with the sensitivity of the apparatus ($\sim 10^{-10}$ amperes). Data were taken at successively higher current levels, to the maximum output of the operational amplifier ($\sim 10^{-2}$ amps), and then repeated for successively lower current levels to the lower limit. In this manner irreversible changes occurring in the sample during a measurement sequence could be detected, and a check on the reproducibility of the data was provided.

### 6. DC Measurements of I-V Characteristics

A study of the current-voltage characteristics of thin film metal-oxide-metal diodes reveals considerable information concerning the nature of the oxide. As well as the current flow mechanism, temperature effects, rectification effects, and time-dependent changes can be investigated.

Measurements were made using a 4-terminal connection to the sample *in situ*. In each case the slowly varying dc bias was applied to the devices after the pulse measurements had been completed. The I-V characteristics of the samples did not change. A schematic of the circuit is shown in Fig. 11. The bias was applied using batteries and a motor driven potentiometer and the current was

monitored by measuring the voltage developed across a series sampling resistor with a Keithley 602 electrometer voltmeter whose output was recorded on the Y channel of a Hewlett Packard Mosley 135M X-Y recorder. The applied voltage was measured with a Keithley 603 electrometer amplifier with the output applied to the X channel of the recorder for low level voltages, less than 1 volt. For the higher voltages the applied bias was monitored directly by the X channel of the X-Y recorder.

The current-voltage characteristics were measured on a dc basis as well as on a pulse basis in order to monitor the I-V characteristics to lower levels than could be obtained on a pulse basis as well as for easier read-out of the characteristics.

Easier read-out of data was necessary in order to plot the data obtained as a function of the temperature of the device. A filament was placed in the vacuum system at a location 10" from the device in the measurements position. The filament current was varied and the temperature of the device was allowed to come to equilibrium. The temperature was monitored by a Pt-Pt10%Rh thermocouple which was located beneath the pressure contact to the center overlayer.

# III. RESULTS OF EXPERIMENTAL STUDIES OF HOT ELECTRON TRANSPORT IN THIN-FILM EMISSION DIODES

## A. Introduction

As stated in section I, the electron process of importance in these devices is in some doubt. A number of investigators[12,13,57-59] have discussed the situation when the transport mechanism appears to be a combination of thermal and field effects. There appears to be a range of barrier heights in which the thermal effects dominate the mechanism, small barriers, a range in which both effects are seen, and a range, large barriers, in which the field effects overshadow the thermal effects. The I-V characteristics of the device must be measured to determine which mechanism is of importance. If the I-V characteristics are measured as a function of the temperature of the device a better understanding of the mechanism involved can be achieved. The emission into vacuum of hot electrons from the diodes lends an insight into the scattering mechanism taking place in the oxide.

The experimental techniques which have been developed for these studies were discussed in some detail in previous sections. These investigations have involved

fabrication and testing of 60 thin film sample sets. The MgO film thicknesses ranged from 60 Å to 680 Å.

B. High Level I-V Characteristics of Thin Film Emission Diodes

The I-V characteristics of the thin film samples were measured using the millisecond-pulse technique discussed in section II-C-4 and also by the slowly varying dc technique discussed in section II-C-6. The level of measurements was restricted to avoid damage to the samples. In the simple band theory of solids, neglecting image forces, the barrier $\varphi_R$ is given by $\varphi_m - \chi_I$, where $\varphi_m$ is the work function of the metal and $\chi_I$ is the electron affinity of the insulator. If $\varphi_R$ is a low value, $\lesssim$ 1 eV, the Schottky mechanism will dominate and no tunnel electrons will be seen. At the higher barrier heights the electrons will not have enough thermal energy to surmount the barrier and tunnel current will be the dominant mechanism. Nelson[26] measured the barrier for Al-$Al_2O_3$-Al devices and found that it was 2.2 eV with no applied bias. For the same type of device, Savoye[12] found that field effects were dominant and that thermal effects were also present, but insignificant. It was believed that a Au-MgO-Au device would exhibit strictly field effects because the

simple barrier picture indicated that a barrier of 4.65 eV would be present at room temperature. This value was obtained from the work of Holscher,[79] $\varphi_{Au} = 5.45$ and Kemp and Neeley,[60] $\chi = 0.8$ eV. If the I-V characteristic was strictly tunnelling, the Fowler-Nordheim equation as applied to solids would indicate the dependence of current on voltage. This equation can be written in the form:

$$J = J_o(F/F_o)^2 e^{-(F_o/F)}$$

where $J_o$ and $F_o$ are parameters of the insulator. Assuming the free electron mass,

$$J_o = 7.2 \times 10^9 \varphi_o^2 \text{ A/cm}^2 \qquad F_o = 6.8 \times 10^7 \varphi_o^{3/2} \text{ V/cm},$$

where $\varphi_o$ is the potential barrier height in electron volts presented by the oxide modified by the image forces. For $\varphi_o = 4.65$ eV,

$$J_o = 1.36 \times 10^{11} \text{ A/cm}^2 \qquad F_o = 6.16 \times 10^8 \text{ V/cm},$$

then:

$$J = 1.36 \times 10^{11} (F/6.16 \times 10^8)^2 e^{-\left(\frac{6.16 \times 10^8}{F}\right)} \text{ A/cm}^2$$

if F is the field present in the insulator. Since the area of each device is $6.45 \times 10^{-2}$ cm$^2$,

$$I = 8.77 \times 10^9 (F/6.16 \times 10^8)^2 e^{-\left(\frac{6.16 \times 10^8}{F}\right)} \text{ amps}.$$

For an insulating film 89 Å thick the device characteristic should look like that shown in Fig. 12, where the currents are labeled in amps per division. Two features

of these characteristics are immediately noticeable, the high voltage necessary before any measurable current can be drawn and the extremely high slope of the curves.

The first evaporated Au-MgO-Au device that was measured in any great detail was PY-G-11(1). This device had an 89 Å thick oxide layer and its I-V characteristic is shown in Fig. 13. In contrast to the theoretical tunnel curves, current is drawn at very low voltages and the slope of the curves is much less than those in Fig. 12. However, the curves are definitely nonlinear.

The Fowler-Nordheim equation can be written as:

$$I = aJ_o(V/sF_o)^2 e^{-F_o s/V}$$

or

$$I/V^2 = aJ_o(1/sF_o)^2 e^{-F_o s/V}$$

where a is the device area and s is the oxide thickness. If one takes the logarithm of each side the expression becomes:

$$\ln(I/V^2) = \ln\left[aJ_o(1/sF_o)^2\right] - F_o s/V$$

so that a plot of $\ln(I/V^2)$ vs. $1/V$ should yield a straight line. The I-V characteristics of device PY-G-11(1) is shown plotted on this Fowler-Nordheim plot in

Fig. 14. It can be seen that the Fowler-Nordheim expression does not hold for this device.

The Richardson-Schottky equation which may be applied to a metal-oxide-metal device, as explained by the simple band theory, is given by van der Ziel:[61]

$$J = AT^2 \, e^{-\varphi_R/kT} \, e^{bV^{1/2}}$$

where

$$b = (q^3/4\pi\epsilon_r\epsilon_o s)^{1/2}(kT)^{-1}$$

In these expressions:

A = Richardson's constant, 120 $A/cm^2 \, {}^\circ K^2$

q = charge of the electron

$\epsilon_r$ = relative dielectric constant of the oxide

$\epsilon_o$ = permittivity of free space

k = Boltzmann's constant

T = temperature in °K.

This expression can also be written as:

$$\ln I = \ln \beta + b \, V^{1/2}$$

so that a plot of ln I vs. $V^{1/2}$ should yield a straight line, if the Schottky mechanism is the dominant mechanism. Such a plot of the I-V characteristics of device PY-G-11(1) is shown in Fig. 15. As can be seen from this figure the Schottky mechanism explains the characteristics quite well.

At this point, however, one must be careful not to assume Schottky emission just because the plot of log I vs. $V^{1/2}$ is a straight line. As pointed out by Hartman,[62] the Pool-Frenkel effect has a similar I-V characteristic. This equation is written as:

$$J = G_o V e^{(2bV^{1/2} - \psi/kT)}$$

where $G_o$ is a constant with the dimensions of a conductivity, $\psi$ is the energy difference between the trap level and the bottom of the conduction band, and all other symbols have already been defined. As can be seen this mechanism would also plot as a straight line on a log I vs. $V^{1/2}$ plot. Furthermore, a bulk-limited conduction mechanism discussed by Mead[63] also plots as a straight line on this type of plot. O'Dwyer[64] has recently machine calculated the voltage-current characteristics for films of a few hundred to a few thousand angstroms thickness with the help of a dielectric model originally proposed by Frolich.[65] His result is also a straight line on a ln I vs. $V^{1/2}$ plot. Jonscher[15] points out that the bulk limitation as proposed above probably does not arise for very thin dielectrics, 150 Å or less, but probably holds for the thicker films.

A number of checks can be made to determine if the Schottky mechanism is involved or if one of the other mechanisms is present. Hartman[62] noted that the dielectric constant, as determined by the slope of the log I vs. $V^{1/2}$ plots, was too high for SiO films if the Schottky or Pool-Frenkel mechanism is the dominant mechanism. He also noted that the zero field intercept of this curve varied as a function of the dielectric thickness, with the intercept becoming higher for thicker films. This should not happen for the Schottky or Pool-Frenkel mechanisms. This intercept gave a much different barrier height than the slope of the $\ln I_o$ vs. $\frac{1}{T}$ plots, and it should be the same for the Schottky mechanism.

If one assumes the Schottky mechanism to be the controlling mechanism for these devices, the slope of the curve in Fig. 15 is b, which can be written as:

$$b = \gamma\, \epsilon_r^{-1/2}\, s^{-1/2}\, T^{-1} .$$

Assuming the low frequency dielectric constant of MgO, which is 9.8,[4] and an oxide thickness of 80 Å, the slope gives a temperature of 330°K. The actual device temperature during measurement was 313°K, as measured by the Pt-Pt10%Rh thermocouple. A calculation of the temperature change of the device, during measurement,

was made. The heat equation for this problem was solved by Savoye[55] and he arrives at the expression:

$$\Delta T = \frac{2}{K}\sqrt{\frac{k}{\pi}}\, J_s\, V_s \sqrt{t}$$

where

$$k = \frac{K}{c\delta} = 3.92 \times 10^{-3}\ \frac{cm^2}{sec} \text{ for glass}$$

K = thermal conductivity = $8.0 \times 10^{-3}$ watts/cm°K

t = pulse length in seconds.

Using these values the expression becomes:

$$\Delta T = 8.9\, J_s\, V_s \sqrt{t}$$

and for a 10 millisecond pulse, with $J_s = 0.126\ A/cm^2$, $V_s = 2.9$ volts,

$$\Delta T = 0.325°K\ .$$

It can be seen that the device did not heat up much during pulse measurements. If the temperature is thus assumed to be 313°K, the relative dielectric constant of the oxide is calculated to be 10.9, which is fairly close to the assumed value of 9.8. Alternatively if the relative dielectric constant is 9.8 and the temperature is 313°K the oxide thickness must be 89 Å instead of the calculated 80 Å. This variation is well within the bounds of the experimental error involved in a deposition rate calibration of evaporated material. Since there is no a priori reason for assuming the high frequency dielectric constant for the Schottky mechanism,

as there is in the Pool-Frenkel[14] or Fowler-Nordheim[12] mechanisms, the Schottky mechanism cannot be ruled out. However, if one assumes the Pool-Frenkel mechanism, the plot of $\ln(I/V)$ vs. $V^{1/2}$ should be straight line with a slope of 2b. Such a plot of the I-V characteristics of device PY-G-11(1) is shown in Fig. 16. Although it is not a straight line over the entire plot, a straight line is drawn on the figure. Assuming an oxide thickness of 89 Å, the slope of this line gives a dielectric constant of $\epsilon_r = 3.17$, which is in good agreement with the high frequency dielectric constant of MgO, which is 2.95[4]. Therefore the Pool-Frenkel mechanism cannot be ruled out on this basis either. However, the curved line on Fig. 16, which is in extremely good agreement with the data points, is a plot of the Schottky equation. It thus appears that the Pool-Frenkel mechanism does not hold.

Devices were studied with oxide thicknesses in the range of 69 Å to 680 Å. In all cases, in which no oxygen gas was admitted during the deposition of the MgO film, the I-V characteristics plotted as a straight line on a $\ln I$ vs. $V^{1/2}$ plot and similar to the curve in Fig. 14 a $\ln \frac{I}{V^2}$ vs. $\frac{1}{V}$ plot and also similar to Fig. 16 for a $\ln \frac{I}{V}$ vs. $V^{1/2}$ plot. Figure 17 presents a summary of

data obtained from the thin samples studied in detail in which the MgO layer was deposited with no oxygen gas admitted during deposition. As can be seen from this curve there is essentially no change in the zero field intercept as a function of oxide thickness, another indication that the current flow mechanism is not bulk dominated.

From the Richardson-Schottky equation with zero field:

$$I_o = aAT^2 e^{-\varphi_R/kT}$$

where a is the area of the device. It can be seen from this expression that $\varphi_R$ can be obtained;

$$\varphi_R = kT \ln \frac{aAT^2}{I_o} .$$

The barriers obtained in this manner are given in Table I. It can be seen that the barriers are in remarkably good agreement. This determination of the barrier height may not be accurate because of the questionable value of the Richardson constant. However, as Hartman[62] pointed out, a change in this constant by an order of magnitude would only change the barrier determined in this manner by about 10%.

Figure 18 shows the Schottky plot of the devices with the thicker (680 Å) insulating films. Although the intercept is not the same, as a consequence of

Table I

BARRIERS FOR DIFFERENT DEVICES AS OBTAINED FROM THE ZERO FIELD INTERCEPT OF THE SCHOTTKY PLOT

| DEVICE NO. | S(Å) | $\phi_R$ (eV) |
|---|---|---|
| PY-G-19(2) | 79 | 0.710 |
| PY-G-11(1) | 89 | 0.714 |
| PY-G-18(2) | 109 | 0.700 |
| PY-G-17(1) | 159 | 0.721 |
| PY-G-20(1) | 680 | 0.695 |
| PY-G-20(3) | 680 | 0.695 |

measuring these devices at a lower temperature the barriers obtained in this manner are nearly the same. The difference in current at a given voltage, and consequently the different intercepts, is caused by a slight difference in device area. The overlayers for these two devices were deposited through a different mask than for the other devices. These barriers are much lower than that predicted by the simple model, so other measurements were necessary in order to determine what the conduction mechanism is. These measurements are described in the following sections but a number of other features of the I-V characteristics became evident during the measurements on these devices.

The forward, overlayer positive, and reverse, overlayer negative, characteristics of each of these devices were identical. This indicates that the barrier is symmetrical, which is not the case for devices fabricated by oxidation of the underlayer metal film. Rectification effects have been seen[27,66] for devices with identical metal electrodes which indicated a non-symmetrical barrier, probably due to an oxide gradient in the oxidized film.

Another feature that was noted was that the I-V characteristics, as measured by the slowly varying dc technique, were the same with the voltage decreasing as with the voltage increasing. Other authors[27,29,59,67] have seen a hysteresis effect, where the retrace differed from the original trace. If the current on the retrace is higher, at the same voltage, than on the original trace, it is probably due to Joule heating. However, to change the current by a noticeable amount the current must be left at the maximum value for about one minute. In the present experiment the voltage was always lowered after less than 30 seconds for measurements to the upper limits and heating was negligible. If the current

on the retrace is lower, at the same voltage, than on the original trace, it is due to the filling of traps[68,69] while the voltage is applied. This in turn increases the effective barrier at the underlayer-oxide interface. As the voltage is decreased, the finite lifetime associated with the trapping sites causes the effective barrier to remain higher and thus the current is lower for the same applied voltage. These traps arise from impurities introduced into the oxide film during oxidation. The impurities are not present in the evaporated MgO films. The results also cast doubt on the Pool-Frenkel and other trap limited mechanisms.

The I-V characteristics of the devices indicate that three problems involved in the oxidized underlayer type device have been removed. These problems were; the oxide must be that of the metal underlayer, the oxide gradient present in oxidized films, and the impurities introduced as a result of oxidizing the underlayer.

## C. Temperature Measurements of the I-V Characteristics of Thin Film Emission Diodes

The I-V characteristics of the devices indicate that the Schottky mechanism is probably the dominant mechanism in the transport of electrons through the oxide film. Since this mechanism is very temperature dependent and the tunnelling mechanism has very little temperature dependence it was decided to measure the I-V characteristics of the devices as a function of temperature. The method for this measurement is described in section II-C-6.

The I-V characteristics of device PY-G-11(1), as a function of temperature, are shown in Fig. 19. It can be seen that there is a large dependence of the I-V characteristics on temperature with a change of less than 100°K giving rise to an increase of current, at a given voltage, of an order of magnitude. This effect is also seen if some of the other mechanisms proposed are present. However, if a plot of the zero field intercepts, of the ln I vs. $V^{1/2}$ plots, is made on a $\ln(I_o/T^2)$ vs. 1/T plot, the slope of this plot should again give $\varphi_R$, as can be seen below:

$$I_o = aAT^2 e^{-\varphi_R/kT}$$

$$I_o/T^2 = aAe^{-\varphi_R/kT}$$

$$\ln(I_o/T^2) = \ln aA - \varphi_R/kT$$

If this slope gives $\varphi_R$ as the same value as $\varphi_R$ obtained from the zero field intercept calculations the mechanism of importance is the Schottky mechanism. A ln I vs. $V^{1/2}$ plot for different temperatures for device PY-G-11(1) is shown in Fig. 20. The intercepts, $I_o$, are plotted on a $\ln(I_o/T^2)$ vs. $10^3/T$ in Fig. 21. The barrier height, $\varphi_R$, obtained in this manner is 0.33 eV as compared to 0.71 eV by the zero field intercept method. This result casts some doubt on the Schottky mechanism. Table II shows the comparison of the barrier heights obtained using the two methods for the devices listed in Table I.

Table II

BARRIER HEIGHTS FOR DIFFERENT DEVICES AS OBTAINED BY THE ZERO FIELD INTERCEPT AND THE SLOPE OF THE $\ln(I_o/T^2)$ vs. 1/T PLOT

| DEVICE NO. | S (A) | $\varphi_R$ (eV) (Zero Field) | $\varphi_R$ (eV) (Slope) |
|---|---|---|---|
| PY-G-19(2) | 79 | .71 | .33 |
| PY-G-11(1) | 89 | .71 | .33 |
| PY-G-18(2) | 109 | .70 | .35 |
| PY-G-17(1) | 159 | .72 | .33 |

As can be seen from this table the results are quite consistent and cannot be explained by a simple Schottky mechanism.

D. Measurements Made on Devices Fabricated with Oxygen Gas Present During Deposition of the Oxide Film

The results on the above devices indicated that the oxide films were not pure MgO. The MgO probably dissociates to some degree during evaporation and probably does not re-combine at the substrate surface to give a stoichiometric film. The result is a film with an excess of magnesium atoms. It was decided to attempt to grow a more stoichiometric film by admitting oxygen gas during the deposition of the MgO film.

Since the pressure in the vacuum system is on the order of $10^{-8}$ Torr during deposition of the MgO films the first attempt to produce stoichiometric films was done with oxygen gas admitted to the system to a pressure of $1 \times 10^{-8}$ Torr, and this device, PY-G-22(2), was measured. Oxygen gas was admitted to a pressure of $10^{-7}$ Torr during fabrication of the next device, PY-G-25(3). A summary of these two devices and one fabricated with no oxygen admitted is shown in Fig. 22. It will be noted that although the I-V characteristics

still plot as a straight line on a ln I vs. $V^{1/2}$ plot, the zero field interecepts are no longer the same. The zero field interecept values of $\varphi_R$ are .780 eV for device PY-G-22(2) fabricated with $10^{-8}$ Torr of oxygen gas and 0.823 eV for device PY-G-25(3) fabricated with $10^{-7}$ Torr of oxygen. It is evident from these curves that something is changing in the MgO film when deposition of the MgO is done with oxygen present in the system.

The plots of $\ln(I_o/T^2)$ vs. $10^3/T$ for these two devices and PY-G-11(1) are shown in Fig. 23. It will be noted that the slopes of the plots decrease with increasing amounts of oxygen present during the MgO deposition. This would indicate a lower barrier, if the mechanism was strictly a Schottky mechanism, for increasing amounts of oxygen, while the zero field intercept indicated a higher barrier. The barriers measured in this manner give $\varphi_R$ of 0.21 eV for PY-G-22(2) and 0.11 eV for PY-G-25(3).

A number of devices were fabricated with the deposition of MgO done in an atmosphere of $10^{-6}$ Torr of oxygen. None of these devices could be measured. These devices either broke down before any current was drawn or they were initially shorts. The devices with MgO thicknesses greater than about 70 Å always

broke down when about 12 volts were applied and those with thinner oxides were all initially shorts. It is believed that the devices with thicknesses less than about 70 Å were shorted due to pinholes.

A number of devices were fabricated in which the MgO was deposited with $10^{-5}$ Torr of oxygen gas present for a short time and then the film was completed after the oxygen had been pumped from the system. The first device fabricated in this manner showed definite rectification effects with higher currents drawn for the overlayer negative than for the overlayer positive, as expected. This device had an MgO film that was 120 Å thick with oxygen present during deposition of the first 30 Å. The oxide layer was again too thick because the device broke down before any appreciable current could be drawn. All subsequent devices fabricated in this manner were either initially shorted or they were also unstable and broke down before any quantitative measurements could be made.

One device, however, was stable long enough for some measurements to be made. The I-V characteristics of this device, PY-G-38(1), are shown in Fig. 24. The curves are labeled in amps per division and + signifies that the overlayer is positive. It can be seen that

the device broke down at about 17.6 volts. The interesting features of these characteristics are the difference in current for the two biases, the characteristics are ohmic to about 6.5 volts, and the sharp rise in current beyond this bias. Figure 25 is a plot of these characteristics on a Fowler-Nordheim plot, $\ln(I_c/V^2)$ vs. $1/V$, where $I_c$ is the actual current minus the ohmic current. As can be seen from these curves the I-V characteristics of this device can be explained quite satisfactorily by the Fowler-Nordheim tunnel equation. The barrier, $\varphi_o$, can be obtained from the slopes of these curves. They are: 1.9 eV for the overlayer positive and 1.74 eV for the overlayer negative. The fact that the barrier is higher for the overlayer positive is expected since the more stoichiometric part of the oxide film is near the underlayer. These results are consistent with the hypothesis that the MgO films are magnesium rich and that admitting oxygen gas during deposition of the MgO film increases the stoichiometry as seen by an increased barrier height. The other devices plotted in this manner still plotted as in Fig. 14.

## E. Low Level I-V Characteristics of Thin Film Emission Devices

It was noted during the study of the I-V characteristics of these devices that at low fields, $\simeq 10^4$ V/cm, the I-V characteristics were ohmic. It was decided to study the I-V characteristics at these low levels in order to get a better understanding of the conduction mechanism.

The first device measured in this manner *in situ* was device PY-G-21(3). The I-V characteristics were linear up to a field of $\gtrsim 10^4$ V/cm and the resistance of the device was $1.3 \times 10^5$ Ω at a temperature of 312°K. The resistance was measured as a function of temperature and is plotted vs. $10^3/T$ in Fig. 26. A similar plot for devices PY-G-22(2), $10^{-8}$ Torr oxygen, and PY-G-25(3), $10^{-7}$ Torr oxygen, are also shown on this figure. Two features of the device resistance are noticeable in this figure. One of these features is that the resistance increases as the amount of oxygen gas increases during MgO deposition, even though the oxide thicknesses are not all the same. PY-G-21(3) and PY-G-22(2) both have an MgO layer of about 90 Å thickness and PY-G-25(3) has an oxide thickness of about 60 Å. The other feature is that the temperature dependence of the resistance is not linear on a plot of this type.

## F. Measurements of Electron Emission into Vacuum from Thin Film Diodes

The present experiment was designed to permit simultaneous measurements of the I-V characteristics of the device and the emission into vacuum from the device. Data was obtained using the millisecond-pulse technique discussed in section II-C-5. Although the experiment was designed to permit measurements on a given emission diode over a range of overlayer film thicknesses, this was never accomplished. After measurements were made on a given device and more gold was deposited to increase the overlayer thickness the devices were always shorted. Consequently the measurements were made on each device with only one overlayer thickness. The overlayer thickness for each device was calculated from the resistivity of the film. The resistance per square of a thin metallic film is typically higher than that predicted by the bulk resistivity.[32] The resistance of a given metal film also depends on the substrate. Thus, although this method is not an accurate method for determining the exact thickness, the ratio of thicknesses can be accurately determined. All films were deposited to a calibrated thickness of 200 Å, except where noted,

see section II-C-2. The thickness of the overlayer for device PY-G-11(1) will be assumed to be 200 Å and the rest of the overlayer thicknesses calculated with respect to this overlayer. The calculations will be based on the assumption that $S_o = K R_s^{-1/2}$, where $R_s$ is the sheet resistance in Ω/square, $S_o$ is the overlayer film thickness, and K is a constant. This emperical relationship has been observed by a number of workers.[20,32,55] The sheet resistance of device PY-G-11(1) is 1.5 Ω/square and a thickness of 200 Å for this value is not unreasonable (see reference 55, Fig. 8) since it lies between the value calculated from the bulk resistivity and Savoye's results for gold on $Al_2O_3$. Table III lists the devices previously

Table III

OVERLAYER THICKNESSES FOR MEASURED DEVICES

| DEVICE NO. | $R_s$ (Ω/square) | $S_o$ (A) |
|---|---|---|
| PY-G-11(1) | 1.50 | 200 |
| PY-G-17(1) | 1.60 | 194 |
| PY-G-18(2) | 1.22 | 222 |
| PY-G-19(2) | 3.39 | 133* |
| PY-G-22(2) | 1.38 | 209 |
| PY-G-25(3) | 1.50 | 200 |

*Deposited to a thickness of 150 Å.

discussed with their sheet resistance and calculated overlayer thicknesses.

The overlayer film thicknesses are of importance because attenuation of the hot electrons occurs in the overlayer film as well as in the oxide film.[12,20,70] The emission transfer ratio, $\alpha$, for device PY-G-11(1) is plotted vs. sample voltage, $V_s$, in Fig. 27. The immediate feature that is seen is that the emission transfer ratio, $\alpha$, decreases with increasing $V_s$, in contrast to the results seen by other investigators.[12,71] Savoye,[12] for example, was able to explain the increase of $\alpha$ with increasing $V_s$ on strong inelastic electron-phonon interactions. His results indicated a mean-free-path of about 7 Å with an energy loss of 0.1 eV per interaction. In this case only a fraction of the electrons would arrive at the overlayer metal with sufficient energy to escape over the vacuum work function barrier. This fraction would be expected to increase with increasing $V_s$ and, depending upon the details of the electron energy distribution, could in principle increase sufficiently rapidly with sample bias to give rise to a net increase in $\alpha$ with $V_s$. However, if these interactions did not occur, or if the interactions were elastic, one would expect that $\alpha$ would decrease with increasing

$V_s$, since injection into the overlayer would then occur at higher energies and the mean-free-path for hot electrons in the metal overlayer is expected to decrease for increasing electron energy.[72,73,74] This effect is seen here experimentally.

Figure 28 is a comparison of emission results for the devices previously discussed in which no oxygen was admitted during the deposition of MgO. Figure 29 is a comparison of emission results for devices fabricated with different amounts of oxygen present during the MgO deposition. The results for device PY-G-11(1) are also plotted on this figure for comparison purposes since it has the oxide thickness closest to that of device PY-G-22(2).

From the data presented in these figures the following observations can be made:

1) The magnitude of the emission transfer ratio, $\alpha$, is seen to decrease with increasing $V_s$ for each MgO thickness regardless of the amount of oxygen gas present during deposition of the MgO.

2) The general shape of the log $\alpha$ vs. $V_s$ curves is similar for all devices except at the low voltage levels where the measurements are not as accurate. Strangely, the main effect of increasing the MgO

thickness is to increase the transfer ratio at a given voltage.

3) The effect of increasing the oxygen pressure during MgO deposition is also to increase the transfer ratio at a given voltage.

G. Attempts to Fabricate a Device with a Single Crystal Oxide

As stated in section I an attempt was to be made to grow an epitaxial device, at least a device with a single crystal MgO film. A number of attempts were made on different substrates but in no case was a single crystal device achieved.

The devices fabricated on the MgO substrates appeared to have highly disoriented layers. These results were true regardless of the method of substrate preparation. Each device was a short circuit between underlayer and overlayer. Ten sample sets, thirty devices, were fabricated with no success.

The devices fabricated on the $CaF_2$ substrates appeared to be slightly more ordered than on the MgO substrates. The MgO film for two of these devices exhibited a ring pattern when studied with LEED. Each device was a short circuit between underlayer and

overlayer. Five sample sets, fifteen devices, were fabricated with no success.

The devices fabricated on the single crystal substrates were done with the substrate temperature at 400°C during deposition of the various layers. The deposition rates were then varied to attempt to achieve epitaxy.

Since a perfect cleavage plane was not achieved with any of these substrates the surfaces were never nearly atomically smooth. The devices had MgO films of about 100 Å thickness, about 15 molecule layers, so it can be seen that the substrate must be very smooth in order to achieve a device with no pinholes.

Another problem that is involved is that during epitaxial growth of a thin film, the film must nucleate[36] so that single crystal growth can occur. This nucleation leads to pinholes in the film until the film has reached a certain thickness. Since these devices must have thin oxide layers it appears that epitaxial growth and non-shorted devices are two competing mechanisms.

Epitaxial growth may be inhibited by the fact that the MgO films are non-stoichiometric with an excess of Mg atoms. In order to achieve stoichiometry and still

have a measurable device the MgO layer must be on the order of 40 Å thick. Thus again, epitaxy and a measurable device are incompatible. The conclusion arrived at is that the epitaxial growth of a measurable device with a stoichiometric film of MgO between two metals may not be impossible, but is surely extremely difficult. Time did not permit the pursuit of this topic any further.

Table IV is a summary of the results of all devices studied extensively.

Table IV

SUMMARY OF DEVICE DATA

| DEVICE NO. | S | $S_o$ | $\varphi_1$ | $\varphi_2$ | R | $P_{O_2}$ |
|---|---|---|---|---|---|---|
| PY-G-11(1) | 89 | 200 | .714 | .33 | - | - |
| PY-G-16(3) | 106 | - | .741 | - | - | - |
| PY-G-17(1) | 159 | 194 | .721 | .33 | - | - |
| PY-G-18(1) | 106 | - | .694 | .34 | - | - |
| PY-G-18(2) | 109 | 222 | .700 | .35 | - | - |
| PY-G-19(2) | 79 | 133 | .710 | .33 | - | - |
| PY-G-20(1) | 680 | - | .695 | - | - | - |
| PY-G-20(3) | 680 | - | .695 | - | - | - |
| PY-G-21(3) | 90 | - | .732 | .34 | $1.3\times10^5$ | - |
| PY-G-22(2) | 90 | 209 | .780 | .21 | $4.25\times10^5$ | $10^{-8}$ |
| PY-G-25(3) | 60 | 200 | .823 | .11 | $7.4\times10^5$ | $10^{-7}$ |
| PY-G-38(1) | 90 | - | 1.9,1.74 | - | $4.35\times10^5$ | $10^{-5}$,- |

In this table:

S = oxide thickness, in Å

$S_o$ = overlayer thickness, in Å

$\varphi_1$ = barrier obtained by zero field intercept method, in eV

$\varphi_2$ = barrier obtained by slope of Arrhenius plot, in eV

R = resistance of device for ohmic part of characteristic, in Ω, at about room temperature

$P_{O_2}$ = pressure of $O_2$ gas admitted during MgO deposition, in Torr

# IV. ANALYSIS OF HOT ELECTRON TRANSPORT PROCESSES IN VACUUM DEPOSITED THIN-FILM EMISSION DIODES

## A. Introduction

The transport of hot electrons in thin film emission diodes can be viewed as involving three stages, which are in principle separable: 1) a process by means of which electrons are injected into the thin oxide film, 2) transport through the oxide film, and 3) transmission of electrons through the overlayer metal film region, with emission into vacuum. A major difficulty in studies of such devices lies in the fact that these processes are not readily separable on an experimental basis.

In preceding sections of this thesis, a series of experiments was discussed which involved the study of the transport of hot electrons through these devices fabricated under a variety of conditions and the subsequent emission into vacuum of these electrons. These efforts were directed toward providing as complete an experimental description of the film properties and the transport processes as possible in order to determine the properties of vacuum deposited thin oxide films.

The present section first presents a brief summary of the important experimental observations of these studies. Analysis of the experimental results is separated into two stages: electron injection into the oxide film, and transmission of a fraction of the injected electrons into vacuum. The processes of importance at each stage are thus as nearly as possible subjected to analysis separately, and the results combined to formulate the complete model for the hot electron transport process in vacuum deposited thin-film emission diodes.

## B. Summary of Experimental Observations

These studies have involved investigations of Au-MgO-Au thin film emission diodes with the MgO film deposited with different amounts of oxygen gas present in the vacuum system and to different thicknesses. The properties of the MgO films changed as the amount of oxygen present in the vacuum system changed during deposition of the MgO film. This change was to higher biases necessary for the same sample current. These observations are consistent with an increase in barrier height with an increase in the amount of oxygen present. This might be expected if the films

are more stoichiometric with more oxygen present during deposition.

The thin film sample I-V characteristics were plotted on a ln I vs. $V^{1/2}$ plot for direct comparison between samples. The data for each sample plotted in this way were fit by straight lines, in qualitative agreement with the simple Richardson-Schottky or Pool-Frenkel equations. The data was plotted on a $\ln(I_o/T^2)$ vs. $1/T$ plot for each device. The data for each sample plotted in this manner were fit by straight lines. However, the data plotted in these two manners gave different barrier heights, if one assumes the Schottky equation, or different trap levels, if one assumes a Pool-Frenkel equation. Thus the data is inconsistent with either of these mechanisms applied in a simple manner to these devices. The data were also inconsistent with the simple Fowler-Nordheim equation adapted for internal field emission since it did not plot as a straight line on $\ln(I/V^2)$ vs. $1/V$ plot.

An emission current into vacuum was observed for all sample types, which was stable and reproducible and free from breakdown effects. The magnitude of the emission transfer ratio, $\alpha$, decreased with increasing sample voltage, $V_s$, and increased for thicker oxide films.

The indications are that the barrier presented to the flow of electrons by the oxide film increases with increasing amounts of oxygen present during the deposition of the MgO. Since no devices could be measured which were fabricated with an oxygen pressure of $10^{-6}$ Torr or greater present during MgO deposition, an attempt was made to produce a device with an oxide layer consisting of two regions with a different composition near either of the metal-oxide interfaces. Although the results indicated that these devices show rectification effects, since the barrier at either interface was different, no devices fabricated in this manner were stable over a large current range and no extensive quantitative results were obtained.

All devices fabricated on single crystal substrates were initially shorted and could not be repaired. The conclusion arrived at is that the epitaxial growth of a measurable device with a stoichiometric film of MgO between two metals may not be impossible, but is extremely improbable.

### C. Discussion of a Model for Injection of Electrons into the Oxide Film

Experimental results have been presented for the I-V characteristics of vacuum deposited thin film

emission diodes which are in agreement with an expression in which $I_s$ is directly proportional to $V_s$ at low fields and in which $\ln I_s$ is proportional to $V_s^{1/2}$ at high fields. However the results are not consistent with a field-controlled emission-limited Pool-Frenkel mechanism whereby electrons are emitted from a discrete trap level into the conduction band over the Coulomb potential barrier under the attendant lowering by the applied electric field. The origin of this equation was in connection with conduction processes in bulk insulators or semiconductors[14] in which the effects of the electron image force on the interface barrier are of less importance in conduction than for very thin films.

The results were also not consistent with the simple Richardson-Schottky equation used for emission into vacuum, modified for emission into the conduction band of the dielectric by multiplying $\epsilon_o$ by $\epsilon_r$. The origin of the Richardson-Schottky equation was in connection with thermionic emission of electrons into vacuum from metals of high work function in which the work function is lowered by the electric field because of image force modification of the metal - vacuum interfacial barrier. These results are not directly applicable to the case of internal electron emission from a metal into an oxide,

since a detailed analysis must consider the influence of the oxide dielectric constant in modifying the electron image force. Emtage and Tantraporn[5] and Pollack[6] obtained results which they attributed to a Schottky emission mechanism. The problem as applied to these devices needs some modification since the multiple image force corrections to the barrier must be made. This problem is solved in Appendix I. The result is:

$$I = aAT^2 e^{-\varphi_R/kT} e^{\frac{.148\ V^{.484}}{kT}}, \qquad (1)$$

for the equation that applies to Schottky type emission into the conduction band of the insulator for high fields. It can be seen that the current dependence on voltage is not exactly the same as for emission into vacuum from a thermionic cathode. However, the zero field intercept of the plot of ln I vs. $V^{.484}$ should still give the barrier height, $\varphi_R$. A plot of ln I vs. $V^{.484}$ for device PY-G-11(1) is shown in Fig. 32 for the various temperatures. As expected the device characteristics plotted as a straight line on this curve. The only difference between this plot and a plot of ln I vs. $V^{1/2}$ is that the zero field intercept is slightly lower for T = 313°K. The value of $\varphi_R$ obtained from the zero field intercept in Fig. 32 is .722 eV as compared

to .714 eV from the zero field intercept of the ln I vs. $V^{1/2}$ plot.

Figure 33 is a plot of $\ln(I_o/T^2)$ vs. $10^3/T$ for $I_o$ obtained from the ln I vs. $V^{.484}$ plots at different temperatures. It can be seen from this figure that the plot is not a "straight line" as it is in Fig. 21. The plot should be a straight line according to Eq. (1) if the barrier is independent of temperature. However, as stated in section III-B, the barrier was expected to be much higher than that measured in these devices. The barrier, however, could be lowered if impurities were introduced into the MgO film allowing energy states in the forbidden gap in the bulk material or at the surface. Since these devices were fabricated and studied in ultra-high-vacuum the probability of introducing foreign impurities into the device is slight. The impurity atoms must then be excess Mg giving rise to a localized energy level. Depending on the number of excess Mg atoms, or oxygen vacancies, and the location of this level in the energy band structure, the barrier could be temperature dependent. Thus the barrier picture as shown in Fig. 30 is complicated by the presence of donors. Calculations of the effective Debye length[80] shows that the square barrier, modified

by the electron image force, is the correct shape for this barrier. The emission data indicates that a height of $\varphi_R \approx .72$ eV is the correct height.

Since the dependence of the barrier height on applied voltage deviates from the ln I vs. $V^{.484}$ law for lower voltages, expression (1) does not hold for low voltages. This expression should thus be written as:

$$I = aAT^2 e^{-\varphi_R/kT} e^{f(V)/kT} \qquad (2)$$

where f(V) is a function of applied voltage and is plotted in Fig. 31. This expression shows that there should be a current at zero applied voltage. However no current is observed at zero applied voltage. Consider that the overlayer is biased positively. This expression then gives the value of the current from the overlayer to the underlayer, or the electron flow from the underlayer to the overlayer. However, at zero applied voltage there is an electron flow from underlayer to overlayer due to thermal agitation which allows electrons to flow over the barrier from underlayer to overlayer. However, since the barrier is symmetrical and the overlayer and underlayer are the same material, gold, at zero applied voltage the same number of electrons should have thermal energy to flow over the barrier from

overlayer to underlayer. In equilibrium this gives rise to equal and opposite currents, so that the measured current at V = 0 is I = 0. As the barrier is lowered for electron flow from underlayer to overlayer it is raised for electron flow from overlayer to underlayer. Thus the correct expression for current from a Schottky type mechanism is:

$$I = aAT^2 e^{-\varphi_R/kT} \left[ e^{f(V)/kT} - e^{g(V)/kT} \right], \qquad (3)$$

where,

$$g(V) = f(V) - eV \; . \qquad (4)$$

From this expression it can be seen that at V = 0

$$g(o) = f(o) \qquad (5)$$

and

$$I = 0 \; .$$

Figure 34 is a comparison between the data for device PY-G-21(3) and Eq. (3). The data points are circled and the solid line is Eq. (3). It can be seen from this figure that there is extremely good agreement between the data and Eq. (3) over 6 orders of magnitude of current and 5 orders of magnitude of voltage. Furthermore, Eq. (3) predicts a linear relationship between I and V for low voltages. The bracketed expression in Eq. (3) can be written as:

$$e^{f(V)}(1 - e^{-eV/kT}) \quad . \tag{6}$$

For fields $\lesssim 10^4$ V/cm, $f(V) \approx K$, thus (6) becomes:

$$e^{K/kT}(1 - e^{-eV/kT}), \tag{7}$$

where K is a constant and $\varphi_R - K = \varphi_o$, the actual barrier height. Expanding $e^{-eV/kT}$ in a Maclaurin's series the bracketed expression becomes:

$$1-\left[1 - \frac{eV}{kT} + \frac{1}{2}\left(\frac{eV}{kT}\right)^2 - \frac{1}{6}\left(\frac{eV}{kT}\right)^3 + \cdots\right] \quad . \tag{8}$$

For voltages on the order of $5 \times 10^{-3}$ volts, which is where the I-V characteristics of the this device, PY-G-21(3), start to deviate from linearity, $\frac{eV}{kT} = 0.186$ and $\frac{1}{2}\left(\frac{eV}{kT}\right)^2 = 0.017$. So it can be seen that below this value of voltage, (3) can be written as:

$$I_o \cong aAT^2 e^{-\varphi_o/kT}\left(\frac{eV}{kT}\right), \tag{9}$$

or,

$$V = IR, \tag{10}$$

where R is given by

$$R = \frac{kTe^{\varphi_o/kT}}{eaAT^2} \quad . \tag{11}$$

For this device at T = 312°K this resistance is $8 \times 10^4$ Ω while the measured resistance was $1.3 \times 10^5$ Ω, which is remarkably good agreement considering that the Richardson constant is involved in this expression.

The data for devices PY-G-17(1), 18(2), and 19(2), which were measured at high voltages only, are shown

in Fig. 35 where ln I is plotted vs. $V^{.484}$. As for device PY-G-11(1) the barriers calculated from the zero field intercept do not change substantially from those calculated from the zero field intercept of the ln I vs. $V^{1/2}$ plots. Figure 36 shows a comparison between the devices fabricated with varying amounts of oxygen present during deposition of the MgO on a ln I vs. $V^{.484}$ plot. The barriers obtained from these plots are given in Table V along with the barriers found for device PY-G-38(1) from the Fowler-Nordheim plots.

Table V

BARRIER HEIGHTS FOR A NUMBER OF DEVICES

WITH DIFFERENT PARAMETERS

| DEVICE NO. | S (Å) | $\varphi_R$ (eV) | $P_{O_2}$ (Torr) |
|---|---|---|---|
| PY-G-11(1) | 89 | .722 | $< 10^{-8}$ |
| PY-G-17(1) | 159 | .724 | $< 10^{-8}$ |
| PY-G-18(2) | 109 | .701 | $< 10^{-8}$ |
| PY-G-19(2) | 79 | .711 | $< 10^{-8}$ |
| PY-G-22(2) | 90 | .792 | $10^{-8}$ |
| PY-G-25(3) | 60 | .833 | $10^{-7}$ |
| PY-G-38(1) | 90 | 1.90, 1.74 | $10^{-5}$, $< 10^{-8}$ |

This table illustrates the fact that the barrier height does not change with oxide thickness but that the barrier height increases with increased oxygen pressure

present during deposition of the MgO film. Figure 37 is a plot of the data for devices PY-G-22(2), MgO deposited at $10^{-8}$ Torr $O_2$, and PY-G-25(3), MgO deposited at $10^{-7}$ Torr $O_2$, on log-log paper. The solid lines drawn on the curves are expression (3) with the appropriate values of $\varphi_R$ for these two devices. Again there is strikingly good agreement between the experimental points and the theoretical curves over six orders of magnitude of current. The values of resistance calculated and experimentally found were again in extremely good agreement. For device PY-G-22(2) the calculated value is $3.9 \times 10^5$ Ω while experimentally it was determined to be $4.3 \times 10^5$ Ω. For device PY-G-25(3) the numbers are $7.1 \times 10^5$ Ω and $7.5 \times 10^5$ Ω respectively.

The remarkably good agreement between Eq. (3) and the data indicates that the Schottky type mechanism, modified for these devices, is the dominant mechanism for injection of electrons into the oxide film. The data also indicate that the barrier presented to the flow of electrons by the oxide is much lower than that predicted by the simple band theory. If the barrier was $\varphi_M - \chi_I$, the barrier would be 4.65 eV regardless of the number of excess Mg atoms or oxygen vacancies. However the barrier is much lower than this and also

depends on the number of excess Mg atoms in a manner such that the barrier is lower for more excess Mg. The fact that the barrier seen is lower than that expected is not altoghether unreasonable. Other authors have seen this same effect[81,82,83] for metal-semiconductor interfaces. Mead[84] gives a semi-emperical analysis in which he characterizes the barrier as $\varphi_M - \chi_S$ for semiconductors of ionic character and independent of metal electrode for semiconductors of covalent bonding.

A brief resume of this analysis is given below, not as a statement to determine the barrier height but as a statement that it could be much lower than $\varphi_M - \chi_I$. Figure 38 is a reproduction of a figure in a classic paper on surface states by Shockley.[85] This figure shows the traditional splitting of atomic energy levels as the wave functions of the atoms overlap. In addition it shows the energy of the surface states as a function of lattice spacing. One fact is evident, that is that there are two distinct regions of surface state behavior. At large separations, the wave functions overlap only slightly and the surface states lie at the band edges. At small separations the wave functions overlap strongly and the surface states are near the center of the gap. This provides a valuable clue to

the behavior of different types of semiconductors with respect to surface states. In essentially ionic materials, the wave functions are atomic in nature and the overlap is small. Surface states are formed by the two types of atoms at the surface of the crystal and their energies lie close to the valence and conduction band edges. The upper surface states are unoccupied and the lower surface states are occupied. Thus the Fermi level at the surface may move from near the conduction band edge to near the valence band edge without creating any surface charge. This behavior is quite consistent with the oversimplified picture of the ionic crystal and it does explain the results for many materials. Until the wave function overlap reaches a critical value the surface states lie at the band edges. A small increase in overlap above this critical value causes the surface states to move rapidly to a region near the center of the forbidden gap.

The above analysis holds for intrinsic semiconductors and insulators. However when impurity atoms are added to the crystal the location of the Fermi level may change. If these atoms give rise to donor levels near the conduction band the Fermi level may be closer to the conduction band than the valence band. If the

impurities occupy interstitial positions in the lattice the wave function overlap would be greater than in the original material. A large density of donor like surface states near the conduction band could exist at the surface.

How do these surface states affect the barrier? The surface states are distributed in energy somewhere in the forbidden gap of the oxide, and when the free surface is charge neutral they are filled to some energy, $E_o$, below the conduction band. This will then locate the Fermi level at the surface. If an electric field is applied at the surface this field will induce charge in the oxide, primarily in the surface states if their density is large, and the Fermi level at the surface will shift from this value. However, the larger the number of surface states per unit energy interval, the smaller the movement of the Fermi level for a given induced charge. The same argument may be applied to the energies of a metal-oxide interface. In the limit of very high surface state density, the Fermi level at the surface is fixed by $E_o$, and the barrier energy is just the difference between the band edge and this Fermi level independent of the contact potential difference between metal and oxide.

Bardeen[87] discusses the behavior of the barrier as a function of surface state density. The conclusion arrived at is that for a high density of surface states the barrier height is nearly independent of the work function of the metal and is about the same as for a free surface. The height of the barrier is thus determined by the location of the surface states and their density.

There is some experimental evidence that excess Mg in MgO gives rise to a localized energy level near the bottom of the forbidden gap or possibly in the valence band.[88,89] These states are low lying donor states and when the crystal is irradiated with UV a current is carried by holes. The donor level in their samples is the ground state of an F center and when irradiated by UV the electron enters the excited state. An electron from the valence band can then be thermally excited into the ground state of the F center giving rise to a hole in the valence band. The current under these conditions is then carried by holes. Other results of Yamaka and Sawamoto[90] found that the current in MgO with an excess of Mg was carried by electrons. Their conclusion comes from the results of measurements of the thermo-electromotive

force at a temperature range of 650°C to 1000°C. These results indicated a donor level in the forbidden gap nearer the bottom of the conduction band.

It can be seen that there is some doubt as to the location of the donor levels in MgO with an excess of Mg. The explanation given by Olson[89] for a low lying donor level can be summarized as follows: The MgO crystal is heated in a magnesium vapor pressure. The excess magnesium thus arrives at the surface and reacts with the crystal. Rather than a diffusion of magnesium atoms into the crystal into interstitial positions this reaction causes diffusion of oxygen to the surface, creating an oxygen vacancy. This oxygen vacancy becomes the site of tightly bound electrons or a low lying donor level. Their analysis excluded Mg atoms in intersititial positions because the crystal cannot accommodate them.

An excess magnesium atom in an interstitial type position would probably give rise to a donor level nearer the conduction band. Since the films studied here are not single crystal films, the excess magnesium could very well occupy positions which are of an interstitial type. The experimental evidence indicated that this must be the case since the barrier is so low.

Thus, there must exist localized donor levels near the conduction band and donor like surface states also near the conduction band.

According to Fig. 33 the barrier height changes as a function of temperature. Figure 39 is a plot of $\ln(I_o/T^2)$ vs. $10^3/T$ for the two devices fabricated with $O_2$ gas present during the deposition of MgO. The results from device PY-G-11(1) are repeated here for comparison. It can be seen that none of these curves plot as straight lines. The zero field intercept of the ln I vs. $V^{.484}$ gives a value of $I_o$ as:

$$I_o = aAT^2 e^{-\varphi_R/kT} \tag{12}$$

Thus

$$I_o/T^2 = aAe^{-\varphi_R/kT} \tag{13}$$

or

$$\ln(I_o/T^2) = \ln aA - \varphi_R/kT \quad . \tag{14}$$

Therefore it can be seen that if $\varphi_R \neq \varphi_R(T)$ the slope of the $\ln(I_o/T^2)$ vs. 1/T plot should be a straight line:

$$d\ln(I_o/T^2)/d(1/T) = -\varphi_R/k \quad . \tag{15}$$

However if $\varphi_R$ is a function of temperature this becomes:

$$d\ln(I_o/T^2)/d(1/T) = -\varphi_R(T)/k - (1/kT)\, d\varphi_R(T)/d(1/T) \tag{16}$$

Thus the slope of these plots will not be proportional to the barrier height, which may explain the difference seen between the barriers found by the two methods in

section III-C since the barriers were found from the slope of the best straight line fit to the data for the $\ln(I_o/T^2)$ vs. $10^3/T$ plots. If $d\varphi_R(T)/dT$ is positive, i.e. if the barrier increases with increasing temperature, then $d\varphi_R(T)/d(1/T)$ is negative and the slope of the $\ln(I_o/T^2)$ vs. $1/T$ plots will give a number which is smaller than the actual barrier. The barrier heights obtained for these three devices from the ln I vs. $V^{.484}$ plots are plotted in Fig. 40 as a function of temperature. It can be seen from this figure that the barrier heights do increase with increasing temperature. Thus the slope of the Arrhenius plot will give a value for the barrier height which is actually less than the real barrier height, as seen in these experiments.

The barrier is the distance, in energy, between the location of the Fermi level and the bottom of the conduction band at the surface. In a bulk n-type semiconductor the Fermi level does move farther from the conduction band with increasing temperature. A similar process must exist for these devices. A discussion of this problem is given in Appendix II.

After oversimplification of the problem a qualitative result was obtained for the barrier height as a

function of temperature and donor concentration. The result is:

$$\varphi = kT\ln\left[(1/2)\left\{N_c/N_d+\left[(N_c/N_d)^2+8N_c e^{\psi/kT}/N_d\right]^{1/2}\right\}\right] \quad (17)$$

This simple calculation shows that the barrier increases for increasing temperature, increases for decreasing donor concentration, and increases faster for increasing temperature as the donor concentration decreases. These results are all consistent with the experimental results. This expression is plotted as the dashed curves in Fig. 40 and it can be seen that the agreement with the experimental results is fairly good on a qualitative basis.

The model developed here for the barrier height depends on the existence of surface states. As previously stated the barrier under these conditions should be nearly independent of the work function of the metal. Savoye[55] found a contact potential difference of $\varphi_{Au}-\varphi_{Al} = .8$ eV in his Al-$Al_2O_3$-Au samples. If the surface state model holds, the barrier should be nearly the same for current flow in either direction, if it does not hold the barrier will be modified by the contact potential difference between the metals. A number of Au-MgO-Al devices were fabricated. These devices were very unstable and usually broke down

before any extensive measurements could be made. One device, PY-A-1(1), was stable long enough to measure the I-V characteristics at T = 313°K. The results of this measurement are shown in Fig. 41 on a ln I vs. $V^{.484}$ plot. The barriers obtained from these plots are: for the Au-MgO interface, $\varphi_{RAu}$ = .702 eV, and for the Al-MgO interface, $\varphi_{RAl}$ = .643 eV. It can be seen that there is some difference between the two electrodes, $\varphi_{RAu}-\varphi_{RAl}$ = .059 eV, but this value is much smaller than the difference in work functions between gold and aluminum. This difference in barriers is about the same value as the difference noted by Mead[83] for different metals on CdSe. Thus the model incorporating surface states to lower the expected barrier is consistent with the observed results even though no quantitative results could be obtained.

We conclude that the current transfer process of importance in these thin film emission diodes is that of field-controlled emission-limited Schottky emission mechanism whereby electrons are emitted from the metal electrode into the conduction band of the insulating film over the image force interfacial barrier under the attendant lowering by the electric field. The simple Schottky equation does not hold but the equation

derived by taking into account the multiple image corrections to the barrier profile give excellent agreement with experimental results. The effective height of the energy barrier at the Au-MgO interface deduced from this analysis is about .7 eV. This value can only be explained if a large density of interface states exist. The barrier height is temperature dependent and also depends on the excess magnesium concentration. This model implies that a large density of surface states, which are all ionized, allows the barrier to be much smaller than initially expected and that the effect of increasing the temperature is to ionize more donors allowing more electrons to enter the conduction band of the MgO. This results in a higher barrier for higher temperatures.

In this model the electrons injected by the Schottky emission process appear in the conduction band of the insulating film, where they are accelerated by the strong electric field toward the positively biased electrode. The processes by means of which the injected electrons are transported through the insulating film are discussed in the next section.

## D. Discussion of Emission into Vacuum

The electron injection process in these thin film emission diodes has thus been characterized as a Schottky emission process. The subsequent transport of the injected electrons through the insulator under the influence of the strong electric field can be expected to involve some energy loss.

Figures 27, 28, and 29 show the emission transfer ratio, $\alpha = I_e/(I_e+I_s)$ as a function of sample bias. Two features of these plots are very striking. One is that the transfer ratio decreases with increasing sample bias and the other is that for only one device, PY-G-25(3), is the sample bias greater than 5.45 volts. Figure 44a shows the energy band diagram for these devices under an applied sample voltage of 4 volts, which is higher than most sample biases reached in these experiments. The straight line with the arrow shows the trajectory of an electron which loses no energy in traversing the oxide and metal overlayer. It can be seen that the electron should not be emitted into vacuum since it does not have enough energy to surmount the metal-vacuum interfacial potential barrier.

The anode-overlayer spacing is large enough so that Schottky emission should not occur from the metal

overlayer into vacuum. The resolution of the measurements was such that emission currents on the order of $10^{-10}$ amps could be measured. For current of $10^{-10}$ amps due to "thermionic" emission a sample bias of $\approx 4.45$ volts would be necessary. Therefore there should be no electrons emitted into vacuum until the sample bias is $\approx 4.45$ volts.

Savoye and Anderson[12] discuss the possibility of preferential emission of electrons through holes in the gold overlayer film. In order for electrons to be emitted from these Au-MgO-Au devices the electrons must be emitted through holes in the gold overlayer film. The energy band diagram appropriate to the fraction of electrons which arrive at the oxide-overlayer interface in the vicinity of a hole is shown in Fig. 44b for a 4 volt sample bias.

In the case of large holes, the field at the underlayer beneath the hole might be expected to decrease fairly rapidly with distance from the edge, and hence the current density would also decrease beneath a hole. In consequence only a fraction of the area of a particular hole would be expected to contribute appreciable emission current.

Electron micrographs of thin gold films deposited on cold substrates indicate that such films consist of a large number of agglomerates, separated by relatively narrow open regions resembling slots, which are characterized by a fairly well defined width.[93,94] We therefore assume that in the present case the holes in the Au overlayer films can be represented by slots of characteristic width d.

The width of the slots for a typical case is difficult to estimate from the electron micrographs, but is on the order of 20-200 Å for a film of about 100 Å thickness.[55] In the present experiments with MgO films varying from 60 Å to 160 Å thickness, the electric field strength at the underlayer beneath a slot might therefore be expected to decrease rapidly with distance from the slot edge. The electron current emitted into the oxide film beneath a slot can be estimated using a solution to the electrostatic problem for the field beneath a slot as a function of the distance from the slot edge.

A solution to the electrostatic problem simplified by neglecting the dielectric discontinuity at the surface has been obtained, and is presented in Appendix III. From this solution, numerical calculations for the

field strength, F(y), as a function of the distance, y, from one edge of the slot were carried out for the ratios of oxide thickness to slot width of interest, assuming all slots are 100 Å wide. Results of these calculations are presented in Fig. 45, where relative field strength, $F/F_o$, is plotted versus y. Notice that the ordinate scale is an expanded scale extending only from 75% to 100%.

The magnitude of $F/F_o$ is seen to decrease rapidly with distance and at a rate strongly dependent on the oxide thickness, as expected.

The relative electron current, $j_{rel}(y)$ resulting from the field F at y is:

$$j_{rel}(y) = \frac{j(y)}{j(-\infty)} = \frac{AT^2 e^{-\varphi_R/kT} e^{\beta[F(y)]^{1/2}}}{AT^2 e^{-\varphi_R/kT} e^{\beta F_o^{1/2}}}$$

$$= e^{\beta F_o^{1/2}\left[(F/F_o)^{1/2}-1\right]} . \qquad (19)$$

We have assumed the simplified form for the Schottky equation since it is nearly correct for the fields of interest. The constant $\beta$ has the value, $\beta = 4.5 \times 10^{-3}$ $(cm/volt)^{1/2}$, for T = 313°K, the temperature at which emission data was taken.

Let there be N such slots per unit area and of length $\ell$. If $\gamma$ is the ratio of overlayer hole area to total overlayer area

$$\gamma = N\ell d \ . \qquad (20)$$

An estimate to the current emitted into the oxide beneath a hole in the overlayer film can thus be made.

The sample current, $I_s$, can be viewed as consisting of two contributions; 1) a contribution from Schottky current density $j_s$ from regions of Au lying beneath the gold overlayer, and 2) a contribution from regions of Au lying beneath holes in the gold overlayer, which is written as $j_{rel}(y) j_s$. This second contribution will depend upon the position, y, under the slot of width d, with $0 \leq j_{rel}(y) \leq 1$. Assuming that $j_s$ is constant, and determined by the magnitude of the applied field at the Au underlayer beneath the Au overlayer, we write for the sample current:

$$I_s = j_s a(1-\gamma) + j_s N\ell a \int_o^d j_{rel}(y)\,dy - I_e \ , \qquad (21)$$

or

$$I_s = j_s a\left[(1-\gamma) + \gamma \frac{1}{d}\int_o^d j_{rel}(y)\,dy\right] - I_e \ , \qquad (22)$$

where a is the sample area and the integration is over a single slot of width d.

A similar expression can be written for the emission current, $I_e$:

$$I_e = j_s a\left[(1-\gamma)P_{oo}\alpha_t + \gamma\frac{1}{d}\int_o^d j_{rel}(y)P_{os}\alpha_H(y)\,dy\right], \quad (23)$$

where $\alpha_t$ is the attenuation factor for the Au film, $P_{oo}$ is the fraction of the electrons which arrive at the overlayer film energetically capable of emission, $P_{os}$ is the fraction of the electrons which arrive at a slot energetically capable of emission, and $\alpha_H(y)$ expresses the transfer ratio through a slot of width d, as a function of position y. For the biases, $V_s$, used in these experiments, $P_{oo} = 0$. Since the sample current beneath a slot is less than the sample current beneath the overlayer and $1-\gamma \approx 1$, $I_s$ and $I_e$ can be written as:

$$I_s = j_s a - I_e \quad (24)$$

$$I_e = j_s a\gamma\frac{1}{d}\int_o^d j_{rel}(y)P_{os}\alpha_H(y)\,dy\,. \quad (25)$$

On this model the measured transfer ratio $\alpha_M$ is:

$$\alpha_M = \frac{I_e}{I_e+I_s} = \gamma\frac{1}{d}\int_o^d j_{rel}(y)P_{os}\alpha_H(y)\,dy\,, \quad (26)$$

or

$$\alpha_M = \gamma\frac{1}{d}\int_o^d P_{os}\alpha_H(y)\,e^{\beta F_o^{1/2}\left\{\left[F(y)/F_o\right]^{1/2}-1\right\}}dy. \quad (27)$$

For an applied field of $F_o = 2.5 \times 10^6$ volts/cm (27) becomes

$$\alpha_M = \gamma\frac{1}{d}\int_o^d P_{os}\alpha_H(y)\,e^{7.1\left\{\left[F(y)/F_o\right]^{1/2}-1\right\}}dy\,. \quad (28)$$

If no energy loss occurred in the oxide all electrons arriving at a slot would be energetically capable of escape, for $F_o = 2.5 \times 10^6$ volts/cm, and a good approximation under these conditions would be $\alpha_H(y) = 1$ for $0 \leq y \leq d$. In this case,

$$\alpha_M = \gamma \frac{1}{d} \int_o^d e^{7.1\left\{\left[F(y)/F_o\right]^{1/2}-1\right\}} dy \quad . \tag{29}$$

This expression for $\alpha_M$ can be integrated numerically for each oxide thickness of interest. This has been done and $\alpha_M$ is plotted vs. S, the oxide thickness, in Fig. 46. This shows that $\alpha$, on the basis of field alone, should go up for thicker oxides. Also shown on this figure are the actual emission ratios, for $F_o = 2.5 \times 10^6$ volts, divided by a suitable $\gamma$. The $\gamma$ used here is not the actual $\gamma$ since the emission transfer ratio drops off as a function of voltage. The $\gamma$ used was one in which the data would then fit the theoretical curve for s = 159 Å. It can be seen in this figure that the other data points fit the curve quite well.

An examination of Fig. 29 shows that an extension of the data to V = 0 leads to values of $\gamma$ on the order of $2 \times 10^{-3}$. This would put a lower bound on $\gamma$ of $2 \times 10^{-3}$. The reason for saying that this value is a lower bound on $\gamma$ is that the term $\alpha_H(y)$ in Eq. (23)

is not a constant of value 1.0 since the electrons arriving near the edge of a slot have a greater probability of being trapped than those arriving at the center of a slot with the same value of $v_x$. This is a consequence of the fringing field at the slot. This value for $\gamma$ is quite reasonable. A comparison with the results of Savoye (see reference 55, Fig. 40) shows that for an overlayer thickness of 200 Å, $\gamma$ has a value of $\approx 6 \times 10^{-3}$ for gold on $Al_2O_3$. As noted in section III-F of this thesis, the sheet resistance of a gold film on MgO is lower than for a gold film on $Al_2O_3$, indicating a more continuous film of gold on MgO, i.e., fewer pin-holes in the gold. This would lead to a smaller value of $\gamma$ for Au on MgO than for Au on $Al_2O_3$, as seen here.

Possible energy loss mechanisms in the MgO film include impurity scattering, impact ionization of valence electrons, and electron-phonon interactions.

Impact ionization of valence electrons can only occur if the energetic electron has kinetic energy $E \geq E_g$, where $E_g$ is the band-gap energy. Because there is a potential barrier of magnitude $\varphi_o$ between the overlayer Fermi level and the bottom of the oxide conduction band and the energy distribution of electrons

in the metal drops off quite rapidly above this level, the maximum kinetic energy available for $V_s$ volts applied is approximately $E_m = eV_s - \varphi_o$. From this the threshold voltage for impact ionization to be possible is $eV_s \geq E_g + \varphi_o$. The band-gap energy, $E_g$, of MgO is 8.7 eV and $\varphi_o \approx .7$ eV. These values show an estimate of the threshold voltage for impact ionization of about 9.4 volts. In the present experiments the maximum applied voltage is always less than 9 volts, hence impact ionization of valence electrons can be ignored.

Electron-phonon interactions, in particular the creation of optical phonons, can be expected to result in a loss in energy. The creation of optical phonons can be expected to result in an energy loss on the order[98] of 0.1 eV per interaction. The mean distance, $\lambda$, required for an electron of energy E to create an optical phonon can be crudely estimated[12] on the basis of the theories of intrinsic breakdown of insulators

$$\lambda \sim \frac{\hbar\omega}{dE/dx} \quad , \tag{30}$$

where $\hbar\omega$ is the optical phonon energy and dE/dx is the rate of energy loss to the lattice with distance x. O'Dwyer[56] gives an expression for dE/dt, for energies less than the valence-band ionization energy, which is

$$dE/dt = \left[\hbar\omega \log(4E/\hbar\omega)\right]/2\tau_o(E) \quad , \tag{31}$$

with

$$1/\tau_o(E) = \sqrt{\frac{m}{2}}\ \frac{e^2\omega}{2}\ \left(\frac{1}{\epsilon_{rh}} - \frac{1}{\epsilon_{r\ell}}\right) E^{-1/2} \quad , \tag{32}$$

in esu, with $\epsilon_{rh}$ and $\epsilon_{r\ell}$ the high and low frequency dielectric constants respectively. Using $dE/dx \sim dE/vdt$ with $E = \frac{1}{2}\, mv^2$, $\lambda$ can be written as

$$\lambda \sim \frac{4\hbar^2}{me^2 \log(4E/\hbar\omega)}\ \left(\frac{E}{\hbar\omega}\right)\ \frac{\epsilon_{rh}\epsilon_{r\ell}}{\epsilon_{r\ell} - \epsilon_{rh}} \quad . \tag{33}$$

For electron energies on the order of the phonon energy and $\epsilon_{r\ell} \simeq 10$, $\epsilon_{rh} \simeq 3$, $\lambda \sim 6.2 \times 10^{-8}$ cm = 6.2 Å. This can be compared with some results obtained from studies of secondary electron emission from MgO, in which a mean free path of about 5 Å is found to be appropriate for describing the internal secondary escape mechanism.[98]

On the basis of this estimate it can be seen that electron-phonon interactions alone cannot explain the results depicted in Figs. 27, 28, and 29. There are two reasons for this: 1) an electron would only lose about 2.6 eV in energy in traversing the thickest of these oxides and most of the electrons incident on a hole in the gold overlayer would escape, at an applied voltage of 4 volts, and 2) the mean free path should increase with increasing electron energy. Therefore on the basis of electron-phonon interactions the

ratio, $\alpha$, would be expected to go up with increasing sample voltage contrary to experimental results.

The term impurity scattering used here included two distinct types of events. In one case the scattering center does contain a weakly bound electron and in the other case it does not.

In the case in which the scattering center does not contain a weakly bound electron the mean free path is equal to the average distance between impurity atoms and can be given by:[99]

$$\lambda \sim \frac{2\epsilon_r^2 E^2}{\pi m^* N_i e^2 \log\left(1 + \frac{\epsilon_r^2 E^2}{e^2 N_i^{2/3}}\right)} . \qquad (34)$$

This again will not explain the experimental results since $\lambda$ again increases with increasing bias and it would be essentially elastic scattering.

For the case in which the impurity does contain a weakly bound electron there exists the possibility of appreciable energy loss per interaction if the scattering site, such as a donor or trap, contains an electron which can be excited into the conduction band of the insulator. Furthermore the mean free path in this case would decrease with increasing sample bias. This can be seen on the basis of the following analysis.

As the electron is accelerated in the conduction band of the oxide it gains energy and when it has gained energy greater than the energy difference between the conduction band minimum in the oxide and the donor level it could lose this energy to the donor electron which is then excited into the conduction band of the oxide. The greater the applied bias the more of these interactions that could occur.

This, however, leads to avalanche phenomena so that for each interaction there are two electrons in the conduction band for each initial electron. This would greatly increase the sample current if a great number of these interactions took place. However this effect is not noted in the sample I-V characteristics which can be completely explained on the basis of a Schottky type mechanism. If the total number of these interactions was small, then the transmission ratio $\alpha$ should increase or at least stay nearly constant with applied voltage.

As can be seen by this qualitative analysis none of the possible energy loss mechanisms can explain the observed behavior for these devices. The most probable explanation is that the oxide emitting surface becomes charged. When a sample current is first drawn, electrons arrive at the slot and those with enough energy are

emitted into vacuum. The remaining portion are not collected by the overlayer immediately but lead to a space charge at the slot. Thus the emitted current is dependent on sample current and time and in this manner indirectly dependent on the sample voltage. This is shown quite dramatically in Fig. 47.

Figure 47a shows the actual scope trace of $I_s$ and $I_e$ vs. $V_s$ for device PY-G-17(1). The pulse amplifier saturates at a given output power and the voltage is then constant beyond this point. The actual $V_s$ vs. time is observed on oscilloscope I (see section II-C-4). The applied voltage was allowed to saturate in this particular measurement and the actual pulse is shown in Fig. 47b. $I_s$ and $I_e$ were not observed as a function of time but were seen on oscilloscope II plotted vs. $V_s$. $I_s$ was seen to reach a maximum value when $V_s$ reached its maximum and remained at that current as evidenced by a bright spot at that point. $I_s$ vs. time can then be inferred from this curve and is shown in Fig. 47b as a constant current of $6.7 \times 10^{-3}$ amps for 6.75 msec. $\leq t \leq$ 10 msec. $I_e$ however was seen to drop to $4.6 \times 10^{-8}$ amps from its maximum of $7.6 \times 10^{-8}$ amps. This drop is shown as a linear drop as a function of time in Fig. 47b but may very well have another time dependence. This is

direct evidence that the oxide in the neighborhood of a slot does become negatively charged by the electrons that are not emitted into vacuum. The total charged area is so slight, however, that it does not affect the sample current.

Thus, although $\alpha$ is a function of applied sample voltage it is actually indirectly dependent upon voltage through the voltage dependence upon current and time. A better functional dependence for $\alpha$ would be $\alpha = \alpha(I,t)$. However, since $I = dQ/dt$ an even better functional dependence would be $\alpha = \alpha(Q,t)$. The total charge, Q, that has arrived at the overlayer is given by:

$$Q = \int_o^t I(\tau)\,d\tau \quad . \tag{35}$$

Again assuming the simple Schottly equation:

$$I = I_o e^{\beta V^{1/2}} \quad , \tag{36}$$

and since V is linearly dependent on time, $V = n^2\tau$:

$$I = I_o\, e^{\beta n \tau^{1/2}} \quad , \tag{37}$$

thus;

$$Q = I_o \int_o^t e^{\beta n \tau^{1/2}}\, d\tau \quad . \tag{38}$$

Integration yields:

$$Q = \frac{2I_o}{\beta^2 n^2}\left[(\beta n t^{1/2} - 1)\, e^{\beta n t^{1/2}} + 1\right]. \tag{39}$$

The results previously mentioned have been obtained on the assumption that $F(y)/F_o$ is a constant value for each device. However since the insulator is charging

up at the emitting slot, $F(y)/F_o$ is actually decreasing as $F_o$ increases. This means that the ratio $j_{rel}(y)$ is actually decreasing as $F_o$ increases so that relatively fewer electrons arrive at the slot as $F_o$ increases, or $\alpha_M$ from Eq. (27) decreases as $F_o$ increases.

Further evidence that the charging of the slot area is the determining factor in the emission results is shown in Fig. 48. In Fig. 48a, $\alpha$ of device PY-G-11(1), at $V_s$ = 2 volts, is plotted vs. the time it took for the voltage ramp to reach 2 volts, i.e., $dV/dt$ is different for each plotted point. Figure 48b is a plot of $\alpha$ with the same parameters, plotted vs. Q, the total charge passed through the insulator as found from Eq. (39). As can be seen from these figures $\alpha$ decreases as a function of time, or total charge, even though the sample current and sample voltage are the same. Similar results were obtained for each device, however on only one other device were the measurements extensive enough to determine a charging "time constant", this was device PY-G-17(1). The results of these two devices are plotted on a log$\alpha$ vs. t plot in Fig. 49. If $\alpha$ can be described as $\alpha = \alpha_o e^{-t/\tau}$ this "time constant", $\tau$, is 2 msec for PY-G-11(1) and 2.4 msec for PY-G-17(1). The decay of the charge is fairly rapid since a succeeding pulse,

on the order of one second later, gave identical results to the first pulse. The electrons are apparently being trapped in surface states which exist in the vicinity of the slots and have a time constant on the order of a millisecond which is in reasonable agreement with the time constants found for slow surface states.[80]

A further note of evidence that the emission current is controlled by charging of the insulator at the slot is given by the fact that no emission into vacuum was observed when the devices were studied using the slowly varying dc method.

The following section presents a brief summary of the important experimental results obtained and a discussion of the conclusions which can be drawn in terms of the preceding analyses.

## V. SUMMARY

This investigation was primarily concerned with the transport of hot electrons through vacuum deposited thin film emission diodes with subsequent emission into vacuum. The studies were specifically carried out on the evaporated Au-MgO-Au system.

The possible mechanisms for current flow from metal electrode to metal electrode are the following: 1) ohmic, 2) space charge limited, 3) tunnelling of electrons into the conduction band of the oxide and subsequent flow to the other electrode, 4) a Poole-Frenkel effect in which the electrons are thermally emitted from traps into the conduction band of the oxide by field enhancement, 5) mechanisms whereby electrons travel through the oxide by jumping from trap to trap, and 6) Schottky emission of electrons into the conduction band of the oxide.

The current-voltage characteristics were nonlinear which ruled out ohmic conduction except at very low field strengths and the current was not proportional to $V^2$ as it should be for space charge limited current.[16] Tunnelling could be ruled out since the functional dependence of I upon V was inconsistent with this mechanism (see Fig. 14). A Poole-Frenkel mechanism could also be ruled out on the same basis (see Fig. 16).

Furthermore when the MgO films were deposited in an oxygen atmosphere the term $\psi$ in the exponent in the equation $I = I_o e^{-\psi/kT} e^{\alpha V^{1/2}}$ becomes larger, which would indicate a lowering of the trap level by producing more stoichiometric films of MgO, if the Poole-Frenkel equation is assumed. It would indicate a higher barrier if the Schottky equation is assumed. It is much more reasonable to assume that the barrier is higher than a lowering of the trap level.

Some authors[15] have observed a power law dependence of current upon voltage in which $I \alpha V$ at low voltages, attributed to ohmic current flow, $I \alpha V^2$ for intermediate voltages, attributed to space charge limited current, and $I \alpha V^n$ where $n > 2$ for higher voltages. The term, n, in the exponent has varied from 4 all the way up to 16. This behavior has been attributed to the hopping of the electron between energy states in the forbidden gap of the insulator and eventual collection by the metal overlayer. Their analysis thus involved two or more changes in current flow mechanism as the voltage is increased. A look at Figs. 34 and 37 show a similar dependence of I upon V which can be completely explained by a Schottky type emission process in which the multiple image correction to the barrier profile has been made.

Using the multiple image correction to the potential barrier profile results in an I-V characteristic which is linear for low voltages and ultimately reaches a dependence such that ln $I \alpha V^{.484}$. The expressions derived using the multiple-image correction, Eq. (1)-(9), were plotted on log-log paper and fit the data over six orders of magnitude of current and four orders of magnitude of voltage. The conclusion drawn is that the electron flow in these devices is that of emission of electrons over the potential barrier into the conduction band of the oxide by a Schottky type process and subsequent acceleration by the strong electric field to the collection electrode.

A number of other features of these devices were brought to light during study of the I-V characteristics. There was no aging effect observed in these devices as noted by nearly every other author. The I-V characteristics were identical for the overlayer biased positively as for the overlayer biased negatively, indicating a symmetrical barrier, when gold was used as both electrodes. There was no hysteresis noted in dc measurement of the device characteristics and the pulse measurements were identical to the dc measurements. The barrier height did not change as the oxide thickness changed.

The barrier height did change as the amount of oxygen present in the vacuum system changed during deposition of the MgO film. The change was to a higher barrier as the oxygen pressure was made higher. Raising the oxygen pressure during deposition of the MgO film probably leads to a more stoichiometric film. The excess Mg present in these films gives rise to donor levels in the "bulk" and at the surface. These levels are near the conduction band so that the barrier is quite low. Decreasing the number of donors leads to a higher barrier since the Fermi level will be lower for fewer donors. The barrier height was also seen to change with temperature as noted by the results depicted in Figs. 39 and 40 and this change could be explained in a qualitative manner by assuming a high density of donor like interface states and "bulk" donors.

Another possible explanation for the nonlinear $\ln(I_o/T^2)$ vs. $1/T$ plots and the different barrier obtained by taking the slopes of these plots would be another current flow mechanism, which is nearly independent of temperature, such as tunnelling, superimposed on the Schottky current but of much smaller magnitude. It is impossible to determine which of these explanations hold or if both do.

The barrier height can be raised significantly by depositing the MgO in a high pressure of oxygen gas, on the order of $10^{-5}$ Torr, as evidenced by device PY-G-38(1). The barrier for this device was raised to about 2 eV and tunnelling became the dominant mechanism for current injection. The barrier to electron flow from overlayer to underlayer for this device was lower because the oxide near the overlayer was deposited after the oxygen had been pumped from the system resulting in a nonsymmetrical barrier. This is further evidence that the barrier goes up as the oxide film becomes more stoichiometric. None of the devices fabricated with a high pressure, $> 10^{-6}$ Torr, of oxygen present during deposition of the MgO were stable long enough to do extensive measurements.

In order to fabricate more stoichiometric devices, which can be measured, the oxide films must be very thin, $\lesssim$ 50 Å, and all devices made with such a thin oxide film were shorted between underlayer and overlayer due to pinholes. This led to the conclusion that single crystal devices may be impossible to attain. This would be especially true if the excess Mg in the films would in some way inhibit epitaxial growth of the oxide film. In this case the films would have to be stoichiometric

and very thin. Furthermore a perfect cleavage plane would have to be attained. None of the devices fabricated on single crystal substrates were single crystal devices, and all were shorts.

The low potential energy barrier is due to a high density of donor like interface states. If this is true the barrier should be nearly the same regardless of the metal used for the electrodes. One device, PY-A-1(1), which was a Au-MgO-Al device, was stable long enough to make one I-V characteristic run. The barrier to current flow from Au → Al was nearly the same as that from Al → Au. The difference between barriers to current flow was of the same order of magnitude as that seen for different metals on CdSe by Mead.[83] This is further evidence that the electron flow is controlled by the metal-oxide interfacial barrier.

Further evidence for Schottky emission is noted by the fact that emission into vacuum is seen from all the devices at very low sample voltages. The sample biases are never large enough to allow emission of electrons into vacuum through the gold overlayer film. Thus the electrons must be emitted through pinholes in the gold film, i.e., directly from the oxide film. The emitted electrons must still overcome a potential barrier at

the oxide-vacuum interface which is the electron affinity of the MgO. If the electrons were not coming over the underlayer-oxide interfacial barrier they would not have enough energy to be emitted into vacuum until the sample bias had reached about 1.0 volt or more. Emission into vacuum was noted from these devices at sample biases less than 0.5 volts. Thus, if the electron affinity of MgO is $\approx$ 0.8 eV, the emission current must be due to the electrons in the tail of the Fermi distribution above the energy level of the oxide conduction band. These electrons then have enough energy to be emitted into vacuum.

The emission ratio, $\alpha = \frac{I_e}{I_e+I_s}$ appears to be higher for the thicker oxide films at any given sample bias. It also appears to be slightly higher at the same field in the oxide. This can be explained on the basis of the electric field strength beneath a slot. The thicker the oxide the greater the electric field strength beneath a slot in the overlayer film. Thus for the thicker oxides more electrons are being emitted into the conduction band of the oxide beneath a slot in the overlayer film, and thus more electrons are arriving at the slot area for the same average field strength in the oxide.

This analysis is complicated by the fact that the oxide is charging negatively at the emitting slot. This is seen by the fact that the emission ratio goes down as the sample bias is increasing. None of the possible scattering mechanisms in the oxide film could account for this dependence of $\alpha$ on $V_s$ and still give sample I-V characteristics consistent with the Schottky mechanism observed here. Thus the emission transfer ratio is dependent on sample bias only to the extent that the bias depends on time or total charge passed through the oxide.

Evidence that $\alpha$ depends on the time is shown in Figs. 47, 48, and 49. Figure 47 shows that if the sample bias is left at the same value for any length of time the sample current remains constant but the emission current decreases rapidly. Thus $\alpha$ decreases as a function of time for a given sample bias. Figures 48 and 49 show that $\alpha$ decreases at a given sample bias as the time it takes to reach that bias increases. The dependence on the time taken to reach a given sample bias is such that $\alpha = \alpha_o e^{-t/\tau}$ where the "time constant" for charging is about 2 msec.

Further evidence that the oxide is charging in the vicinity of an emitting slot is the fact that no

emission into vacuum was observed when the devices were studied using the slowly varying dc technique.

Thus, although these devices are poor cold cathode electron emitters, a number of other uses may be possible. Since the metal-oxide interfacial potential barrier can be varied, depending upon deposition parameters, an array of these devices with different barriers could be used as light detectors such that a signal could be picked off at different points on this array, depending on the frequency of the light. The results obtained from device PY-G-38(1) indicates that these devices with different barrier heights at each interface could be designed as rectifiers. Much more work would be necessary to achieve either of these "practical" devices.

# APPENDIX I

## Application of the Schottky Emission Problem to a Metal-Insulator-Metal Diode

The following analysis for internal Schottky emission uses a physical model similar to that assumed for the case of emission into vacuum. The process of electron injection into the conduction band of the oxide film is analyzed in terms of the simple band theory of solids,[75] in which the metal overlayer and metal underlayer are idealized according to the Sommerfeld model. The oxide is assumed to present a barrier to electron conduction of height $\varphi_R$, modified by the electron image force. The energy level diagram appropriate for the potential barrier in this case shown in Fig. 30, drawn for a rectangular barrier height, $\varphi_R$, of 0.72 eV and an oxide thickness, S, of 100 Å with the zero of energy taken at the Fermi energy of the Au underlayer. The single image correction and the multiple image correction to this barrier are also shown.

The exact expression for the multiple-image correction to the potential energy of an electron in a medium with dielectric constant $\epsilon_r\epsilon_o$ between infinite parallel plane electrodes is derived by Savoye (see ref. 55, Appendix II). The result is:

$$eV_i = - \frac{e^2}{8\pi\epsilon_r\epsilon_o} \left\{ \frac{1}{2x} + \sum_{n=1}^{\infty} \left[ \frac{ns}{(ns)^2 - x^2} - \frac{1}{ns} \right] \right\} \quad \text{(I-1)}$$

This expression gives the image correction in joules. Using the appropriate values this expression becomes:

$$eV_i = - \frac{3.59}{\epsilon_r x} \left\{ 1 + \frac{2x}{s} \sum_{n=1}^{\infty} \frac{1}{n\left[ (s/x)^2 n^2 - 1 \right]} \right\} \text{(ev)}. \quad \text{(I-2)}$$

In this expression the distance, x, of the electron from one plate and the total dielectric thickness, S, are in Å. Assuming the low frequency dielectric constant of MgO the expression becomes:

$$eV_i = - \frac{.367}{x} \left\{ 1 + \frac{2x}{s} \sum_{n=1}^{\infty} \frac{1}{n\left[ (s/x)^2 n^2 - 1 \right]} \right\} . \quad \text{(I-3)}$$

This expression can be written as:

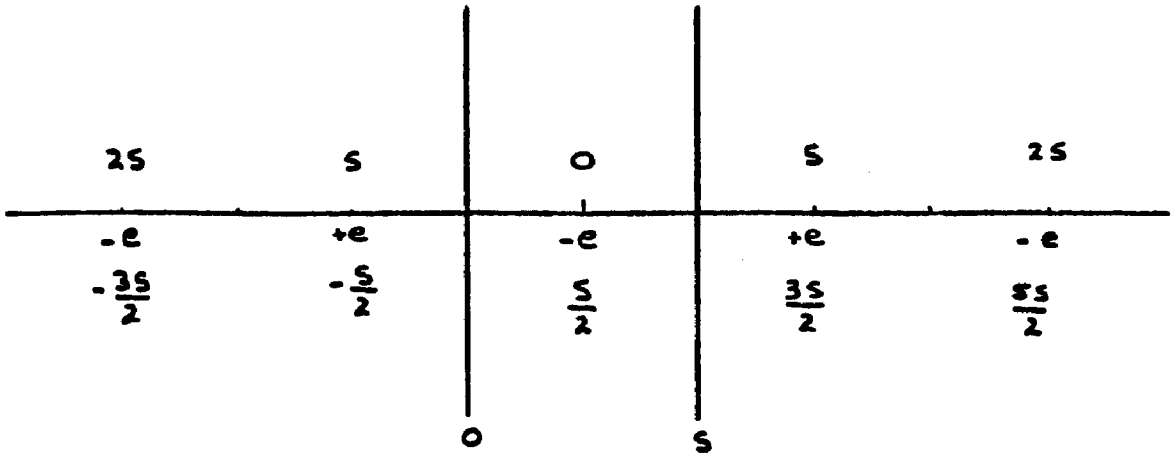
$$eV_i = - \frac{.367}{x} \left[ 1 + C\left(\frac{x}{s}\right) \right], \quad \text{(I-4)}$$

where $- \frac{.367}{x}$ is the single image potential energy and $C\left(\frac{x}{s}\right)$ is the multiple-image correction. Since this series has no closed form some approximations must be made. When x = s/2 expression (I-3) becomes:

$$eV_i = - \frac{.367}{x} \left\{ 1 + \sum_{n=1}^{\infty} \frac{1}{n(4n^2 - 1)} \right\} , \quad \text{(I-5)}$$

The easiest method for obtaining this expression in simpler form is to solve the porblem with the electron midway between the two electrodes. Since the force on the electron is zero in this case, a method differing from Savoye's must be used. In this case the coulomb

potential of all the image forces will be calculated at the center of the dielectric and the potential energy of the electron thus found by multiplying this expression by -e. Let the electrode spacing be S, with one electrode taken as the origin as shown in the diagram below. The positions and signs of the image charges are noted below the x axis with the distance from the electron noted above the x axis.




The total coulomb potential can be written by inspection:

$$V_i = \frac{e}{4\pi\epsilon_r\epsilon_o}\left\{\frac{2}{s} - \frac{2}{2s} + \frac{2}{3s} - \frac{2}{4s} + \frac{2}{5s} \cdots\right\} \qquad \text{(I-6)}$$

or

$$V_i = \frac{e}{2\pi\epsilon_r\epsilon_o s}\sum_{n=1}^{\infty}\frac{(-1)^{n+1}}{n} . \qquad \text{(I-7)}$$

Thus the potential energy of the electron at the midpoint between the electrodes is:

$$eV_i = -\frac{e^2}{2\pi\epsilon_r\epsilon_o s}\sum_{n=1}^{\infty}\frac{(-1)^{n+1}}{n} \qquad \text{(I-8)}$$

The series $\sum_{n=1}^{\infty} \frac{(-1)^{n+1}}{n}$ is convergent[76] and is the Taylor series for ln(x+1) evaluated at x = 1.[77,78]

The Taylor series expansion for f(x) is given by:

$$f(x) = \sum_{n=o}^{\infty} \frac{f^{(n)}(x_o)}{n!} (x-x_o)^n , \qquad \text{(I-9)}$$

thus:

$$\ln(x+1) = \sum_{n=1}^{\infty} \frac{x^n (-1)^{n+1}}{n} . \qquad \text{(I-10)}$$

For x = 1 this becomes:

$$\ln(2) = \sum_{n=1}^{\infty} \frac{(-1)^{n+1}}{n} . \qquad \text{(I-11)}$$

So we can write the potential energy of the electron as:

$$eV_i = - \frac{e^2 \ln 2}{2\pi \epsilon_r \epsilon_o s} . \qquad \text{(I-12)}$$

According to Simmons (see ref. 11, Eq. (33) and Fig. 4) an extremely good approximation to the multiple image correction is of the form:

$$eV_i = - \frac{Ks^2}{x(s-x)} . \qquad \text{(I-13)}$$

To find the value of K one must equate this expression to expression (I-12) at $x = \frac{s}{2}$, one gets:

$$K = \frac{e^2 \ln 2}{8\pi \epsilon_r \epsilon_o s} . \qquad \text{(I-14)}$$

Thus the expression

$$eV_i = - \frac{e^2 \ln 2}{8\pi \epsilon_r \epsilon_o} \left[\frac{s}{x(s-x)}\right] \qquad \text{(I-15)}$$

is an extremely good approximation to the multiple image correction and this expression is plotted in Fig. 30. Putting in the appropriate values

$$eV_i = -.508\left[\frac{s}{x(s-x)}\right], \qquad \text{(I-16)}$$

where dimensions x and s are in Å.

From Eq. (I-18) it can be seen that the actual barrier $\varphi_o$ is given by

$$\varphi_o = \varphi_R - .508\left[\frac{s}{x(s-x)}\right](eV). \qquad \text{(I-17)}$$

Thus when an electric field is applied, the barrier to electron flow becomes

$$\varphi(x) = \varphi_o - eV\frac{x}{s} \qquad \text{(I-18)}$$

or

$$\varphi(x) = \varphi_R - .508\left[\frac{s}{x(s-x)}\right] - eV\frac{x}{s}. \qquad \text{(I-19)}$$

The resulting barriers for a field of $3 \times 10^6$ V/cm, which corresponds to an applied voltage of 3 volts across the 100 Å thick oxide film, is also shown in Fig. 30. Even though Eq. (I-19) is a simplified approximation to the true multiple image modification it is still extremely difficult to work with. To apply this expression to the Schottky equation the maximum of the potential energy of the electron when a field is applied must be found. Let $eV_i|_F$ be the potential energy of an electron in an applied field.

$$eV_i|_F = -.508\left[\frac{s}{x(s-x)}\right] - eV\frac{x}{s} \qquad \text{(I-20)}$$

$eV_i|_{F_{max}}$ is found when $\frac{d(eV_i|_F)}{dx} = 0$ or

$$.508\left[\frac{s-2x}{x^2(s-x)^2}\right] - \frac{eV}{s} = 0 \; . \qquad \text{(I-21)}$$

The solution to (I-23) cannot be found for general values of s and V. Thus the problem will be solved numerically for an oxide thickness of 100 Å and compared to the solutions found for the single image problem. The values of $-eV_i|_{F_{max}}$ are plotted against F in Fig. 31. As can be seen from this figure the dependence of the potential maximum on applied electric field deviates from a straight line on a $\ln(eV_i|_{F_{max}})$ vs. ln(F) plot for fields less than about $10^5$ V/cm. At the fields where the curve is linear the dependence is not proportional to $V^{1/2}$ but to $V^{.484}$, using Simmon's multiple image approximation. Since the barrier height is $\varphi_R + eV_i|_{F_{max}}$ it can be seen that the barrier is lower for the multiple image correction than for the single image correction for all applied fields of interest.

Thus $eV_i|_{F_{max}}$ can be written as

$$eV_i|_{F_{max}} = -DV^{.484} \; . \qquad \text{(I-22)}$$

Therefore, if Richardson's equation is written

$$J = AT^2 e^{-\Phi/kT} \qquad \text{(I-23)}$$

$$\Phi = \varphi_R - DV^{.484} \quad . \qquad \text{(I-24)}$$

So the Schottky equation for a dielectric sandwiched between two metal electrodes beoomes

$$J = AT^2 \, e^{-\varphi_R/kT} \, e^{DV^{.484}/kT} \quad . \qquad \text{(I-25)}$$

Using the values obtained in this manner this equation becomes

$$J = AT^2 \, e^{-\varphi_R/kT} \, e^{.148V^{.484}/kT} \quad . \qquad \text{(I-26)}$$

# APPENDIX II

## Barrier Height as a Function of Temperature and Excess Mg Concentration

The barrier height is defined as the energy difference between the bottom of the conduction band and the Fermi level at the interface. In a bulk semiconductor this difference, in the bulk, increases for an increase in temperature for an n-type semiconductor. The location of the Fermi level as a function of temperature is found by the condition of charge neutrality in equilibrium, the total positive charge is set equal to the total negative charge. If surface states are present the charge involved with these must also be taken into account. For a device of this type however, the condition of charge neutrality must be imposed on the entire device and not just for the oxide.

Figure 42 is a schematic energy band diagram for a metal showing how the barrier changes under different conditions. Figure 42a shows the barrier presented to the flow of electrons out of the metal when the interface is a gold-vacuum interface. In these devices the MgO films deposited have an excess of Mg atoms which give rise to a donor level quite a distance from the conduction band.[88,89,90] If no surface states were present the

barrier presented to the flow of electrons from the metal, Au, to the oxide, MgO, would be $\varphi_R = \varphi_M - \chi_I$ as previously stated. The energy band diagram for this problem is shown in Fig. 42b. This picture shows that the donors near the interface must be ionized in order to get a barrier of this height. The distribution of ionized donors is schematically shown on this figure by the separation between signs. The result is a sheet of negative charge just within the metal. Thus it can be seen that to lower the barrier from $\varphi_M$ to $\varphi_M - \chi_I$ a positive charge density must be set up in the oxide. To lower the barrier even further, more positive charge must reside in the oxide and therefore more negative charge in the metal. Since all the "bulk" donors are ionized near the surface this "extra" positive charge must come from ionized donor like interface states. The energy band picture for this situation is shown in Fig. 42c. Thus a large density of donor like interface states must exist at the Au-MgO interface.

This picture is somewhat misleading since it deals with a metal-bulk oxide contact. In reality there is another metal-oxide interface very near the one pictured here. To determine what the potential energy of an electron is the oxide looks like, Poisson's equation must

be solved using the proper boundary conditions. This problem has been solved by Geppert[91] for an intrinsic oxide and he found that the depression of the potential energy profile at the mid-point between the two metal interfaces was $2.74 \times 10^{-19}$ eV using the following parameters, $\varphi_R = 1$ eV, $\epsilon_r = 9$, $s = 100$ Å and $T = 300$°K. Thus, for an intrinsic oxide the barrier is essentially flat. Roberts[92] found a potential energy depression at the mid-point between electrodes of $5 \times 10^{-13}$ eV for an n-type semiconductor with the following parameters, $N_d = 10^{16}/cm^3$, $\varphi_R = 0.7$ eV, $E_c - E_d = 1.2$ eV, $\epsilon_r = 10$, $s = 100$ Å, and $T = 300$°K. The parameters used in this problem are nearly the same as those involved in a Au-MgO-Au device and the mid-point potential energy depression is again negligible. Thus Figs. 42b and 42c would show flat bands terminating on another electrode for a device of this type.

The above analysis did not include image forces and when these are included the potential barrier will have the shape shown in Fig. 30, as calculated in Appendix I.

The charge neutrality condition for the device is a very complicated expression since it must include all charges. Since the oxide film is not a single crystal,

the energy band diagram does not strictly hold. In this case there is probably no single discrete donor level, there may be traps at various levels due to lattice inperfections which apparently do not affect the conduction mechanism, the surface states probably have a band of discrete allowed energy levels, and there may very well be acceptor levels at the interface and in the oxide. The charge neutrality condition can be written as:

$$P_t + N_d^+ + p = n + N + N_t' + N_a^- + n_t \qquad \text{(II-1)}$$

where: $P_t$ = number of unoccupied donor like surface states

$N_d^+$ = number of ionized "bulk" donors

$P$ = number of holes in the valence band

$n$ = number of electrons in the conduction band

$N$ = negative charge just inside the metal electrodes

$N_t'$ = number of filled "bulk" traps

$N_a^-$ = number of ionized donors

$n_t$ = number of occupied acceptor like surface states.

Since the Fermi level at the surface is near the conduction band and the band gap is so large, coupled with the fact that the bands are flat,[91,92] the number of holes in the

valence band and the number of ionized acceptors can be ignored if they are low lying in the forbidden gap. The acceptor like surface states can also be ignored. Thus (II-1) can be written as

$$P_t + N_d^+ = n + N + N_t' \quad . \tag{II-2}$$

If the further assumptions are made that at the temperature involved in these studies all the donor like surface states are ionized and $N = P_t$ this expression can be written as

$$N_d^+ = n + N_t' \quad . \tag{II-3}$$

Each of the terms in (II-3) are expressed by either a series or an integral. If one more assumption is made that the donors and traps have a single discrete level this becomes:

$$\frac{N_d}{2e^{\frac{E_f - E_d}{kT}} + 1} = N_c e^{(E_f - E_c)/kT} + \frac{N_t}{2e^{\frac{E_t - E_f}{kT}} + 1} \tag{II-4}$$

This expression is very simplified but is still extremely difficult to handle because there are four unknowns. If one ignores the traps a qualitative solution can be made for the barrier as a function of temperature.

This extremely simplified solution then becomes:

$$\frac{N_d}{2e^{\frac{E_f - E_d}{kT}} + 1} = N_c e^{(E_f - E_c)/kT} \tag{II-5}$$

Let

$$E_c - E_f = \varphi_R$$

$$E_f - E_d = E_c - E_d - (E_c - E_f) = \psi - \varphi_R \qquad \text{(II-6)}$$

Then the expression becomes

$$N_d/(2e^{\psi/kT} + e^{\varphi_R/kT}) = N_c/e^{2\varphi_R/kT} \qquad \text{(II-7)}$$

which can be solved for $\varphi_R$. This solution is:

$$\varphi_R = kT \ln \frac{1}{2}\left\{N_c/N_d + \left[(N_c/N_d)^2 + 8N_c e^{\psi/kT}/N_d\right]^{1/2}\right\} \qquad \text{(II-8)}$$

So it can be seen that $\varphi_R$ increases for increasing T, increases for decreasing $N_d$, and increases faster with T for smaller $N_d$.

# APPENDIX III

## Calculation of the Fringing Field, F, at a Plane Electrode, Beneath a Slot in an Opposing Plane - Parallel Electrode

The variation of field F(x) at the underlayer, which determines $j_s(x)$ as a function of position, x, under a slot of width, d, in the overlayer can be obtained approximately by the following method:* Fig. 43a shows the geometry assumed; the insulating film thickness is s with dielectric constant $\epsilon_r\epsilon_o$, the slot width is d. This problem is idealized in Fig. 43b, where an electrostatic problem is indicated in which we have assumed no dielectric discontinuity, and also that the slot is infinitely deep.

This electrostatic problem can be solved by a Schwarz-Christoffel transformation.[95,96] The z-plane representation is shown in Fig. 43b, and the transformation to the upper half of the w-plane shown in Fig. 43c is accomplished by:

$$dz/dw = K(w-a)^{1/2}(w-b)^{1/2}/w(w-1). \qquad \text{(III-1)}$$

---

*Note that in this appendix x is taken as the distance from the slot edge, while in the text it is the coordinate perpendicular to the overlayer plane.

To find the value of K and the relationship between a and b one must integrate in the complex plane. In these expressions $z = x+jy$ and $w = u+jv$.

$$\int_D^C dz = \int_D^C \frac{dz}{dw}\, dw \qquad \text{(III-2)}$$

In the z plane, $\int_D^C dz = js$, while in the w plane this integral can be taken along a semi-circle of very large radius, such that $w = Re^{j\theta}$, $dw = jRe^{j\theta}d\theta$, and $|Re^{j\theta}| = R \gg a$, $R \gg b$, and $R \gg 1$, then:

$$js \simeq \int_o^\pi K \frac{(Re^{j\theta})^{1/2}(Re^{j\theta})^{1/2}}{Re^{j\theta}Re^{j\theta}}\, jRe^{j\theta}d\theta$$

$$= \int_o^\pi jKd\theta = j\pi K \,. \qquad \text{(III-3)}$$

Therefore

$$K = s/\pi \,. \qquad \text{(III-4)}$$

Another integration that can be made is

$$\int_A^B dz = \int_A^B \frac{dz}{dw}\, dw \,. \qquad \text{(III-5)}$$

In this case $\int_A^B dz = js$, and now integrate along a small semi-circle in the w-plane such that $w = re^{j\theta}$, where $|re^{j\theta}| = r \ll a$, $r \ll 1$, $r \ll b$ so that

$$js \simeq \int_o^\pi K \frac{(ab)^{1/2}}{re^{j\theta}(-1)}\, jre^{j\theta}d\theta = -j\frac{s}{\pi}(ab)^{1/2}\pi \,. \qquad \text{(III-6)}$$

Therefore $ab = 1$. Thus (III-1) can be written as

$$dz/dw = (s/\pi)(w-a)^{1/2}(w-b)^{1/2}/w(w-1) \quad , \qquad \text{(III-7)}$$

which cannot be integrated easily. The substitution

$$p^2 = (w-b)/(w-a) \qquad \text{(III-8)}$$

yields:

$$z = \frac{2s}{\pi} \int \frac{(b-a)^2 p^2 dp}{a(1-a)(p^2-1)(p^2-b^2)(b+p^2)} \quad . \qquad \text{(III-9)}$$

Letting $a = \frac{1}{b}$ results in

$$z = \frac{2s}{\pi} \int \frac{(b+1)^2 (b-1) p^2 dp}{(1-p^2)(b^2-p^2)(b+p^2)} \qquad \text{(III-10)}$$

or

$$z = \frac{2s}{\pi}\left[ \int \frac{dp}{1-p^2} - \int \frac{b\,dp}{b^2-p^2} - \int \frac{(b-1)\,dp}{b+p^2} \right] \quad . \qquad \text{(III-11)}$$

Integration yields

$$z = \frac{s}{\pi}\left\{ \ln\left|\frac{1+p}{1-p}\right| - \ln\left|\frac{b+p}{b-p}\right| - \frac{2(b-1)}{\sqrt{b}} \tan^{-1}\left(\frac{p}{\sqrt{b}}\right) \right\} . \qquad \text{(III-12)}$$

The constants of integration have been set equal to zero and this fixes the origin of the z-plane. It is noted that when $p = 0$, $w = b$, and $z = 0$, this information is shown in Fig. 43b and c. As $w \to a$, $z \to -d$, but $p \to \infty$ so $z \to -s(b-1)/\sqrt{b}$ . Therefore

$$d/s = (b-1)/\sqrt{b} \quad . \qquad \text{(III-13)}$$

The transformation from the w-plane to the $\chi$-plane where the field is uniform is given[97] by

$$\chi = \frac{V_o}{\pi} \log w \quad . \qquad \text{(III-14)}$$

The field strength, F, is given by

$$F = \left|\frac{d\chi}{dz}\right| = \left|\frac{d\chi}{dw}\frac{dw}{dz}\right| , \qquad \text{(III-15)}$$

thus

$$F = \left(\frac{V_o}{s}\right)\frac{w-1}{(w-a)^{1/2}(w-b)^{1/2}} . \qquad \text{(III-16)}$$

Now as $w \to o$, $z \to -\infty$, and $F \to V_o/s$ as it should, therefore we write

$$F = F_o \frac{w-1}{(w-a)^{1/2}(w-b)^{1/2}} . \qquad \text{(III-17)}$$

For negative real w this gives the field at the underlayer and the calculations need only to be made for $-1 \leq w \leq 0$. At $w = -1$, $z = -d/2 + js$, and from symmetry the field will be the same on either side of the point on the underlayer beneath the center of the slot. A numerical calculation of $F(z)$ at $z = x+js$ for $x \leq -d/2$ can be made choosing $-1 \leq w \leq 0$, evaluating $F/F_o$ from (III-17) and finding x from

$$x/s = \mathrm{Re}\left\{\frac{1}{\pi}\left[\ln\left(\frac{1+p}{1-p}\right) - \ln\left(\frac{b+p}{b-p}\right) - \frac{2(b-1)}{\sqrt{b}}\tan^{-1}\left(\frac{p}{\sqrt{b}}\right)\right]\right\} \qquad \text{(III-18)}$$

where $p^2$ is given in (III-8).

It will be assumed that d = 100 Å and the appropriate values for d/s for these devices will then be; 1.67, 1.28, 1.12, .92, and .63.

The calculations for the field strength at the underlayer metal beneath the slot in the overlayer were carried out numerically and the results are shown plotted as $F/F_o$ vs. distance from one edge of the slot in Fig. 45.

## BIBLIOGRAPHY


1. C. A. Mead, "The Tunnel-Emission Amplifier," Proc. IRE 48, 359 (1960).
2. C. A. Mead, "Operation of Tunnel-Emission Devices," J. Appl. Phys. 32, 646 (1961).
3. D. V. Geppert, "Internal Field Emission and Low Temperature Thermionic Emission into Vacuum," Proc. IRE 48, 9, 1644 (1960).
4. N. F. Mott and R. W. Gurney, Electronic Processes in Ionic Crystals, Oxford Clarendon Press (Oxford), 1940.
5. P. R. Emtage and W. Tantraporn, "Schottky Emission through Thin Insulating Films," Phys. Rev. Letters 8, 267 (1962).
6. S. R. Pollack, "Schottky Field Emission through Insulating Layers," J. Appl. Phys. 34, 877 (1963).
7. R. H. Fowler and L. Nordheim, "Electron Emission in Intense Electric Fields," Proc. Roy. Soc. (London) A199, 173 (1928).
8. P. S. Schnupp, "Kronig-Penny-Type Calculations for Electron Tunneling through Thin Dielectric Films," Phys. Stat. Sol. 21, 567 (1967).
9. T. E. Hartman, "Tunnelling of a Wave Packet," J. Appl. Phys. 33, 3427 (1962).

10. R. Stratton, "Voltage-Current Characteristics for Tunnelling through Insulating Films," J. Phys. Chem. Solids 23, 1177 (1962).

11. J. G. Simmons, "Generalized Formula for the Electric Tunnel Effect between Similar Electrodes Separated by a Thin Insulating Film," J. Appl. Phys. 34, 1793 (1963).

12. E. D. Savoye and D. E. Anderson, "Injection and Emission of Hot Electrons in Thin-Film Tunnel Emitters," J. Appl. Phys. 38, 3245 (1967).

13. W. Tantraporn, "Electron Current through Metal-Insulator-Metal Sandwiches," Solid State Elect. 7, 81 (1964).

14. J. Frenkel, "On Pre-Breakdown Phenomena in Insulators and Electronic Semiconductors," Phys. Rev. 54, 647 (1938).

15. A. K. Jonscher, "Electronic Properties of Amorphous Dielectric Films," Thin Solid Films 1, 213-234 (1967), Elsevier, Amsterdam.

16. M. A. Lampert, "Injection Currents in Insulators," Proc. IRE 50, 1781 (1962).

17. M. A. Lampert and F. Edelman, "Theory of One-Carrier Space-Charge-Limited Currents Including Diffusion and Trapping," J. Appl. Phys. 35, 2971 (1964).

18. J. Lindmayer, J. Reynold, and C. Wrigley, "One Carrier Space-Charge-Limited Currents in Solids," J. Appl. Phys. 34, 809 (1963).

19. J. Cohen, "Tunnel Emission into Vacuum," J. Appl. Phys. 33, 1999 (1962).

20. C. A. Mead, "Transport of Hot Electrons in Thin Gold Films," Phys. Rev. Letters 8, 56 (1962). Erratum, Phys. Rev. Letters 9, 46 (1962).

21. H. Kanter and W. A. Feibelman, "Electron Emission from Thin Al-$Al_2O_3$-Au Structures," J. Appl. Phys. 33, 3580 (1962).

22. R. E. Collins and L. W. Davis, "Electron Distribution of Hot Electrons in Al," Appl. Phys. Letters 2, 213 (1963), and "The Transport of Hot Electrons in Al-$Al_2O_3$-Al Tunnel Cathodes," Solid State Elect. 7, 445 (1964).

23. J. G. Simmons, "Intrinsic Fields in Thin Insulating Films between Dissimilar Electrodes," Phys. Rev. Letters 10, 10 (1963).

24. R. Holm, "The Electric Tunnel Effect Across Thin Insulator Films in Contacts," J. Appl. Phys. 22, 569 (1951).

25. T. Hartman, "Tunnelling through Asymmetric Barriers," J. Appl. Phys. 35, 3283 (1964).

26. O. L. Nelson and D. E. Anderson, "Potential Barrier Parameters in Thin-Film Al-$Al_2O_3$-Metal Diodes," J. Appl. Phys. 37, 77 (1966).

27. O. L. Nelson, Studies of Potential Barrier Parameters in Thin-Film Metal-Oxide-Metal Devices, Ph.D. Thesis, University of Minnesota, 1965.

28. J. L. Miles and P. H. Smith, "The Formation of Metal Oxide Films Using Gaseous and Solid Electrolytes," J. Electrochem. Soc. 110, 1240 (1963).

29. M. Scharfe, The Gaseous Anodization of Tantalum, M.S.E.E. Thesis, University of Minnesota, 1966.

30. G. S. Anderson, W. N. Meyer, and G. K. Wehner, "Sputtering of Dielectrics by High-Frequency Fields," J. Appl. Phys. 33, 2991 (1962).

31. P. D. Davidse and L. I. Maissel, "Dielectric Thin Films through R.F. Sputtering," J. Appl. Phys. 37, 574 (1966).

32. L. Holland, Vacuum Deposition of Thin Films, John Wiley and Sons, Inc., New York, 1956.

33. H. M. O'Bryan, "Evaporation Technique for Highly Refractory Substances," Rev. Sci. Instr. 5, 125 (1934).

34. L. A. Harris, "Structural Effects in Thin-Film Sandwich Emitters," J. Appl. Phys. 35, 268 (1964).

35. M. McColl and C. A. Mead, "Electron Current Through Thin Mica Films," Trans. Metall. Soc. AIME 233, 502 (1965).

36. D. W. Pashley, "Epitaxy in Thin Surface Films," Metall. Adv. Elect. Mat. 19, 175-207 (1962).

37. C. Davisson and L. H. Germer, "Diffraction of Electrons by a Crystal of Nickel," Phys. Rev. 30, 705-740 (1927).

38. D. E. Anderson, A. B. Laponsky, and W. T. Peria, Research in Physics of Electron Emission and Electron Tube Technology, Third Interim Report, Contract No. AF 33(657)-10475, University of Minnesota, Minneapolis, Minnesota, October 16, 1963 to April 15, 1964.

39. T. J. Szczech, Ph.D. Thesis, University of Minnesota, 1966.

40. T. Tom and C. F. Brothers, "The Role of Sublimation Pumping in Conjunction with Ion Pumping," Northern California Vacuum Society Meeting, October 1965.

41. L. D. Hall, "Electronic Ultra-high Vacuum Pump," Rev. Sci. Instr. 29, 367 (1958).

42. W. M. Brubaker, "A Method for Greatly Enhancing the Pumping Action of a Penning Discharge," Trans. 6th. Nat. Vac. Symp., 1959, 302, Pergamon Press, London, 1960.

43. R. Riesz and G. H. Dieke, "The Analysis and Purification of Rare Gases by Means of Electric Discharges," J. Appl. Phys. 25, 196 (1954).

44. K. H. Behrndt and R. W. Love, "Control of Deposition Rate and Film Thickness with the Crystal Oscillator," Vacuum Symposium Trans. 87, 1960.

45. S. J. Lins and H. S. Kukuk, "Resonance Frequency Shift Thin-Film Thickness Monitor," Vacuum Symposium Trans. 333, 1960.

46. D. E. Anderson, Studies of Thin Film Hard Superconductors, Report No. 2, Contract No. DA-44-009-AMC-812(T) University of Minnesota, Minneapolis, Minnesota, October 26, 1965-October 25, 1966.

47. P. W. Palmberg, D. C. Johnson, and H. J. Boll, "Construction of Hemispherical Grids," Rev. Sci. Instr. 35, 244 (1964).

48. P. W. Palmberg, North American Rockwell Science Center, Thousand Oaks, California, Private Communicatio

49. F. Kloss and L. Herte, "Advances in RF-Induced Plasma Sputtering," SCP and Solid State Tech., 45 (1967).

50. First International Conference on Electron and Ion Beam Science and Technology, John Wiley and Sons, Inc., 1965.

51. R. T. Bayard and D. Alpert, "Extension of the Low Pressure Range of the Ionization Gauge," Rev. Sci. Instr. 21, 571 (1950).

52. F. L. Schuermeyer and J. A. Crawford, "Interpretation of Low Voltage Photomeasurements in Metal-Insulator-Metal Films," Appl. Phys. Letters 9, 317 (1966).

53. R. E. Weber, Work Function and Structural Studies for Alkali-Covered Semiconductors, Tech. Report AFAL-TR-67-355, University of Minnesota, Minneapolis, Minnesota, February 1968.

54. W. R. Miller, Jr. and N. N. Axelrod, "Modified Faraday Cage," Rev. Sci. Instr. 37, 1096 (1966).

55. E. D. Savoye, Extraction and Injection of Hot Electrons in Thin Film Emission Diodes, Ph.D. Thesis, University of Minnesota, 1966.

56. J. J. O'Dwyer, "Dielectric Breakdown in Solids," Phil. Mag. Suppl. 1 (Adv. in Phys.) 1, 349 (1958).

57. W. W. Dolan and W. P. Dyke, "Temperature-and-Field Emission of Electrons from Metals," Phys. Rev. 95, 327 (1954).

58. R. H. Good, Jr. and E. W. Müller, "Field Emission," Encyclopedia of Physics 21, 176-231 (1956).

59. T. B. Linnerooth, Alkali Ion Doping of the Metal-Oxide Interface, M.S. Thesis, University of Minnesota, 1965.

60. J. C. Kemp and V. I. Neeley, "Wave Functions for F Centers in MgO," Phys. Rev. 132, 215 (1963).

61. A. van der Ziel, Solid State Physical Electronics, Second Edition, Prentice Hall, Englewood Cliffs, New Jersey, 1968, p. 149.

62. T. E. Hartman, J. C. Blair, and R. Bauer, "Electrical Conduction through SiO Films," J. Appl. Phys. 37, 2468 (1966).

63. C. A. Mead, "Electron Transport Mechanisms in Thin Insulating Films," Phys. Rev. 128, 2088 (1962).

64. J. J. O'Dwyer, "Current-Voltage Characteristics of Dielectric Films," J. Appl. Phys. 37, 599 (1966). "Electric Current in Thin Dielectric Films," Bull. Am. Phys. Soc. 10, 389 (1965).

65. H. Frolich, "On the Theory of Dielectric Breakdown in Solids," Proc. Roy. Soc. (London) A188, 521 (1947).

66. S. R. Pollack and C. E. Morris, "Electron Tunnelling through Asymmetric Films of Thermally Grown $Al_2O_3$," J. Appl. Phys. 35, 1503 (1964).

67. D. A. Lavrinets, Electron Scattering in $Ta_2O_5$ Thin Films, M.S.E.E. Thesis, University of Minnesota, 1969.

68. E. Pittrelli, "Tunnel Emission into an Insulating Film with Traps," Solid-State Electr. 6, 667 (1963).

69. D. Meyerhofer and S. A. Ochs, "Current Flow in Very Thin Films of $Al_2O_3$ and BeO," J. Appl. Phys. 34, 2535 (1963).

70. H. Kanter, "Slow Electron Transfer through Evaporated Au Films," J. Appl. Phys. 34, 3629 (1963).

71. I. W. Hickmott, "Anomalous Transmission of Low-energy Electrons through Thin Metal Films," J. Appl. Phys. 34, 1569 (1963).

72. S. M. Sze, J. L. Moll, and T. Sugano, "Range-Energy Relation of Hot Electrons in Gold," Solid State Electronics 7, 509 (1964).

73. J. J. Quinn, "The Range of Hot Electrons and Holes in Metals," Appl. Phys. Letters 2, 167 (1963).

74. K. Motizuki and M. Sparks, "Range of Excited Electrons and Holes in Metals and Semiconductors," J. Phys. Soc. Japan 19, 486 (1964).

75. A. J. Dekker, Solid State Physics, Prentice Hall, Inc., Englewood Cliffs, New Jersey, 1957, Chapter 11.

76. G. B. Thomas, Jr., Calculus and Analytic Geometry, Addison-Wesley Publishing Company, Inc., Reading, Massachusetts, 1953, p. 614.

77. E. Hille, Analytic Function Theory, Ginn and Company, 1959, Vol. I, p. 197.

78. A. E. Taylor, Advanced Calculus, Ginn and Gompany, 1955, p. 562.

79. A. A. Holscher, "A Field Emission Retarding Potential Method for Measuring Work Functions," Surface Science 4 (1966).

80. A. Many, Y. Goldstein, and N. B. Grover, Semiconductor Surfaces, John Wiley and Sons, Inc., New York, 1965, p. 138.

81. W. E. Meyerhof, "Contact Potential Differences in Silicon Crystal Rectifiers," Phys. Rev. 71, 727 (1947).

82. W. G. Spitzer and C. A. Mead, "Barrier Height Studies on Metal-Semiconductor Systems," J. Appl. Phys. 34, 3061 (1963).

83. C. A. Mead, "Surface States on Semiconductor Crystals; Barriers on the Cd (Se:S) System," Appl. Phys. Letters 6, 103 (1965).

84. C. A. Mead, "Metal-Semiconductor Surface Barriers," Solid-State Elect. 9, 1023 (1966).

85. W. Shockley, "On the Surface States Associated with a Periodic Potential," Phys. Rev. 56, 317 (1939).

86. L. Pauling, The Nature of the Chemical Bond, Cornell University Press, Ithaca, New York, 1960.

87. J. Bardeen, "Surface States and Rectification at a Metal Semiconductor Contact," Phys. Rev. 71, 717 (1947).

88. E. Yamaka and K. Sawamoto, "Photoinduced Hall Effect in MgO," Phys. Rev. 101, 565 (1956).

89. E. Olson, Radiation Induced Electrical Phenomenon in the Alkaline Earth Oxides, Ph.D. Thesis, University of Minnesota, 1969.

90. E. Yamaka and K. Sawamoto, "Electrical Conductivity and Thermo-electric Motive Force in MgO Single Crystals," J. Phys. Soc. Japan 10, 176 (1955).

91. D. V. Geppert, "Theoretical Shape of Metal-Insulator-Metal Potential Barriers," J. Appl. Phys. 34, 490 (1963).

92. G. G. Roberts, "Equilibrium Space Charge Distribution in Semiconductors," Brit. J. Appl. Phys. 18, 749 (1967).

93. K. L. Chopra, L. C. Bobb, and M. H. Francombe, "Electrical Resistivity of Thin Single-Crystal Gold Films," J. Appl. Phys. 34, 1699 (1963).

94. C. A. Neugebauer, Physics of Thin Films, Ed. by G. Hass and R. E. Thun, Academic Press, New York and London, 1964.

95. R. V. Churchill, Complex Variables and Applications, McGraw-Hill Book Company, Inc., New York, Toronto, and London, 1960.

96. S. Ramo and J. R. Whinnery, Fields and Waves in Modern Radio, Second Edition, John Wiley and Sons, Inc., New York and London, 1953.

97. W. J. Gibbs, Conformal Transformations in Electrical Engineering, Chapman and Hall, Ltd., London, 1958.

98. W. S. Khokley and K. M. van Vliet, "Escape Mechanism of Secondary Electrons in Polar Crystals," Phys. Rev. 128, 1123 (1962).

99. A. J. Dekker, Solid State Physics, Prentice Hall, Inc., Engelwood Cliffs, New Jersey, 1957, Chapter 13.

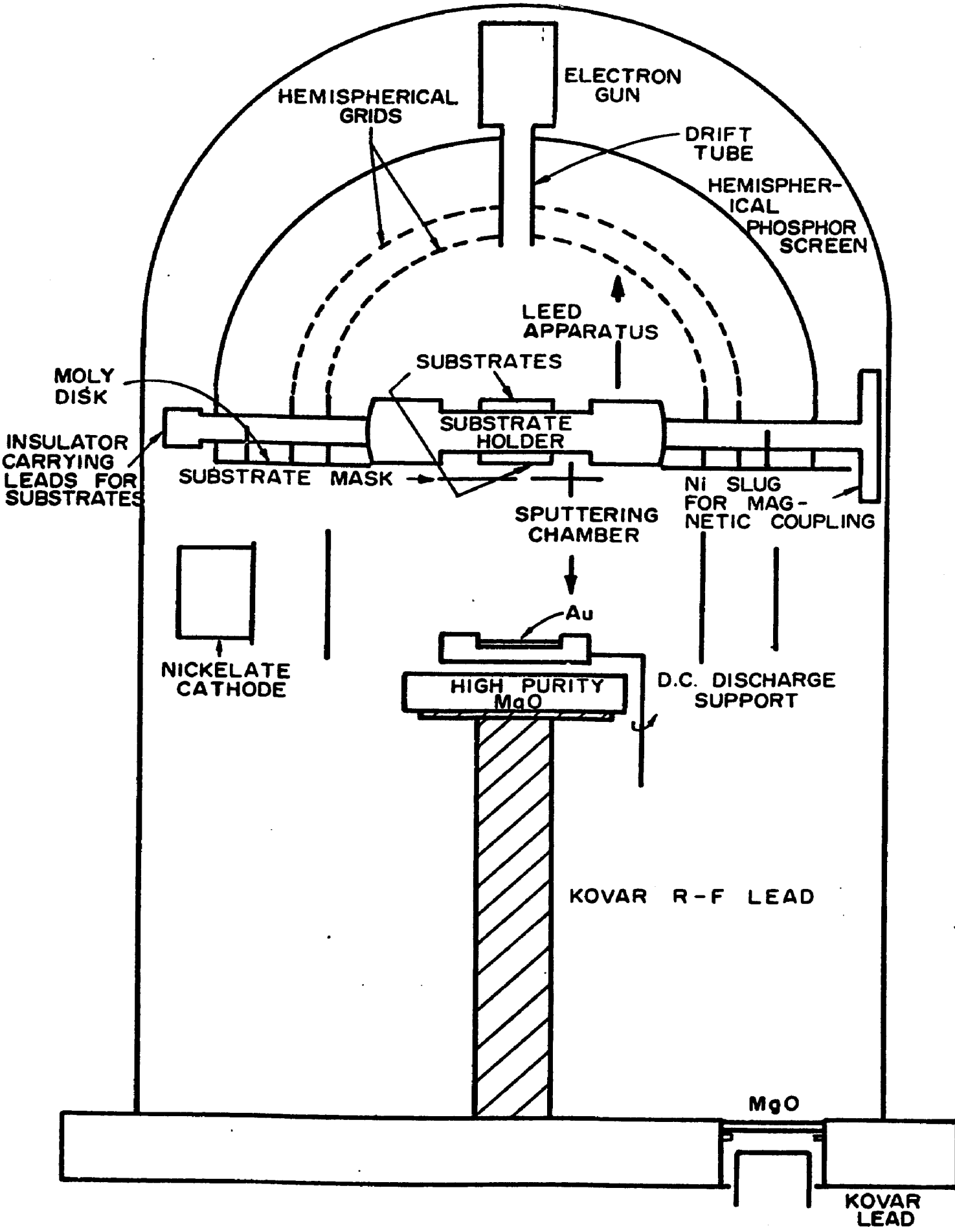
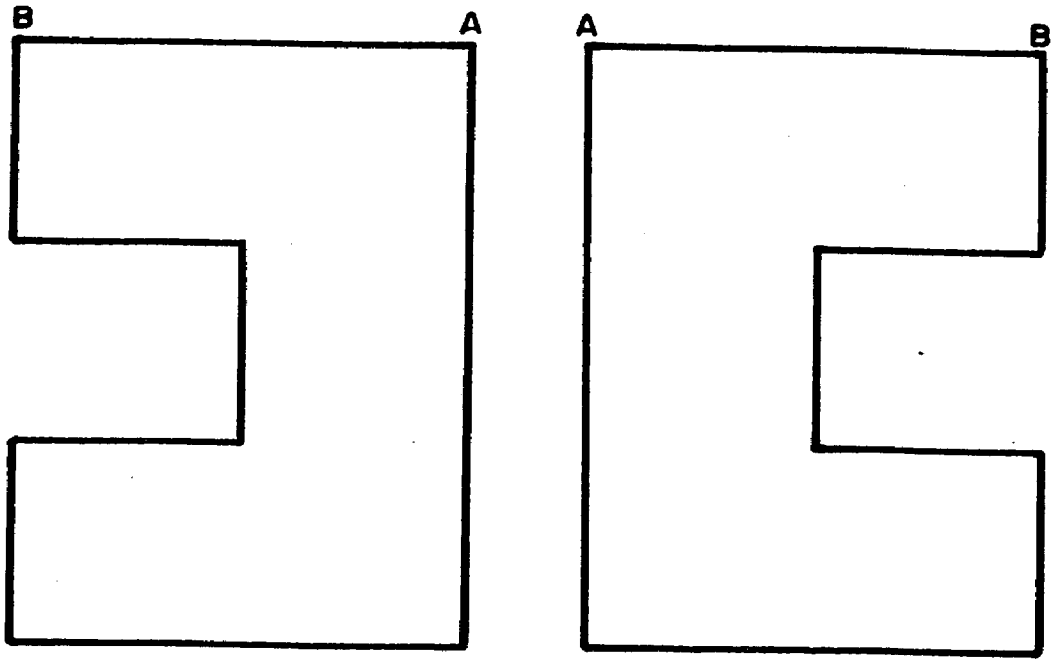
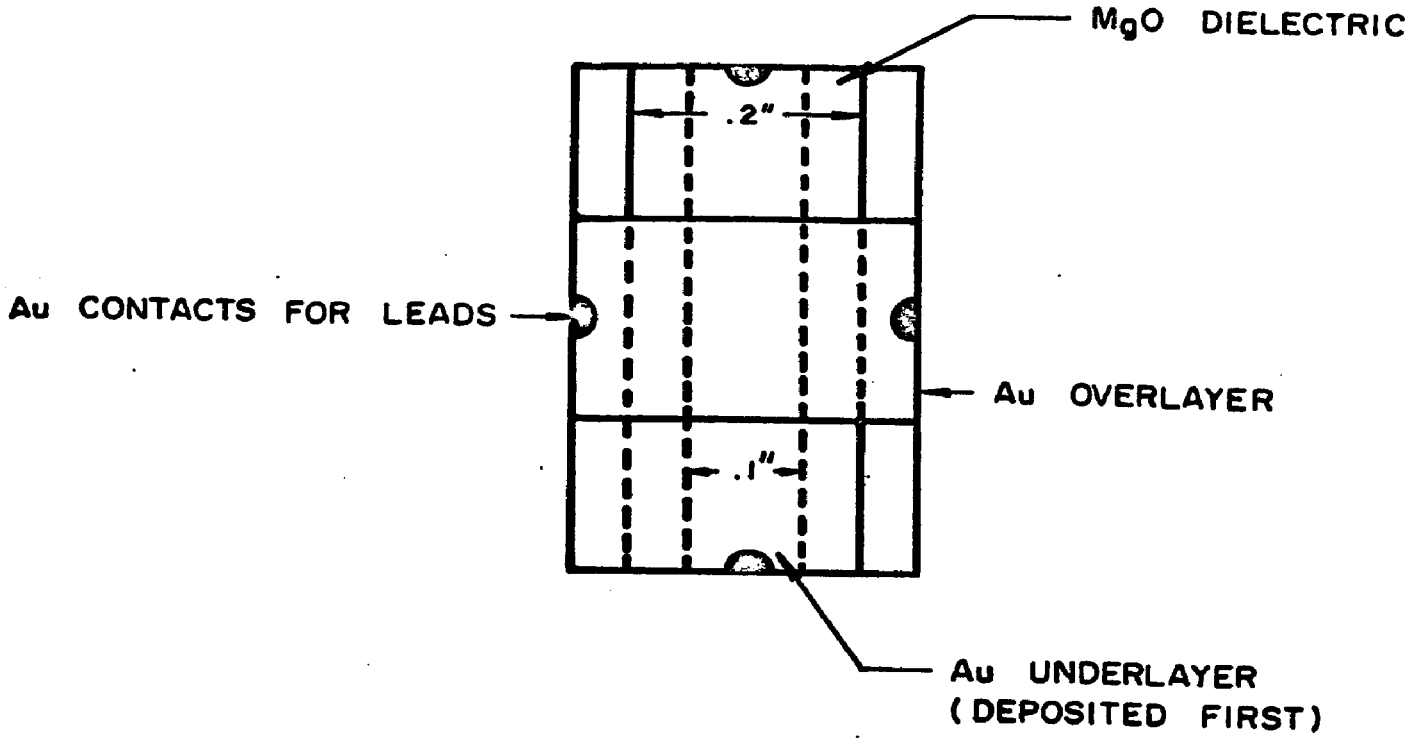



Figure 1. Schematic Representation of Initial Vacuum System Used for Depositing Ordered Au-MgO-Au Emission Diodes




2a. Substrate Masks




2b. Substrate with Au-MgO-Au Thin-Film Diode

Figure 2

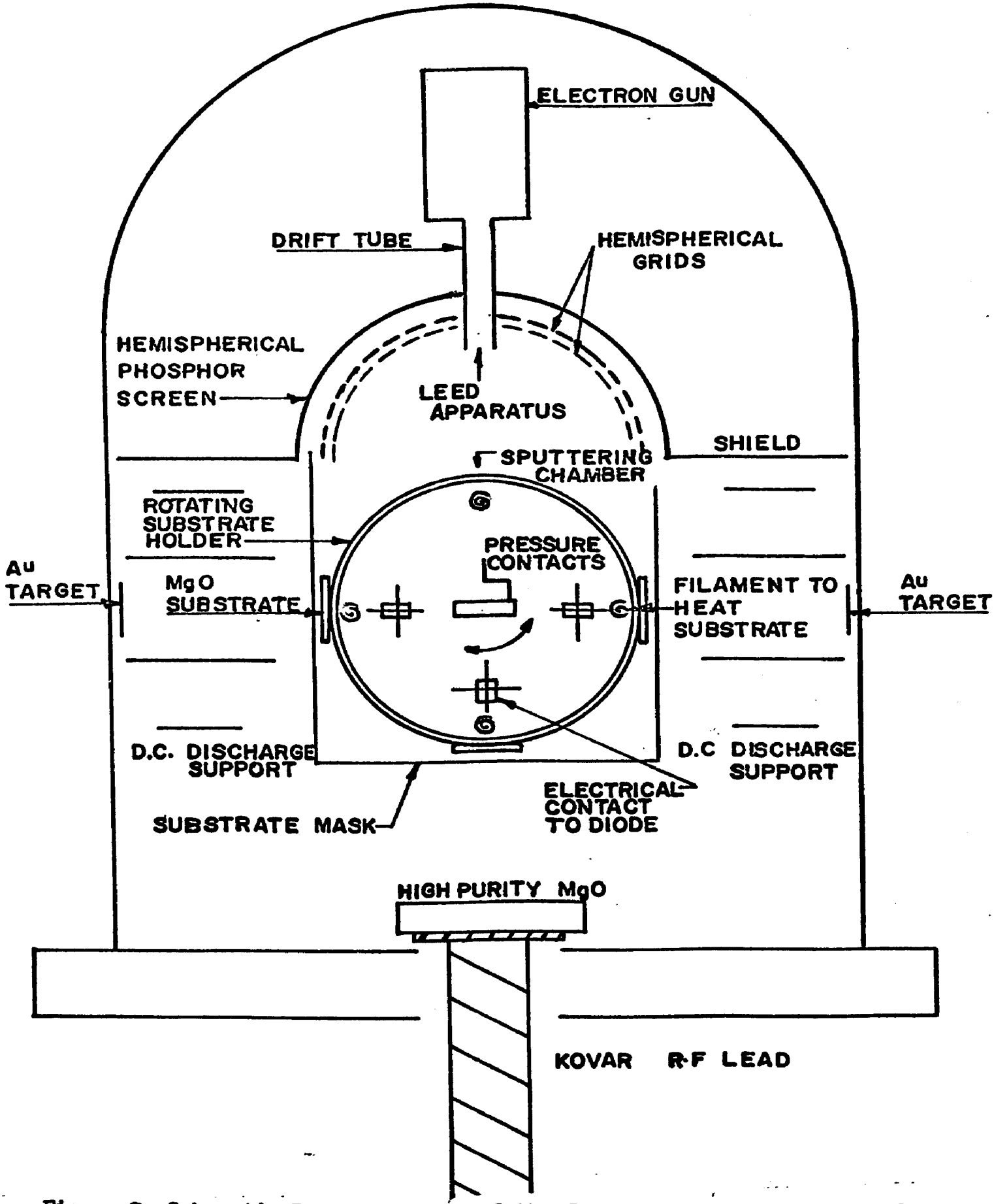



Figure 3. Schematic Representation of the Second Vacuum System Used for Depositing Ordered Au-MgO-Au Emission Diodes

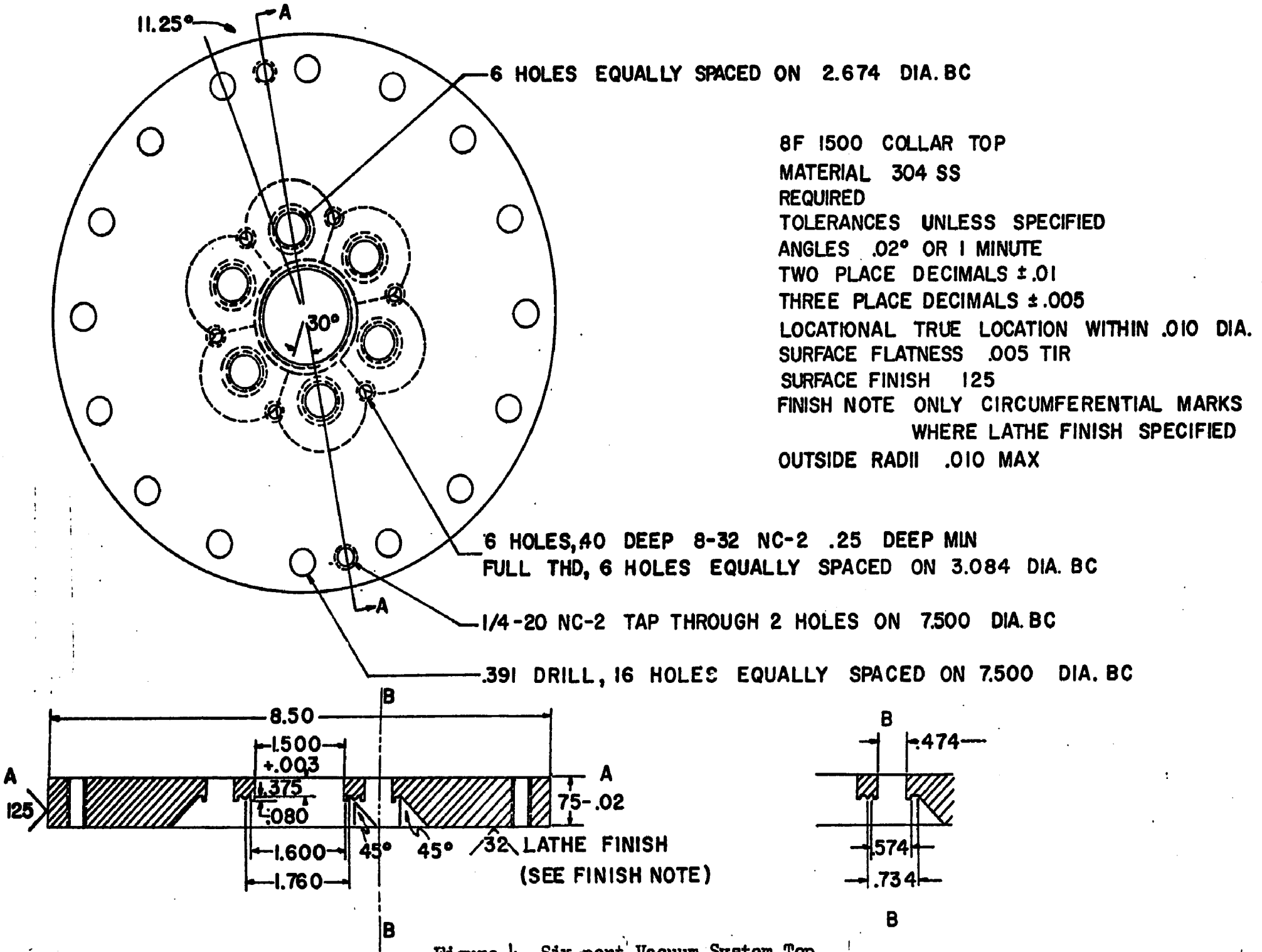



Figure 4. Six-port Vacuum System Top

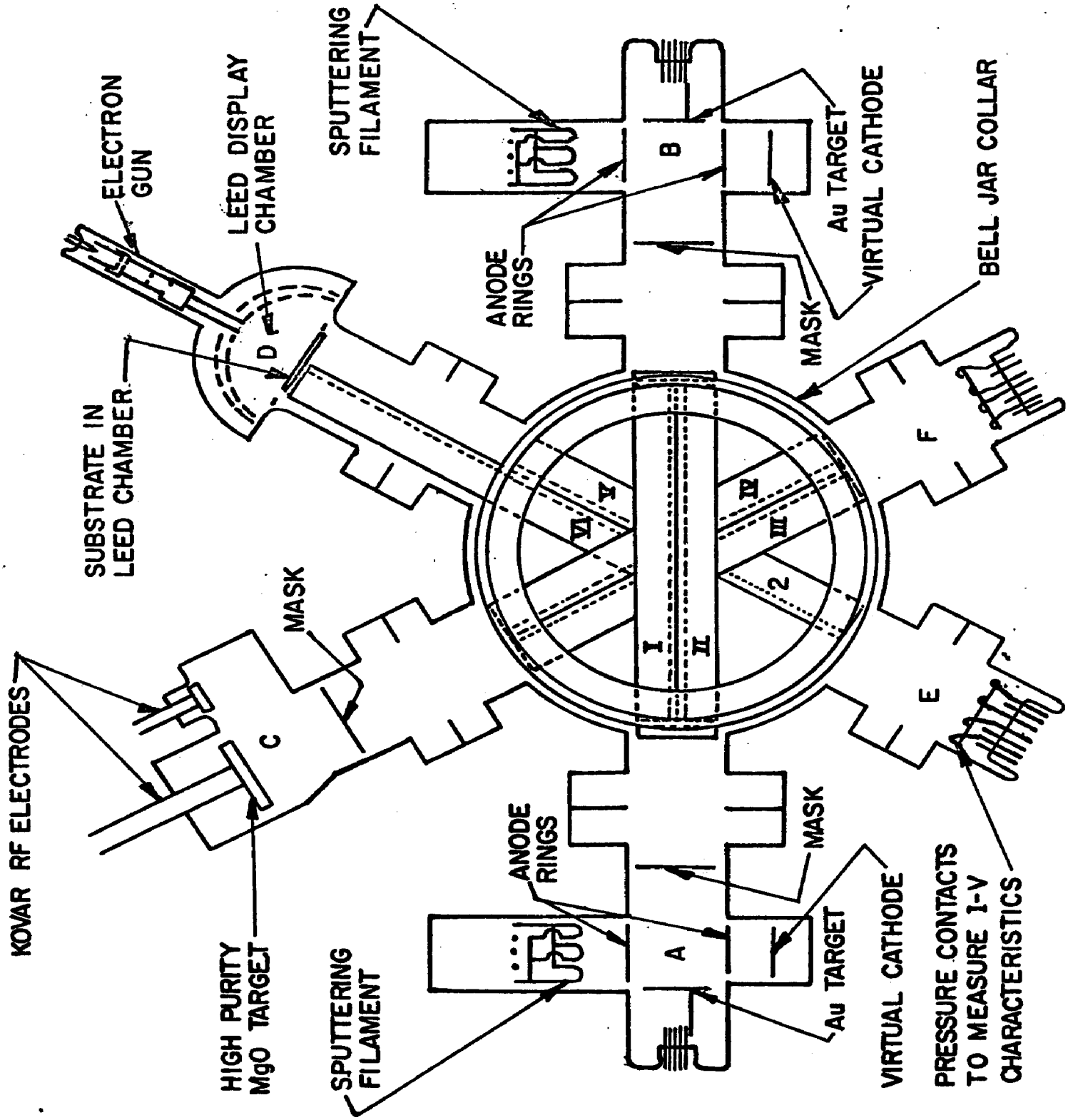



Figure 5. Schematic View of Six-port Vacuum System

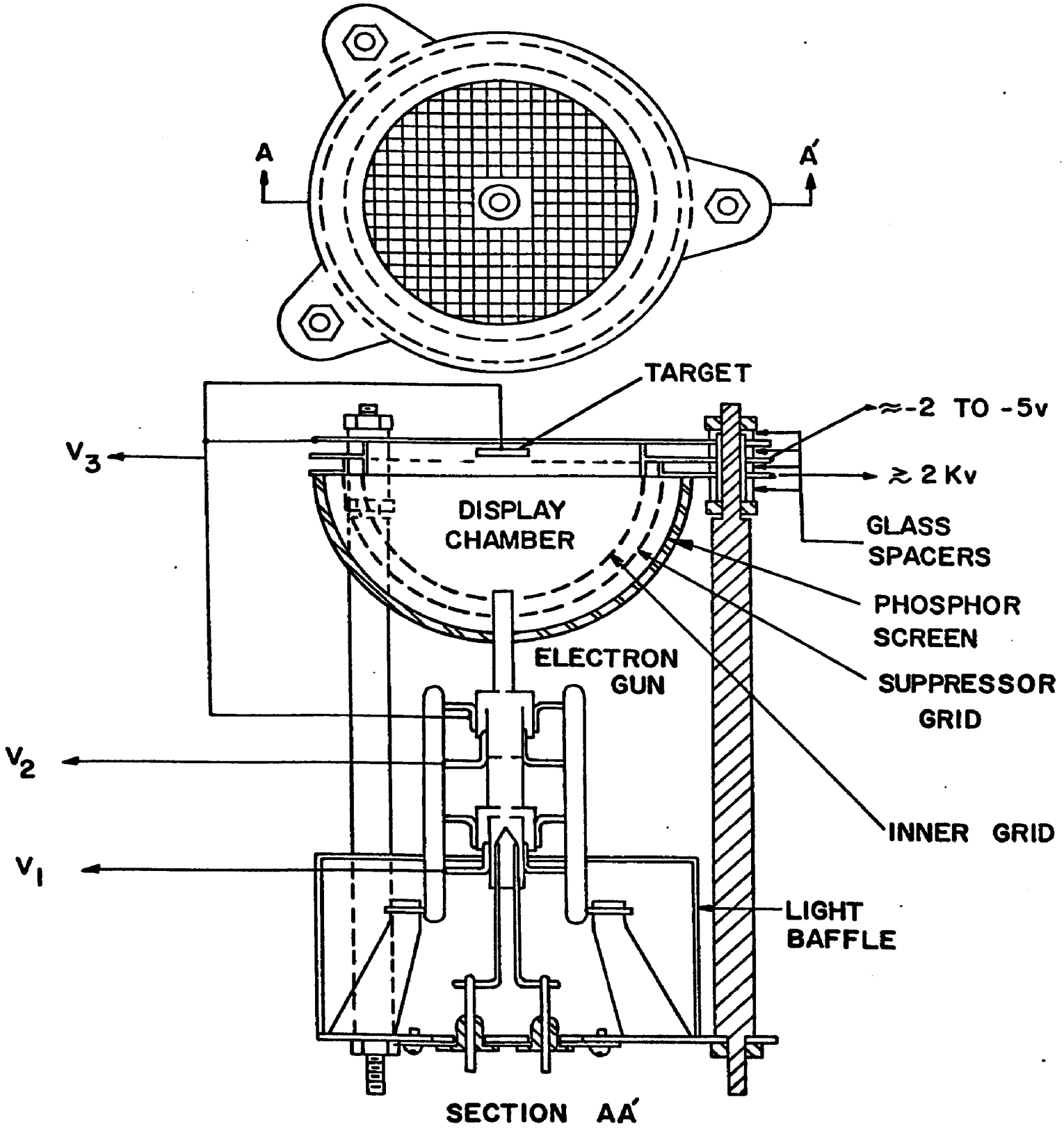



Figure 6. Detail of LEED Unit

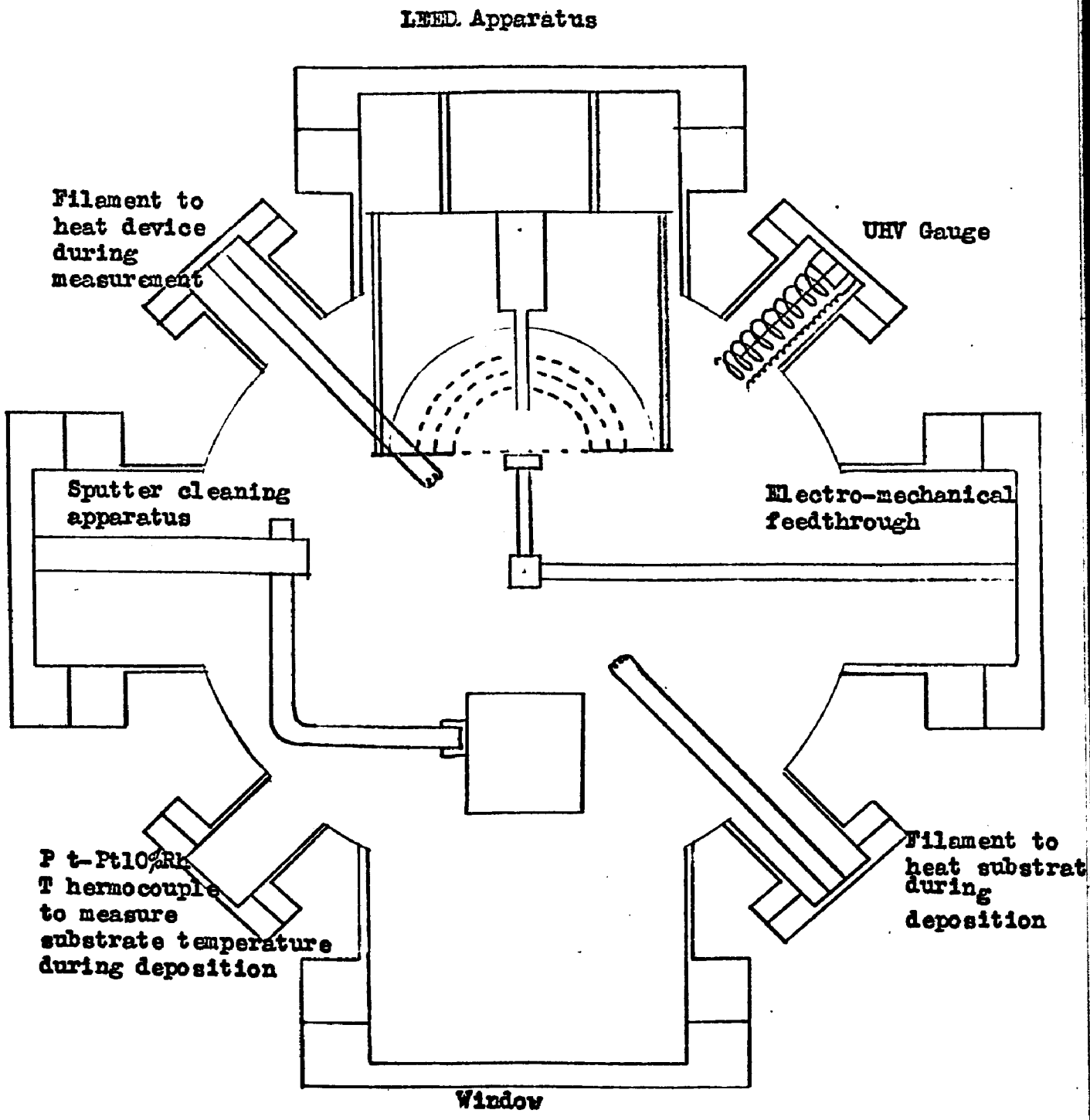
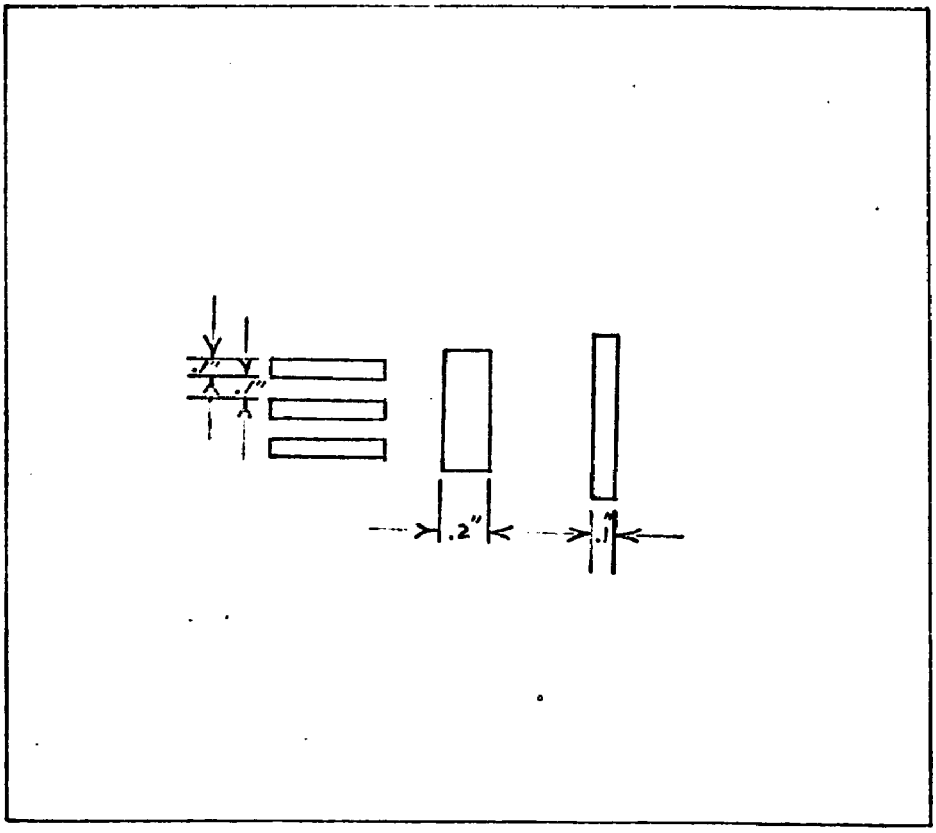
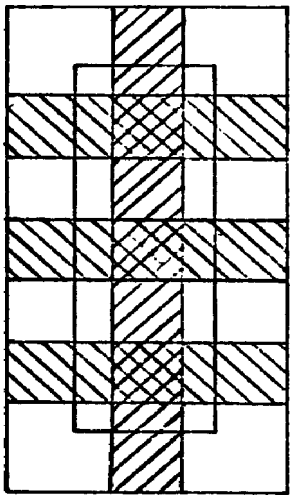



Figure7. Schematic Representation of Bell-jar Section of Final Vacuum System




8a. Mask for Final Vacuum System



8b. Substrate with 3 Metal-Insulator-Metal Emission Diodes

Figure8

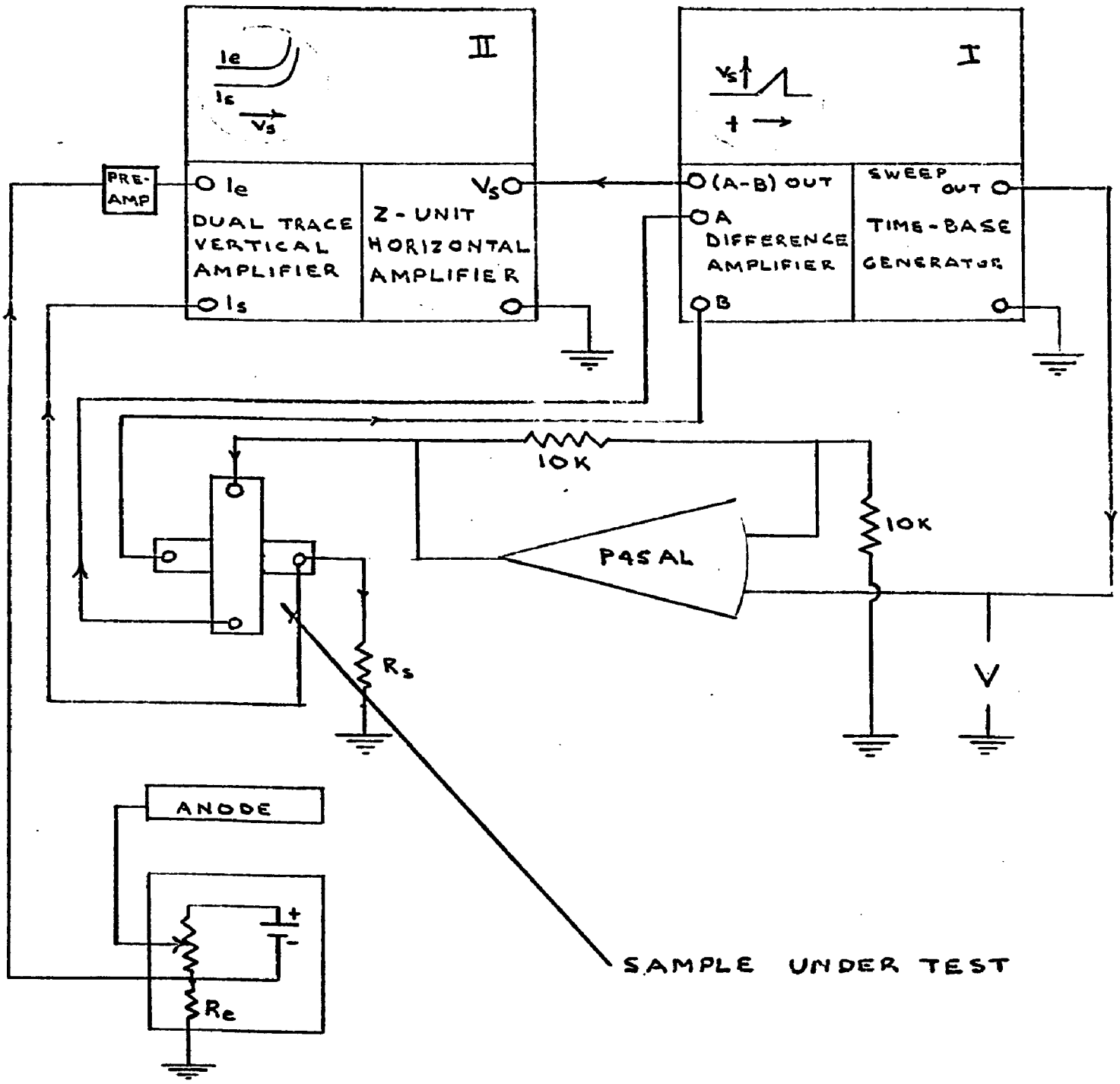


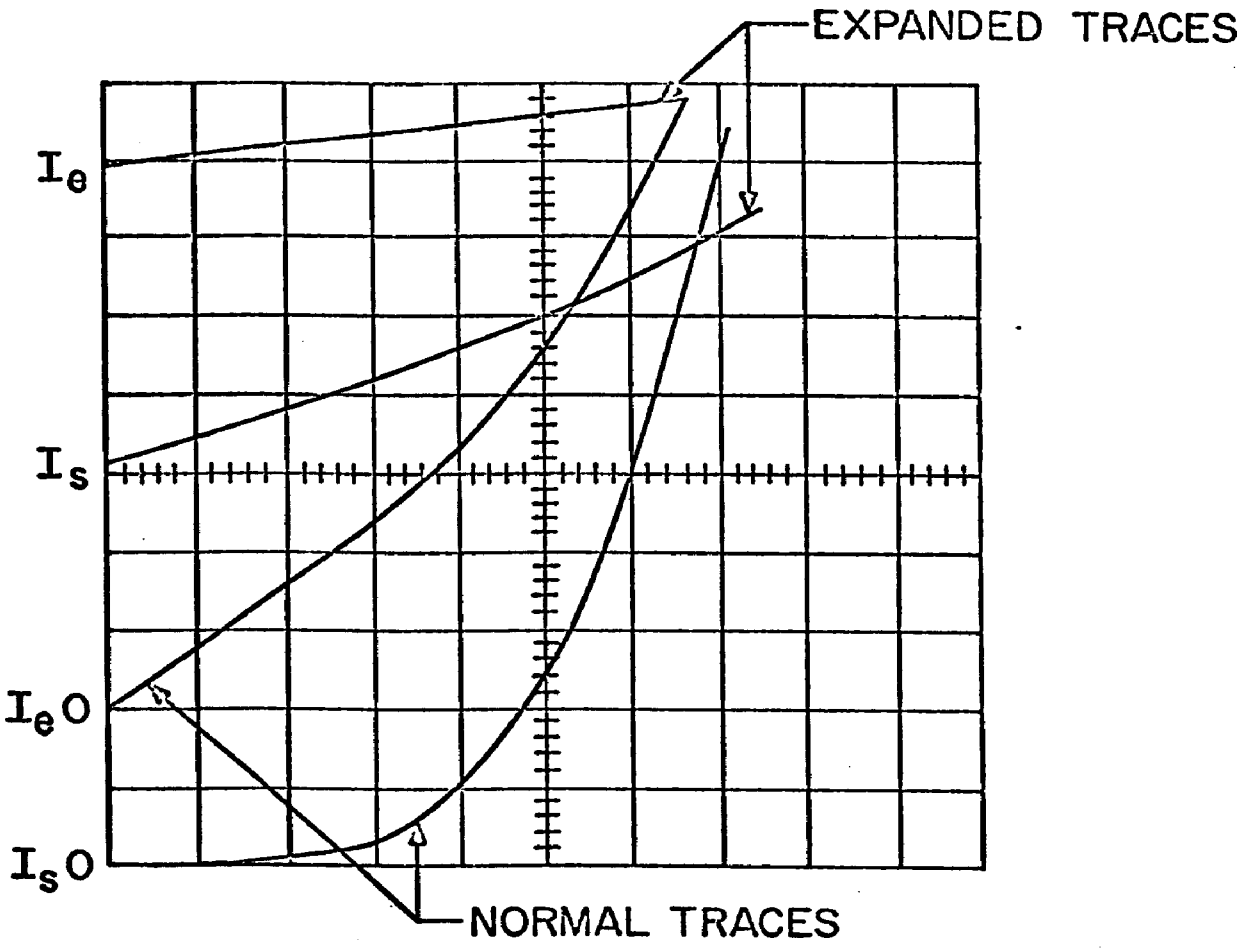

Figure 9. Circuit Used for Millisecond-Pulse Measurements of Thin-Film Hot Electron Emission Diodes

$I_s$ AND $I_e$ vs. $V_s$ FOR Au - MgO - Au

SAMPLE NO. PY-G-17

OVERLAYER NO. 1, 310° K

10 MILLISECOND PULSE




SCALES:

VERTICAL: $I_s$: 1 m A / DIVISION

$I_e$: $10^{-8}$ A / DIVISION

HORIZONTAL: $V_s$: 1.0 V / DIVISION

$V_s$: EXPANDED 0.1 VOLTS/DIVISION

ZERO SUPPRESSED 6.0 VOLTS

Figure 10. Results of Millisecond-Pulse Measurement Technique, Showing I-V Characteristics and Expanded Traces.

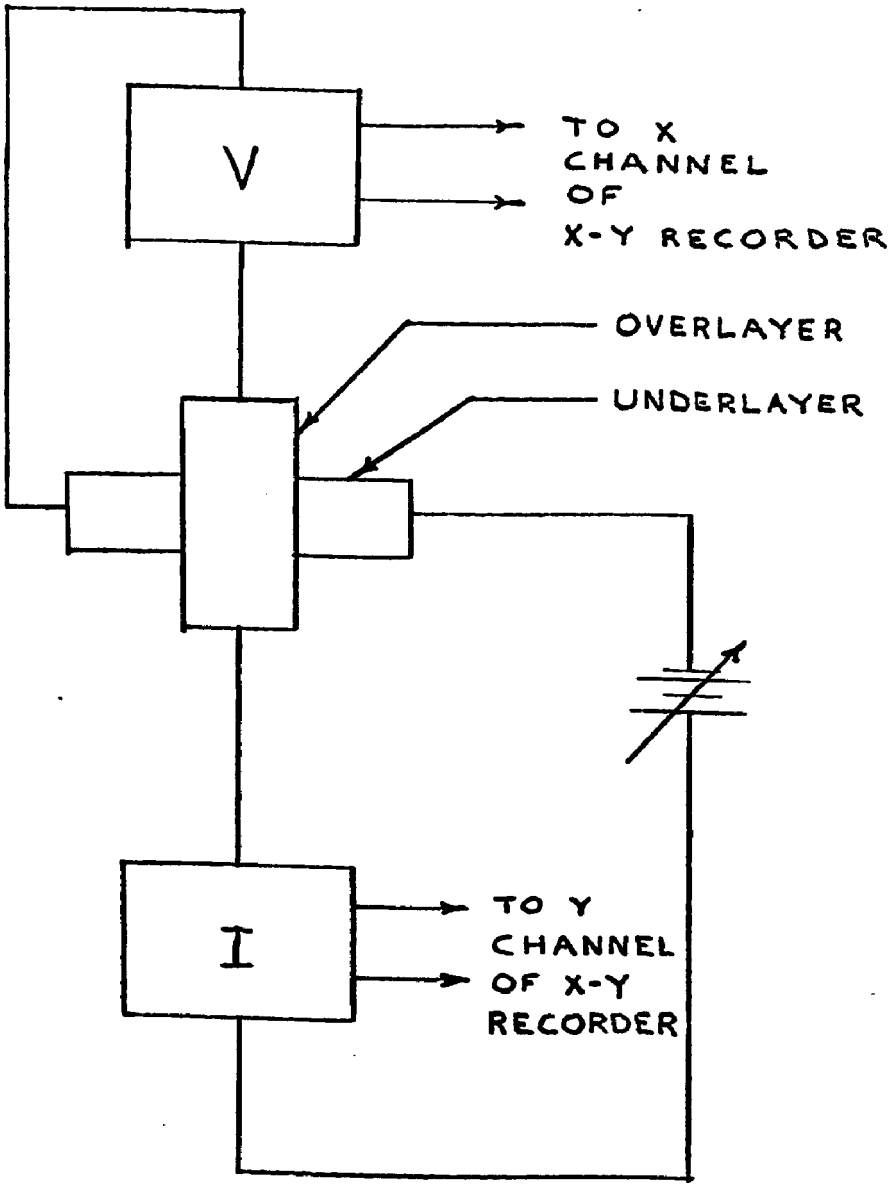



Figure 11. Schematic of DC Measurement Technique for Au-MgO-Au Emission Diodes

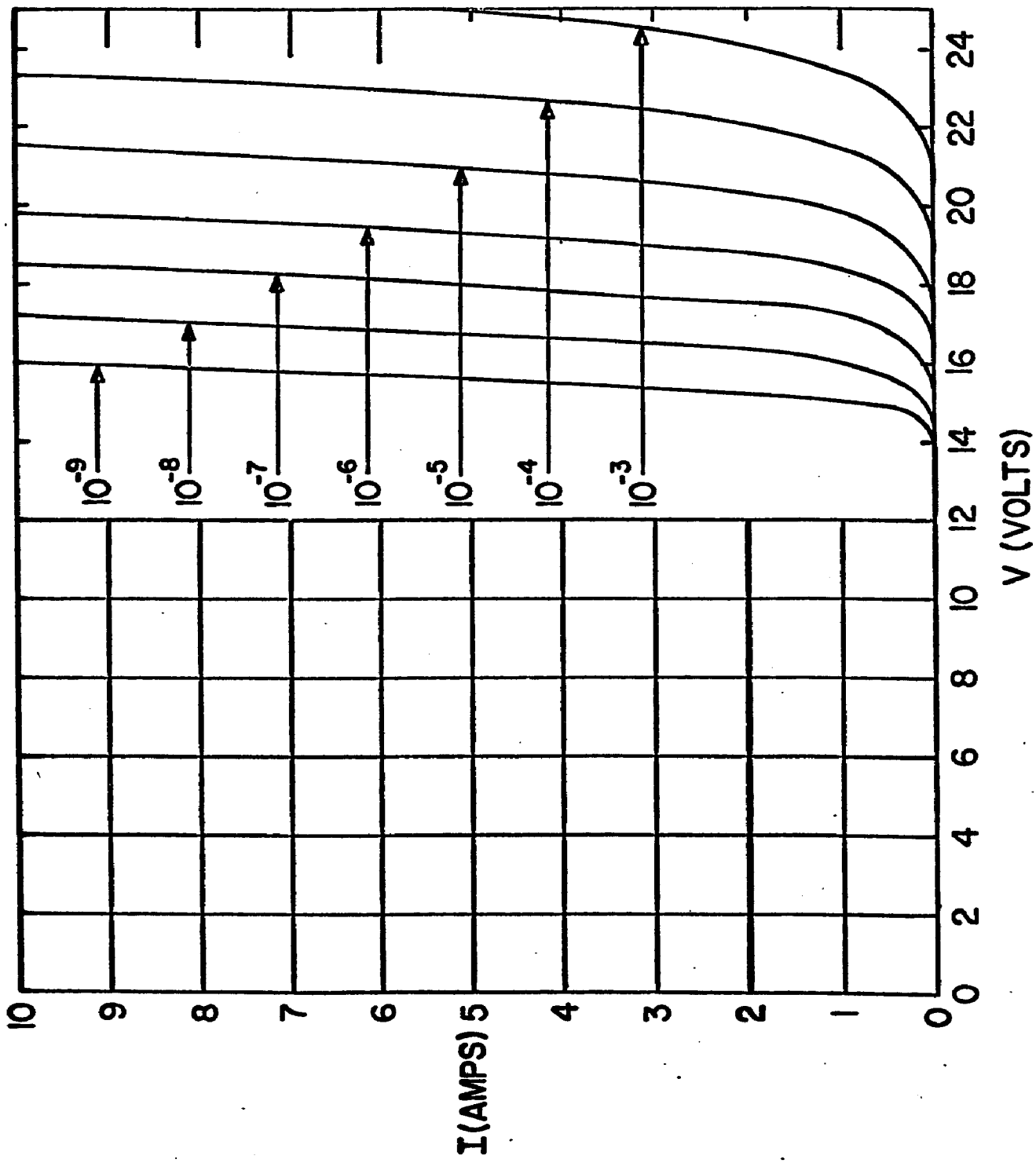



Figure 12. Tunnel I-V Characteristics of a Au-MgO-Au Device with an 89Å Thick Oxide

I-V CHARACTERISTICS FROM
DEVICE PY-G-II
OVERLAYER I 313°K
89 Å OXIDE

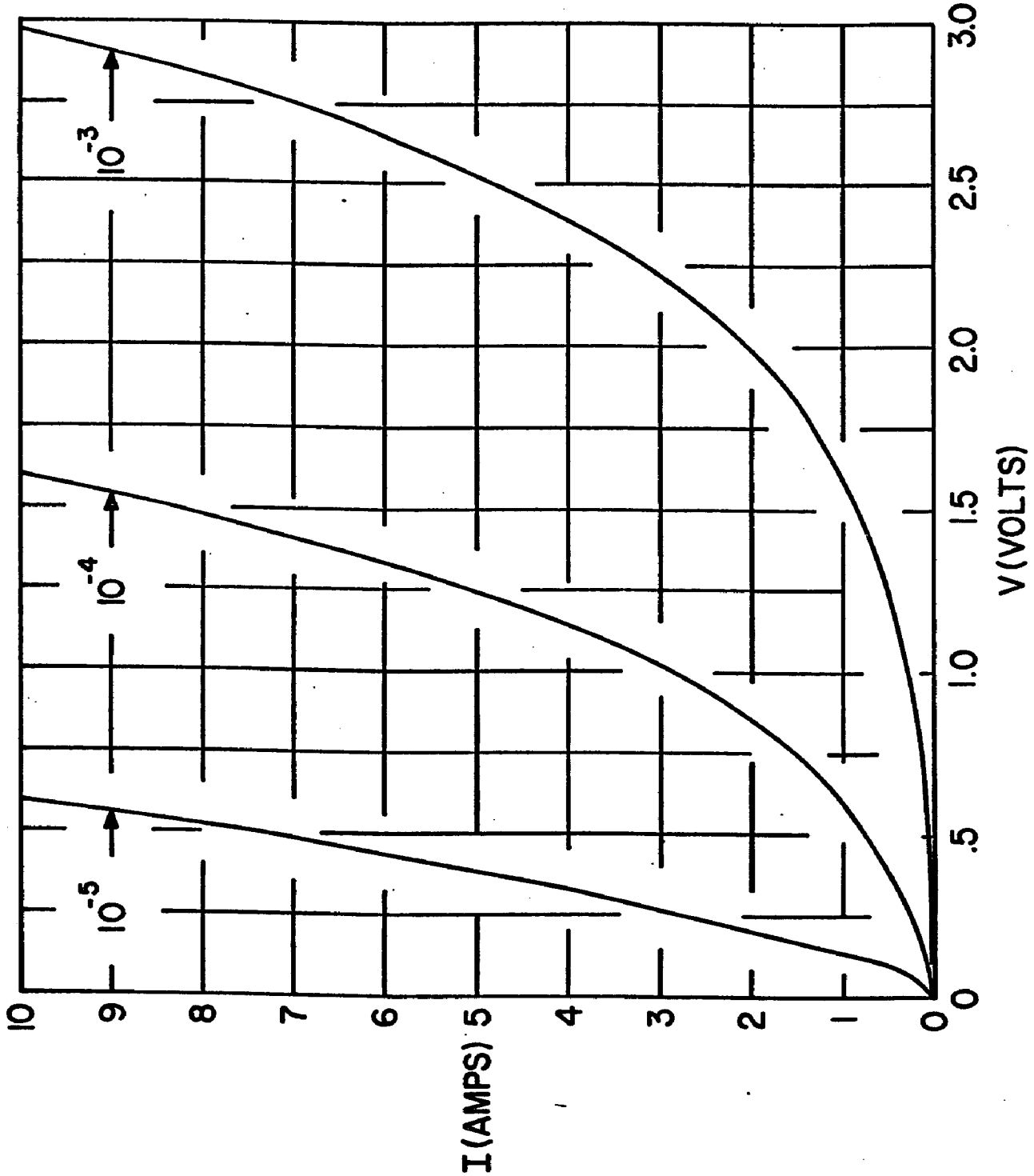



Figure 13

FOWLER-NORDHEIM PLOT OF I-V CHARACTERISTICS OF DEVICE PY-G-11 OVERLAYER 1

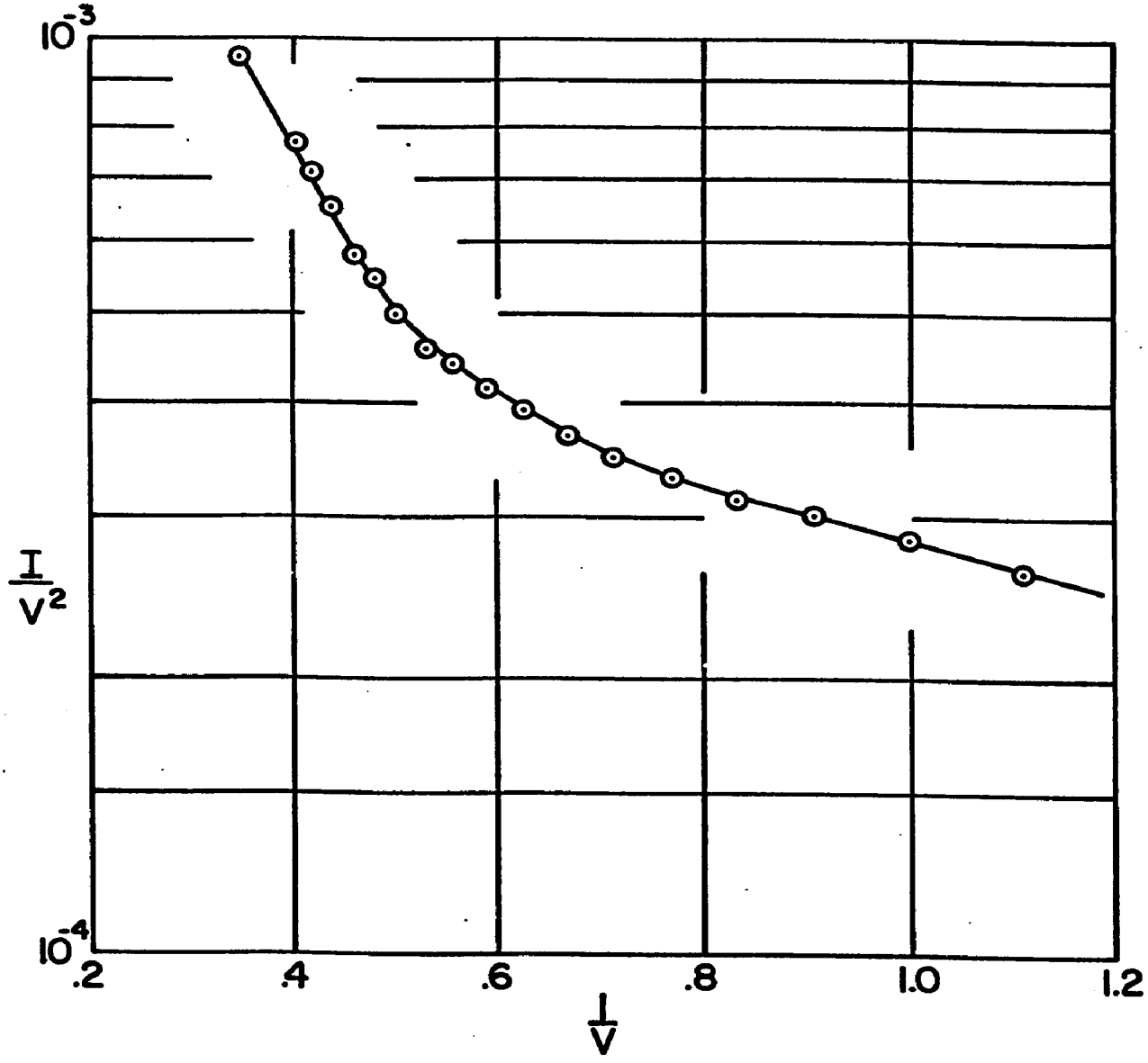



Figure 14

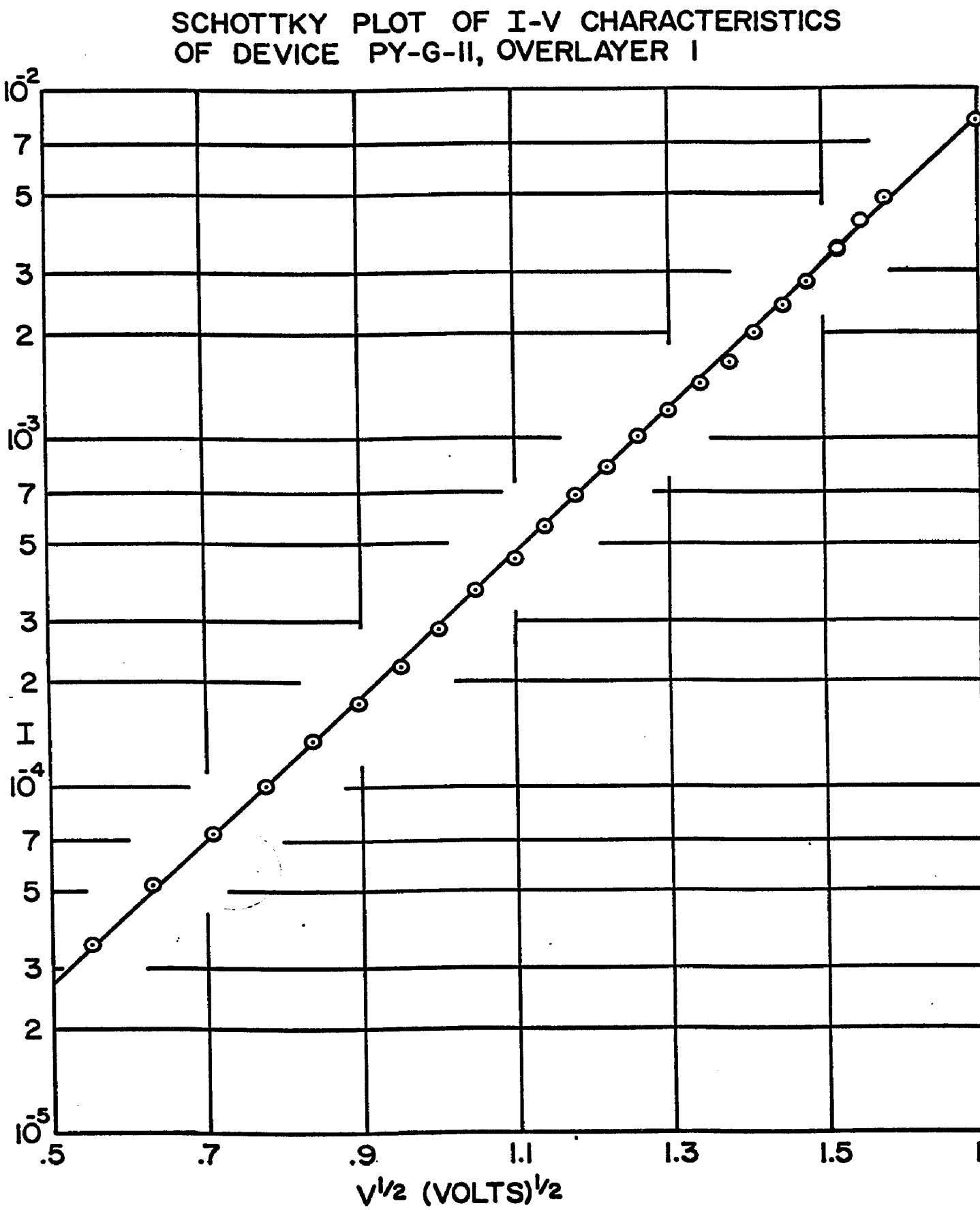

SCHOTTKY PLOT OF I-V CHARACTERISTICS
OF DEVICE PY-G-11, OVERLAYER 1
$10^{-2}$
7
5
3
2
$10^{-3}$
7
5
3
2
I
$10^{-4}$
7
5
3
2
$10^{-5}$
.5
.7
.9
1.1
1.3
1.5
$V^{1/2}$ (VOLTS)$^{1/2}$

Figure 15

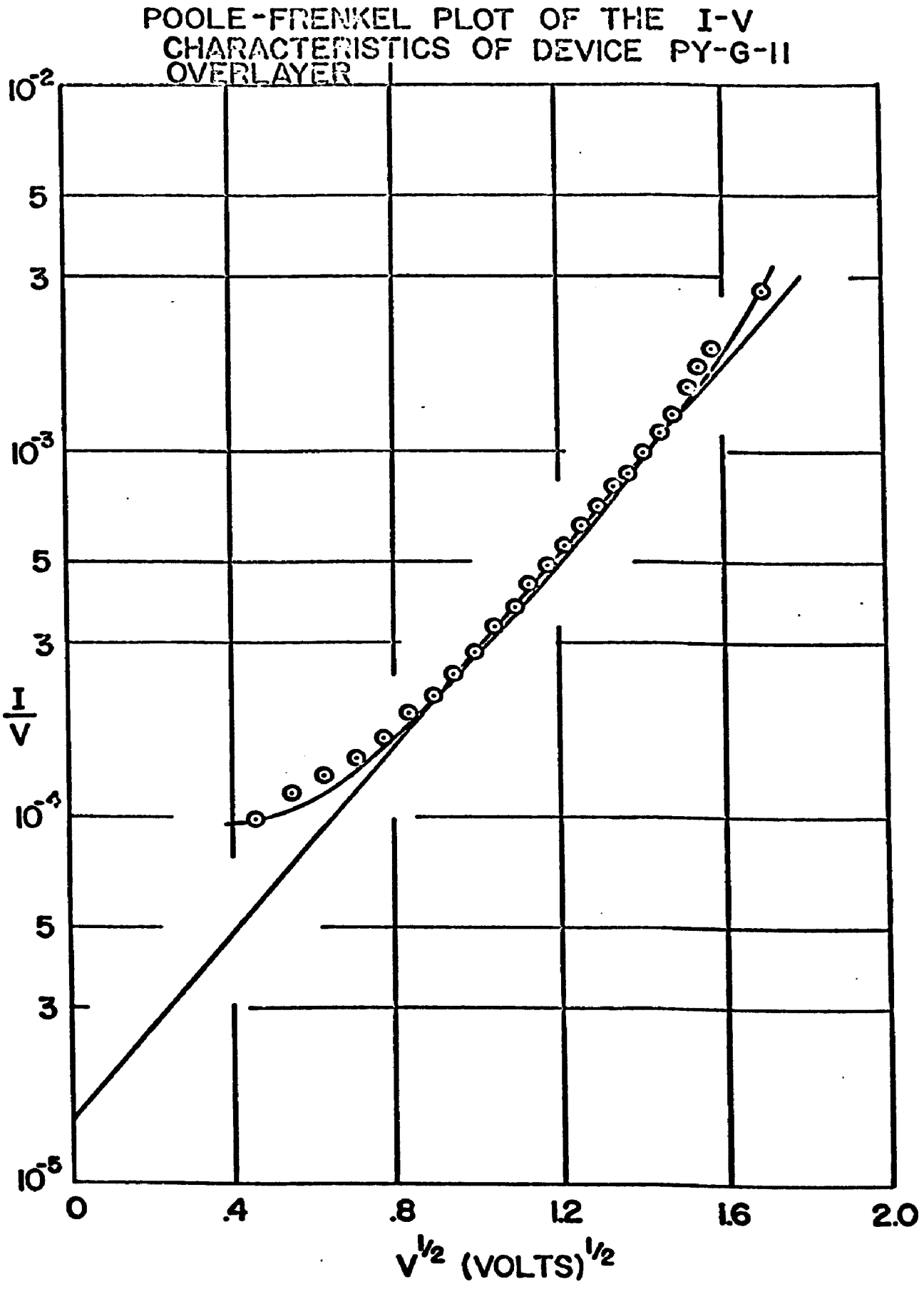

POOLE-FRENKEL PLOT OF THE I-V CHARACTERISTICS OF DEVICE PY-G-II OVERLAYER
10-2
5
3
10-3
5
3
I/V
10-4
5
3
10-5
0
.4
.8
1.2
1.6
2.0
V1/2 (VOLTS)1/2

Figure 16

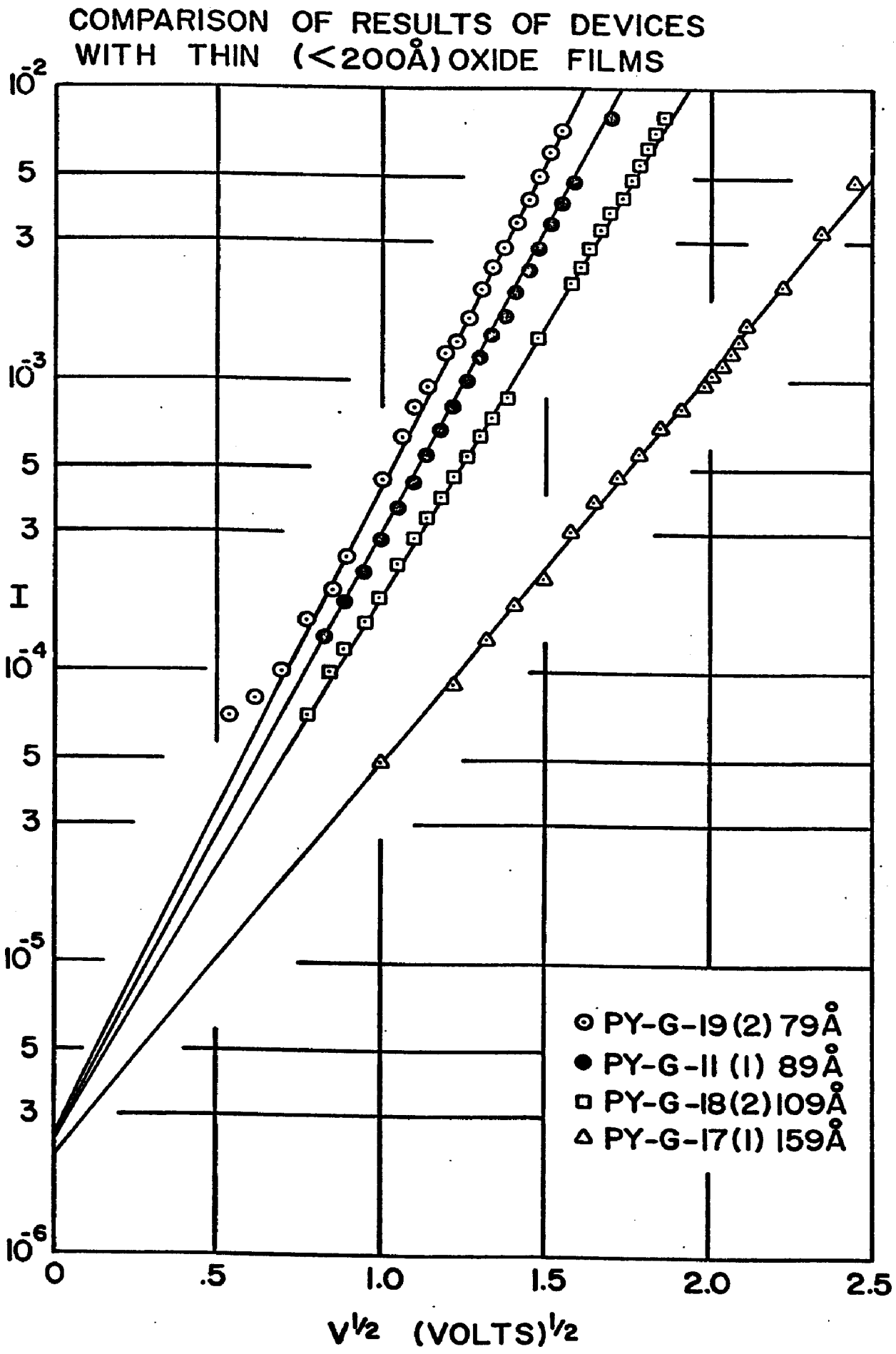

COMPARISON OF RESULTS OF DEVICES
WITH THIN (<200Å) OXIDE FILMS
$10^{-2}$
5
3
$10^{-3}$
5
3
I
$10^{-4}$
5
3
$10^{-5}$
5
3
$10^{-6}$
0
.5
1.0
1.5
2.0
2.5
$V^{1/2}$ (VOLTS)$^{1/2}$
PY-G-19(2) 79Å
PY-G-11 (1) 89Å
PY-G-18(2) 109Å
PY-G-17(1) 159Å

Figure 17

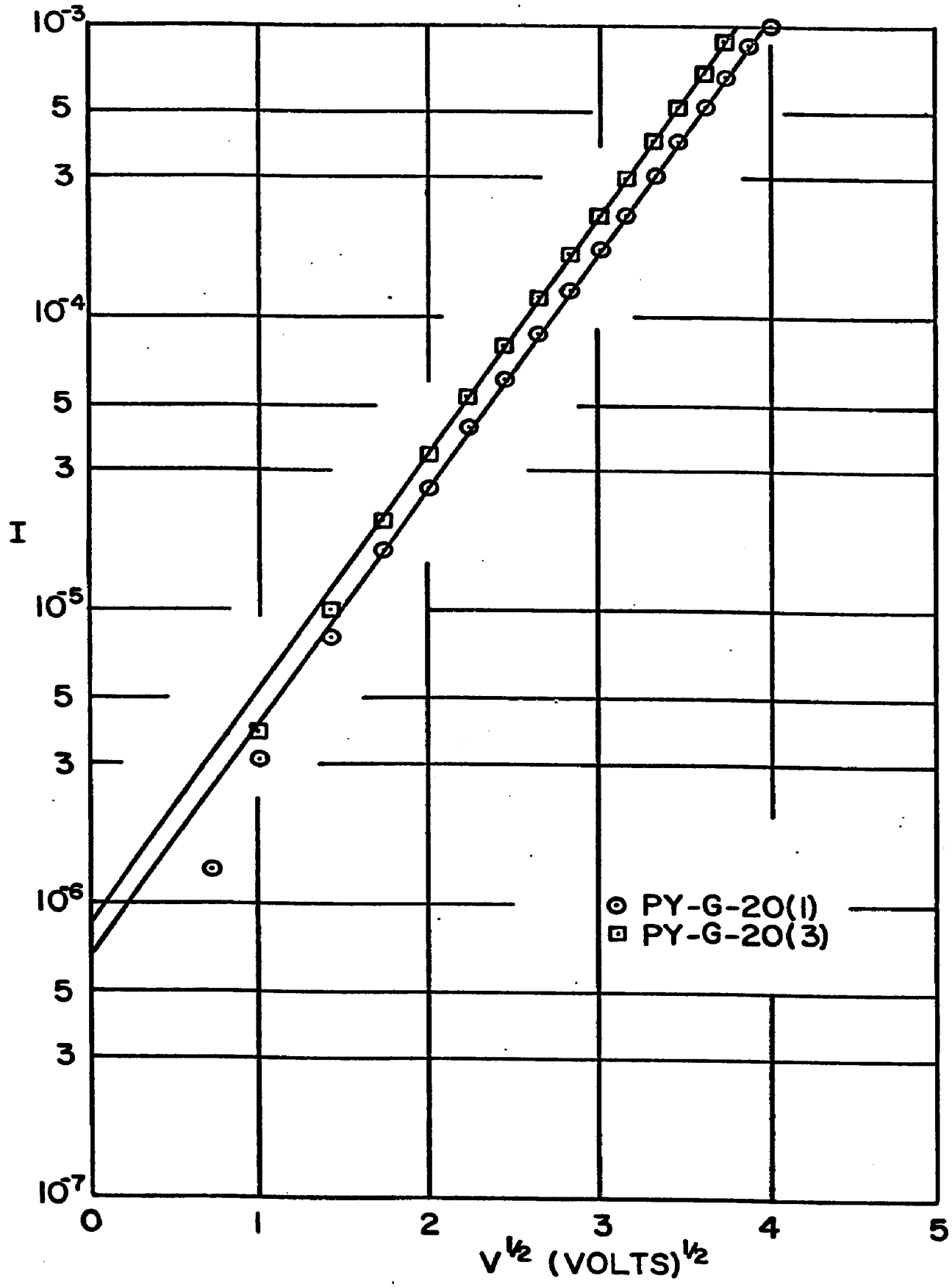

Ln I VS. V^1/2 PLOT FOR TWO DEVICES WITH THICKER OXIDE FILMS (680 Å)
10^-3
5
3
10^-4
5
3
I
10^-5
5
3
10^-6
5
3
10^-7
0
1
2
3
4
5
V^1/2 (VOLTS)^1/2
PY-G-20(1)
PY-G-20(3)

Figure 18

TEMPERATURE DEPENDENCE OF I-V CHARACTERISTICS OF DEVICE PY-G-II OVERLAYER I

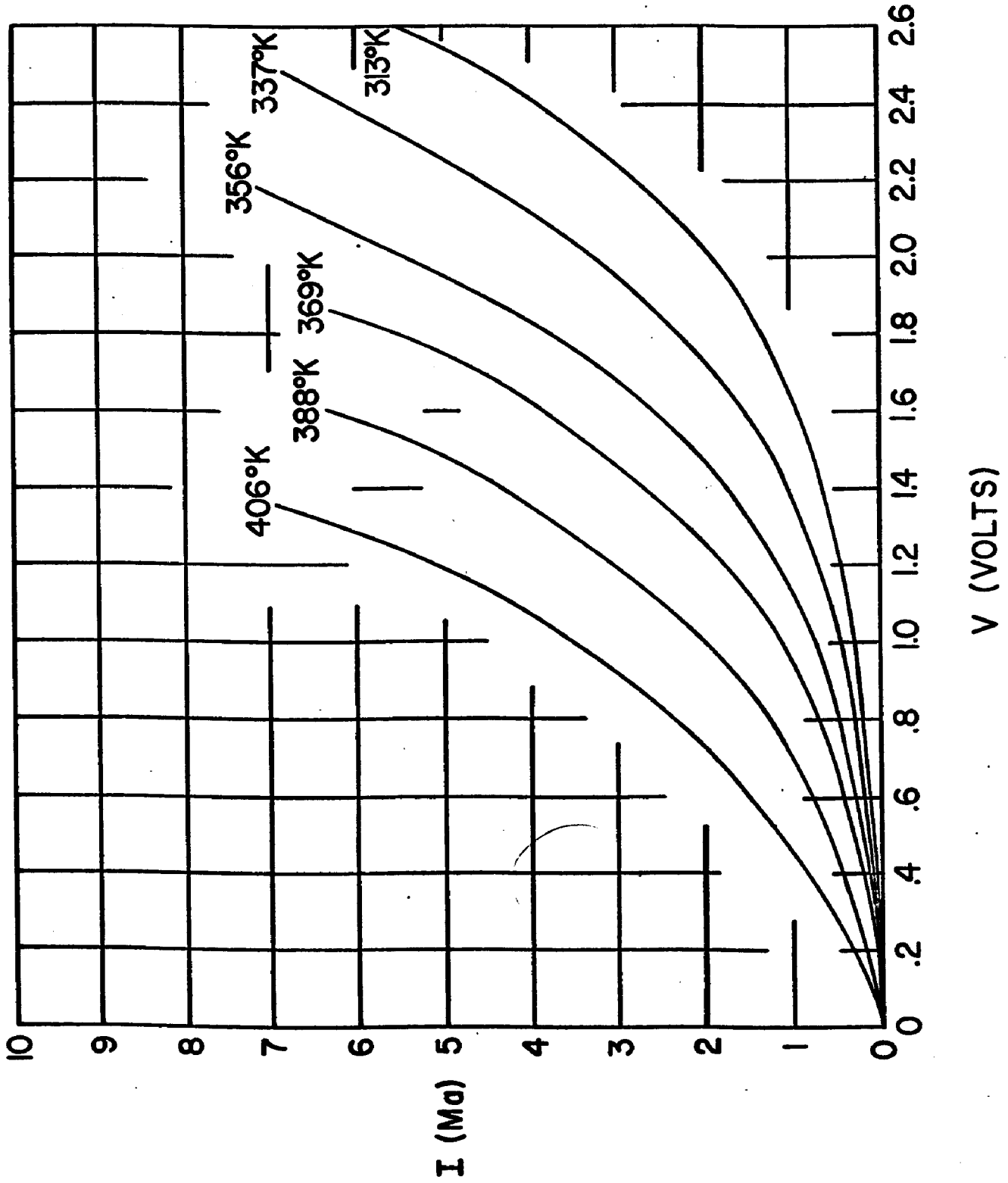



Figure 19

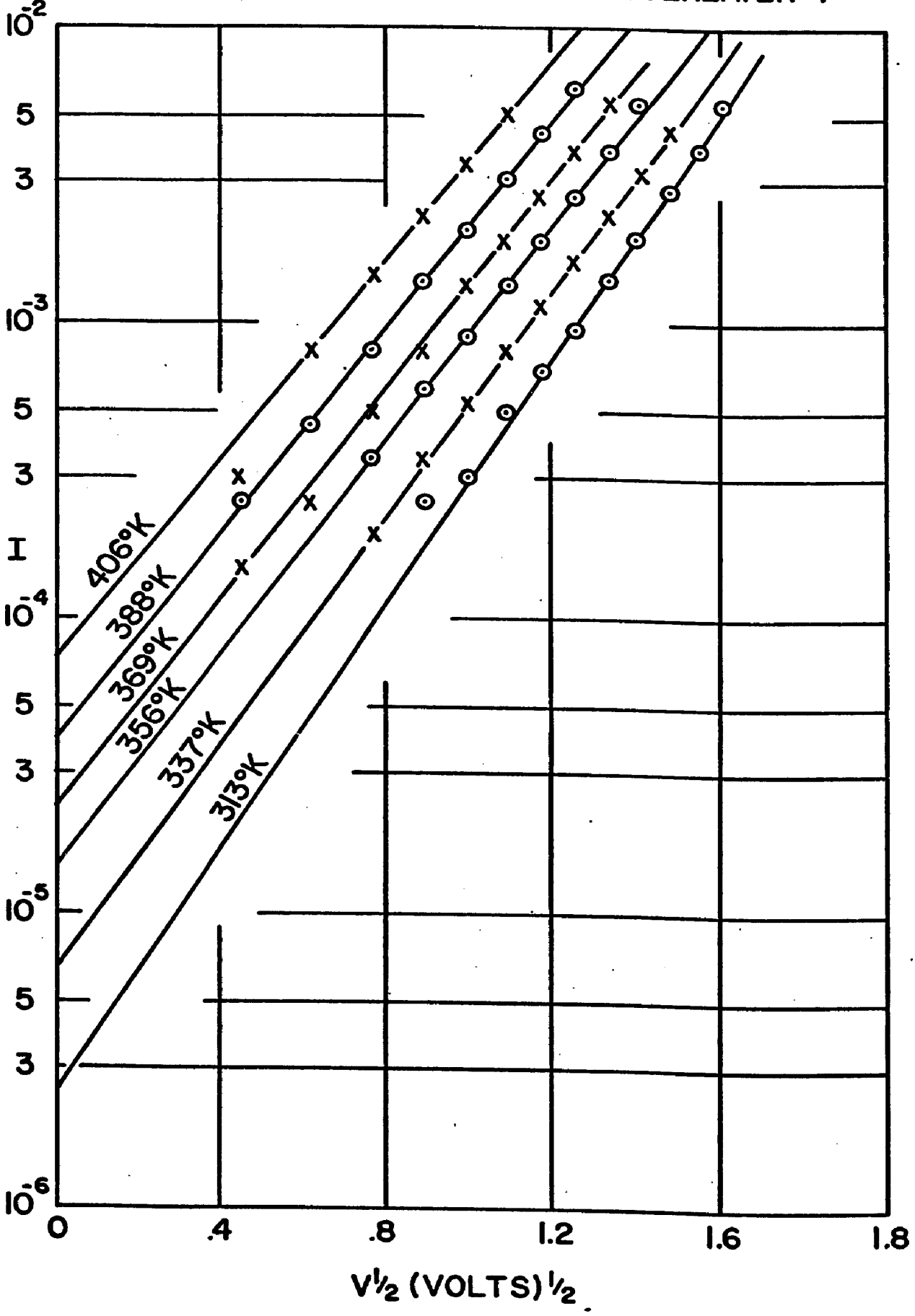

Ln I vs. V½ AS A FUNCTION OF TEMPERATURE FOR DEVICE PY-G-II OVERLAYER I
I
10⁻²
5
3
10⁻³
5
3
10⁻⁴
5
3
10⁻⁵
5
3
10⁻⁶
406°K
388°K
369°K
356°K
337°K
313°K
0
.4
.8
1.2
1.6
1.8
V½ (VOLTS)½

Figure 20

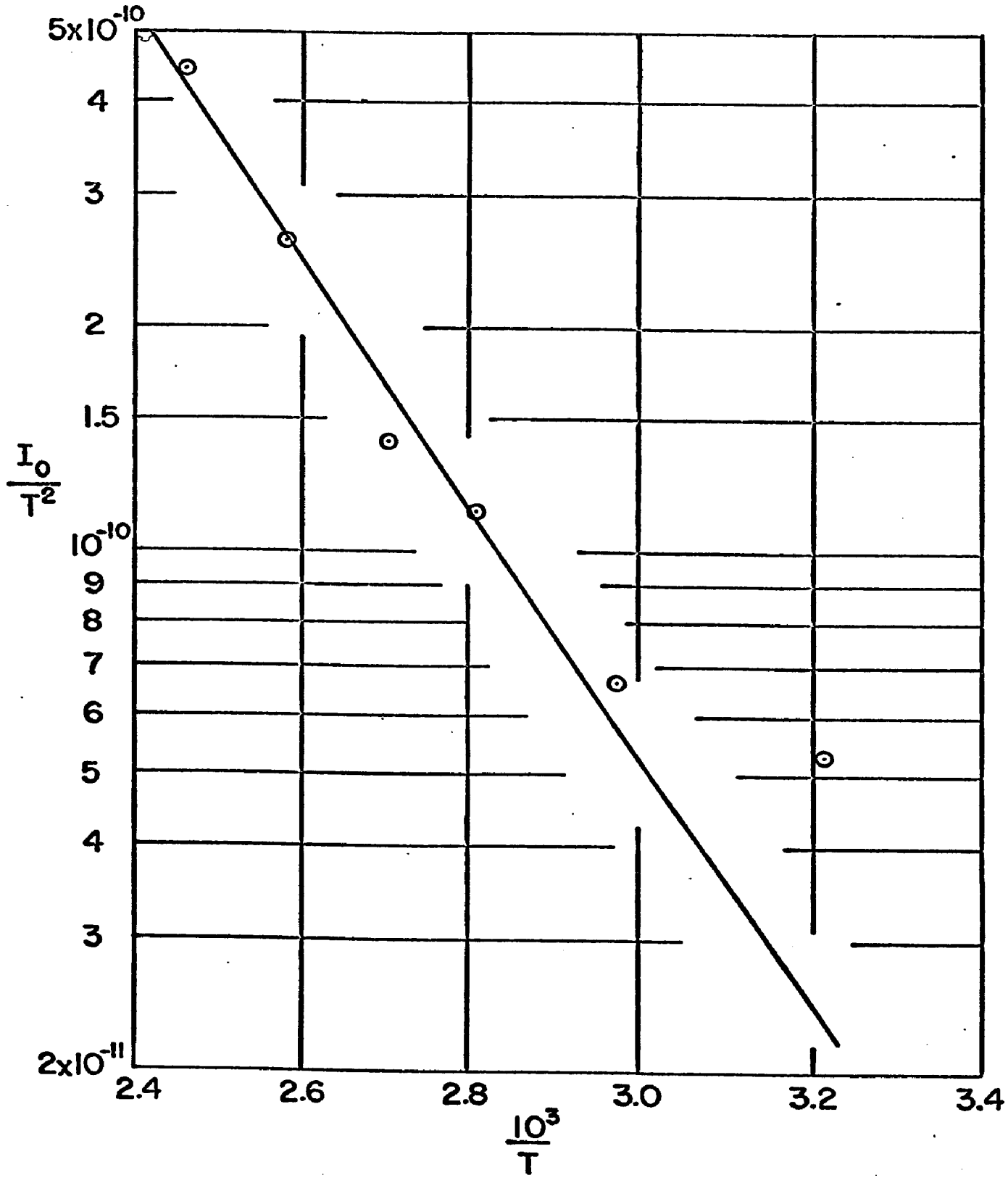

Ln ($I_0/T^2$) VS. $10^3/T$ FOR DEVICE PY-G-II, OVERLAYER I.
$5\times10^{-10}$
4
3
2
1.5
$10^{-10}$
9
8
7
6
5
4
3
$2\times10^{-11}$
$\frac{I_0}{T^2}$
2.4
2.6
2.8
3.0
3.2
3.4
$\frac{10^3}{T}$

Figure 21

COMPARISON OF RESULTS WITH DIFFERENT PRESSURES OF OXYGEN PRESENT DURING FABRICATION

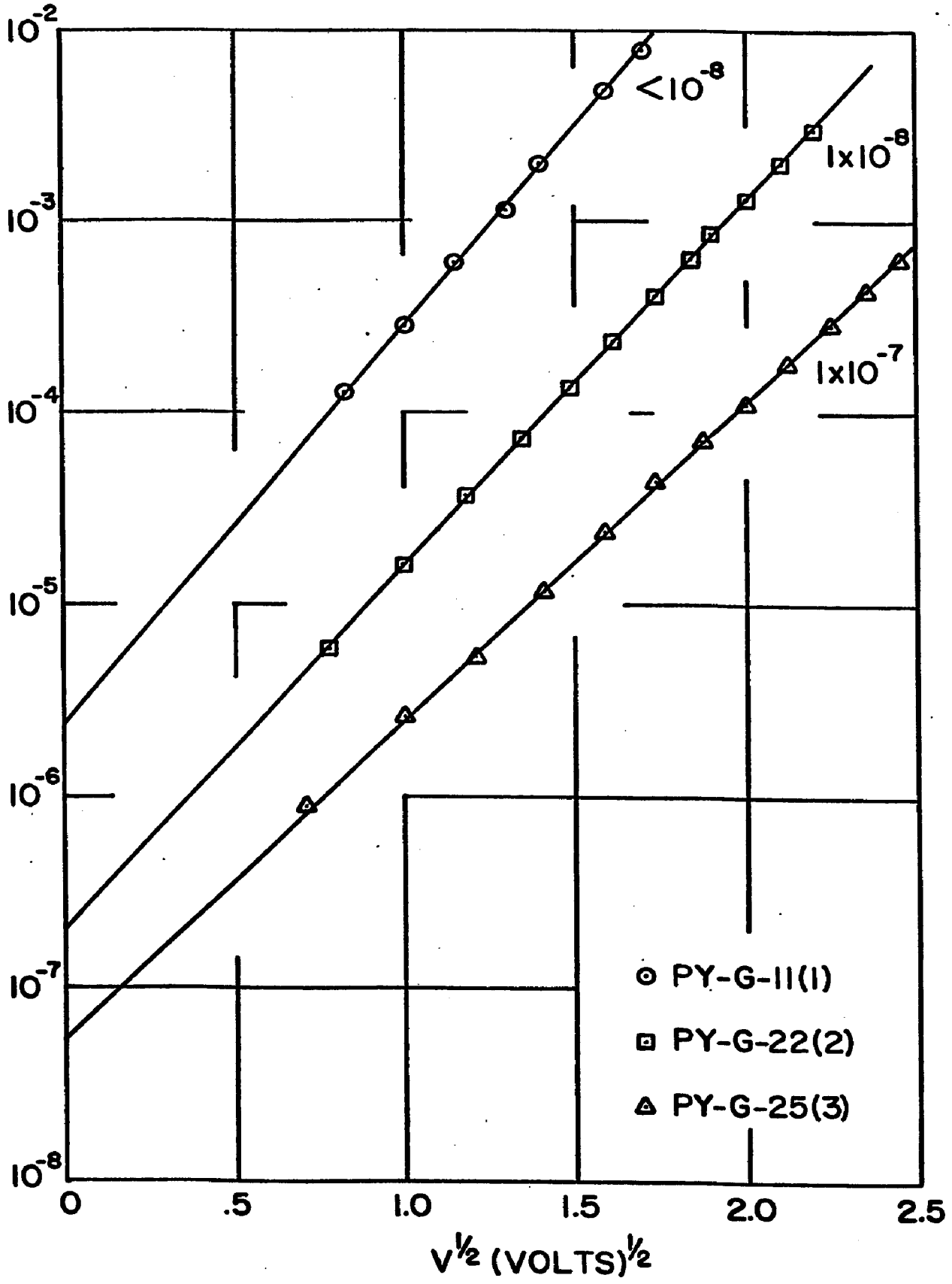



Figure 22

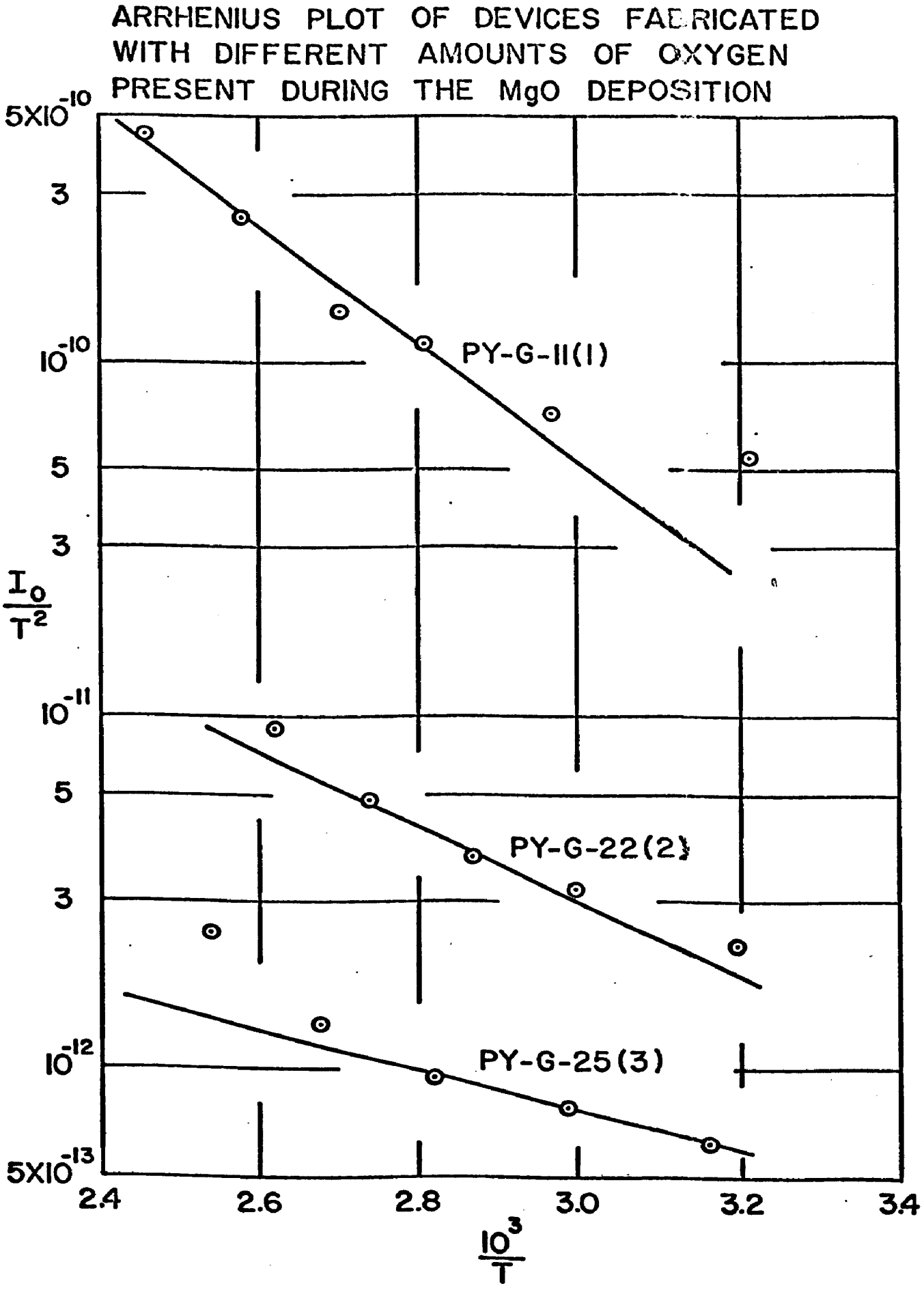
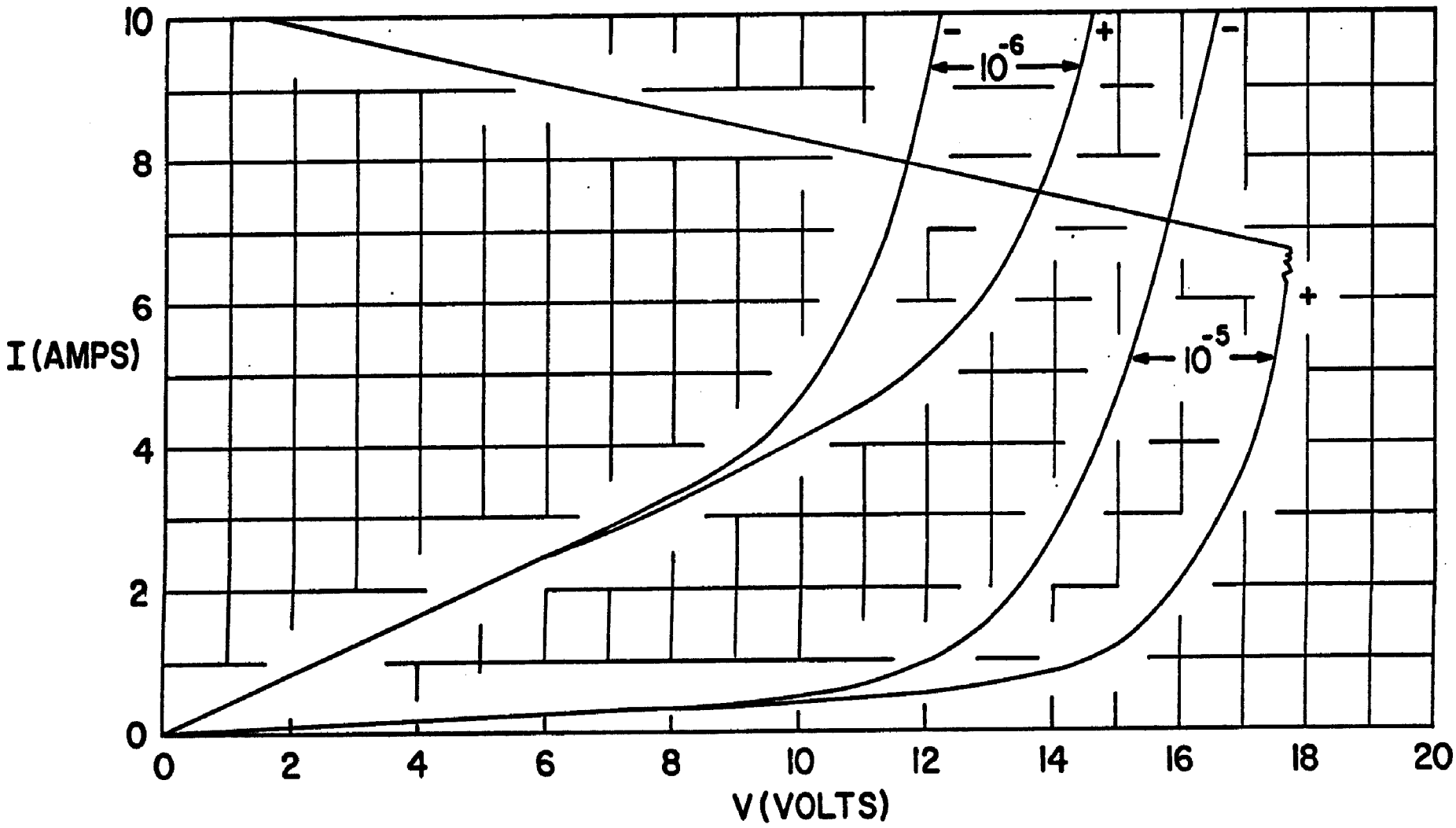

ARRHENIUS PLOT OF DEVICES FABRICATED WITH DIFFERENT AMOUNTS OF OXYGEN PRESENT DURING THE MgO DEPOSITION
5X10-10
3
10-10
5
3
10-11
5
3
10-12
5X10-13
I0/T2
PY-G-11(1)
PY-G-22(2)
PY-G-25(3)
2.4
2.6
2.8
3.0
3.2
3.4
10^3/T

Figure 23

# I - V CHARACTERISTICS OF DEVICE PY-G-38(1)



FOWLER-NORDHEIM PLOT OF I - V CHARACTERISTICS OF DEVICE PY-G-38(1)

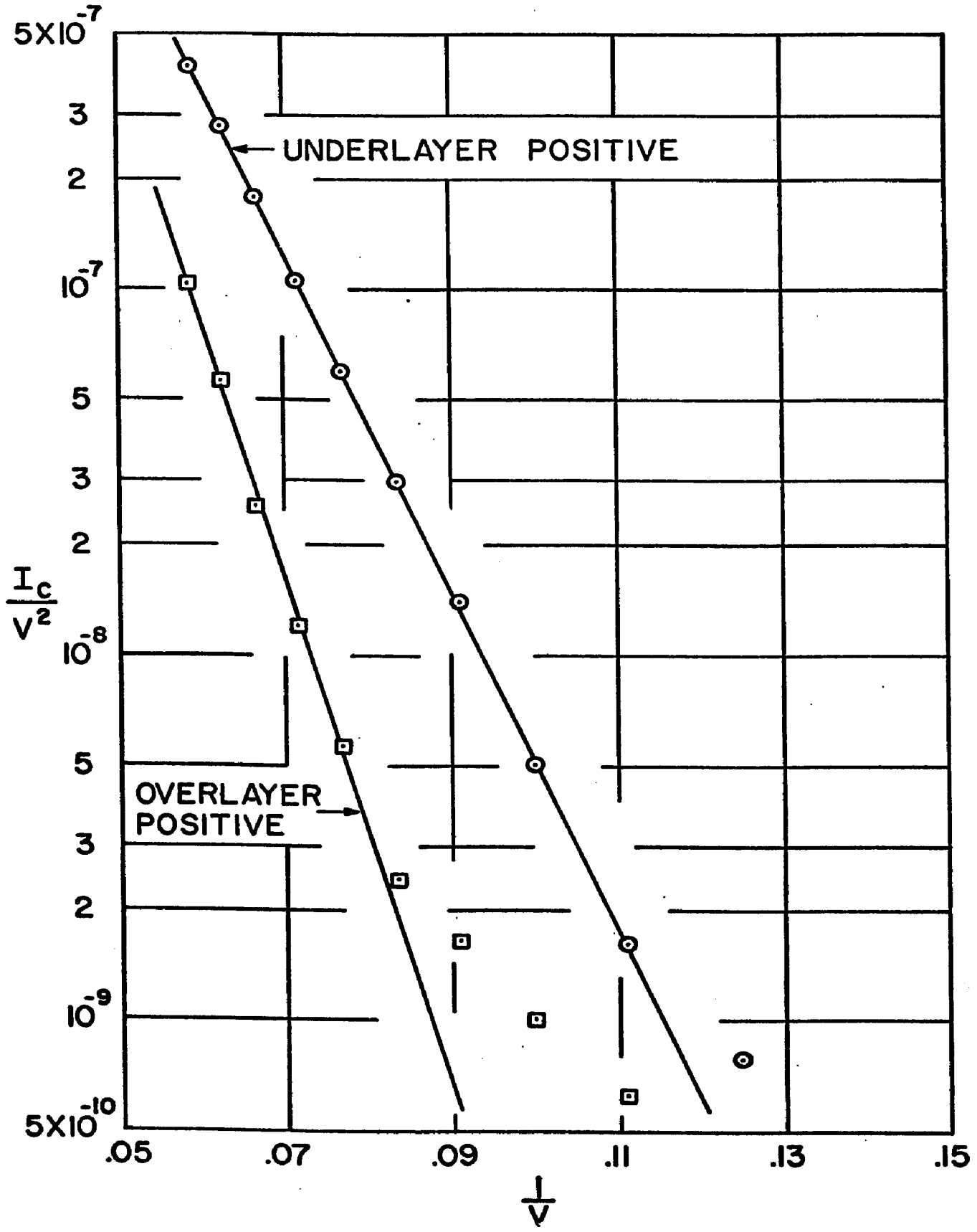



Figure 25

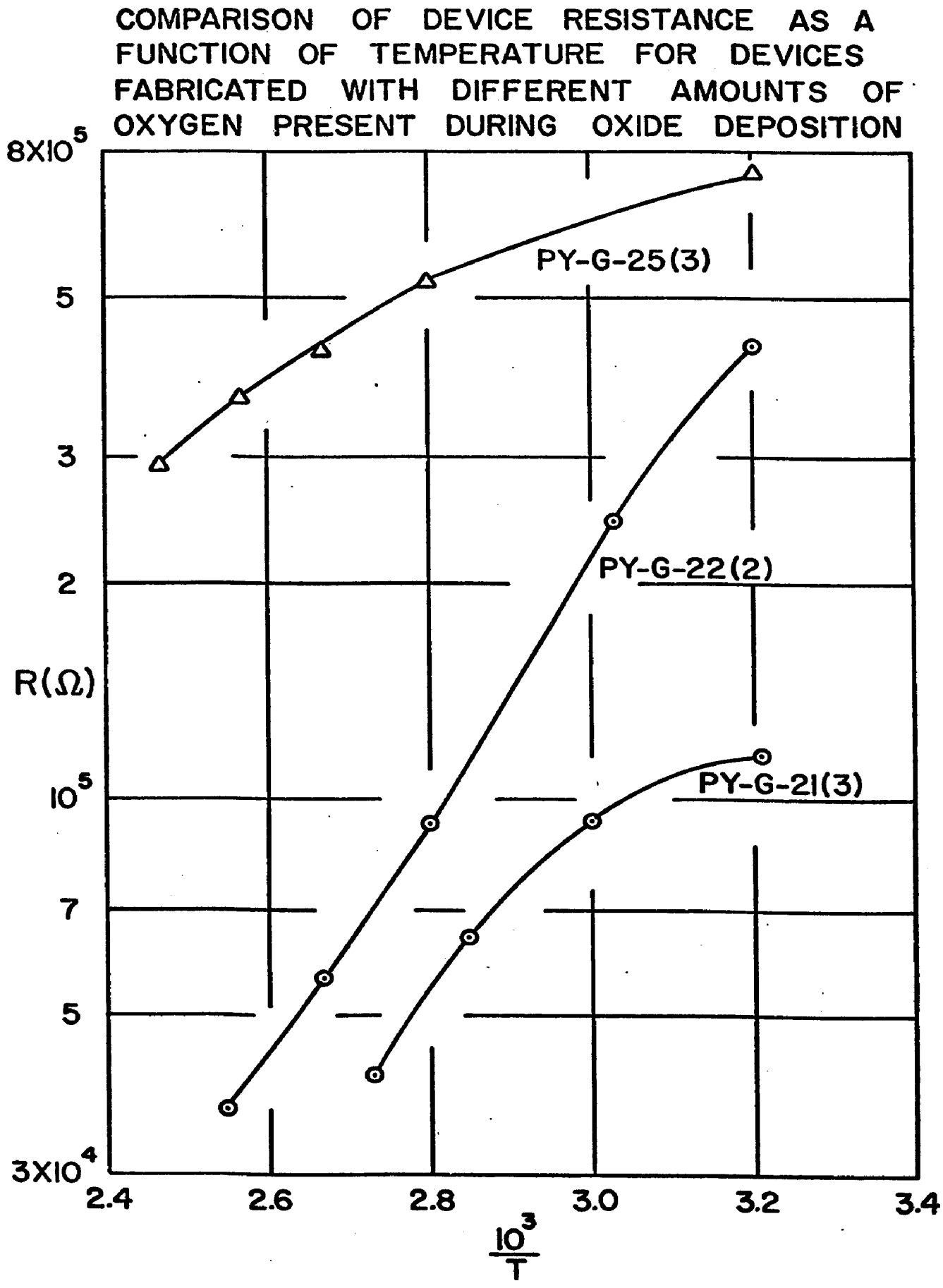

COMPARISON OF DEVICE RESISTANCE AS A FUNCTION OF TEMPERATURE FOR DEVICES FABRICATED WITH DIFFERENT AMOUNTS OF OXYGEN PRESENT DURING OXIDE DEPOSITION
8X10^5
5
3
2
R(Ω)
10^5
7
5
3X10^4
PY-G-25(3)
PY-G-22(2)
PY-G-21(3)
2.4
2.6
2.8
3.0
3.2
3.4
10^3/T

Figure 26

EMISSION TRANSFER RATIO, $\alpha$, VS. SAMPLE VOLTAGE, $V_S$, FOR DEVICE PY-G-11(1)

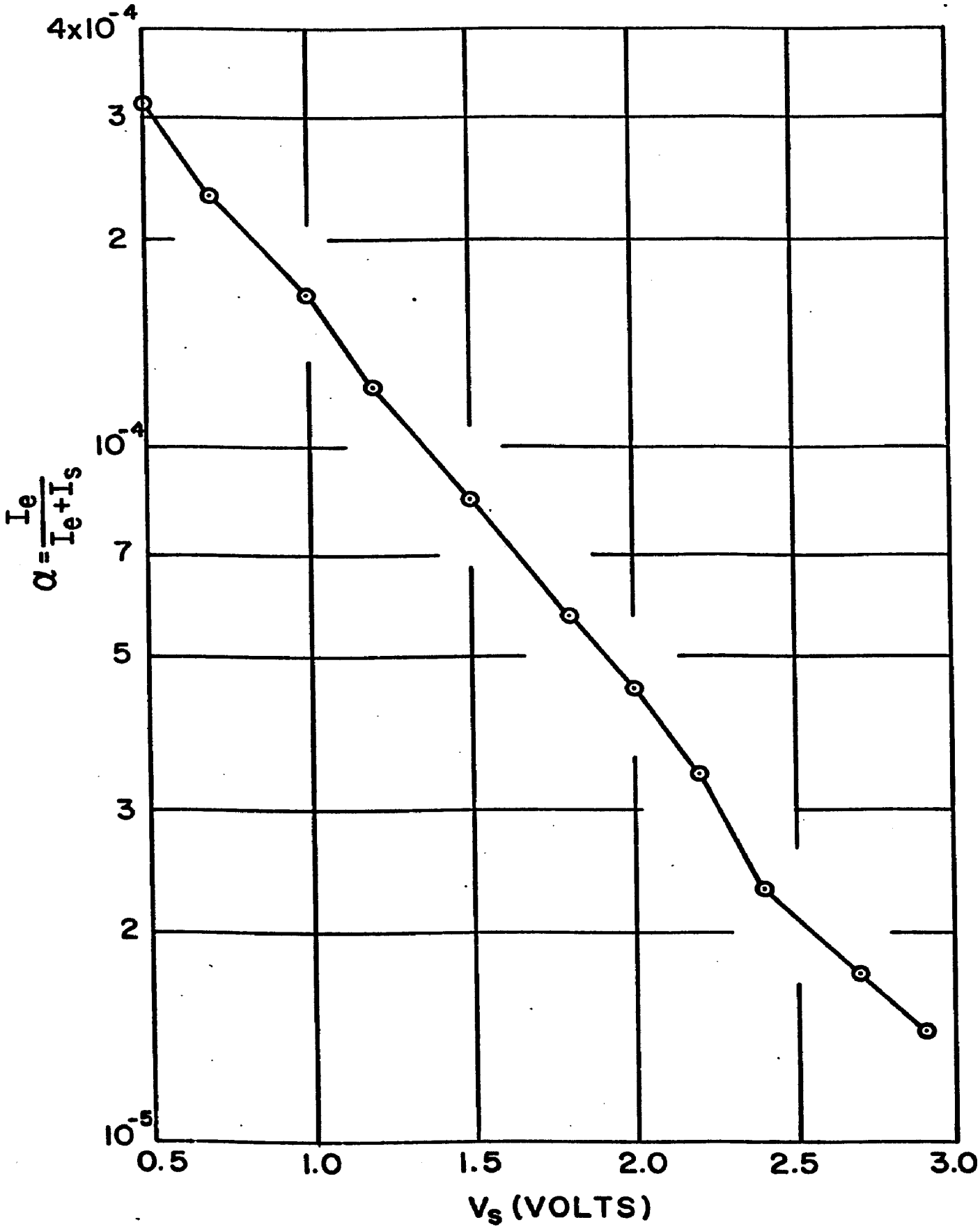



Figure 27

COMPARISON OF EMISSION TRANSFER RATIO FOR DEVICES WITH DIFFERENT OXIDE THICKNESSES

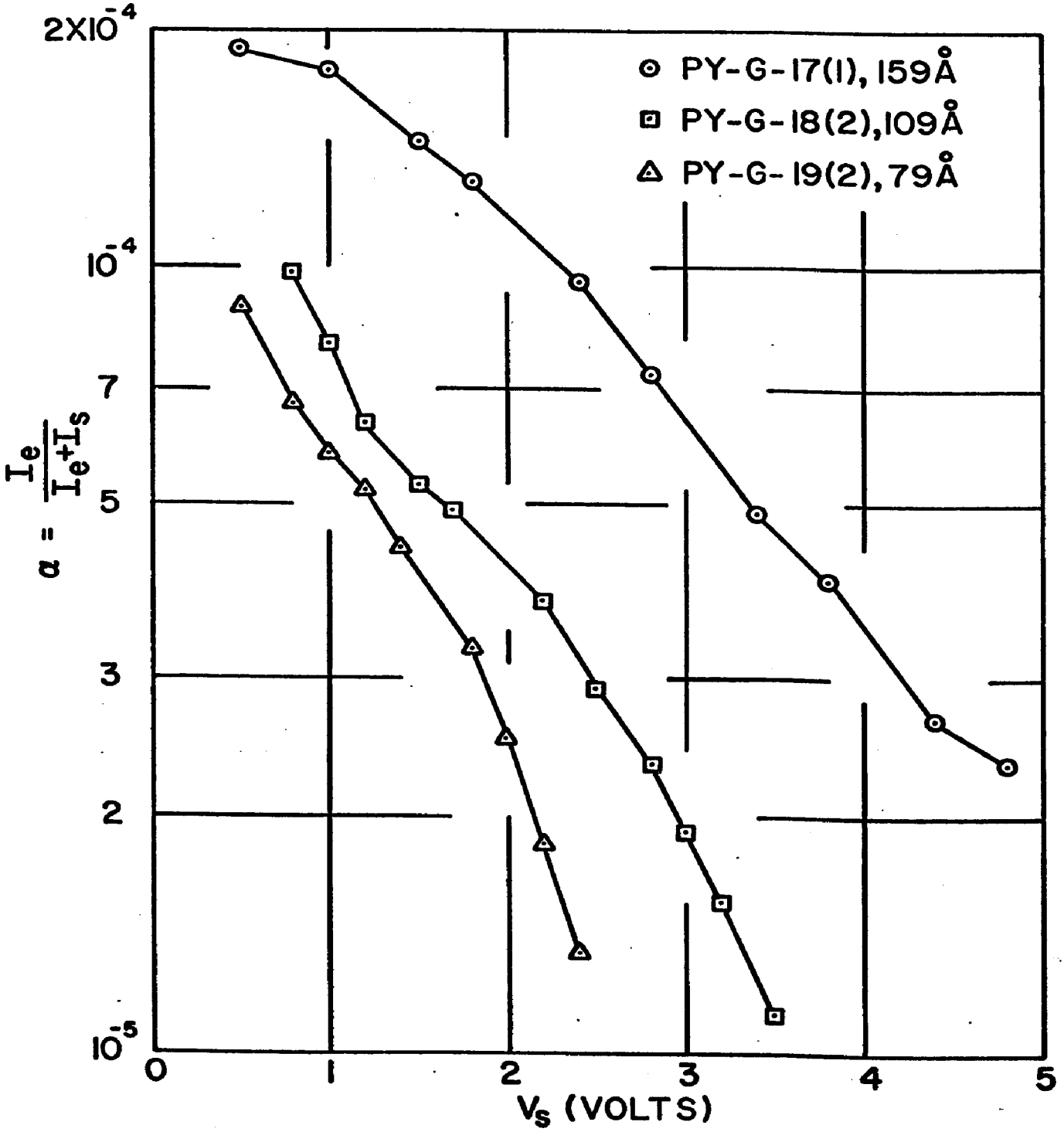



Figure 28

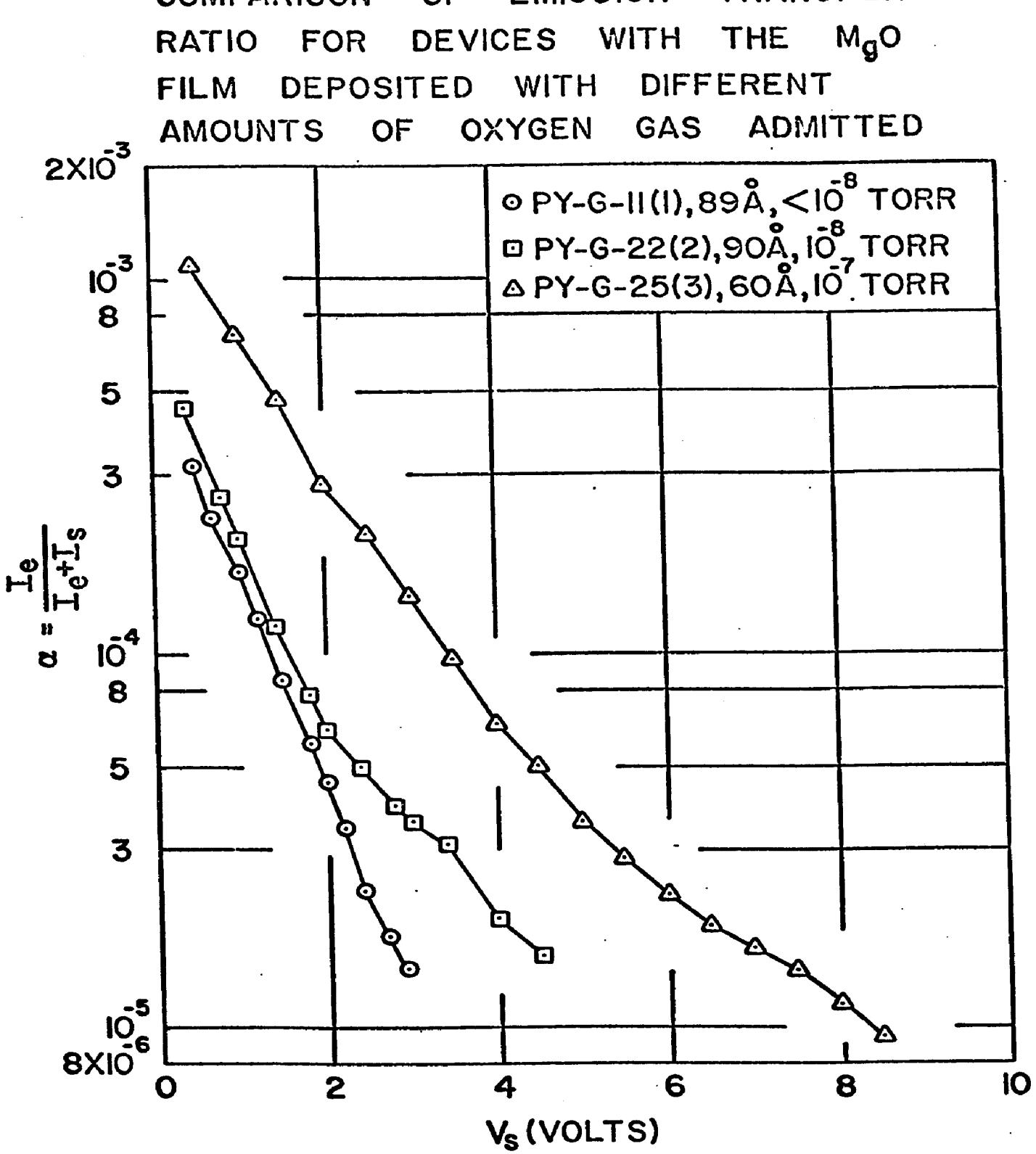

COMPARISON OF EMISSION TRANSFER RATIO FOR DEVICES WITH THE MgO FILM DEPOSITED WITH DIFFERENT AMOUNTS OF OXYGEN GAS ADMITTED
⊙ PY-G-11(1), 89Å, <10⁻⁸ TORR
⊡ PY-G-22(2), 90Å, 10⁻⁸ TORR
△ PY-G-25(3), 60Å, 10⁻⁷ TORR
α = Ie / (Ie+Is)
2X10⁻³
10⁻³
8
5
3
10⁻⁴
8
5
3
10⁻⁵
8X10⁻⁶
0
2
4
6
8
10
Vs (VOLTS)

Figure 29

POTENTIAL BARRIER PRESENTED BY A DIELECTRIC FILM BETWEEN TWO METALS SHOWING ELECTRON IMAGE FORCE MODIFICATION

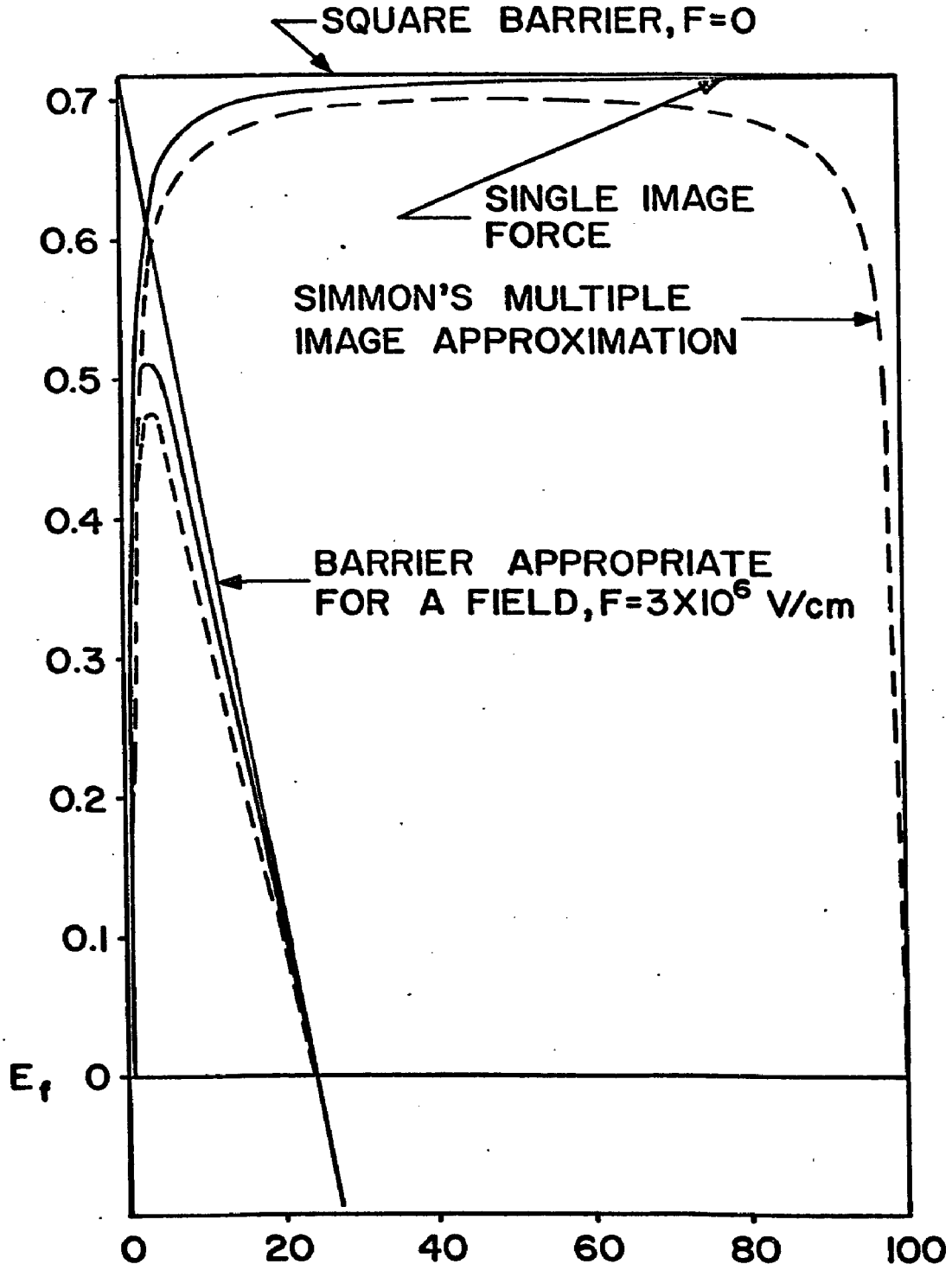



Figure 30

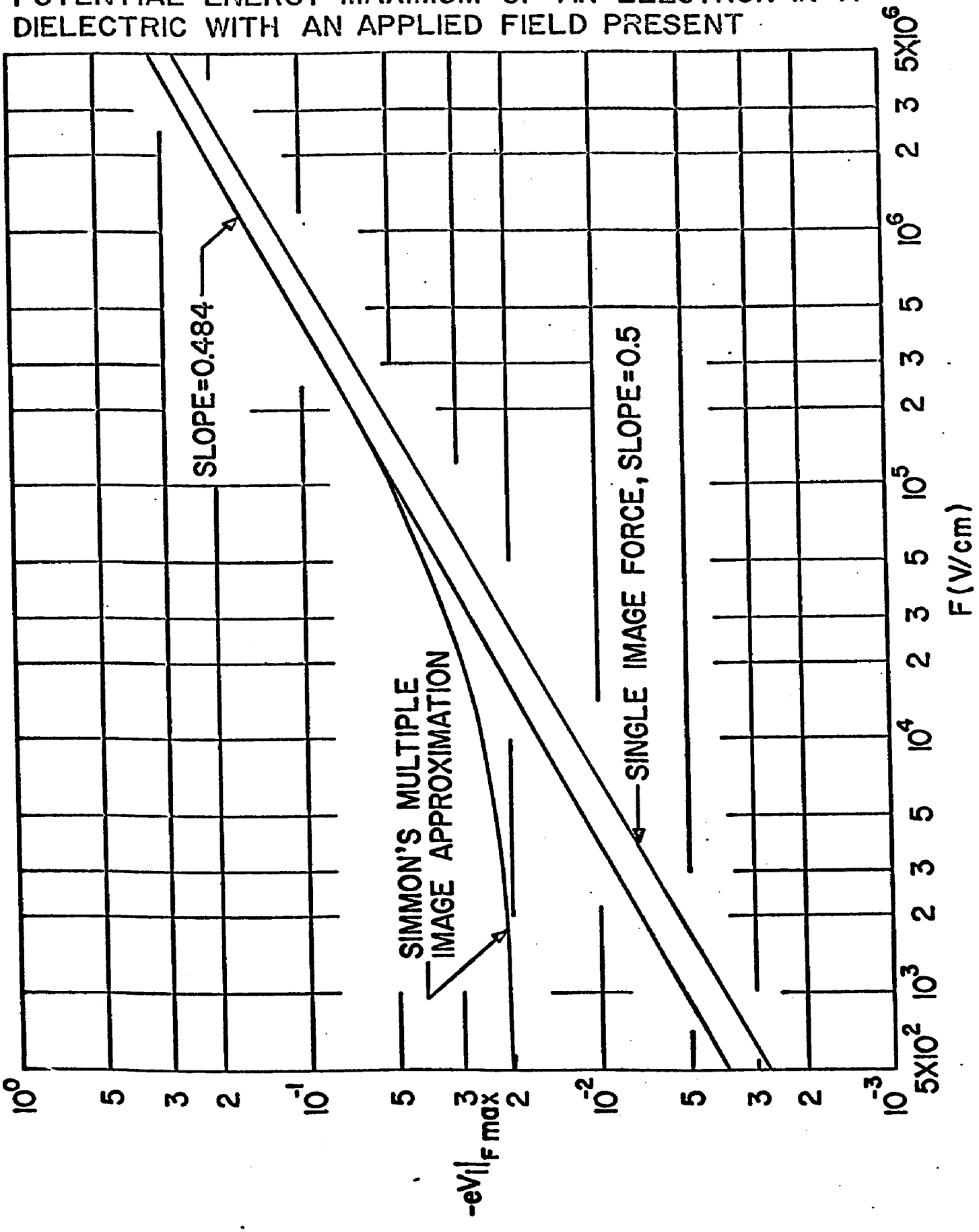

POTENTIAL ENERGY MAXIMUM OF AN ELECTRON IN A DIELECTRIC WITH AN APPLIED FIELD PRESENT
SLOPE=0.484
SINGLE IMAGE FORCE, SLOPE=0.5
SIMMON'S MULTIPLE IMAGE APPROXIMATION
F(V/cm)
$-eV|_{F\,max}$

Figure 31

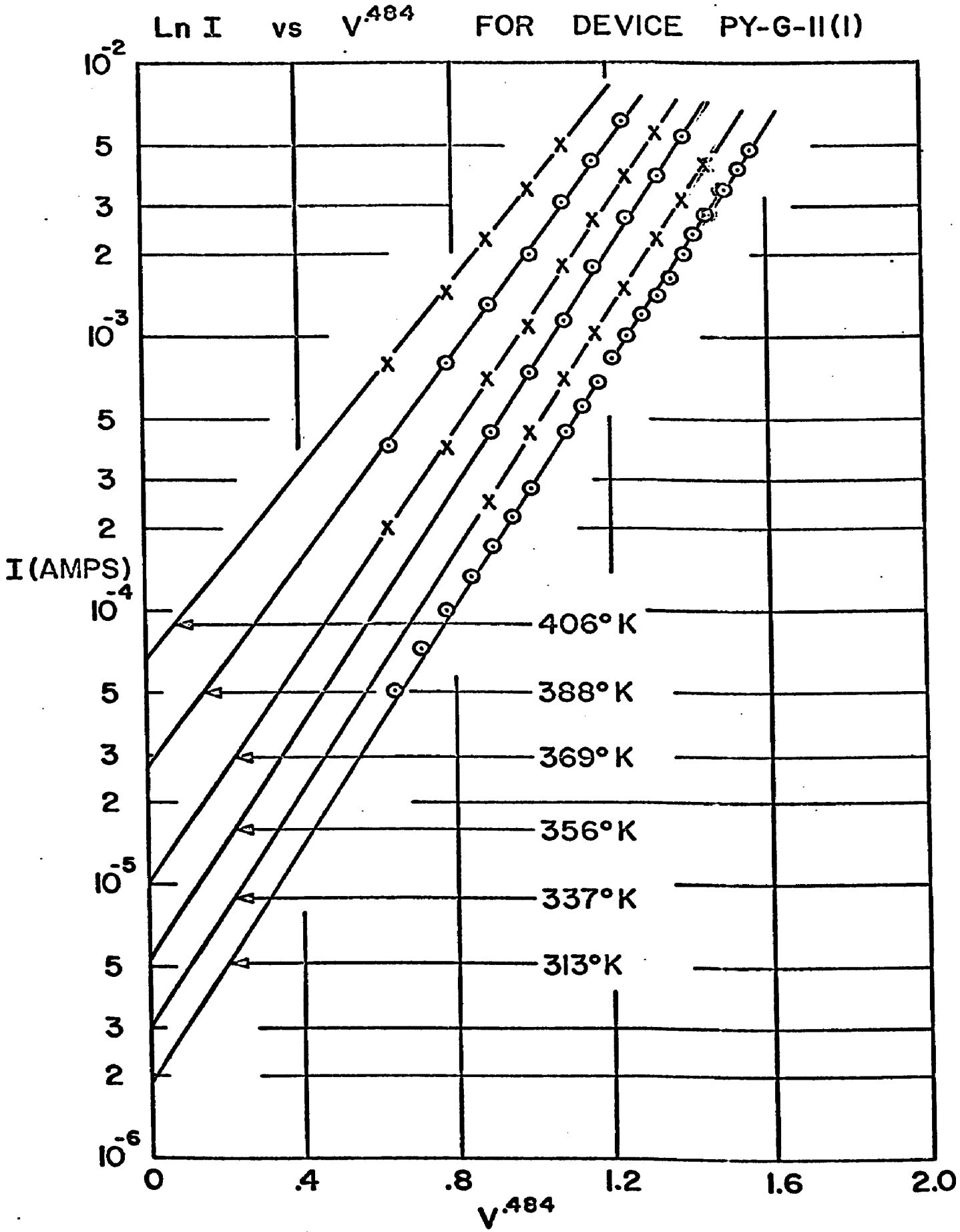

Ln I vs V.484 FOR DEVICE PY-G-II(I)
I(AMPS)
10-2
5
3
2
10-3
5
3
2
10-4
5
3
2
10-5
5
3
2
10-6
406° K
388° K
369° K
356° K
337° K
313° K
0
.4
.8
1.2
1.6
2.0
V.484

Figure 32

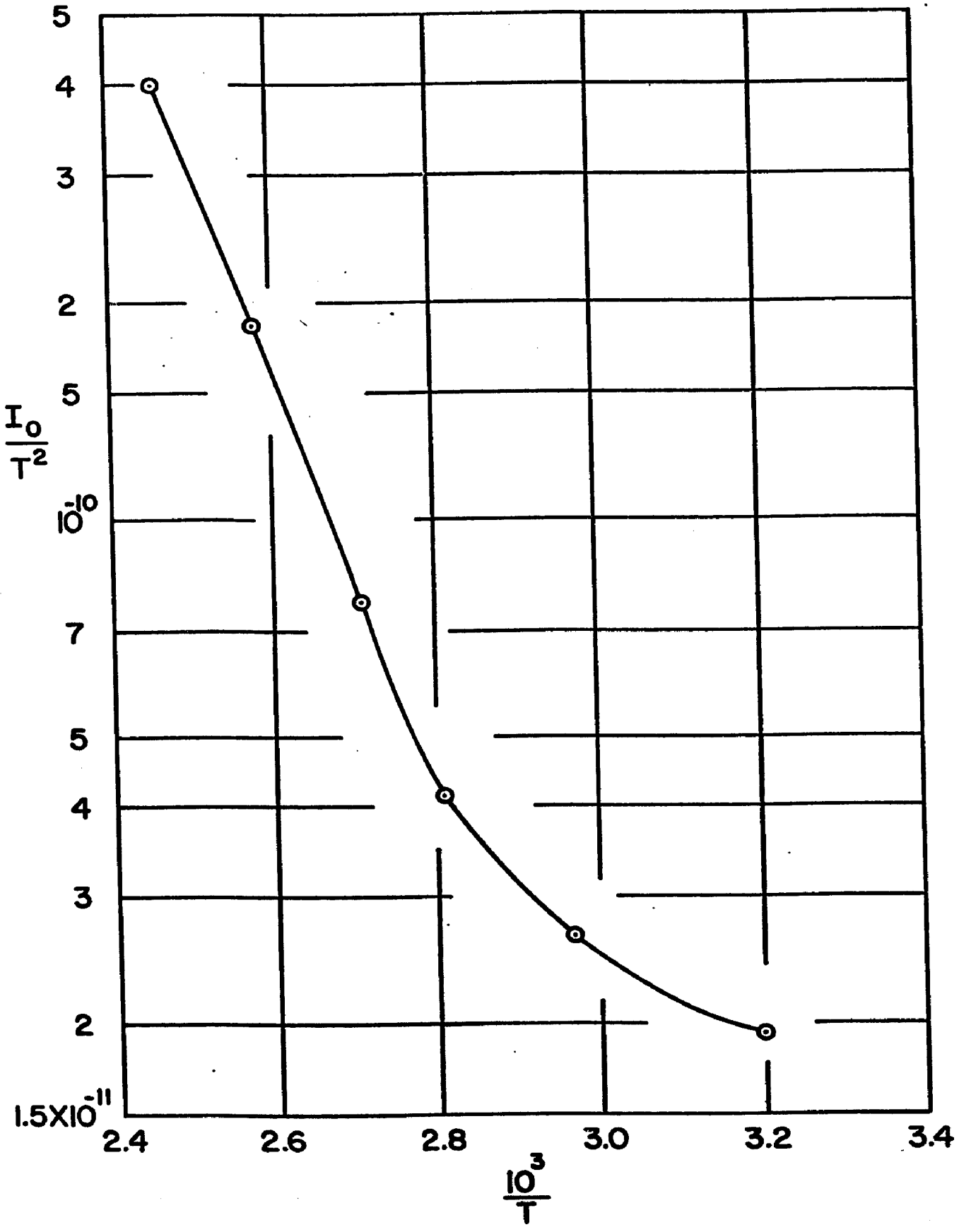

Ln $I_o/T^2$ VS. $10^3/T$ FOR DEVICE PY-G-11(1) WHERE $I_o$ IS FOUND FROM THE Ln I VS. $V^{.484}$ PLOTS
5
4
3
2
5
$10^{-10}$
7
5
4
3
2
$1.5X10^{-11}$
$\frac{I_o}{T^2}$
2.4
2.6
2.8
3.0
3.2
3.4
$\frac{10^3}{T}$

Figure 33

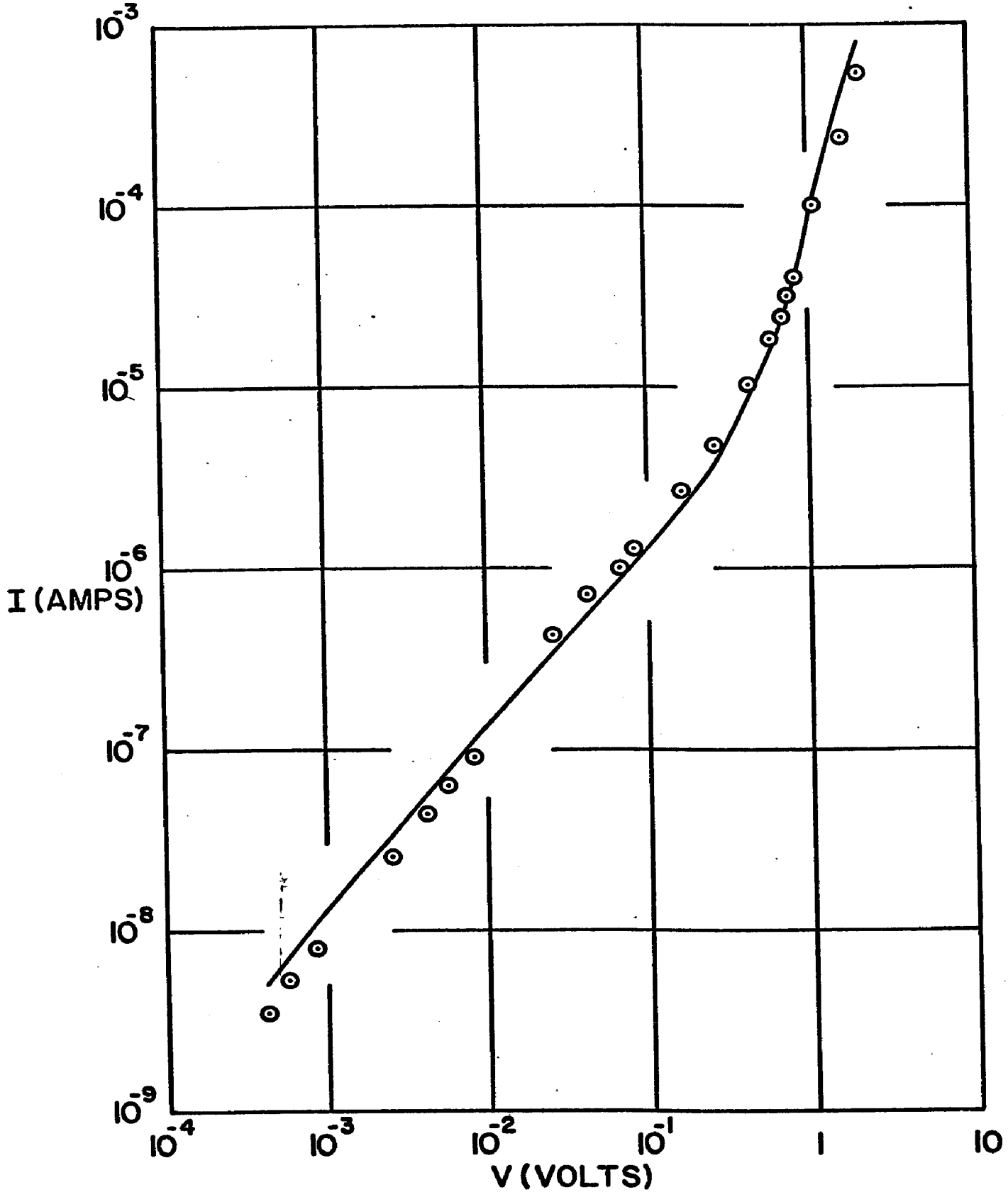

COMPARISON BETWEEN THE DATA FOR
DEVICE PY-G-21(3) AND EQUATION 3
$10^{-3}$
$10^{-4}$
$10^{-5}$
$10^{-6}$
$10^{-7}$
$10^{-8}$
$10^{-9}$
I (AMPS)
$10^{-4}$
$10^{-3}$
$10^{-2}$
$10^{-1}$
1
10
V (VOLTS)

Figure 34

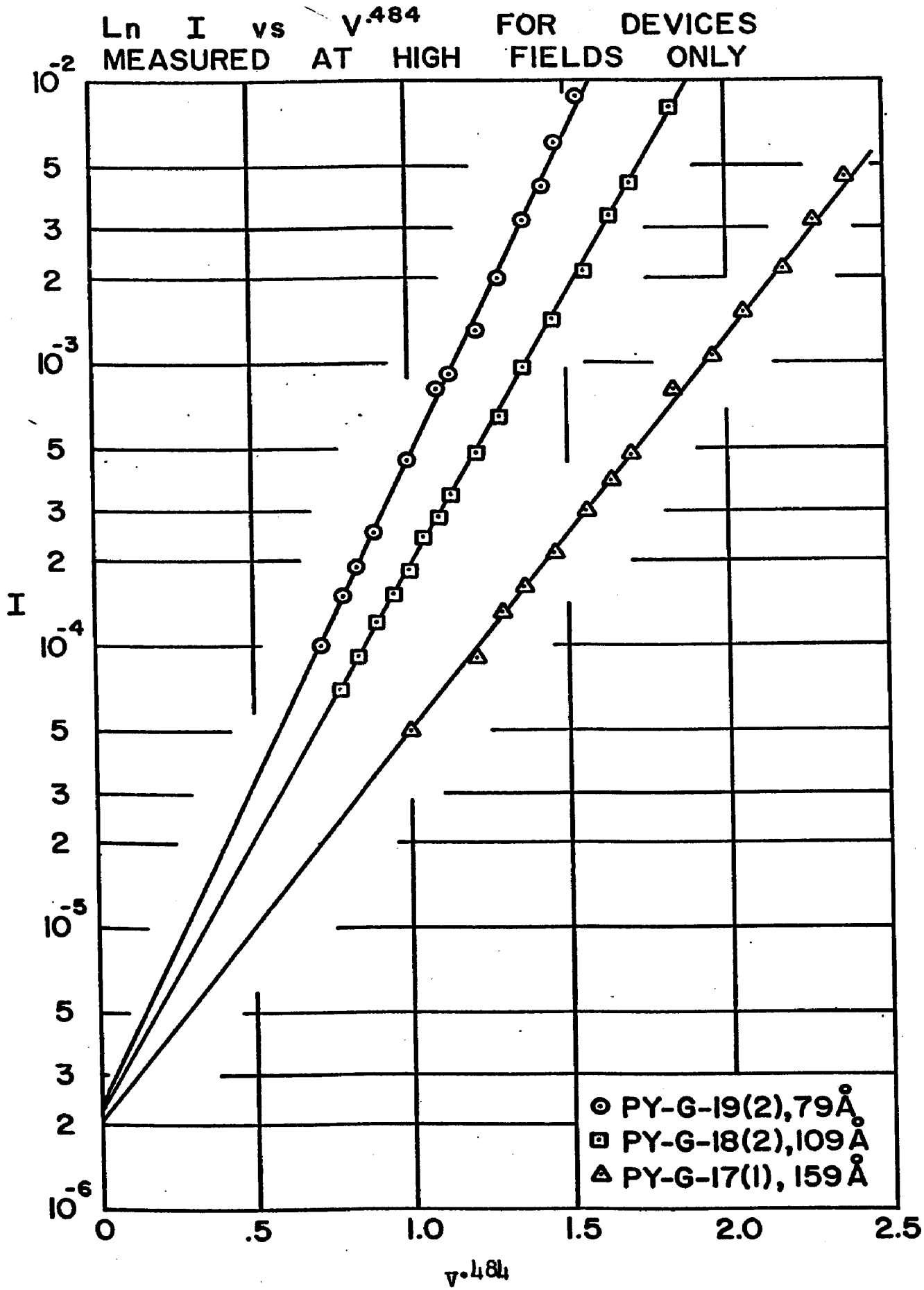

Ln I vs V.484 FOR DEVICES
MEASURED AT HIGH FIELDS ONLY
I
V.484
10-2
5
3
2
10-3
5
3
2
10-4
5
3
2
10-5
5
3
2
10-6
0
.5
1.0
1.5
2.0
2.5
PY-G-19(2),79Å
PY-G-18(2),109Å
PY-G-17(1), 159Å

Figure 35

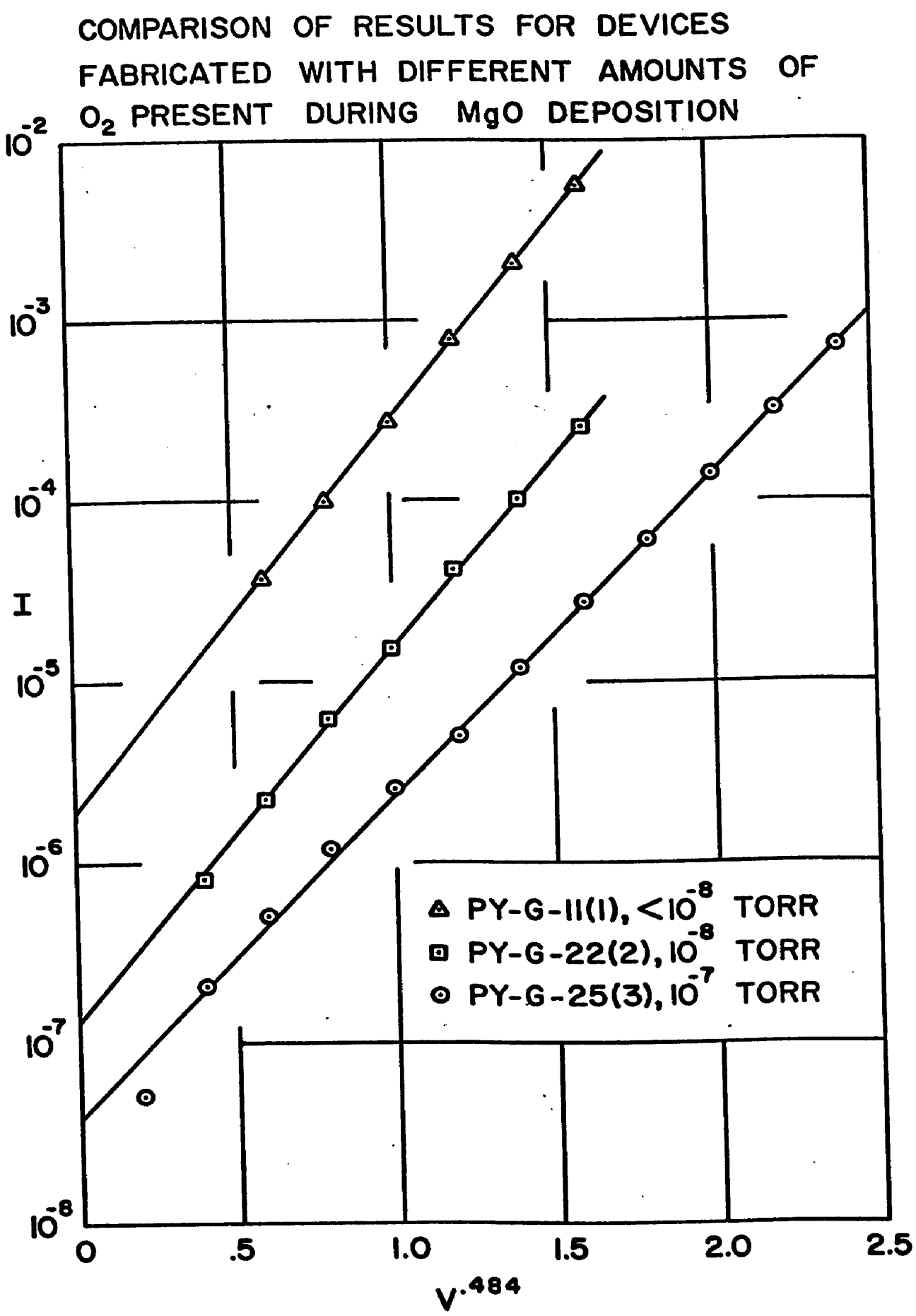

COMPARISON OF RESULTS FOR DEVICES FABRICATED WITH DIFFERENT AMOUNTS OF $O_2$ PRESENT DURING MgO DEPOSITION
$10^{-2}$
$10^{-3}$
$10^{-4}$
I
$10^{-5}$
$10^{-6}$
$10^{-7}$
$10^{-8}$
0
.5
1.0
1.5
2.0
2.5
$V^{.484}$
PY-G-11(1), $<10^{-8}$ TORR
PY-G-22(2), $10^{-8}$ TORR
PY-G-25(3), $10^{-7}$ TORR

Figure 36

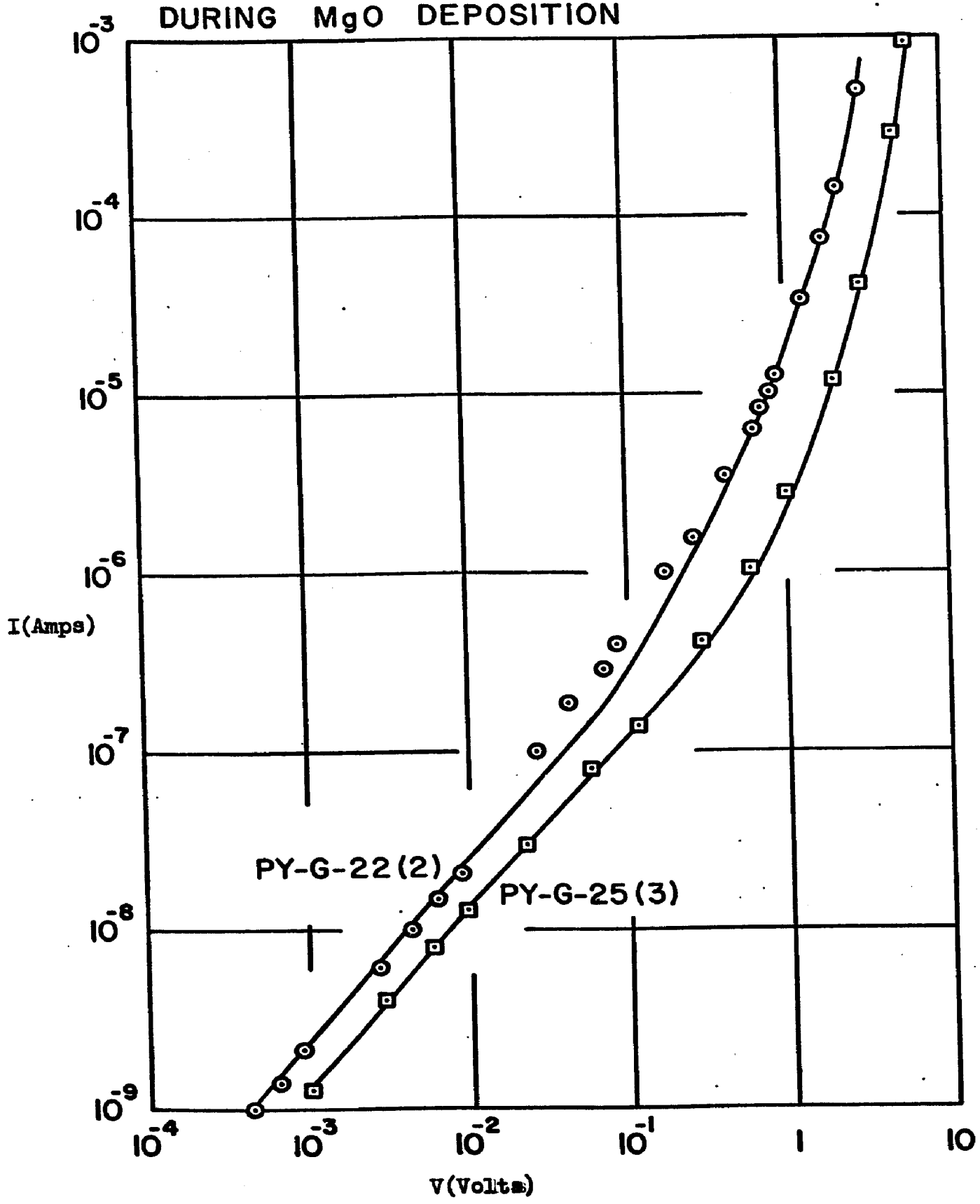

COMPARISON BETWEEN EXPERIMENTAL DATA AND EQUATION 3 FOR DEVICES FABRICATED WITH OXYGEN PRESENT DURING MgO DEPOSITION
$10^{-3}$
$10^{-4}$
$10^{-5}$
$10^{-6}$
$10^{-7}$
$10^{-8}$
$10^{-9}$
I(Amps)
PY-G-22(2)
PY-G-25(3)
$10^{-4}$
$10^{-3}$
$10^{-2}$
$10^{-1}$
1
10
V(Volts)

Figure 37

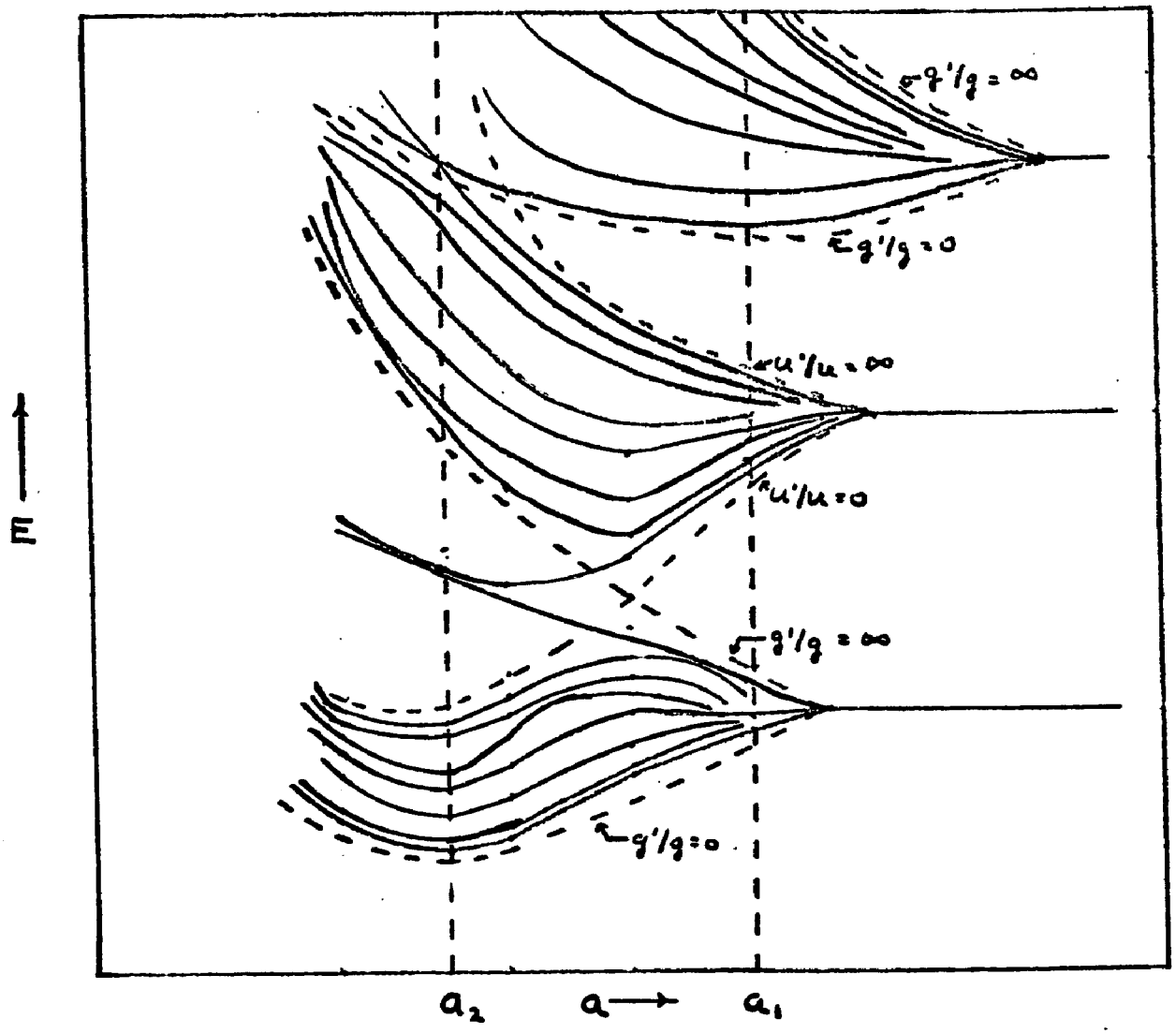



Figure 38. Energy Bands as a Function of Interatomic Spacing for a Simple Linear Chain

$Ln(I_o/T^2)$ VS $10^3/T$ FOR DEVICES FABRICATED WITH DIFFERERENT AMOUNTS OF OXYGEN PRESENT DURING MgO DEPOSITION

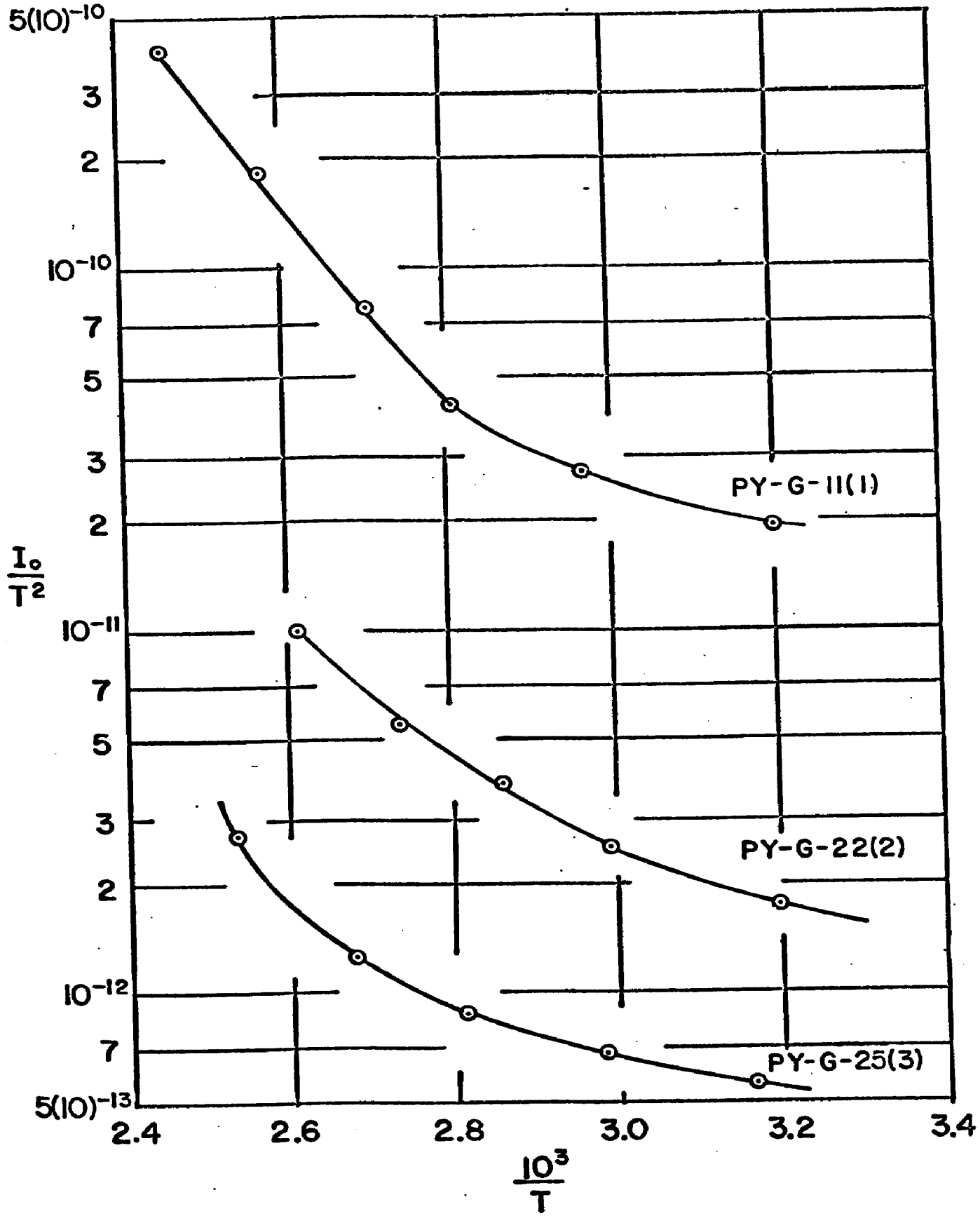



Figure 39

# BARRIER HEIGHTS AS A FUNCTION OF TEMPERATURE

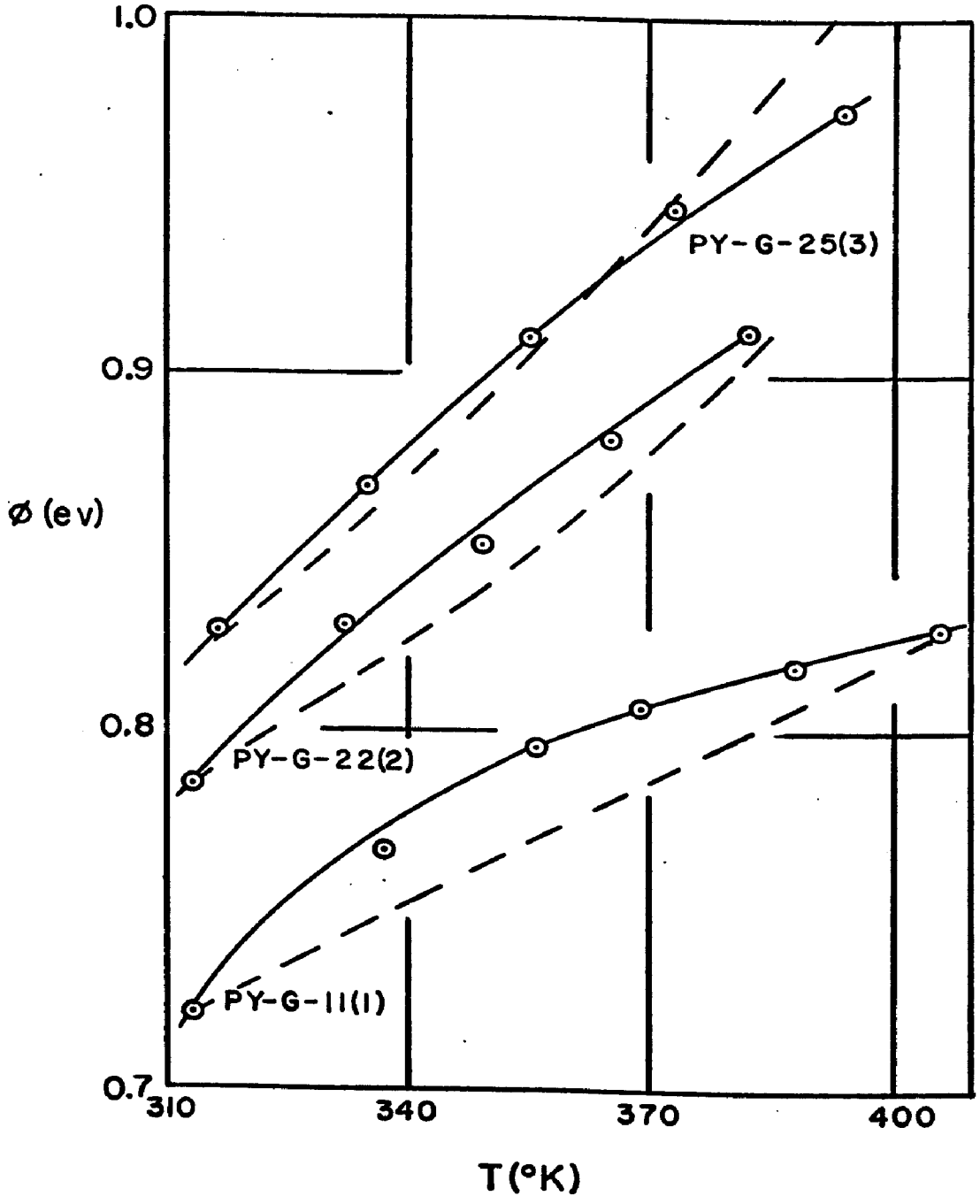



Figure 40

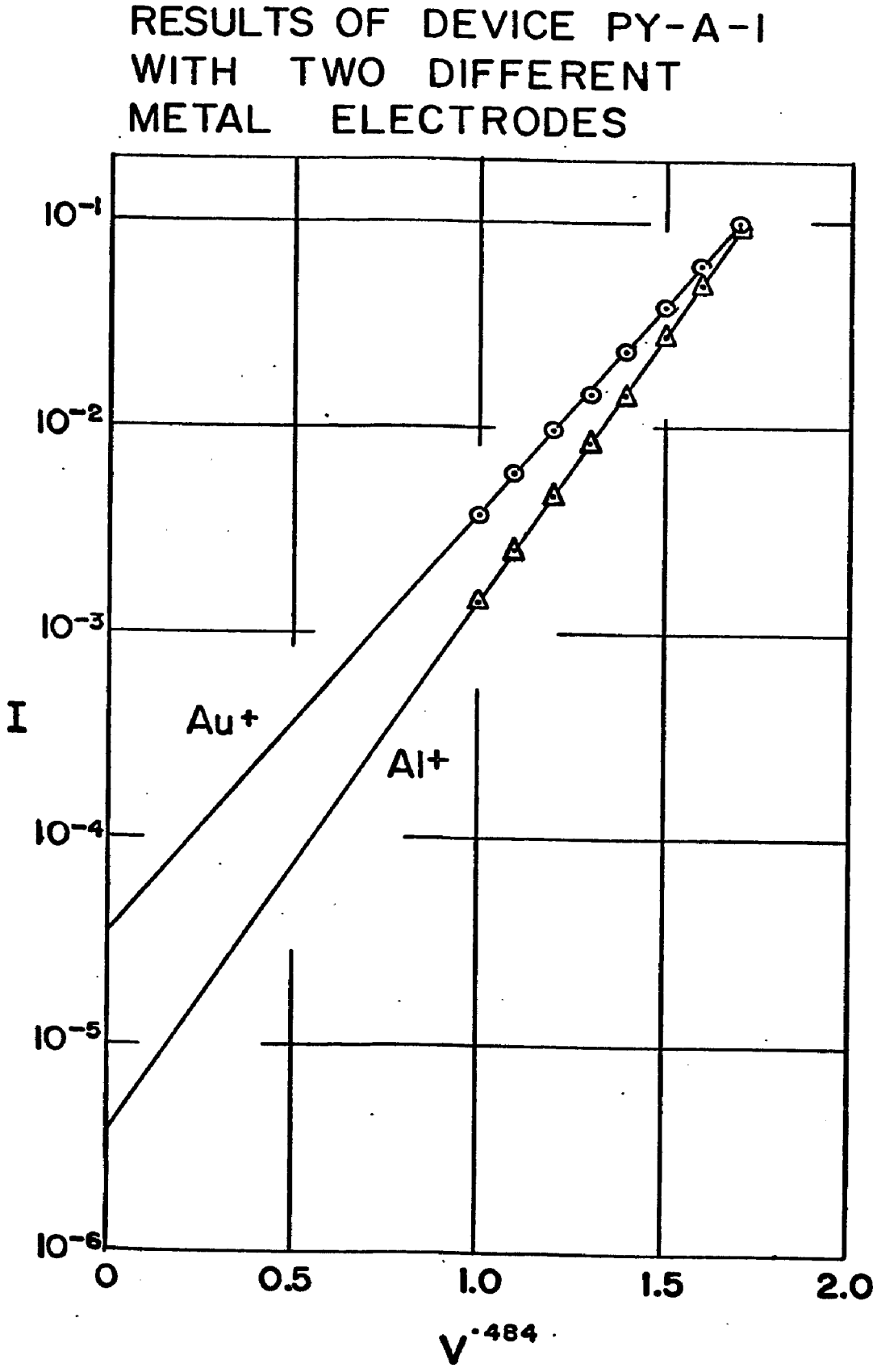
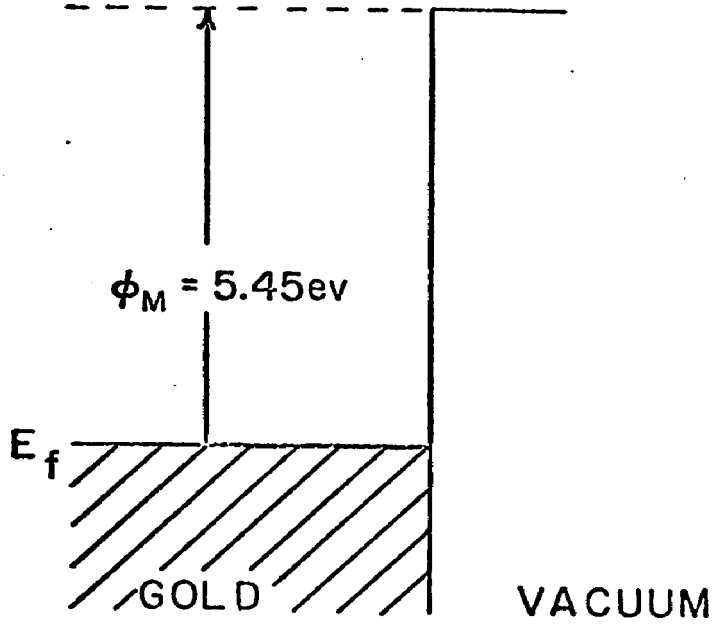
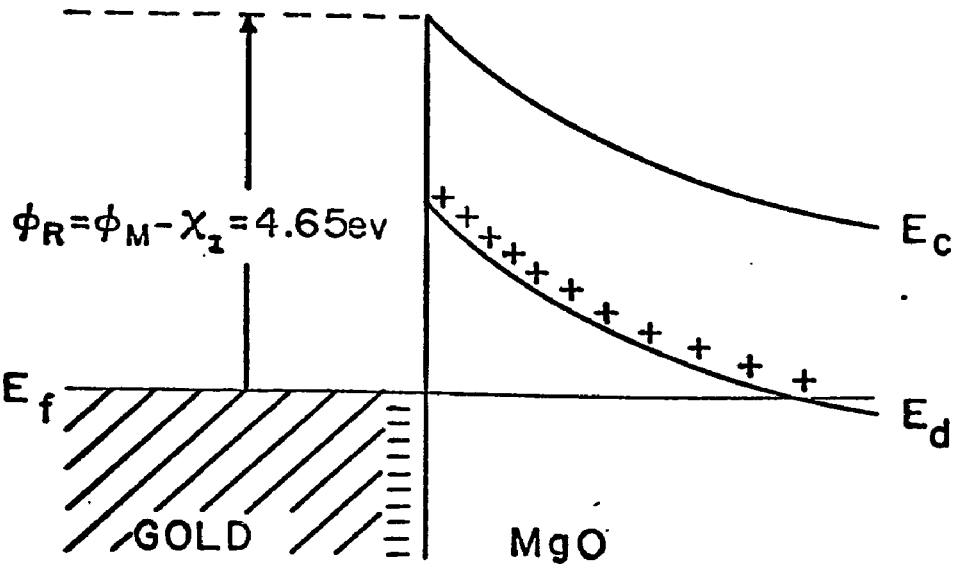

RESULTS OF DEVICE PY-A-1
WITH TWO DIFFERENT
METAL ELECTRODES
10⁻¹
10⁻²
10⁻³
10⁻⁴
10⁻⁵
10⁻⁶
I
Au+
Al+
0
0.5
1.0
1.5
2.0
V·484

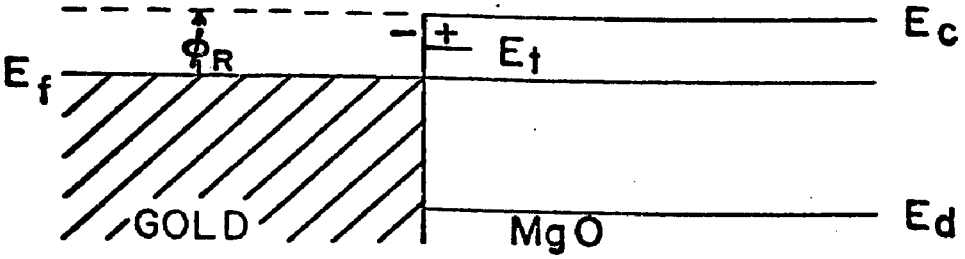
Figure 41




a. ENERGY BAND PICTURE FOR A GOLD–VACUUM INTERFACE

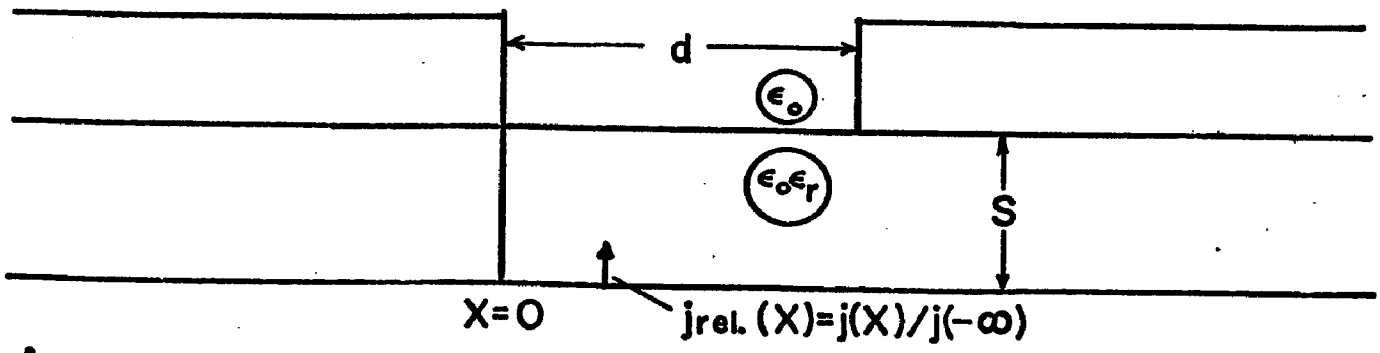



b. ENERGY BAND PICTURE FOR A GOLD–MgO INTERFACE IF NO INTERFACE STATES EXIST

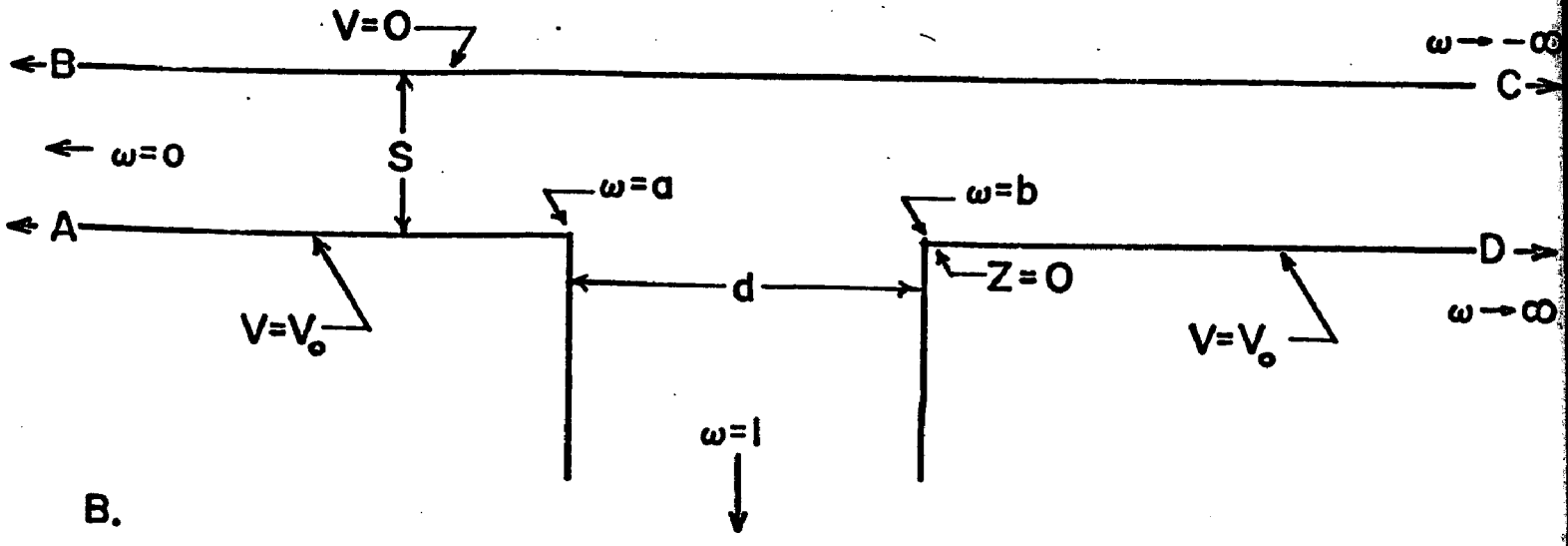



c. ENERGY BAND PICTURE FOR A GOLD-MgO INTERFACE WITH A HIGH DENSITY OF DONOR LIKE INTERFACE STATES

Figure 42




A.




B.

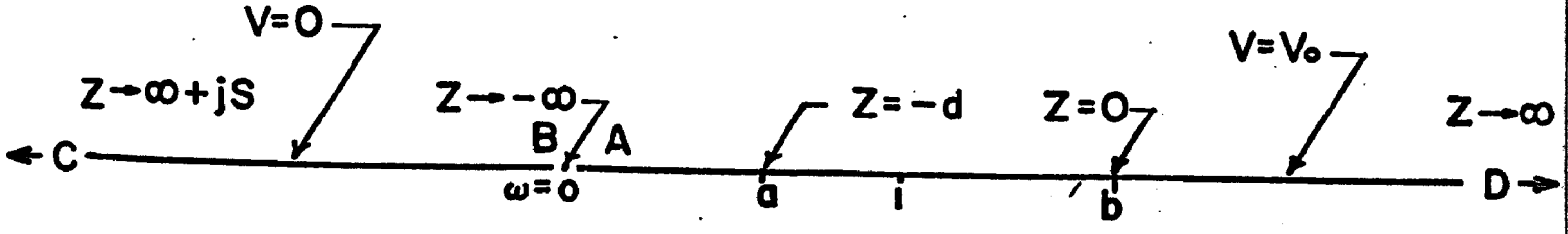
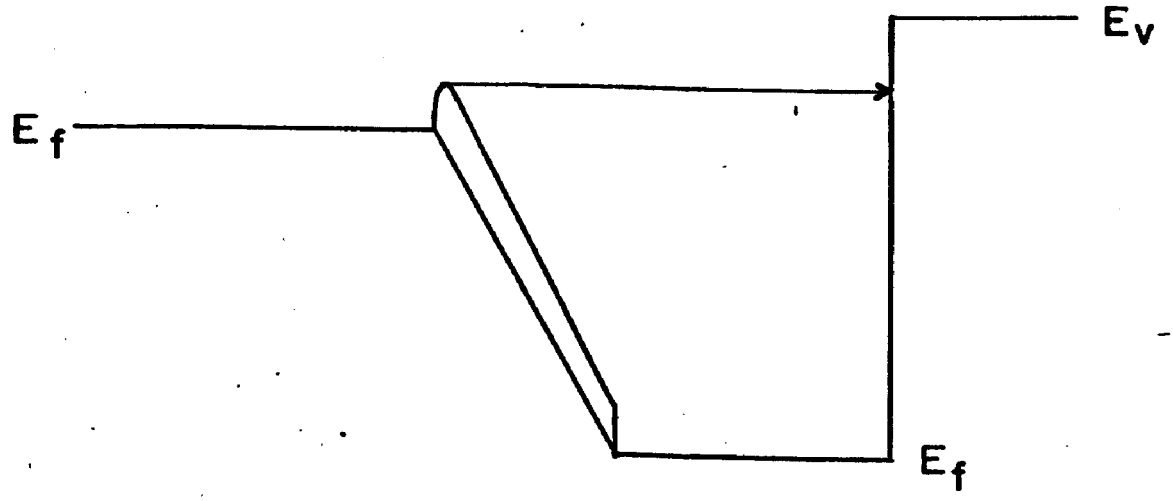
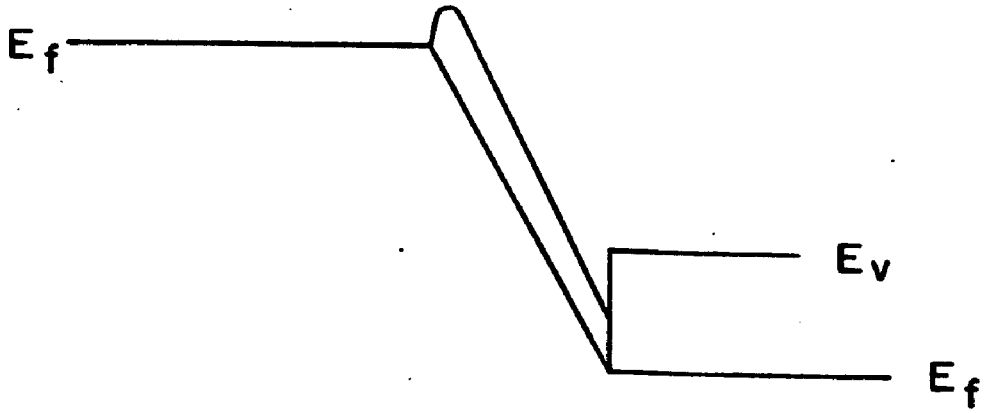



DIAGRAM INDICATING DETAILS OF THE CALCULATION OF ELECTRIC FIELD VARIATION AT A PLANE ELECTRODE OPPOSITE A SLOTTED ELECTRODE

Figure 43




44a. ENERGY LEVEL DIAGRAM FOR AN APPLIED SAMPLE BIAS OF 4 VOLTS SHOWING THAT NO ELECTRONS SHOULD BE EMITTED THROUGH THE OVERLAYER




44b. ENERGY LEVEL DIAGRAM APPROPRIATE FOR EMISSION THROUGH HOLES IN THE GOLD OVERLAYER FILM

Figure 44

FIELD STRENGTH AT THE UNDERLAYER
BENEATH A SLOT IN THE OVERLAYER

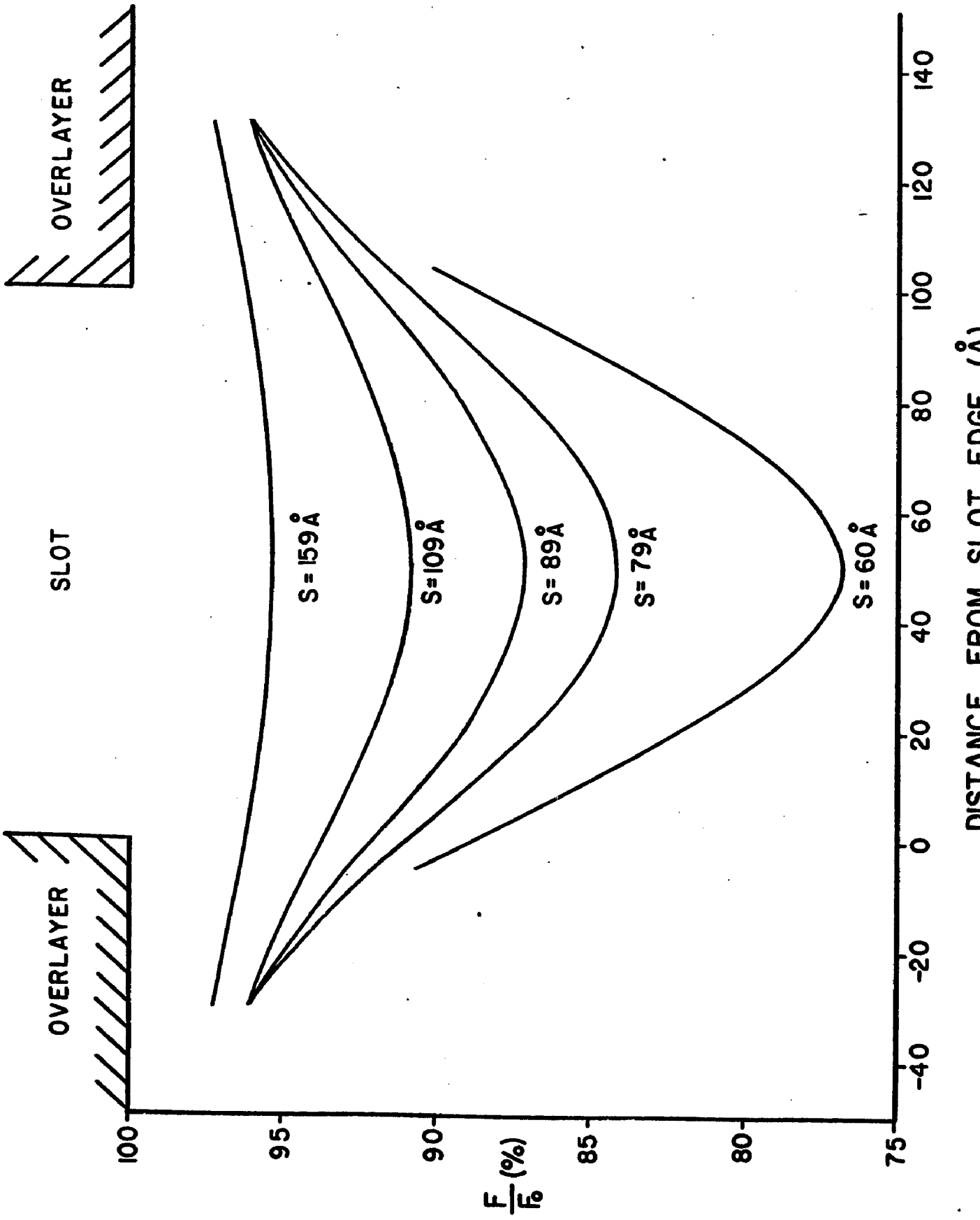



Figure 45

$\alpha = \frac{I_e}{I_e + I_s}$ AS A FUNCTION OF OXIDE THICKNESS

ASSUMING NO ENERGY LOSS IN THE OXIDE

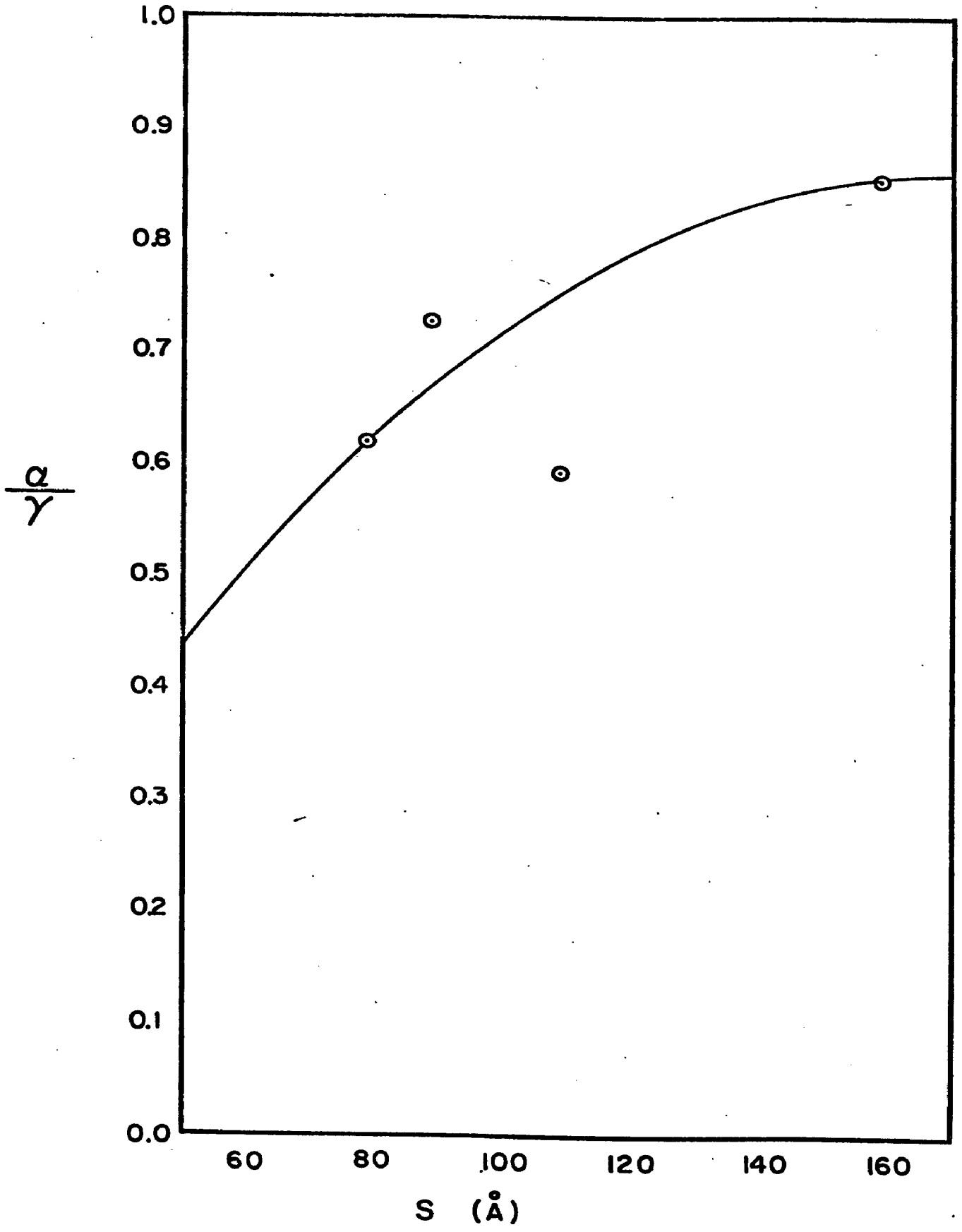
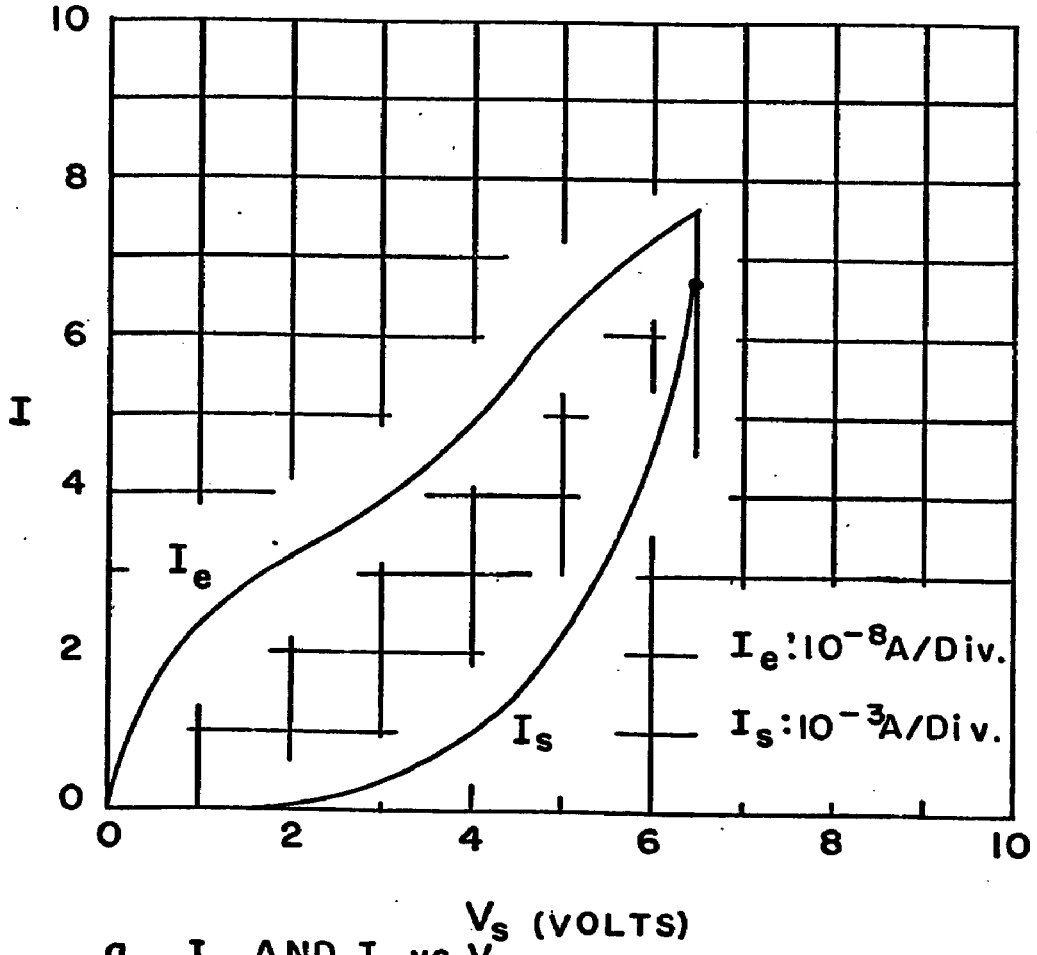
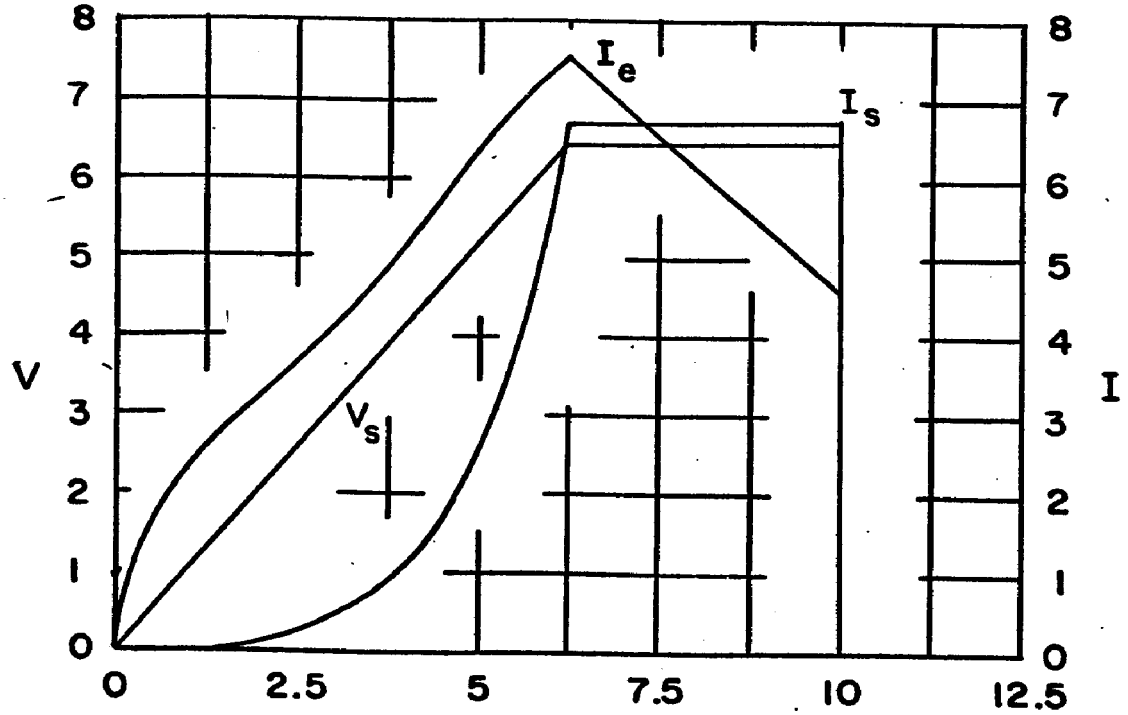



Figure 46

EVIDENCE OF CHARGING AT AN EMITTING SLOT, DEVICE PY-G-17(1)

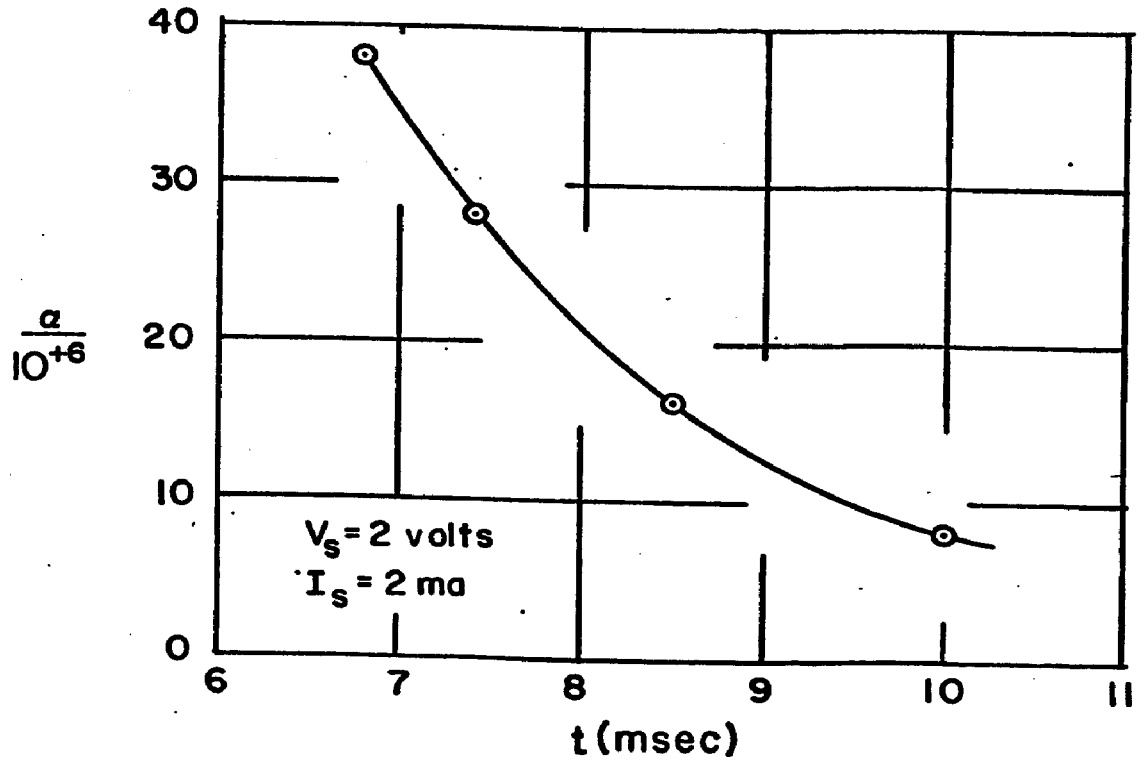



a. $I_e$ AND $I_s$ vs. $V_s$

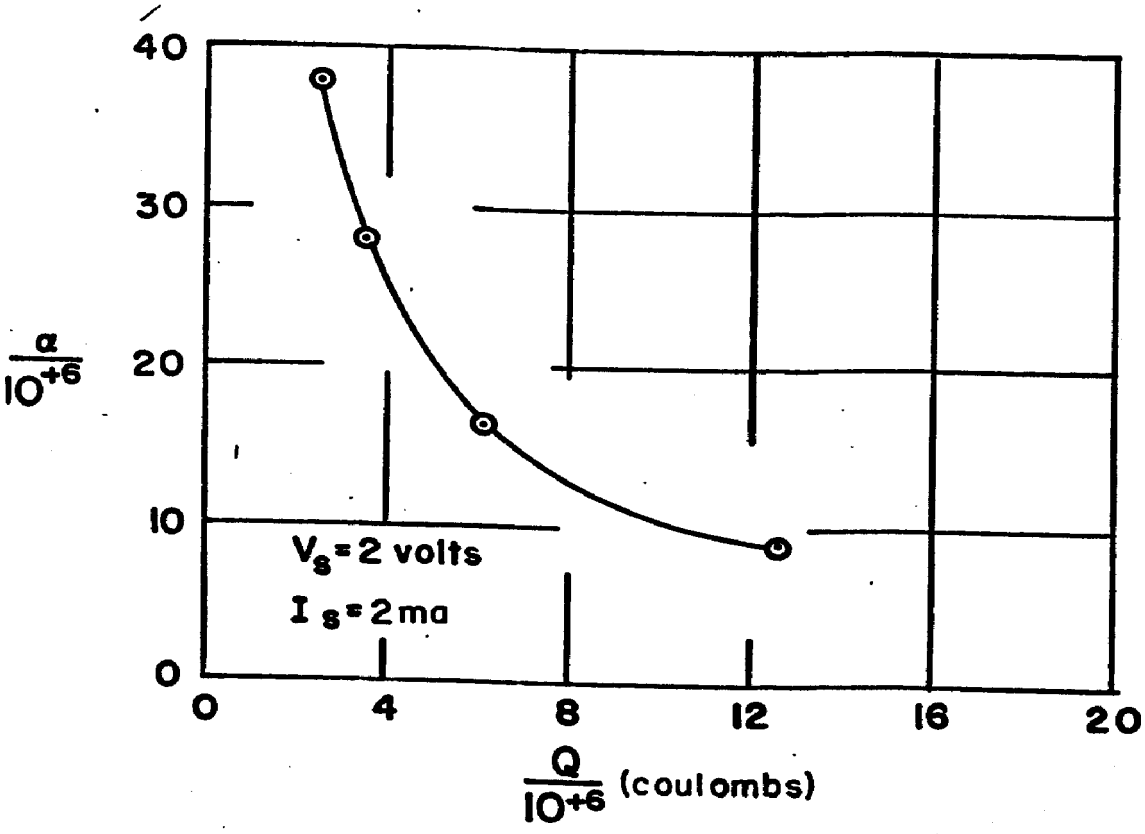



b. $I_e$, $I_s$, AND $V_s$ vs. TIME.

Figure 47




a. EMISSION TRANSFER RATIO VS. TIME REQUIRED TO REACH $V_s$ = 2 VOLTS




b. EMISSION TRANSFER RATIO VS. TOTAL CHARGE PASSED THROUGH THE DEVICE

Figure 8

TIME CONSTANTS FOR CHARGING
OF THE INSULATOR BENEATH A SLOT

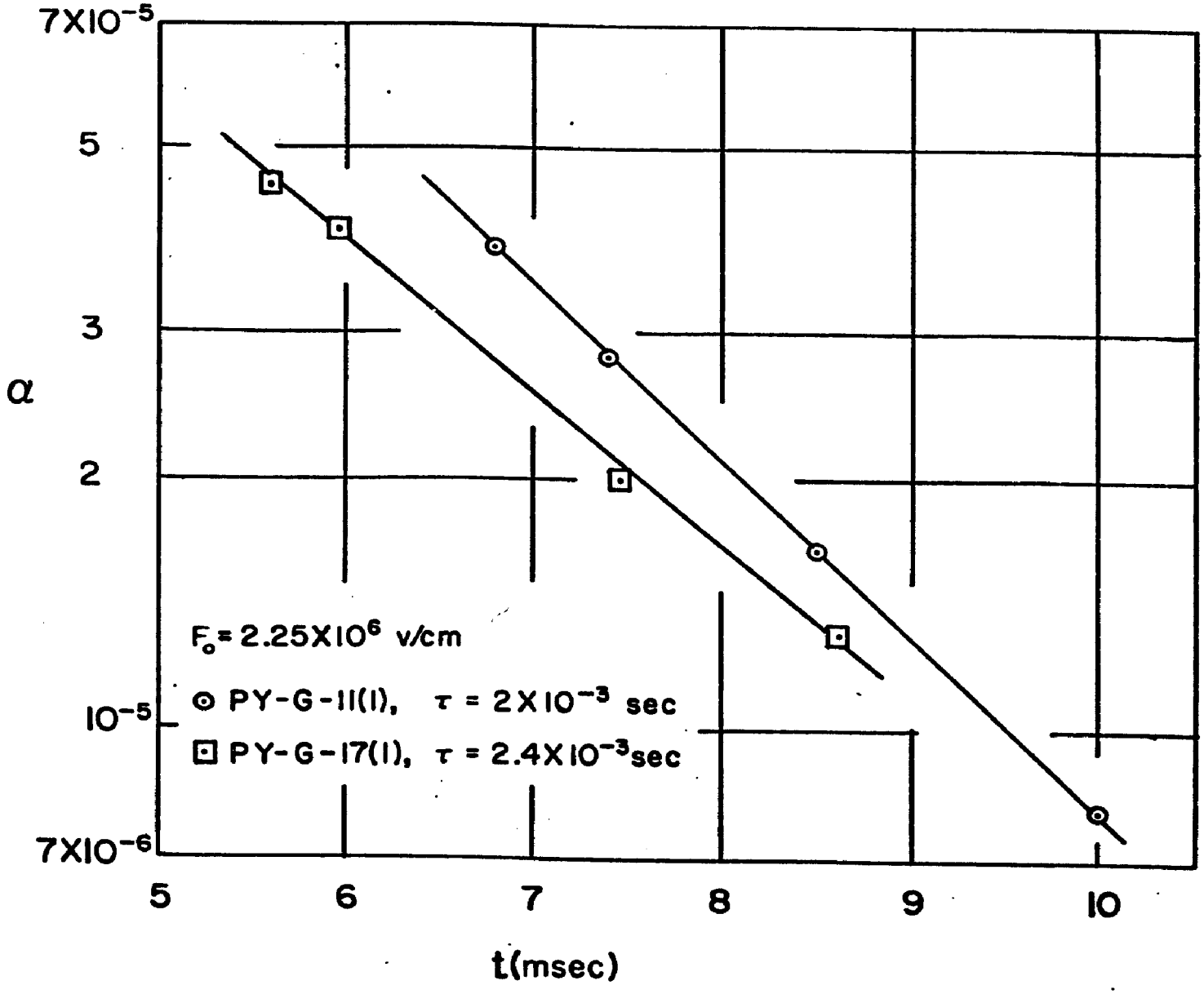



Figure 49